AFAPL-TR-66-52

ALLISON METHOD OF CHEMICAL ANALYSIS

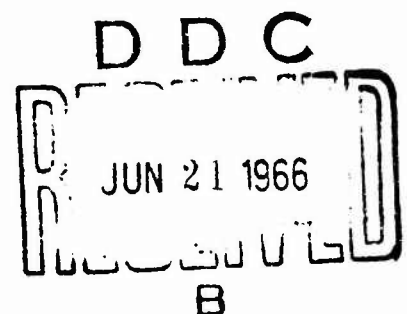Herbert F. Mildrum
Bernhard M. Schmidt

University of Dayton

TECHNICAL REPORT AFAPL-TR-66-52

May 1966

DDC

JUN 21 1966

B

Distribution of this document is unlimited.

NOTICES

When Government drawings, specifications, or other data are used for any purpose other than in connection with a definitely related Government procurement operation, the United States Government thereby incurs no responsibility nor any obligation whatsoever; and the fact that the Government may have formulated, furnished, or in any way supplied the said drawings, specifications, or other data, is not to be regarded by implication or otherwise as in any manner licensing the holder or any other person or corporation, or conveying any rights or permission to manufacture, use, or sell any patented invention that may in any way be related thereto.

Copies of this report should not be returned to the Research and Technology Division unless return is required by security considerations, contractual obligations, or notice on a specific document.

ALLISON METHOD OF CHEMICAL ANALYSIS

Herbert F. Mildrum
Bernhard M. Schmidt

FOREWORD

This technical report has been reviewed and is approved.

Robert D. Sherrill, Chief
Ground Support Branch
Support Technology Division
Air Force Aero Propulsion Laboratory

ABSTRACT

This report describes the theoretical study and experimental circuit investigations conducted on the Allison effect apparatus used for chemical analysis.

The inherent electrical behavior of an Allison effect apparatus has been well defined by using modern high speed oscillographic techniques and frequency selective equipment. A continuous radio frequency spectrum characterized by numerous resonances rapidly diminishes into the noise level at 4000 megahertz. A theoretical analysis of the apparatus has generated a valid equivalent circuit model. A review of the extensive data indicates that the Allison effect apparatus functions primarily as a phase comparator for radio frequencies in the 30 to 100 megahertz range. An rf-optical interaction in the cells, possibly by means of the Cotton-Mouton effect, is thought to produce a characteristic light modulation effect when phase matching occurs.

TABLE OF CONTENTS

TABLE OF CONTENTS (Cont'd)

ILLUSTRATIONS

vii

ILLUSTRATIONS (Cont'd)

ILLUSTRATIONS (Cont'd)

ILLUSTRATIONS (Cont'd)

ILLUSTRATION (Cont'd)

ILLUSTRATIONS (Cont'd)

LIST OF TABLES

INTRODUCTION

This report summarizes the theoretical and experimental circuit analysis of an Allison effect apparatus. The authors of this report are the principal investigators whose coordinated efforts were consolidated to accomplish the technical aspects of the program.

The general philosophy adopted, following a thorough review of all published literature on the experiment, was that, with the application of modern circuit analysis theory and experimental techniques, significant contributions could be made toward the development of a circuit theory describing the Allison effect apparatus.

Many years have passed since Beams and Allison[1] searched for a time lag in the Faraday effect. These first experiments soon were followed by other experiments which investigated an unusual phase of the original observations, viz., the Allison effect. This effect consisted of light intensity minima which appeared in the optical signal as the delay line lengths were adjusted. These minima were located at trolley positions (trolleys were used to change the lengths of the delay lines) characteristic of the materials in the sample cell. The minima were very "sharp"; that is, the position of the trolley on the delay line was unusually well resolved for a particular minimum. Best of all, minima appeared even when the subject material was present as an exceedingly dilute concentration in a host solvent.

There was, however, an unfortunate difficulty: the attenuation in intensity, though well localized, was so small as to be marginal for many observers. Matters were not improved by the fluctuating magnesium spark used for the light source. It developed that training and experience were necessary, even in the case of those observers who could discipline themselves to differentiate between the true signal and the random spark fluctuations. The observation of minima was, therefore, subjective, and, even at present, no objective measurements of minima have been made that are acceptable to the general scientific community.

The history of the Allison effect is long and highly documented. It is no secret that the subject is a matter of some controversy, most of which occurred in the first years of this, some forty year old, investigation. The objections were centered mainly around (1) the reported resolution of minima, (2) the reported sensitivity of the effect, (3) the inability to produce generally acceptable objective experimental evidence of the minima, and (4) the apparent lack of a theoretical basis for such a physical phenomenon.

The major reason for continuing the investigation of the Allison effect is quite obvious. The techniques and the reported sensitivity would make the Allison effect apparatus an important tool in physical and chemical research and in applied chemical analysis.

Each of the preceding objections will be considered in turn. The resolution of minima was criticized because of the apparently slow risetime of current in the coils. The measured low signal frequencies had periods which were orders of magnitude beyond the short interval of time calculated by dividing the minima displacement resolution by the speed of light. This objection was raised by investigators who did not realize the complexity of the signal with which they were dealing, largely because the necessary high resolution electronic test equipment was not then available.

It was suspected at the start of this present investigation that the transient generated in the spark gap breakdown would be rich in high radio frequency components. This proved to be the case, and it can be demonstrated that the reported displacement resolution is indeed within the range of possibility should these significant high radio frequency values be responsible for the effect.

In these days, one is not astonished to read that a given method is capable of detecting a physical entity to within a sensitivity of one part in 10^{11} or 10^{12}. This is a common claim in the case of semiconductor physics, magnetic resonance, and nuclear physics. Were the Allison effect to be published tomorrow, this aspect would evoke little disbelief, but forty years ago the then fantastic sensitivity (which could explain contradictory findings by observers who did not appreciate the necessity for extreme purity of samples) may have had much to do with the formulation of adverse opinion in view of the marginally detectable effect. Further, the medium under investigation is a liquid, and, since even today this phase is least understood, it is unwise to make categorical statements about possibility and impossibility concerning liquids.

While it is always most desirable in scientific experiments to obtain pointer readings, graphic recordings, or photographs as experimental evidence of a particular effect, the inability to produce such evidence should not be the sole basis for an adverse judgement. In some cases, the effect may be so marginal that only visual sensing can detect it. For this reason, and also because the eye remains the most precise instrument capable of selecting a desired optical signal in the presence of considerable background fluctuation, it is clear that subjective experimental evidence still warrants serious consideration. Finally, since the major obstacle to the production of pointer readings for the Allison effect is technological, it seems probable that new advances will make possible the application of enhancement techniques to the experiment.

There is no general agreement on the theoretical basis of the Allison effect: that it is a magneto-optic effect or an electro-optic effect or a combination of both is uncertain. It may be that absorption plays a part in producing the observed phenomenon. Whatever the case, intense electric and magnetic fields at many frequencies between 200 kilohertz to 100 megahertz are present at the reference and sample solenoids during the transient that takes place when the capacitor discharges through the spark gap into the electrical system. Field

orientations vary through the course of the transient so that suitable components of electric and magnetic fields are available, at least momentarily, for the stimulation of either or both types of optical effects. It would, in fact, be surprising if optical effects were missing, a point which can be further strengthened; it is certain that several optical effects do occur during the electrical discharge. If the Allison effect is linked to the magneto-optic effect or the electro-optic effect or both, it will be necessary eventually to obtain explicit expressions for the field intensities in the cells before the effect can be linked theoretically with any of the several magneto-optic and electro-optic effects.

SECTION I

THEORETICAL CIRCUIT ANALYSIS

The theoretical circuit analysis presented in this section has been compiled from a thorough survey of past reference material on the Allison effect experiment. The result of these efforts, in conjunction with new experimental evidence, has been extensively reported by Schmidt[2] in a systematic chronologically ordered log. The material presented in this section has been abstracted from this source.

A. MAJOR PREMISE

The major premise is the existence of the effects, <u>viz.</u>, the minima reported by Allison[1]. From this point onward, then, the following quotations will also form the accepted experimental foundation for the theoretical deliberations:

(a) Allison, "The dimensions of the cells, therefore, do not affect the results, a conclusion which is also supported by other variations of the apparatus mentioned in the sequel"[3].

(b) Allison and Murphy, "The positions of the minima are not changed, within the errors of observations, by wide variations in the resistance, capacitance, or inductance of the circuit, though the distinctness of the minima is affected by such changes"[4]. This statement is qualified as follows: The last phrase, after the comma, is included for information only, since "distinctness" is a subjective factor; it is not part of the experimental basis. A further qualification is given by M. Roquemore[5], "Dr. Allison and M. Roquemore were able to shift minima trolley positions by putting parallel plate capacitors with adjustable glass dielectrics directly across the solenoids. By sliding the glass dielectric in and out, hence changing the capacitance, minima were noted to shift. According to Allison, this was the first time minima were shifted due to changing circuit components ... . It might be concluded that minima do not shift due to value changes in the charging capacitor and solenoids but can be shifted by changing capacitance of parallel plate capacitors placed in parallel across the solenoids".

(c) Allison, "A variety of ways of charging C have been employed with success, the positions of the minima being unchanged with such variations"[6].

(d) Allison, "The divergence between scale readings on two different devices is usually not more than a few millimeters, except toward the extreme ends of the scale, where it becomes somewhat greater"[6].

(e) Allison, "The minima have been read without rectification of the current, ..."[7].

(f) Allison, "They (the minima) have also been observed when only one-half of the bilaterally symmetrical wire system is in use"[7].

(g) Roquemore, "What can be concluded is that using visual observation, minima disappear during humid conditions"[5].

(h) The literature reports that the positions of minima for a given compound remain independent of the concentration of the compound [7, 8, 9]. Extremely small traces, say 1:10[11], have been observed to cause minima at the positions expected for that compound"[8].

(i) The Allison effect offers a means for isotope discrimination. For a given element, the minimum position varies with the isotope [10, 11, 12, 13, 14, 15].

(j) Minima positions for a given substance vary in a regular way with the frequency of the light used in the experiment[3].

(k) While an extremely pure host solvent or substance must be used in the "unknown" cells, there is no particular restriction on the purity of the carbon bisulfide in the reference cell. This information was obtained in a discussion with M. Roquemore. The importance of solvent purity is discussed by Cooper[9].

The theoretical analysis has disclosed that the time varying currents in the solenoids are much more complex than had previously been supposed. The approach to the problem was as follows: Several degrees of refinement were envisioned; the "resolution" of the circuit analysis was to be improved successively by considering first order, second order, third order, and so on, solutions where more and more detail was entered into the theoretical circuit. Since the theoretical circuit is always an idealization of the actual physical circuit, one approaches the latter as a limit. The decision as to what constitutes the first order elements, the second order elements, and so on, is a matter of engineering judgement assisted, where possible, by first-hand experimental information.

B. CIRCUIT MODEL I

1. Identification of Circuit

The first order solution based upon Circuit Model I, Figure 1, considers the system as a collection of lumped circuit elements, which is quite appropriate, considering the long wavelength of the fundamental frequency of the damped oscillation.
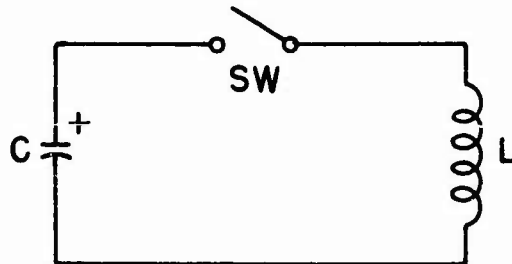
Figure 1. Circuit Model I

This simplified model consists of the lumped components represented in Figure 1 as a charged capacitor (C), the inductance of the lines and coils (L), and the spark gap as a switch (Sw). An oscillatory transient takes place in the circuit the instant the switch is closed. For a reasonably high-Q circuit, the natural angular frequency of oscillation is given rather accurately by the expression:

$$\omega_o = 1/(LC)^{1/2} \tag{1}$$

A comparison of the resonant frequency characteristics of the electrical circuits described in the apparatus of earlier papers, along with those currently in use at Auburn University and at APL (Aero Propulsion Laboratory), is presented in Table I.

The capacitance and coil inductance for the components are relatively simple to calculate from well-known formulas[16].

$$C = 8.85 \times 10^{-12} \, \varepsilon_r (N-1)A/t \quad \text{farads} \tag{2}$$

where:

    N is the number of plates
    A is the area of one side of one plate in square centimeters
    t is the thickness of dielectric in centimeters
    ε_r is the dielectric constant relative to air

$$L = n^2 \left[r^2 /(9r + 10 \ell) \right] \text{microhenrys} \tag{3}$$

6

where:

        n is the number of turns
        r is the radius in inches
        l is the length of coil in inches

      The lengthy wire path connecting the coils to the capacitor does not serve to isolate the components of the resonant circuit at the frequency values calculated because the length of wire involved is considerably less than the average wavelength corresponding to those frequencies. For example, one megahertz corresponds to a wavelength of 300 meters. The total length of wire connecting a coil to the capacitor would need to be around 80 meters before one would be faced with a really significant transmission line problem. The effect of the added long wire leads on the circuit at these frequencies would be to increase the magnitude of the inductance value. Variations in trolley position would cause a vernier adjustment of the inductance and thus of the frequency of resonance. In order to estimate the magnitude of inductance added by the leads, one may apply the expression for the inductance per unit length of a parallel wire transmission line:

$$L = 0.41\ n(d/r)\ \text{microhenrys per meter of line} \qquad (4)$$

where r is the radius of the wire and d is the spacing of the two wires in the same units. For d/r ratios of 100 and 1000, the additional inductances are, respectively, 1.8 and 2.8 microhenrys per meter of parallel wire line. For a specific example, consider the apparatus used by Cooper[17]. Here we have added to a single coil (26 microhenrys) the inductance of a 16 meter parallel wire transmission line (No. 18 wires spaced 20cm) with a d/r ratio of approximately 400. The additional inductance is approximately 38 microhenrys; this correction, in light of the range of coil inductances reported (3.5 - 51 microhenrys), is by no means negligible. The capacitance between wires enters as a second order correction. It amounts to approximately 5 picofarads per meter of parallel wire line.

Table 1. Comparison of System Resonant Frequencies

Reference	Total Circuit Inductance Microhenries	Charging Capacitor Picofarads	System Resonant Frequency f_0 in Megahertz*	
			Calculated	Measured
Allison (3, 7)	16.75	500-6400	1.56 -0.44	---
Cooper (17)	32.00	6400	0.35	---
Schmidt (2)	37.50	18, 300	0.192	0.192
Mildrum (18)	45.50	15, 600	0.191	0.200

* Hertz is defined as a unit of frequency, formerly designated as cycles per second.

Photographic evidence of experimental observations of the resonant frequency of the system located at APL were recorded by means of a fast sweep speed cathode ray oscilloscope and is presented in Figure 2.
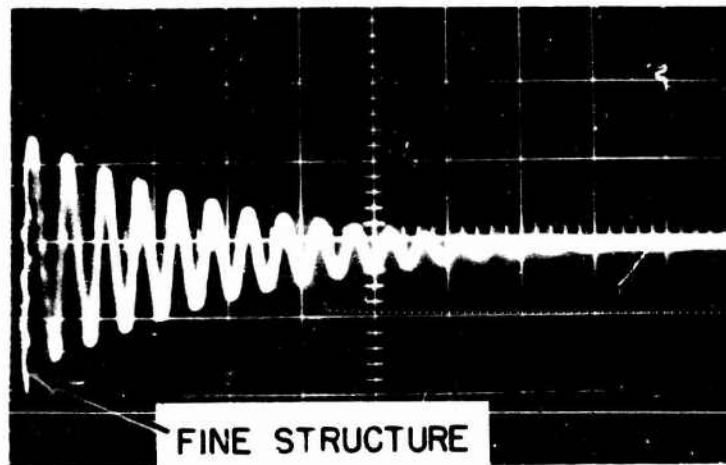
Figure 2.   Resonant Frequency Voltage Signal Across One Solenoid; Horizontal Speed 10μs/cm; Vertical Sensitivity 2 Kv/cm

The spark gap breaks down at approximately 5300 volts. It can be observed that a damped train of oscillations occurs for each breakdown of the spark gap. A fine structure was observed on the first half-cycle, but the remaining cycles were a clean, exponentially damped sinusoidal wave.

The numerical results shown in Table I and the appearance of the voltage transient (Figure 2) furnish strong experimental evidence in favor of the following conclusions:

(a)   The duration of the electric spark was 80 microseconds.

(b)   The spark was not interrupted during this interval of time; that is, the gap provided a high conductivity path during the damped oscillation and closely approximated an ideal switch.

(c)   Circuit Model I is valid for approximating the frequency of the basic oscillatory transient. In other words, the frequency can be computed by considering the natural resonance of the charging capacitor and the parallel equivalent inductance of the two branches connected across the capacitor.

Consider item (c) first. It is evident that there is no other way to account for the low frequency which was observed. If the spark lasted for a brief microsecond or so and then the coils were disconnected electrically, they would "ring"

8

at a frequency near, but slightly lower than, the self-resonant frequency of the inductor, because the distributed capacitance is augmented by the capacitance of the wires and lines connected to the coil. Still, this frequency would unquestionably be much higher than that observed. Only the large charging capacitor can account for the low value observed.

Item (a) follows immediately. Item (b) follows from the fact that the ragged first lobe of the waveform was followed by a smooth exponentially damped sinusoid. No discontinuities or distortions were observed in the waveform, and such certainly would have been evident had the spark been interrupted during the transient. The fast CRO would have exhibited any submicrosecond break or discontinuity. This verifies the assertion that the high-frequency spark is a fairly linear and bilateral resistance because the plasma does not have time to disperse during the low points in the cycle. The spark gap resistance must be very low because of the relatively low damping factor; indeed, we can calculate the resistance fairly accurately from experimental results.

Circuit theory tells us that the Q of a resonant circuit is approximately equal to the number of cycles required for the resonance to damp out. We may take the Q as being approximately 15. Also at resonance

$$2\pi f_o L = 1/(2\pi f_o C) = 10^6/(2\pi \times 190 \times 10^3 \times 0.0183) \tag{5}$$

or

$$2\pi f_o L = 45 \text{ ohms} \tag{6}$$

Now, since

$$Q = 2\pi f_o L/R \tag{7}$$

we find

$$R = 3.0 \text{ ohms} \tag{8}$$

But

$$R = R_{spark} + R_{coils} + R_{lines} \tag{9}$$

The effective series resistance of the capacitor will be negligible. From Section II, B, 3, we find that the a.c. resistance of a coil at 200 KHz is about 0.6 ohm, and one might set the a.c. resistance of the connecting lines and wires at about the same value. Since there are two circuits in parallel, the parallel equivalent resistance of wires, lines, and coils is approximately 0.6 ohm. We may thus conclude that the resistance of the spark is 2.5 ohms. Since the envelope of the transient follows a true exponential curve, this value will be the resistance of the spark rather than the average value of a gradually varying spark resistance.

With the knowledge of this parameter, an estimate of the intensity of the spark may be obtained. It is necessary only to calculate the current in the

circuit; this value squared times the spark resistance represents the power dissipated at that instant, which in turn leads to a value for the maximum possible radiation intensity.

The circuit of Figure 1 (Circuit Model I) is redrawn for convenience and is designated as Figure 3. We are interested in the varying current developed in the spark gap. Note that the charged capacitor has been replaced by an equivalent circuit consisting of a neutral capacitor in series with a constant voltage (V_o), the voltage which exists on the capacitor at the instant of gap breakdown. This voltage appears as a step function in the circuit when the gap breaks down.
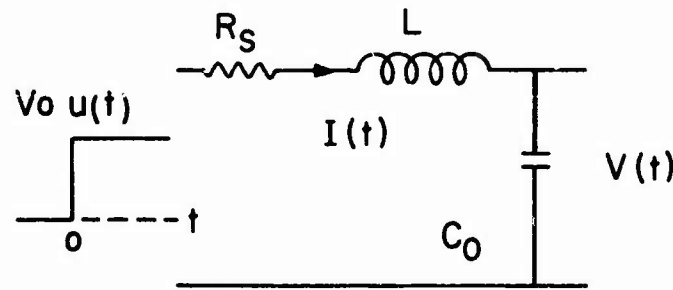
Figure 3. Simplified Representation of Spark Gap, Charging Circuit, and Lines

The response of this circuit to the step function $V_o u(t)$, where $u(t)$ is the unit step function, is obtained readily by transform algebra:

$$\frac{V_o}{s} = I(s) \left[R_s + sL + \frac{1}{sC_o} \right] \qquad (10)$$

whence, after some manipulation

$$I(s) = \frac{V_o}{L} \left[1 / \left\{ (s + \frac{R_s}{2L})^2 + (\frac{1}{LC_o} - \frac{R_s^2}{4L^2}) \right\} \right] \qquad (11)$$

and, taking the inverse transformation,

$$I(t) = \frac{V_o}{L} \left[\frac{1}{LC_o} - \frac{R_s^2}{4L^2} \right]^{-1/2} e^{-\frac{R_s}{2L} t} \sin \left[\frac{1}{LC_o} - \frac{R_s^2}{4L^2} \right]^{1/2} t \qquad (12)$$

We can calculate the current-time waveform by substituting the numerical values obtained in the measurements: 5300 volts, 0.0183 microfarads, 33.5 microhenrys, and 3.0 ohms respectively for V_o, C, L, and R. The result is:

$$I(t) = 140 e^{-0.46 \times 10^5 t} \sin (1.3 \times 10^6 t) \text{ amperes} \qquad (13)$$

10

This equation represents the current in the spark gap. The current in one of the coils is half this value since there is roughly an even division between the two branches. Figure 4 shows a fairly accurate plot of expression (13), the current transient in the spark gap. (The theoretical frequency was used; this is a little higher than the measured frequency.) During the first lobe, the current rises to a peak value of 130 amperes. The spark gap power at this instant is 50.7 kilcwatts.
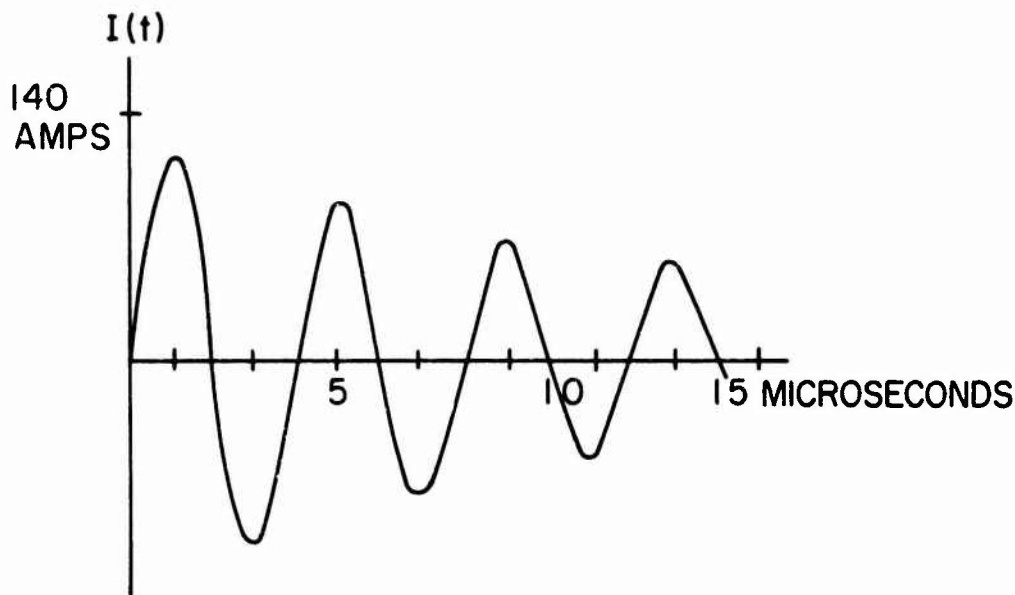
Figure 4. Current Transient in Spark Gap

Note again that the current transient in either of the solenoids is given by this same figure; it is a matter only of multiplying the ordinate by 0.5. Thus, the current in a solenoid builds up to 65 amperes in about 1.3 microseconds. A change in trolley position from the balanced position will cause an unequal distribution in the current. This, in turn, will result in slightly different rise times in the two branches.

2. Observations Regarding Circuit Model I

Since the minima appear as the trolley position is varied, it is only natural to suspect that the small variation in frequency might be associated with the phenomenon. The first order solution predicted almost exactly the low frequency damped oscillatory wave train that is initiated when the spark gap breaks down. One thinks of possible resonance effects or of transitions connected with the atoms or nuclei in question. Unfortunately, this would require identical frequencies and identical rates of change of frequency with trolley displacement; this sort of requirement is nct consistent with the experimental observations of Allison and Murphy [4], and Allison [6]. In other words, the change in inductance (and therefore frequency) per Allison unit on one apparatus may be quite different

from the change in inductance per Allison unit on another apparatus. Further, the minima positions are, within reasonable limits, insensitive to the frequency. Neither is $\Delta f/f$ per Allison unit a constant from apparatus to apparatus. At this point in the analysis, there is no obvious factor that suffers a constant variation per Allison unit on each different apparatus except the time differential in propagation of an electromagnetic wave.

A review of the literature shows that the first order solution represents nearly all the quantitative electric circuit knowledge possessed by the early investigators of the Allison effect. Evidently, only Snoddy [19] suspected that there were higher frequency components involved. In considering the work of the earlier experimentalists, one must be careful to remember that accurate oscillographic equipment, capable of response to frequencies above a fraction of a megahertz, was not available in those days.

C. CIRCUIT MODEL II

1. Theoretical Considerations

The fine grain electrical complexity of the apparatus is such that it will not be feasible to attempt a theoretical solution of a circuit model that contains every electrical detail. What needs to be done is to employ an intuitive approach which catalogs the features into first order, second order, third order, etc., magnitudes of importance. Engineering judgement then tells us which of the fine grain details may be ignored so that we may have a manageable problem.

Circuit Model I is an example of a first order problem which takes into account only the gross features. This circuit predicts the existence of an oscillatory transient with a fundamental frequency somewhere in the nominal range of 0.2 to 1.5 megahertz. Actually the frequency could be somewhat lower or higher for unusually large or unusually small charging capacitors.

It is necessary to go beyond this oversimplified model because the frequency range above may not be involved in the reported effect which is marginal enough to defy clear objective confirmation by an arbitrary observer. Accordingly, the effect may be caused by weaker frequency components stemming from second or even third order details in the electric circuit.

The purpose of Circuit Model II is to investigate the effect of some of the finer details. Let us examine the typical apparatus to see which additional elements can be added without complicating the problem excessively. A second order solution is desired at this point.

To gain an appreciation of the complexity of the total problem, of several points, consider this single point alone: The typical circuit has overall dimensions such that it would be an effective radiator at frequencies of the order of 50 megahertz and higher. Radiation impedances would need to be included at appropriate

points in order to completely represent the apparatus by an equivalent circuit. It is well known that the theoretical determination of these impedances is virtually impossible for any but the simplest geometrical shapes. Our physical circuit, viewed as an antenna, is for this reason alone beyond exact theoretical representation. Circuit Model II will neglect the radiation impedance.

Another feature of the physical circuit is the combination of distributed and lumped reactances. Of course, at extremely high frequencies, several hundred megahertz, all the physical circuit should be viewed as a distributed circuit if exact representation is necessary; but even in our case, the circuit is so large physically that at frequencies where the coils and capacitors behave essentially as lumped elements, the long lead wires and the parallel line delay elements still must be thought of as distributed elements.

The parallel wire lines should be represented as transmission lines in Circuit Model II; however, the lead wires connecting the various elements of the circuit have a distributed capacitance that might well be neglected because of the large line-to-ground spacing in the apparatus. This will be done, but the distributed inductance of these leads is appreciable and must be considered; in a second order calculation the distributed inductance of the lead wires will be given a lumped inductance representation.

There is, in addition, a skin effect problem. Measurements of the coils have disclosed a wide range in the skin effect resistance. This will hold both for the lead wires and the parallel lines. Unfortunately, the a. c. resistance is a nonlinear function of the frequency; this again makes for an extremely formidable theoretical project were an exact solution over a wide frequency range required. Accordingly, a method will be employed to linearize the problem: Analyses will be performed for a number of frequency intervals, in each of which the a. c. resistance will be assumed constant at some nominal value appropriate to that range.

The capacitor charging circuit of a typical apparatus has a relatively high output impedance to even the low radio frequencies. It is reasonable to neglect this portion of the apparatus in Circuit Model II. We will start at the moment the gap breaks down and study the behavior of the circuit for a short time thereafter, a time much shorter than the period of the 60 Hz power frequency used to drive the rectifier and charging circuit.

Numerous small distributed reactances and resistances will be overlooked in Circuit Model II; engineering judgement applies here.

The spark gap will be thought of as a switch plus a linear resistance. The d. c. arc has, of course, a highly nonlinear characteristic, exhibiting a negative slope and even hysteresis; however, as shown by Cobine [20], the high

13

frequency spark has a characteristic which approaches that of a linear bilateral resistance because the products of ionization do not have time to disperse during the short periods associated with the high frequency.

Finally, it is realized that there are two parallel branches connected to the capacitor and that in the end, we will be interested in relative time delay along with the effects of cross coupling through mutual elements; however, our first interest in Circuit Model II is to discover something about the important frequencies and the rise times of voltage and current. We will, accordingly, study only one of the two parallel branches at this time. The elaboration of Circuit Model II will cover the relative behavior of the two parallel branches. Figure 5 illustrates the more complex Circuit Model II.
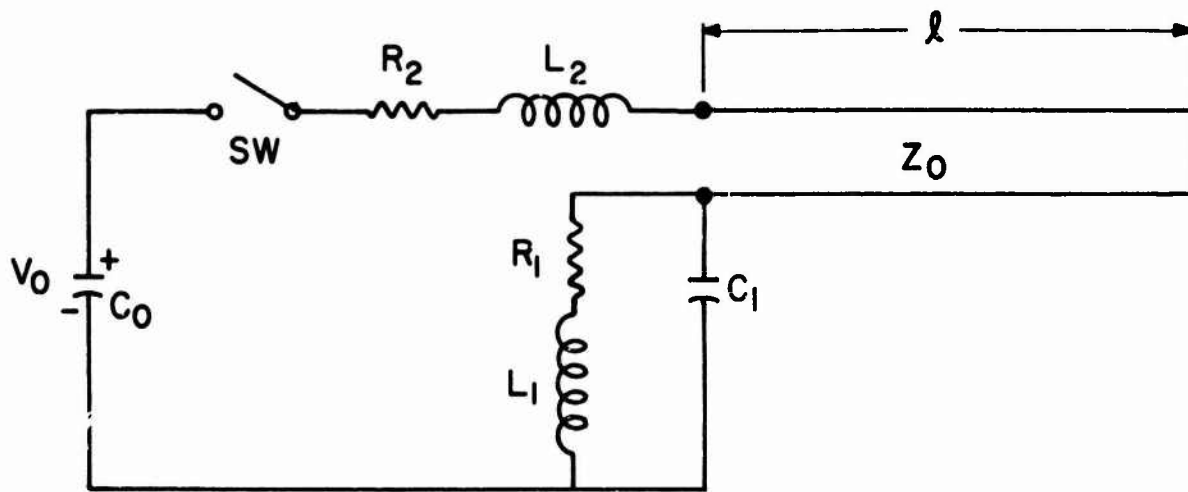
Figure 5. Circuit Model II

2. Identification of Circuit

Capacitor C_o is the charged capacitor which supplies the energy for the electrical pulse. Voltage V_o is the value attained at the moment the gap breaks down. Components L_1, R_1, and C_1 represent the sample coil inductance, the a. c. resistance, and the distributed capacitance (including that of the sample coil). The adjustable parallel wire delay line is represented by characteristic impedance Z_o and length ℓ. Inductance L_2 collects the distributed series inductance of various lead wires. Resistance R_2 represents the linear high-frequency spark resistance and the a. c. resistance of the lead wires. The spark gap itself is represented by the ideal switch SW and part of the R_2 resistance.

Let us now assign some specific values to these parameters in order to get order of magnitude results. The characteristic impedance of a lossless parallel wire line is given by the well known formula,

$$Z_o = 120 \ln (d/r) \text{ ohms} \tag{14}$$

where d is the center-to-center spacing and r is the radius of the conductor.

Cooper's [17] d/r ratio is approximately 400; for this ratio, $Z_o = 720$ ohms. Let length ℓ be taken as 10 meters. Inductance L_2 will average approximately 10 microhenrys. Resistance R_2 is difficult to estimate with precision; however, a rough but realistic value can be arrived at in the following way: Experimental observations indicate that the damped train of oscillations contains about 15 complete cycles (Figure 2). This, we know from electrical circuit theory, describes a circuit with a Q of approximately 15. Assuming a total line-plus-coil inductance of 50 microhenrys and a frequency of 1 megahertz, we find the inductive reactance of the first order circuit to be about 300 ohms. Since

$$Q = \omega L/R, \tag{15}$$

we find that R_2 is in the neighborhood of 20 ohms. We will use this value tentatively.

Capacitor C_o has a wide range in typical experiments, however, we will use 1000 picofarads.

There remains the coil itself; for this we can utilize the precise measurements performed on the helix used in our own experiments. These are contained in Section II, B.

a) At 1 megahertz, L_1 is 37 microhenrys, R_1 is 1.3 ohm, and C_1 (the distributed capacitance) is 8 picofarads.

b) The parameter which varies most with frequency is R_1 which ranges from 0.63 ohm at 0.2 megahertz to 5 ohms at 4 megahertz.

c) The Q of the helix is nominally 175 around 1 megahertz and reaches a maximum of 240 around 3 megahertz.

d) The self-resonant frequency of the helix is approximately 9.2 megahertz.

3. Identification of Critical Frequencies

In order to identify the critical frequencies of the circuit, the question we must now ask is, "What happens 1, 10, 100, and so on, nanoseconds after the switch is closed?" The important point here is that time implies frequency. If we are interested in the circuit's behavior during the first and tenth nanosecond, then we must consider frequencies of the order of, respectively, 1000, and 100 megahertz. The gross characteristics during the first 10 nanoseconds must include frequencies of the order of 100 megahertz, etc.

It will be assumed that the gap will break down in approximately 1 nanosecond. The circuit behavior for a short time (nanoseconds) thereafter may be

determined with reasonable assurance by assuming that a step function is applied to the modified circuit shown in Figure 6. The justification for this approximation is as follows: Capacitor C_o will not discharge by a large fraction during the first few nanoseconds after the breakdown of the gap. (This assertion must withstand the test of self-consistency at the end of the analysis.) For the high frequencies under consideration, the transmission line may be replaced by pure resistance Z_o. The wave front which is transmitted down the line at the application of the voltage step will be reflected at the short circuit which terminates the line and will reappear at the terminals, but this will take time $2\ell/c$ (where c is the velocity of light). The behavior we are studying takes place before the wave front returns. The reflection will be taken up subsequently. Finally, since the frequencies we deal with here are so high that the inductive branch of the helix equivalent circuit has an admittance that is negligible compared with that of the distributed capacitance C_1, it will be assumed that only the capacitance is significant.
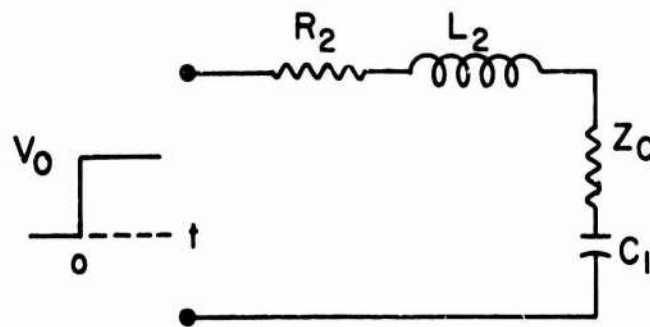
Figure 6. High Frequency Approximation of Circuit Model II

For the values assumed, the reflection time $2\ell/c$ is 66 nanoseconds and the period of the series $L_2 C_1$ resonance frequency is roughly 56 nanoseconds. In speaking of frequencies above 30 megahertz, the second order analysis based on this approximation holds true for at least 25 to 30 nanoseconds.

The most important result to be gained from this approximation of Circuit Model II is the time-dependent voltage that appears across capacitor C_1 during the first 10 or so nanoseconds because this, of course, is the voltage which is applied to the physical helix around the fluid sample. If the Allison effect is related to an electro-optic effect, such as the Kerr effect, this voltage is responsible for the electric field which induces the conditions necessary for the effect.

We delay the solution of this circuit until the purpose of this particular section (identification of critical frequencies) is completed.

There is a critical point around 60 nanoseconds when the reflected wave begins to appear at the terminals of the transmission line. This behavior should be investigated in conjunction with the 56 nanosecond period of the series resonance due to L_2 and C_1.

As time progresses beyond this point, we must consider the behavior of the complete circuit of Figure 4. This would be a relatively simple transient problem were it not for the multiple reflections taking place along the transmission line. These must be taken into account as well as the obvious self-resonance of the helix. The latter will introduce a critical frequency around 10 megahertz.

4. Solution of the High Frequency Approximation

For a solution to the high frequency approximation of Circuit Model II, we can proceed as follows; the circuit of Figure 7 is redrawn and relabeled for convenience. Since we are interested in the time-varying voltage developed across C_1 (and perhaps in the current through it), we set $R = (R_2 + Z_o)$, $L = L_2$, and $C = C_1 C_o / (C_1 + C_o) \simeq C_1$. Note however that, while it was not mentioned previously, the charging capacitor C_o is so large compared to C_1 that we may neglect its contribution to the series equivalent capacitance.
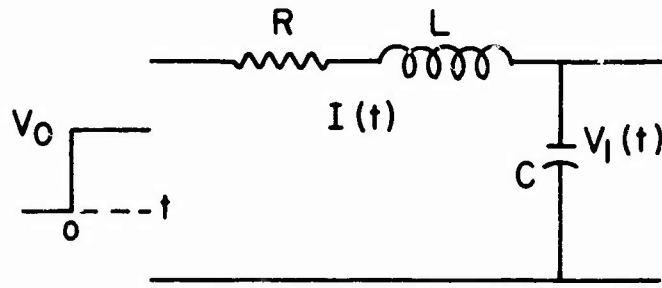
Figure 7. Simplified Representation

The response of this circuit to the step function $V_o u(t)$, where $u(t)$ is the unit step function, is obtained readily by transform albegra. Referring to expression (12) and substitution of the proper subscripts for circuit components, the actual time varying voltage $V_1(t)$ is obtained by starting with

$$V_1(s) = I(s)/(sC) \tag{16}$$

The following substitutions will simplify the expressions:

$$a = R/2L, \text{ and} \tag{17a}$$

$$\omega = \left[1/LC - R^2/4L^2 \right]^{1/2} \tag{17b}$$

Then

$$V_1(s) = \frac{V_o}{LC} \frac{1}{s\left[(s+a)^2 + \omega^2\right]} \tag{18}$$

17

and, taking the inverse transformation,

$$V_1(t) = \frac{V_o}{LC} \left[A e^{-at} \sin(\omega t + \alpha) + LC \right] \tag{19a}$$

where

$$A e^{j\alpha} = \frac{1}{\omega(-a + j\omega)} \tag{19b}$$

Expression (19) looks promising because after some complicated behavior, which may be oscillatory, the value settles down to V_o, as it should if a true step function were applied. In addition, the initial condition requires that $V_1(t)$ be zero when $t = 0$. Substitution of (19b) into (19a) when $t = 0$ does indeed yield this expected result.

The next step is to substitute values for our specific problem because the solution changes radically, depending on whether ω is real, zero, or imaginary. The voltage rise may be heavily damped or there may be ringing or perhaps an overshoot.

If our numerical values are substituted, we find

R = 730 ohms,

L = 10 microhenrys,

C = 8 picofarads,

so that

$a = 3.7 \times 10^7 \sec^{-1}$, and

$\omega = 1.1 \times 10^8$ radians per second,

the results being held to two significant figures.

With a little manipulation, expression (19) becomes

$$V_1(t) = V_o \left[1 + e^{-at} \sqrt{\frac{a^2}{\omega^2} + 1} \; \sin\left(\omega t + \tan^{-1} \frac{-\omega}{-a}\right) \right] \tag{20}$$

and substituting,

$$V_1(t) = V_o \left[1 + e^{-3.7 \times 10^7 t} \sin(1.1 \times 10^8 t - 1.9) \right] \tag{21}$$

A quick numerical check shows that this describes a damped oscillatory transient which settles down to value V_o. There is a sharp rise with a 30% overshoot which peaks at approximately 32 nanoseconds. The 10% to 90% risetime may be as short as 15 nanoseconds. The transient is depicted approximately to scale in Figure 8. An accurate point-by-point plot can, of course, be obtained by substitution in expression (21).
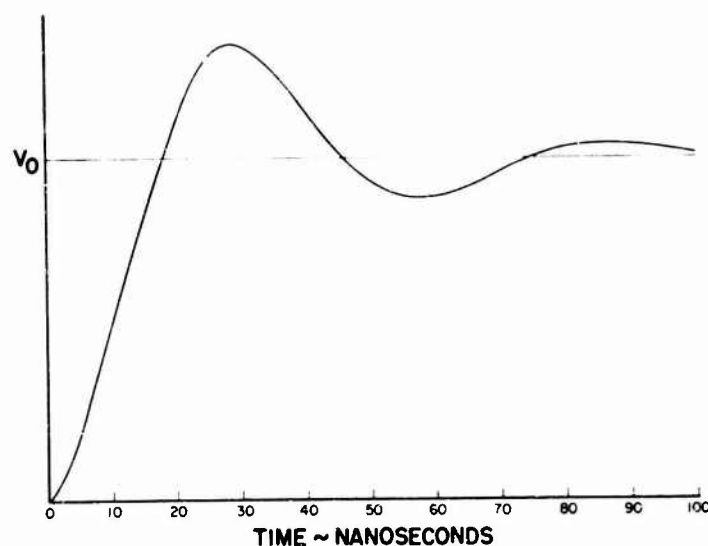
Figure 8. Approximate Appearance of $V_1(t)$

It must be remembered that this result is valid only for the first 66 nanoseconds. During this time the voltage wave given by $Z_0 I(t)$ has been contained by the transmission line. It has traveled down the line, been reflected with change in sign at the shorted termination, and now at 66 nanoseconds reappears at the input terminals of the line. By this time the voltage $Z_0 I(t)$ at the input terminals of the line has damped out to a small value so that the leading edge of the reflected wave appears roughly as a new step excitation of the circuit of Figure 6, and the whole calculation process must be repeated, but with a much more complex input signal. The reflection at 66 nanoseconds is just the first of a series of multiple reflections, although subsequent reflections would have ever decreasing amplitudes. It is likely that we need be concerned only with the first reflection which effects a significant increase in the amplitude of the second peak shown in Figure 7.

Experimental observations shown in Figures 9 and 10 substantiate this approximation. The transient voltage waveforms of each solenoid were superimposed for comparison. These waveforms exhibit an initial 30 nanosecond rise time characteristic, and then develop a peak amplitude 150 per cent higher at 90 nanoseconds elapsed time after the initial impulse.

The effect of successive reflections on the waveform can be noted in Figure 10 where the amplitude was observed to decrease in time after the initial response.

If numbers are substituted in the expression (12) for the current, there results

$$I(t) = 0.94 \times 10^{-3} \, V_0 e^{-3.7 \times 10^7 t} \sin 1.1 \times 10^8 t \tag{22}$$

Examination of the formula shows that the current rises rapidly and reaches a peak amplitude of approximately $0.58 \times 10^{-3} V_0$ amperes at about 14 nanoseconds. Thus, if the breakdown potential of the spark gap were 5000 volts, the peak current would be 2.9 amperes at 14 nanoseconds. Note that this current is the displacement current in the distributed (turn-to-turn) capacitance of the helix.

19
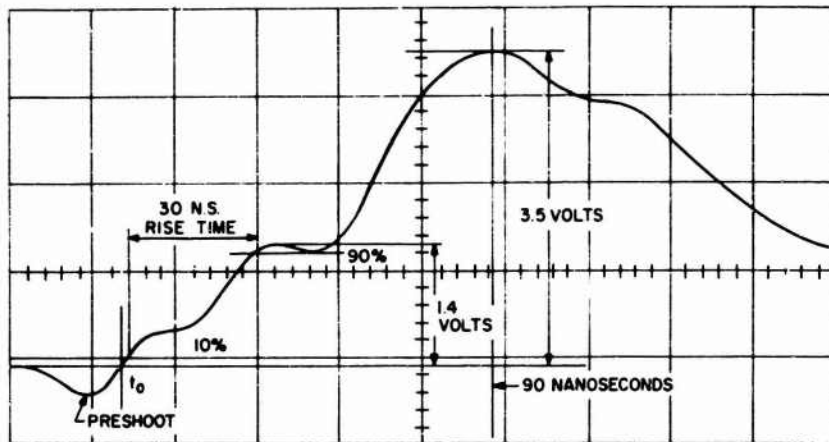
Figure 9. Pulse Generator Input

Pulse Generator Input: 5 volts at 10 nanoseconds rise time
pulse duration 80 microseconds
100 pulses per second

Vertical Sensitivity: 1 volt/cm

Horizontal Sensitivity: 20 nanoseconds/cm
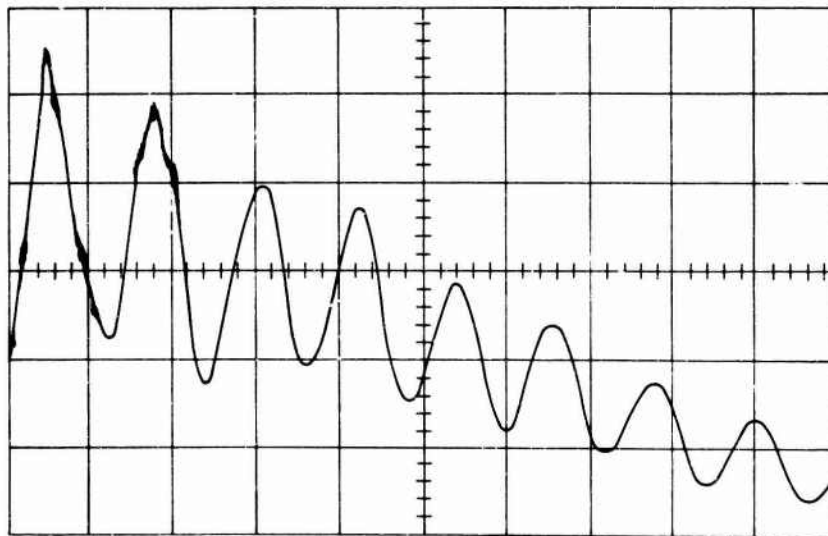
Figure 10. Pulse Generator Input

Pulse Generator Input: 5 volts at 10 nanoseconds risetime
pulse duration 80 microseconds
100 pulses per second

Vertical Sensitivity: 1 volt/cm

Horizontal Sensitivity: 0.2 microseconds/cm

20

It is a cylindrical current-sheath flowing in the axial direction; however, there is a pitch to the winding on the helix so that the current sheath may execute a screw-like motion which would give rise to some axial magnetic field component. Since the distributed capacitance is between the turns of the coil, one would expect the displacement current to flow in a direction that is <u>normal</u> to the direction of the wire. This normal direction is tilted by a small angle (depending on the pitch) from the axial direction of the helix. Thus, the helix could very well form an equivalent one turn coil (or more, depending on the pitch) for the displacement current, and this would furnish a small axial magnetic field which would cause Faraday rotation; further, the fast rise time computed above would apply.

5. A General Solution for Circuit Model II

A general solution for Circuit Model II can now be formulated by first replacing the short circuited transmission line by its single frequency input impedance.

$$Z_{in} = jZ_o \tan(\omega \ell/c) \tag{23}$$

Then, the charged capacitor and the switch may be replaced by a series equivalent consisting of an uncharged capacitor in series with a step function with amplitude V_o. The step function may be handled on a single frequency basis by utilizing its Fourier transform. Next, an expression can be formulated which gives the current in the inductance L_1 (this is the current in the physical sample coil) for any given frequency. In principle, one may then compute the envelope of the frequency spectrum of the current pulse, and from this (also in principle) construct the actual current pulse. In setting up a numerical solution, it will be necessary to recall that the resistances R_1 and R_2 are frequency dependent; however, as was observed previously, the values may be held constant over incremental frequency ranges. The voltage across the inductor may be calculated by multiplying the inductor current by the impedance of the inductor RL branch. Figure 11 illustrates the details discussed above.
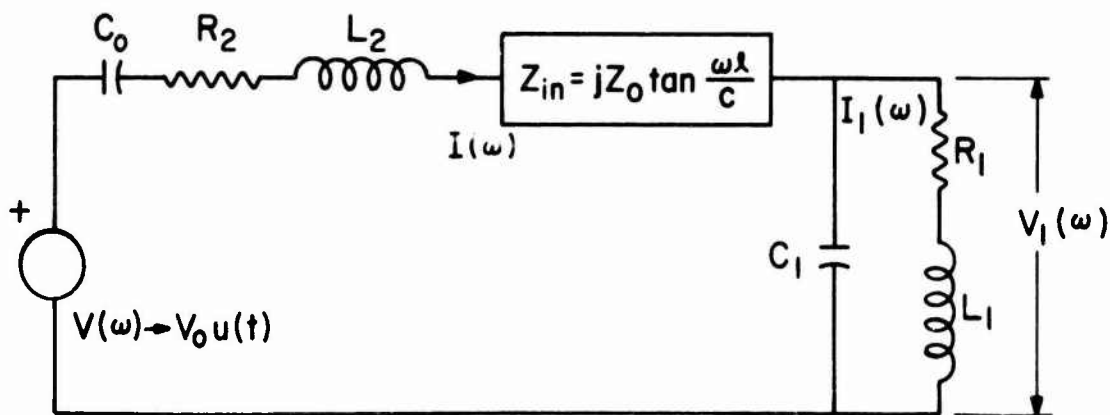
Figure 11. Circuit Model II Rearranged for Analysis

21

The expression for the single frequency impedance as seen by the equivalent voltage source is as follows:

$$Z(\omega) = R_2 j\omega L_2 + jZ_o \tan\frac{\omega\ell}{c} + \frac{(R_1+j\omega L_1)}{j\omega C_1(R_1+j\omega L_1 + \frac{1}{j\omega C_1})} + \frac{1}{j\omega C_o} \tag{24}$$

The current $I(\omega)$ is found by calculating the quotient,

$$I(\omega) = V(\omega)/Z(\omega) \tag{25}$$

Current $I_1(\omega)$ is given by

$$I_1(\omega) = \frac{1}{j\omega C_1 (R_1+j\omega L_1 + 1/j\omega C_1)} \; I(\omega) \tag{26}$$

and voltage $V_1(\omega)$ is given by

$$V_1(\omega) = (R_1+j\omega L_1) \; I_1(\omega) \tag{27}$$

Voltage $V(\omega)$ must be obtained from the Fourier spectrum of $V_o u(t)$, where $u(t)$ is the unit step function. Fourier transform methods show that this frequency spectrum has a hyperbolic character, thus

$$V(\omega) = \frac{V_o}{j\omega} \tag{28}$$

It remains only to substitute numbers for the parameters and perform the laborious computations.

One of the most interesting elements of the circuit is the terminal impedance of the transmission line. Note that there will be many frequencies where Z_{in} will be an open circuit resulting in zeros for I_1 and V_1. Again, because of the periodic nature of Z_{in}, it also will behave as a short-circuit for many other frequencies.

A more sophisticated approach to the solution would entail the use of Laplace transform methods; whether or not it is easier remains to be seen. The immediate difficulty is the treatment of the transmission line input impedance. This can be handled as follows:

$$Z_{in}(\omega) = jZ_o \tan(\frac{\ell}{c}\omega) = Z_o \tanh(\frac{\ell}{c}j\omega) \tag{29}$$

Taking the transform

$$Z_{in}(s) = Z_o \tanh(\frac{\ell}{c}s) \; \text{or} \; Z_o \frac{e^{\frac{\ell}{c}s} - e^{\frac{\ell}{c}s}}{e^{\frac{\ell}{c}s} + e^{\frac{\ell}{c}s}} \tag{30}$$

the transformed impedance of expression (24) becomes

$$Z(s) = R_2 + sL_2 + Z_o \tanh \frac{\ell}{c} s + \frac{R_1 + sL_1}{(1 + sC_1 R_1 + s^2 L_1 C_1)} + \frac{1}{sC_o} \qquad (31)$$

The transform of the source voltage is simply

$$V(s) = \frac{V_o}{s} \qquad (32)$$

The transform of the current from the source is

$$I(s) = \frac{V_o}{s Z(s)} \qquad (33)$$

The transform of the solenoid current is

$$I_1(s) = \frac{1}{(1 + sC_1 R_1 + s^2 L_1 C_1)} I(s) \qquad (34)$$

or

$$I_1(s) = \frac{V_o}{s(1 + sC_1 R_1 + s^2 L_1 C_1) Z(s)} \qquad (35)$$

And, finally, the solenoid voltage is

$$V_1(s) = (R_1 + sL_1) I_1(s) \qquad (36)$$

In all these expressions, remember that V_o and Z_o are simple real constants. The small letter c is the speed of light.

To solve the problem, "all" that needs to be done is to take the inverse transformation of expressions (35) and (36) and one will have the explicit time varying current and voltage of the solenoid. We will not attempt to perform this operation at the present stage of the analysis. It is already clear from the previous work that the result will be a damped oscillatory transient with considerable fine structure on the first cycle or cycles. The frequency of the long transient is given by Circuit Model I. The immediate fine structure is given by the high frequency approximation of Circuit Model II. All this information in addition to information concerning the remaining fine structure is contained in the general solutions, expressions (35) and (36).

D. CIRCUIT MODEL III

1. Theoretical Considerations

The experimental observations and measurements indicate that the circuit detail described in Section I, Part C is sufficient to predict the observations;

23

accordingly, we may extend these details slightly to take into account the presence of two parallel circuits and the mutual inductance between the sample and reference coils, thus obtaining Circuit Model III which should contain the essential parameters that are active in the Allison effect apparatus.

Figure 12 displays the equivalent circuit. Capacitor C_O is the charging capacitor; its initial voltage (at breakdown of the gap) is represented by the step function generator; this is conventional and correct. The arrow means that the time domain representation of $V(\omega)$ is the step function $V_O u(t)$. Function $u(t)$ is the conventional symbol for the unit step function. Voltage V_O is the numerical value of the gap breakdown voltage. Resistance R_O is mainly the arc resistance; we will include therein the small a.c. resistance of the lead wires connecting the capacitor and spark gap to the trolley lines and the common line. Inductance L_O is the inductance of these same lead wires.

In this equivalent circuit the spark gap is considered to be a passive switch; this is in keeping with the experimental observations. Also,

$$Z_1 = jZ_O \tan \frac{\omega \ell_1}{c}, \text{ and } Z_2 = jZ_O \tan \frac{\omega \ell_2}{c} \tag{37}$$

in this circuit model.
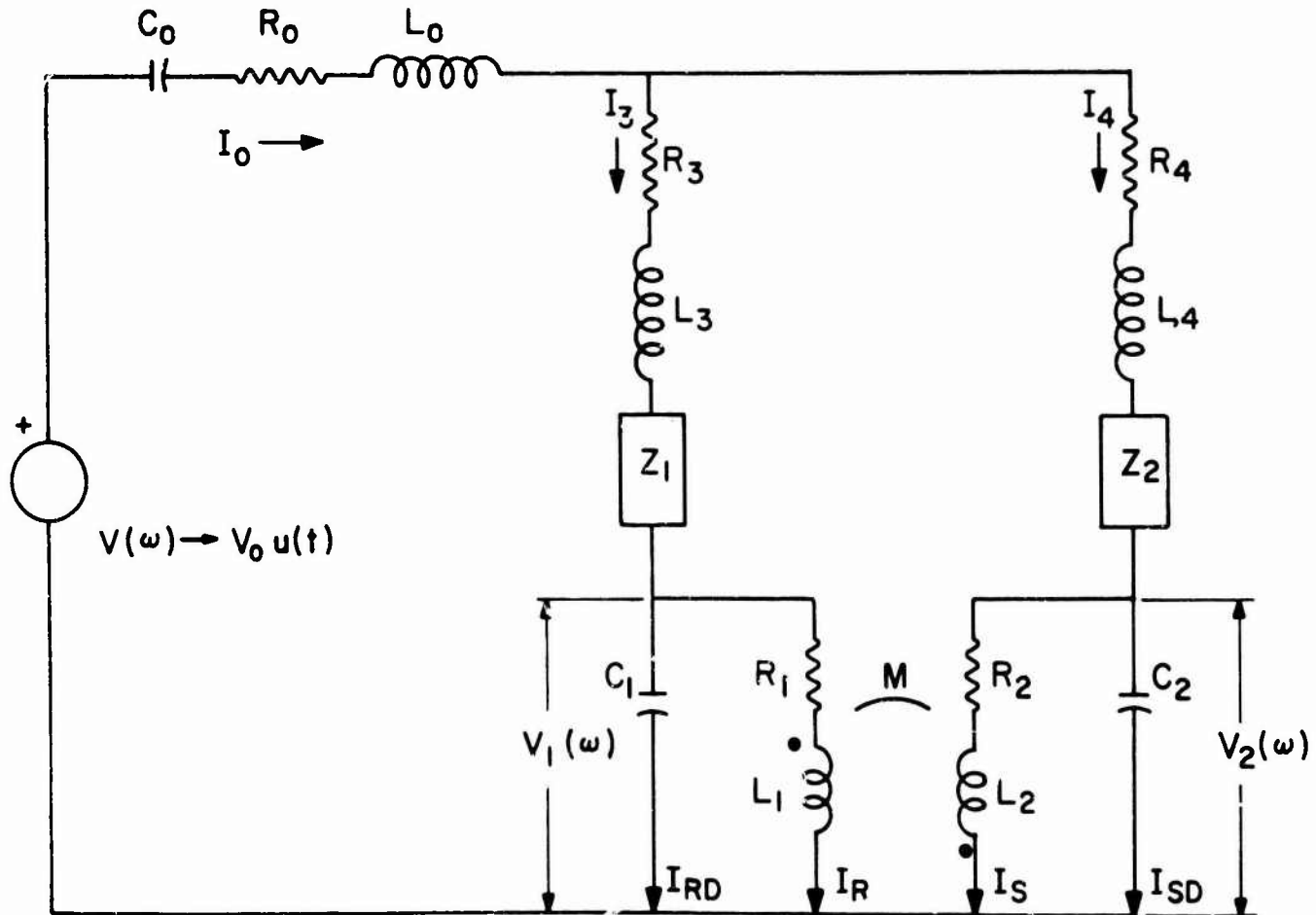
Figure 12. Circuit Model III

24

There are two parallel paths; one through the reference coil circuit and another through the sample coil circuit. Resistance R_3 and Inductance L_3 belong to the lead wires from the trolley lines to the reference solenoid (and to any other lead wires which may be in this branch of the circuit). Impedance Z_1 is the input impedance of the parallel wire delay line in the reference circuit. Its value is a function of the characteristic impedance Z_o of the line, the angular frequency ω, the length of the line ℓ_1, and the speed of light c.

The reference solenoid is represented by the group C_1, R_1, and L_1 which are respectively the distributed capacitance, the a.c. resistance, and the inductance of the coil. There is a mutual inductance M between the reference solenoid and the sample solenoid.

The parameters in the parallel sample branch represent circuit elements corresponding to those in the reference branch.

The dots at the ends of the inductances are the conventional dotted polarity for the mutual inductance. This is not arbitrary for an Allison effect apparatus, since it is the intention that the Faraday rotation in one solenoid be counteracted by the Faraday rotation in the other.

The various branch currents are indicated on the equivalent circuit as well as the coil voltages. The two distinct coil currents, the inductive current, and the displacement current, were discussed in Part C.

Now that the equivalent circuit has been established, we are faced with its solution. What are the desired currents and voltages? The answer to this question depends upon the frequency range of importance; unfortunately, we are not yet in a position to specify such frequency values. Thus, it is logical to solve for the voltages V_1 and V_2 and currents I_R, I_S, I_{RD}, I_{SD}, and I_o.

A little thought will show that there is good motivation for separating the basic solution into a low frequency solution and the solution of a high frequency problem. At low frequencies, approximately the order of 1 MHz for our apparatus, the distributed capacitance of the coil is not very important. For example, current I_{RD} is negligible compared to current I_R. The entire circuit can be simplified by an approach in which the current through the distributed capacitance is neglected. This yields a close low frequency approximation (see Figure 13). Naturally, the mutual inductance is important at these frequencies because the major current flows through the inductances. The parallel wire transmission lines may accurately be replaced by their inductances at the low frequencies.

At high frequencies, of the order of tens of megahertz, the distributed capacitance becomes the dominant element of the solenoid. The flow of current through the inductance becomes negligible in comparison with that shunted through the distributed capacitance, and the mutual inductance becomes ineffective as a

circuit element. During the first moments of the impulse, the parallel wire transmission lines may be replaced by resistances equal to the characteristic resistances of the respective lines (these ordinarily are the same for an Allison effect apparatus), and the approximation will hold good until the reflections return from the shorted terminations (trolleys). This approximate model is illustrated in Figure 14. The charging capacitance is so large that its reactance is completely negligible for the high frequencies. The small lead wire resistances in the parallel paths will be overwhelmed by the extremely large inductive reactances of the lead wires; in any case, they could be considered as being part of R_R and R_S. The inductances of the lead wires must be retained; there is a small distributed capacitance, but it is not nearly so effective as that of the solenoid where the turns are in close proximity.
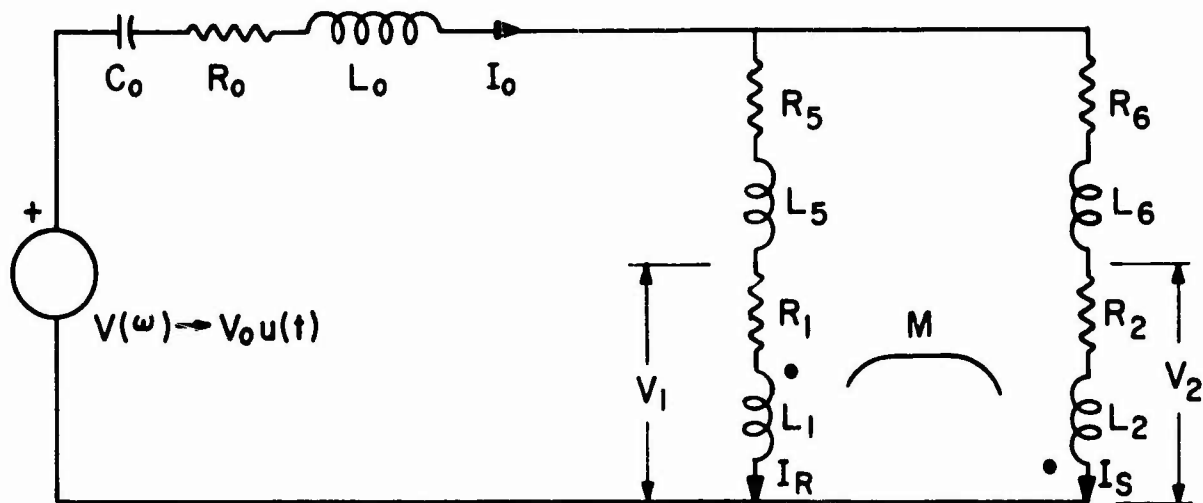
Figure 13.   Low Frequency Approximation of Circuit Model III
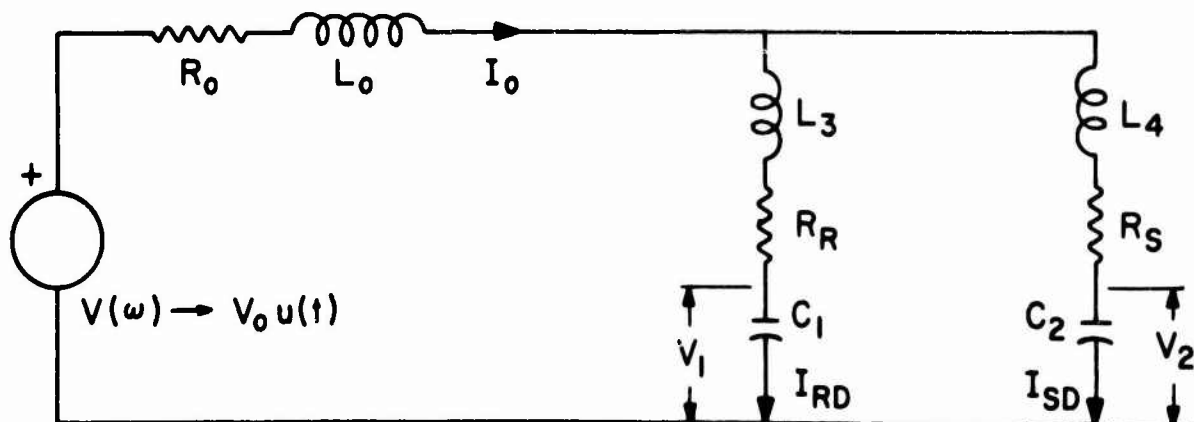
Figure 14.   High Frequency Approximation of Circuit Model III

There is a serious flaw in the high frequency approximation shown in Figure 14. One must remember that the Allison effect is produced by an adjustment of the trolley position; in our approximation, the adjustment is of no importance during the first moments of the impulse because the wave

front has not had time to discover that the transmission lines are terminated by short circuits. Even when the wave fronts make this discovery, it takes an additional period of time to "report" the fact to the circuit. That is, the resistance representation is good until the impulse has had time to travel down and back again. Specifically, the time is equal to $2\ell_1/c$ for line 1, and $2\ell_2/c$ for line 2. (The impulses may return at different times.)

This means that there is a delay built into the Allison effect <u>if it is caused by high frequency components of the RF spectrum.</u> Thus, in order that trolley position have any significance in the Allison effect, we are forced to the conclusion that a minimum time interval of at least $2\ell_2/c$ must elapse before the Allison effect can take place. The actual time limit, however, could exceed this because of the relative lengths of ℓ_1 and ℓ_2. In reality, this result is more general than it appears: it would be true also for the low frequency case; however, the limited resolution at low frequencies would make a delay of this order (6.7 nanoseconds per meter length of the parallel wire line) an insignificant factor.

The physical implications of this interesting aspect must be explored; there are four additional delay factors to be integrated into the overall picture: (1) the time required for light to travel from the spark gap to the average location of the first solenoid; (2) the time required for light to travel the center spacing of the solenoids; (3) the possibility of a delay between the initiation of the electrical impulse and the generation of light; (4) a possible delay attributed to the unknown cause of the Allison effect itself. However, before this can be done we must arrive at an acceptable high frequency approximation.

One obvious change is to retain the Z_1 and Z_2 representations for the transmission lines; these are correct for any frequency above a few hundred KHz. (The high frequency transmission line expressions make use of the fact that the inductive reactance per unit length is very much greater than the a.c. resistance per unit length).

A second change could be made in the high frequency approximation for Circuit Model III; this, however, would anticipate the nature of the mechanism responsible for the Allison effect. Suppose, for example, that there were some high frequency resonance absorption in the sample; the equivalent circuit would then include a high Q series RLC branch across capacitor C_2. Since any such additional features are conjecture at this point, they will be omitted until a more substantial basis for their inclusion is found.

Figure 15, then, shows a high frequency approximation of Circuit Model III that holds good beyond the first few nanoseconds and that would be responsive to variations in trolley position. The limit of validity would be the time required for the appearance of an appreciable current in the inductive branch of the solenoid equivalent circuit. The specific value for the time limitation is obtained by solving the low frequency approximation. Input impedances Z_1 and Z_2 are given

in explicit form in Figure 12. The a.c. resistances R_3 and R_4 (of the lead wires) are included so that the impedance of the reference branch or of the sample branch cannot go to zero, as it could otherwise under series resonance conditions.
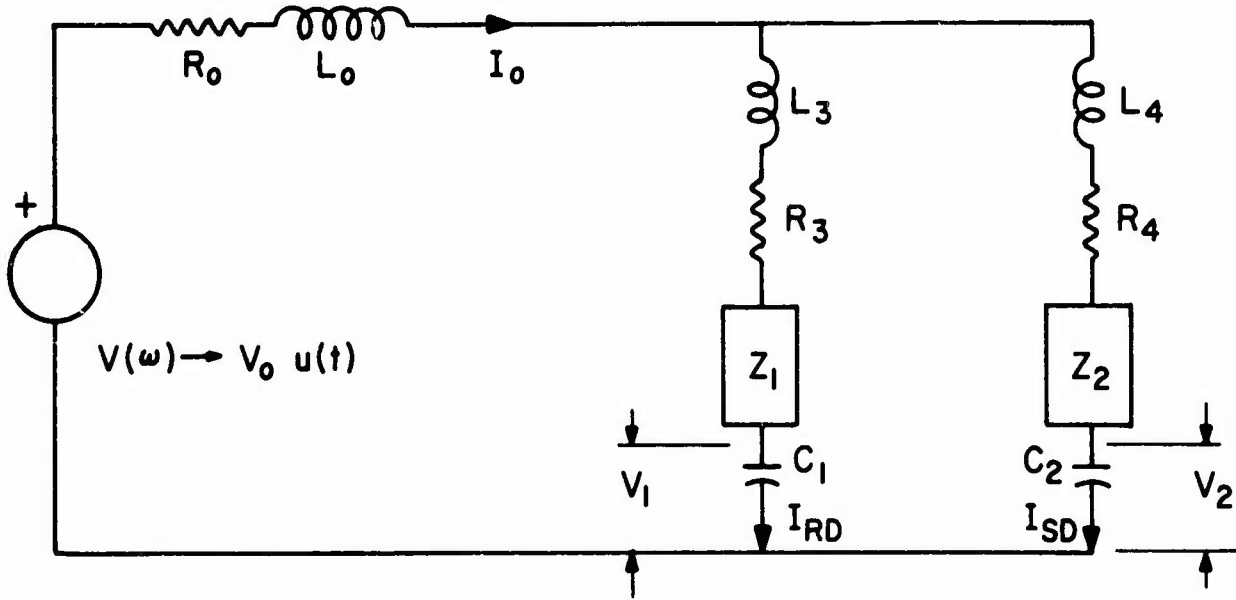
Figure 15. A Second High Frequency Approximation of Circuit Model III

The major reason for resorting to these approximations is that they are much easier to solve than the general circuit while still yielding identical answers for the extreme frequency values. We may use these "asymptotic" solutions to check the general solution.

2. Solution of Low Frequency Approximation

We may solve the low frequency approximation of Circuit Model III (see Figure 13) by applying Kirchhoff's voltage and current laws. Three simultaneous equations are written as follows (Note: The Laplace transformation method is being used):

$$\frac{V_o}{s} = (R_o + sL_o + \frac{1}{sC_o}) I_o + (R_1 + R_5 + sL_1 \cdot sL_5) I_R - sMI_s \tag{38}$$

$$\frac{V_o}{s} = (R_o + sL_o + \frac{1}{sC_o}) I_o - sMI_R + (R_2 + R_6 + sL_2 + sL_6) I_s \tag{39}$$

$$O = I_o - I_R - I_s \tag{40}$$

28

The following substitutions will allow ease of manipulation:

$$A = (R_o + sL_o + \frac{1}{sCo}) \tag{41}$$

$$B = (R_1 + R_5 + sL_1 + sL_5) \tag{42}$$

$$C = sM \tag{43}$$

$$D = (R_2 + R_6 + sL_2 + sL_6) \tag{44}$$

Substituting,

$$\frac{V_o}{s} = A I_o + B I_R - C I_s \tag{45}$$

$$\frac{V_o}{s} = A I_o - C I_R + D I_s \tag{46}$$

$$O = I_o - I_R - I_s \tag{47}$$

$$I_R = \frac{\begin{vmatrix} A & 1 & -C \\ A & 1 & D \\ 1 & 0 & -1 \end{vmatrix}}{\begin{vmatrix} A & B & -C \\ A & -C & D \\ 1 & -1 & -1 \end{vmatrix}} \frac{V_o}{s} = \frac{\Delta R}{\Delta} \frac{V_o}{s} \tag{48}$$

where

$$\Delta = A(B + 2C + D) + BD - C^2 , \text{ and} \tag{49}$$

$$\Delta_R = (D + C) \tag{50}$$

$$I_s = \frac{\begin{vmatrix} A & B & 1 \\ A & -C & 1 \\ 1 & -1 & 0 \end{vmatrix}}{\Delta} \frac{V_o}{s} = \frac{\Delta s}{\Delta} \frac{V_o}{s} \tag{51}$$

where

$$\Delta_s = (B + C) \tag{52}$$

Voltages V_1 and V_2 follow easily once the branch currents are known.

29

$$V_1 = I_R(R_1 + sL_1) - I_s(sM) \tag{53}$$

$$V_2 = -I_R(sM) + I_s(R_2 + sL_2) \tag{54}$$

Substituting,

$$E = (R_1 + sL_1) \tag{55}$$

$$F = (R_2 + sL_2) \tag{56}$$

$$V_1 = \frac{V_o}{s}\left[\frac{DE + CE - CB - C^2}{\Delta}\right] \tag{57}$$

$$V_2 = \frac{V_o}{s}\left[\frac{BF + CF - CD - C^2}{\Delta}\right] \tag{58}$$

In these expressions, the form (V_o/s) is the Laplace transformation of the step function $V_o u(t)$, where V_o is the voltage on the charging capacitor at the instant of spark gap breakdown.

For ease of inspection and analysis, it is convenient to summarize the results in one group.

Table II. Formulas for Circuit of Figure 13

$$I_R = \frac{V_o}{s}\left[\frac{D+C}{\Delta}\right] \tag{48}$$

$$I_s = \frac{V_o}{s}\left[\frac{B+C}{\Delta}\right] \tag{51}$$

$$V_1 = \frac{V_o}{s}\left[\frac{DE + CE - CB - C^2}{\Delta}\right] \tag{57}$$

$$V_2 = \frac{V_o}{s}\left[\frac{BF + CF - CD - C^2}{\Delta}\right] \tag{58}$$

$$I_o = \frac{V_o}{s}\left[\frac{B + 2C + D}{\Delta}\right] \tag{59}$$

$$\Delta = A(B + 2C + D) + BD - C^2 \tag{49}$$

$$A = R_o + sL_o + \frac{1}{sCo} \tag{41}$$

$$B = (R_1 + R_5 + sL_1 + sL_5) \tag{42}$$

30

$$C = sM \tag{43}$$

$$D = (R_2 + R_6 + sL_2 + sL_6) \tag{44}$$

$$E = (R_1 + sL_1) \tag{55}$$

$$F = (R_2 + sL_2) \tag{56}$$

In order to obtain the time varying solutions for the voltages and the currents, it will be necessary to make the proper substitutions, arrange the numerator and denominator in polynomial form, and then employ standard methods to perform the inverse Laplace transformation.

The whole problem could be simplified for a particular apparatus if the actual numerical values were substituted at this point so that the expressions could be condensed.

The results can be anticipated by inspecting the solutions. First, we have an exponentially damped oscillatory train of waves, provided the resistance is not so great as to cause critical damping or overdamping. The fundamental frequency will not be greatly different from that value calculated previously for the equivalent single branch. It will be slightly higher because the net inductance is somewhat reduced by the mutual inductance.

A change in relative phase angle between the two currents in the two solenoids, along with some relative amplitude variation, is accomplished by changing the trolley position. That is, inductance L_6 is changed; accordingly, factors D and Δ will vary.

When the trolleys both are fixed and the solenoids are moved relative to each other, the only variation is in M, the mutual inductance. This causes variation in factors C and Δ in the expressions. It should be noted that the mutual inductance M may be replaced by the expression $k\sqrt{L_1 L_2}$ where k is the coefficient of coupling between the coils. For our apparatus, the variation of M or k with distance may be determined from Figures 25 and 29 of Section II.

In an Allison effect experiment, it is possible to produce minima either by adjusting the trolley position or by displacing a solenoid the same distance[1]. If the low frequency model were applicable to the Allison effect, it should be possible to demonstrate the fact by showing that variations in L_6 and M (or k) produce the same effect. What needs to be done is to find expressions for L_6 and for M as functions of displacement. For a particular apparatus, L_6 must be separated into the inductance of the connecting leads and the inductance of the parallel wire lines. The latter inductance varies linearly with displacement,

31

i.e., so many Henrys per meter displacement. Thus, L_6 will have the form

$$L_6 = L_8 + dL_{10} \tag{60}$$

where L_8 is the lead inductance and d is the displacement. Factor L_{10} is the inductance per unit displacement of the trolley.

The mutual inductance must be expressed in the form containing the distance explicitly. One must construct a graph of M versus d from the referenced figures and then obtain an expression by curve fitting techniques. Distance d should be the center-to-center spacing of the solenoids.

The final step of the analysis will entail differentiation of all voltage and current expressions with respect to the displacement variable d and comparison of results.

3. Study of the First High Frequency Approximation

It seems that Figure 14 is not significant for the Allison effect experiment because it does not reflect the variation of trolley position, as discussed a few pages earlier; however, it gives a true picture of the rise time of the impulse in a particular solenoid. From this standpoint, it should be analyzed, for there may be some preconditioning or preorientation of the molecules in the substances contained in the cells. Let us at least examine the behavior of a purely reactive circuit.

The major effect of the neglected resistance will be damping of the impulses predicted for the purely reactive circuits; this is a standard technique, used to simplify the study of filter circuits. The circuit becomes that of Figure 16 and the analysis, via the Laplace transformation method, follows.
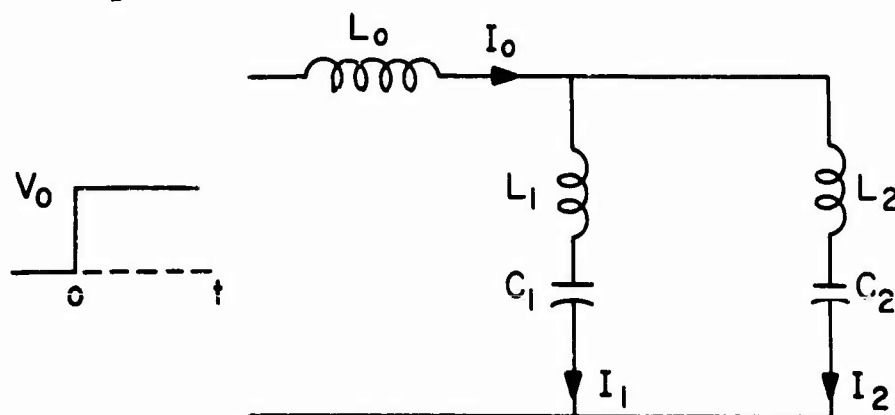
Figure 16. Pure Reactance Idealization of Figure 11

32

Some liberty has been taken with the notation to simplify the format of the expressions. Inductances L_1 and L_2 belong to the lead wires in the parallel branches. The solenoid inductance and mutual inductance are not effective at the high frequencies considered here, for reasons previously discussed. The solenoids are represented solely by capacitors C_1 and C_2, the distributed capacitances of the coils. Currents I_1 and I_2 are used in place of I_{RD} and I_{SD}. The voltages across capacitors C_1 and C_2 are identical to the solenoid voltages V_1 and V_2. Inductance L_o is that of the lead wires up to the nodes where the two parallel branches begin. A step function $V_o u(t)$ is applied. Its Laplace transformation is V_o/s where V_o is the spark gap breakdown voltage.

The first step is to determine the input impedance $Z_{in}(s)$ of the circuit. We calculate the admittances of the two parallel branches, adding them to get the total admittance of the parallel circuit. When the reciprocal of the total admittance is added to the impedance of L_o, the desired result, $Z_{in}(s)$, is obtained.

$$Z_1 = sL_1 + \frac{1}{sC_1} = \frac{s^2 L_1 C_1 + 1}{sC_1} \tag{61}$$

$$Y_1 = \frac{sC_1}{s^2 L_1 C_1 + 1} \tag{62}$$

$$Y_2 = \frac{sC_2}{s^2 L_2 C_2 + 1} \tag{63}$$

$$Y_{12} = Y_1 + Y_2 \tag{64}$$

$$Y_{12} = \frac{s^3 (L_2 C_2 C_1 + L_1 C_1 C_2) + 5(C_1 + C_2)}{(s^2 L_1 C_1 + 1)(s^2 L_2 C_2 + 1)} \tag{65}$$

$$Z_{in} = sL_o + \frac{1}{Y_{12}} \tag{66}$$

$$Z_{in} = \frac{s^4 (L_o L_2 C_2 C_1 + L_o L_1 C_1 C_2 + L_1 C_1 L_2 C_2) + s^2 (L_o C_1 + L_o C_2 + L_1 C_1 + L_2 C_2) + 1}{s^3 (L_2 C_2 C_1 + L_1 C_1 C_2) + s(C_1 + C_2)} \tag{67}$$

Simplifying by substitution,

$$Z_{in} = \frac{s^4 C + s^2 D + 1}{s^3 A + sB} \tag{68}$$

where

$$A = (L_2 C_2 C_1 + L_1 C_1 C_2) \tag{69}$$

$$B = (C_1 + C_2) \tag{70}$$

$$C = L_o L_2 C_2 C_1 + L_o L_1 C_1 C_2 + L_1 C_1 L_2 C_2) \tag{71}$$

$$D = (L_o C_1 + L_o C_2 + L_1 C_1 + L_2 C_2) \tag{72}$$

It is easiest to begin by solving for the current in the circuit containing the spark gap and the charging capacitor.

$$I_o(s) = \frac{V_o}{s} \left(\frac{1}{Z_{in}(s)} \right) = V_o \left[\frac{s^2 A + B}{s^4 C + s^2 D + 1} \right] \tag{73}$$

$$I_o = \frac{A}{C} V_o \left[\frac{s^2 + \frac{B}{A}}{s^4 + \frac{D}{C} s^2 + \frac{1}{C}} \right] \tag{74}$$

By further substitution,

$$I_o = \frac{A}{C} V_o \left[\frac{s^2 + a_o}{s^4 + bs^2 + f} \right] \tag{75}$$

$$I_o = \frac{A}{C} V_o \left[\frac{s^2 + a_o}{(s^2 + g)(s^2 + h)} \right] \tag{76}$$

where

$$g = \frac{b - \sqrt{b^2 - 4f}}{2} \tag{77}$$

$$h = \frac{b + \sqrt{b^2 - 4f}}{2} \tag{78}$$

The expression factors into the following standard form; the inverse transformation for which is found in tables of Laplace transform pairs.

$$I_o(s) = \frac{s^2 + a_o}{(s + i\sqrt{g})(s - i\sqrt{g})(s + i\sqrt{h})(s - i\sqrt{h})} \frac{A}{C} V_o \tag{79}$$

34

After "some manipulation", the expression for the time varying current factors into the following form:

$$I_o(t) = \frac{A}{C} V_o \frac{1}{(h-g)} \left[\frac{(a_o - g)}{\sqrt{g}} \sin \sqrt{g} t - \frac{(a_o - h)}{\sqrt{h}} \sin \sqrt{h} t \right] \tag{80}$$

$$a_o = \frac{B}{A} \tag{81}$$

$$g = \frac{1}{2} \left[\frac{D}{C} - \sqrt{\left(\frac{D}{C}\right)^2 - \frac{4}{C}} \right] \tag{82}$$

$$h = \frac{1}{2} \left[\frac{D}{C} + \sqrt{\left(\frac{D}{C}\right)^2 - \frac{4}{C}} \right] \tag{83}$$

Now an interesting pattern is beginning to emerge. First it can be seen that the factors a_o, g, and h all have the dimensions of angular frequency squared. Let us leave the abstract form and relabel these frequencies so that the expression has a more familiar appearance. Call a_o, g, and h by the names, respectively, ω_o^2, ω_1^2, ω_2^2. Only ω_1 and ω_2, however, are "working" frequencies. Angular frequency ω_o is merely a reference frequency, although it does, of course, depend upon the constants of the circuit. The result of this maneuver then yields the expression:

$$I_o(t) = \frac{A}{C} V_o \frac{1}{(\omega_2^2 - \omega_1^2)} \left[\frac{(\omega_o^2 - \omega_1^2)}{\omega_1} \sin \omega_1 t + \frac{(\omega_2^2 - \omega_o^2)}{\omega_2} \sin \omega_2 t \right] \tag{84}$$

Note from the previous formulas for g and h, that angular frequencies ω_1 and ω_2 are disposed symmetrically about some central value. It is verified easily that when L_o is negligible, these two frequencies tend toward coincidence as L_1 approaches L_2 and C_1 approaches C_2. Further, for these same conditions, angular frequency ω_o, the reference frequency, tends toward this central value. Since ω_2 is always greater than ω_1, one is led to believe that the two sinusoidal terms are additive, as indicated above. This latter assertion is true for vanishing L_o, but it should be checked out for the general case. One thing that should be remembered in the special case of an Allison effect apparatus is that C_1 and C_2 are usually equal to each other; the distributed capacitances of two identical solenoids are equal. The only qualification to this would be based upon the dielectric properties of the substances filling the cells in the solenoids. Another item of concern is that the quantity under the radical in the expression for g and for h should be positive; that is, $(D^2)/4C$ should be greater than, or at least equal to, unity. This fact has been verified for the case C_1 equals C_2, with L_o having any desired value.

The remainder of the analysis consists of calculating currents I_1 and I_2 and the voltages across capacitors C_1 and C_2. The currents are found by using the current division formula. Thus,

$$I_1 = \frac{Y_1}{Y_{12}} I_o \tag{85}$$

$$I_2 = \frac{Y_2}{Y_{12}} I_o \tag{86}$$

The desired voltages are found in each case by multiplying the respective branch current into the impedance of the capacitor. (Recall that this latter circuit element represents the solenoid). Thus,

$$Vc_1 = \frac{I_1}{sC_1} \tag{87}$$

$$Vc_2 = \frac{I_2}{sC_2} \tag{88}$$

These expressions can be solved by the Laplace transform method. After some manipulation, the transform solutions are found to be:

$$I_1 = V_o \frac{s^2 (A - L_1 C_1 C_2) + C_1}{s^4 C + s^2 D + 1} \tag{89}$$

$$I_2 = V_o \frac{s^2 (A - L_2 C_2 C_1) + C_2}{s^4 C + s^2 D + 1} \tag{90}$$

$$Vc_1 = V_o \frac{s^2 L_2 C_2 + 1}{s(s^4 C + s^2 D + 1)} \tag{91}$$

$$Vc_2 = V_o \frac{s^2 L_1 C_1 + 1}{s(s^4 C + s^2 D + 1)} \tag{92}$$

where the symbols are the same as those defined earlier in this section.

When the inverse transformations are taken, the time-varying voltages and currents emerge. For convenience, all the current and voltage expressions are summarized in Table III. The symbols used in the formulas are identified as well; note that the inductance and capacitance parameters have subscripts and that these refer to the elements in the circuit of Figure 16. The reader is cautioned to give the symbol C (no subscript) its proper interpretation, i.e., that of expression (71).

36

Table III. Formulas for Circuit of Figure 17

$$I_o(t) = \frac{A}{C} V_o \frac{1}{(\omega_2^2 - \omega_1^2)} \left[\frac{(\omega_o^2 - \omega_1^2)}{\omega_1} \sin \omega_1 t + \frac{(\omega_2^2 - \omega_o^2)}{\omega_2} \sin \omega_2 t \right] \quad (84)$$

$$I_1(t) = \frac{C_2}{\Omega_2^2 C} V_o \frac{1}{(\omega_2^2 - \omega_1^2)} \left[\frac{(\Omega_2^2 - \omega_1^2)}{\omega_1} \sin \omega_1 t + \frac{(\omega_2^2 - \Omega_2^2)}{\omega_2} \sin \omega_2 t \right] \quad (93)$$

$$I_2(t) = \frac{C_1}{\Omega_1^2 C} V_o \frac{1}{(\omega_2^2 - \omega_1^2)} \left[\frac{(\Omega_1^2 - \omega_1^2)}{\omega_1} \sin \omega_1 t + \frac{(\omega_2^2 - \Omega_1^2)}{\omega_2} \sin \omega_2 t \right] \quad (94)$$

$$Vc_1(t) = \frac{V_o}{\Omega_2^2 C} \left[\frac{\Omega_2^2}{\omega_1^2 \omega_2^2} - \frac{(\Omega_2^2 - \omega_1^2)}{\omega_1^2 (\omega_2^2 - \omega_1^2)} \cos \omega_1 t - \frac{(\omega_2^2 - \Omega_2^2)}{\omega_2^2 (\omega_2^2 - \omega_1^2)} \cos \omega_2 t \right] \quad (95)$$

$$Vc_2(t) = \frac{V_o}{\Omega_1^2 C} \left[\frac{\Omega_1^2}{\omega_1^2 \omega_2^2} - \frac{\Omega_1^2 - \omega_1^2}{\omega_1^2 (\omega_2^2 - \omega_1^2)} \cos \omega_1 t - \frac{(\omega_2^2 - \Omega_1^2)}{\omega_2^2 (\omega_2^2 - \omega_1^2)} \cos \omega_2 t \right] \quad (96)$$

$$\omega_o = \sqrt{\frac{B}{A}} \quad (97)$$

$$\omega_1 = \sqrt{\frac{1}{2} \left[\frac{D}{C} - \sqrt{\left| \frac{D}{C} \right|^2 - \frac{4}{C}} \right]} \quad (98)$$

$$\omega_2 = \sqrt{\frac{1}{2} \left[\frac{D}{C} + \sqrt{\left| \frac{D}{C} \right|^2 - \frac{4}{C}} \right]} \quad (99)$$

$$\Omega_1 = \sqrt{1/L_1 C_1} \quad (100)$$

$$\Omega_2 = \sqrt{1/L_2 C_2} \quad (101)$$

$$A = (L_2 C_2 C_1 + L_1 C_1 C_2) \quad (69)$$

$$B = (C_1 + C_2) \quad (70)$$

$$C = (L_o L_2 C_2 C_1 + L_o L_1 C_1 C_2 + L_1 C_1 L_2 C_2) \quad (71)$$

$$D = (L_o C_1 + L_o C_2 + L_1 C_1 + L_2 C_2) \quad (72)$$

Only the angular frequencies ω_1 and ω_2 are active frequencies in these expressions. The other substitutions ω_o, Ω_1, and Ω_2 have the dimensions of angular frequency, but these are reference frequencies; the substitutions were made for convenience in interpretation.

The set of branch voltage and branch current expressions verifies the fact that, in general, two distinct frequencies will be present in the system at the initiation of the transient which occurs when the spark gap breaks down. Let us substitute the actual parameter symbols in equations (98) and (99) to get the explicit values for these frequencies.

$$f_1 = \frac{1}{2\pi}\left\{\frac{1}{2}\left(\frac{L_oC_1 + L_oC_2 + L_1C_1 + L_2C_2}{L_oL_2C_2C_1 + L_oL_1C_1C_2 + L_1C_1L_2C_2}\right.\right.$$
$$-\left[\left(\frac{L_oC_1 + L_oC_2 + L_1C_1 + L_2C_2}{L_oL_2C_2C_1 + L_oL_1C_2C_1 + L_1C_1L_2C_2}\right)^2\right.$$
$$\left.\left.\left.- \frac{4}{L_oL_2C_2C_1 + L_oL_1C_1C_2 + L_1C_1L_2C_2}\right]^{1/2}\right)\right\}^{1/2} \tag{102}$$

$$f_2 = \frac{1}{2\pi}\left\{\frac{1}{2}\left(\frac{L_oC_1 + L_oC_2 + L_1C_1 + L_2C_2}{L_oL_2C_2C_1 + L_oL_1C_1C_2 + L_1C_1L_2C_2}\right.\right.$$
$$+\left[\left(\frac{L_oC_1 + L_oC_2 + L_1C_1 + L_2C_2}{L_oL_2C_2C_1 + L_oL_1C_2C_1 + L_1C_1L_2C_2}\right)^2\right.$$
$$\left.\left.\left.- \frac{4}{L_oL_2C_2C_1 + L_oL_1C_1C_2 + L_1C_1L_2C_2}\right]^{1/2}\right)\right\}^{1/2} \tag{103}$$

Physically, the inductance L_o is that of the lead wires to the nodes where the parallel paths (reference and sample circuits) begin. The inductances L_1 and L_2 are respectively the net load wire inductances of the reference branch and the sample branch of the circuit. The solenoid inductances are of course by-passed by the distributed capacitances of these coils; capacitors C_1 and C_2 represent the distributed capacitances. In this idealization, the inductances of the parallel wire transmission lines should not be included because the lines appear as resistances until the reflections return from the shorted terminations.

Note again the important effect of the lead wire inductance, L_o. It is instrumental in separating frequencies f_1 and f_2 and, more important, in causing both frequencies to appear in some measure in each branch (and, thus, coil). That is, $\Omega_1 \neq \omega_1$ and $\Omega_2 \neq \omega_2$ if inductance L_o is nonzero.

38

Turning to the physical significance of this fact, we find that a given frequency, f_1 for example, may be present in three places in the apparatus. The light given off by the spark is probably modulated by a signal containing, for one, the frequency f_1 since the intensity must be some function of the current which causes it. This light is then twice exposed to signals containing f_1 as a Fourier component while it traverses the two cells in the apparatus; however, there will be no effect unless electro-optic and/or magneto-optic effects take place in the fluids in the cells. If such effects do take place, then the light will be modulated three times, in different ways, by the frequency f_1.

Another physical effect would be produced by the beat frequency $(f_2 - f_1)$ which would be generated in the system. Frequencies f_2 and f_1 may be high, but they could be sufficiently near each other so that the beat frequency would be optically observable. While trolley position adjustments are not reflected in the idealized circuit that we are considering in this section, it might be possible that the zero beat conditions could be produced by such variations in the actual circuit; a change in the appearance of the light could easily result.

In summary, it can be seen that the lead wire inductance plays an important role in determining (1) the phase and relative amplitudes of the initial frequency components in the solenoids, and (2) the rise time of the transient in the two branches. A good approximation of the leading edges of the transients in the respective coils can be obtained from the formulas (93) through (96). In using these expressions, one must remember that the currents are the displacement currents in the distributed capacitances of the solenoids; the conduction currents which follow much later are given by the solutions of the low frequency approximation. The cross-over area, where both the displacement currents and the conduction currents are effective, is best defined by the solutions to the general circuit (Figure 12).

When the current expressions are used to study the Allison effect, it must not be forgotten that a given segment of the light beam does not "see" the two currents (or voltages) simultaneously. There is a small but important time delay due to the transit time of the light segment between cells; thus, $t_2 = t_1 + (\ell/c)$ where ℓ is the center-to-center spacing of the cells.

4. Solution of Circuit Model III

The solution of the general circuit, see Figure 12, would begin with the application of Kirchhoff's laws to the four meshes and three of the nodes. These seven equations may be reduced to four simultaneous equations which, in principle, will allow us to evaluate the four currents associated with the two solenoids. We are searching for the transient solution; accordingly, use of the Laplace transformation is indicated. The following pages summarize the important steps of this first phase of the solution, which yields the Laplace transformations of the desired currents. A second phase of the solution would be that of finding the inverse transformations so that the time-varying forms of the currents would be known.

Obviously, the key problem in the solution will be the handling of the transmission line term involving the hyperbolic tangent. It is suggested that the reader review Section C, especially equations (29) to (31) for the theory associated with short-circuited transmission lines. Note that in a final solution of this problem, the physical adjustment of the trolley position is reflected in the theoretical expressions by a variation of length ℓ_1 and/or ℓ_2.

Solution 1:

The seven equations which follow represent the application of Kirchhoff's voltage law to the four simple meshes of Figure 12 and the application of Kirchhoff's current law to the upper three nodes, or junction points. The Laplace transformation of the step function generator is V_0/s. The shorted transmission line input impedance in Laplace transform form has been discussed previously. (Note: Some investigators, notably Allison, employ a delay-introducing line of the parallel wire, short-circuited variety in the lead wire branch.) This may be accounted for here by introducing a term, $Z_{00} \tanh (\ell_o s/c)$. This is added to the $R_0 + sL_0 + 1/sC_0$ sum. Length ℓ_o is that of the parallel wire line. (In reference to line length, the length ℓ used in the expression is not the total length of wire in the transmission line; thus a wire length of 2ℓ is used to make a 2-wire transmission line of length ℓ). The purpose of the additional delay line is to account for a possible time delay between the electrical breakdown of the spark gap and the generation of light by the excited or ionized vapors.

$$\frac{V_o}{s} = I_0\left[R_o + sL_o + \frac{1}{sC_o}\right] + I_1\left[R_3 + sL_3 + Z_{02}\tanh\left(\frac{\ell_1}{c}s\right)\right] + I_{RD}\frac{1}{sC_1} \qquad (104)$$

$$\frac{V_o}{s} = I_0\left[R_o + sL_o + \frac{1}{sC_o}\right] + I_2\left[R_4 + sL_4 + Z_{02}\tanh\left(\frac{\ell_1}{c}s\right)\right] + I_{SD}\frac{1}{sC_1} \qquad (105)$$

$$0 = -I_{RD}\frac{1}{sC_1} + I_R\left[R_1 + sL_1\right] - I_S\, sM \qquad (106)$$

$$0 = -I_{SD}\frac{1}{sC_2} + I_S\left[R_2 + sL_2\right] - I_R\, sM \qquad (107)$$

$$I_o = I_1 + I_2 \qquad (108)$$

$$I_1 = I_R + I_{RD} \tag{109}$$

$$I_2 = I_S + I_{SD} \tag{110}$$

$$A = R_o + sL_o + \frac{1}{sC_o} \tag{111}$$

$$B = R_3 + sL_3 + Z_{01} \ \tanh\left(\frac{\ell_1}{c}s\right) \tag{112}$$

$$C = R_4 + sL_4 + Z_{02} \ \tanh\left(\frac{\ell_1}{c}s\right) \tag{113}$$

$$D = \frac{1}{sC_1} \tag{114}$$

$$E = R_1 + sL_1 \tag{115}$$

$$F = sM \tag{116}$$

$$G = R_2 + sL_2 \tag{117}$$

$$H = \frac{1}{sC_2} \tag{118}$$

It becomes convenient, because of difficulty in manipulation, to make the above substitutions. All these letters have the dimension of impedance. Symbol A should be modified by the addition of $Z_{00} \tanh(\ell_o s/c)$ if an additional delay line is employed in the lead wire branch.

$$\frac{V_o}{s} = I_R(A+B) + I_S(A) + I_{RD}(A+B+D) + I_{SD}(A) \tag{119}$$

$$\frac{V_o}{s} = I_R(A) + I_S(A+C) + I_{RD}(A) + I_{SD}(A+C+H) \tag{120}$$

$$0 = I_R(E) + I_S(-F) + I_{RD}(-D) + I_{SD}(0) \tag{121}$$

$$0 = I_R(-F) + I_S(G) + I_{RD}(0) + I_{SD}(-H) \tag{122}$$

The seven simultaneous equations may be reduced to the above four by substitution.

$$\begin{pmatrix} A+B & A & A+B+D & A \\ A & A+C & A & A+C+H \\ E & -F & -D & 0 \\ -F & G & 0 & -H \end{pmatrix} \cdot \begin{pmatrix} I_R \\ I_S \\ I_{RD} \\ I_{SD} \end{pmatrix} = \begin{pmatrix} \dfrac{V_o}{s} \\ \dfrac{V_o}{s} \\ 0 \\ 0 \end{pmatrix} \tag{123}$$

The same four equations are shown here in matrix form.
One step in the solution of the simultaneous equations
requires evaluation of the determinant Δ of the 4 by 4
impedance matrix. The simultaneous equations are
solved in the usual manner.

$$I_R = \frac{V_o}{s} \left(\frac{CDG + DGH + CDH + BFH + DFH}{\Delta} \right) \tag{124}$$

$$I_{RD} = \frac{V_o}{s} \left(\frac{CEH + CEG + EGH - BFH - CF^2 - F^2 H}{\Delta} \right) \tag{125}$$

$$I_S = \frac{V_o}{s} \left(\frac{BHE + HED + BHD + CFD + HFD}{\Delta} \right) \tag{126}$$

$$I_{SD} = \frac{V_o}{s} \left(\frac{BGD + BGE + GED - CFD - BF^2 - F^2 L}{\Delta} \right) \tag{127}$$

Δ = ACEG + AEGH + ABEG + BCEG + BEGH + ADEG + CDEG + DEGH +
ACDG + ADGH + ABDG + BCDG + BDGH + ABEH + ADEH + ACEH +
BCEH + CDEH + ADFH + ACDH + ABDH + BCDH ·· AF^2 H - BCF^2 -
BF^2 H - CDF^2 - DF^2 H -ACF^2 - ABF^2 (128)

Solutions for the four coil currents in Laplace transformation
form are shown above. The time-varying solutions are to be
found by replacing the symbols with the expressions for which
they stand and then finding the inverse transformations. The
first phase of the solution is completed by the following ex-
pressions (also in Laplace transformation form) for the coil
voltages.

$$V_1 = I_{RD} \frac{1}{sC_1} = DI_{RD} \tag{129}$$

$$V_2 = I_{SD} \frac{1}{sC_2} = HI_{SD} \tag{130}$$

Substituting,

$$V_1 = \frac{V_o}{s}\left(\frac{DCEH + DCEG + DEGH - DBFH - DCF^2 - DF^2H}{\Delta} \right) \quad (131)$$

$$V_2 = \frac{V_o}{s}\left(\frac{HBGD + HBGE + HGED - HCFD - HBF^2 - HF^2D}{\Delta} \right) \quad (132)$$

The complexity of the general solution logically would lead one to consider a computer approach. Until there is good justification for completing the general solution, it would be well to continue with the study of other equally important aspects of the total problem, using the circuit analysis results obtained by making reasonable approximations in the general equivalent circuit.

5. Solution of the Second High Frequency Approximation

At this time, we should carry through the complete solution of the second high frequency approximation of Circuit Model III, as shown in Figure 15. This circuit will take into account the effects of trolley adjustment and will give a good answer for the events that take place during the early part of the transient, especially those events which take place between the initial rise time and the time when the inductive current begins to build up appreciably in the solenoids. This latter phase of the problem has been discussed already and a solution is available by the processing of expressions (48) through (59) of Section I, D, 2. The simplification afforded is this: The currents I_R and I_S are negligibly small in these early instants; consequently, the mutual inductance is ineffective.

The applicable solutions may be derived from the general solutions of Section I, D, 4 by recognizing that impedances E and G take on "infinite" values for this assumption. It is merely a matter of dividing numerator and denominator by the product EG and then keeping what is left after E and G separately are allowed to approach infinitely large values.

$$I_{RD} = \frac{V_o}{s}\left[\frac{C + H}{AC + AH + AB + BC + BH + AD + CD + DH} \right] \quad (133)$$

$$I_{SD} = \frac{V_o}{s}\left[\frac{B + D}{AC + AH + AB + BC + BH + AD + CD + DH} \right] \quad (134)$$

$$V_1 = \frac{V_o}{s}\left[\frac{DC + DH}{AC + AH + AB + BC + BH + AD + CD + DH} \right] \quad (135)$$

43

$$V_2 = \frac{V_o}{s} \left[\frac{HB + HD}{AC + AH + AB + BC + BH + AD + CD + DH} \right] \quad (136)$$

To find further simplification we must turn our attention to the physical apparatus itself. First, one may drop the C_o from symbol A because this large capacitance is effective only during the later stages of the transient. It would be well worthwhile to add $Z_{oo} \tanh(\ell_o s/c)$ to symbol A since the Allison equipment employs such a delay line in the lead wire system, and, since the presence of the reported minima seems to depend upon the length ℓ_o[18].

Next, there is no particular reason why the following simplifications could not be made:

$$R_3 = R_4 \quad (137)$$

$$L_3 = L_4 \quad (138)$$

$$Z_{oo} = Z_{o_1} = Z_{o_2} = Z_o \quad (139)$$

These equations imply only that a symmetry is present in the construction of the apparatus; this degree of freedom certainly is permitted by items (a) and (b) of Section I, A. The common Z_o value assumes merely that the same parallel wire line structure (wire size and spacing) is used in the three delay lines.

It is tempting to make the two capacitors C_1 and C_2 equal because the two coils are identical; however, it is precisely here that the circuit could be influenced by the specific substances in the sample and reference cells. The electric fields between the wires in the coil do extend into the fluids contained in the cells (see the sketch of Figure 17). Consequently, the electric susceptibility (and thus dielectric constant) of the fluid must make some contribution to the respective distributed capacitance. Should the susceptibility be frequency dependent, then the capacitances C_1 and C_2 will be frequency dependent. In any event, C_1 and C_2 should retain their identities in the analysis.
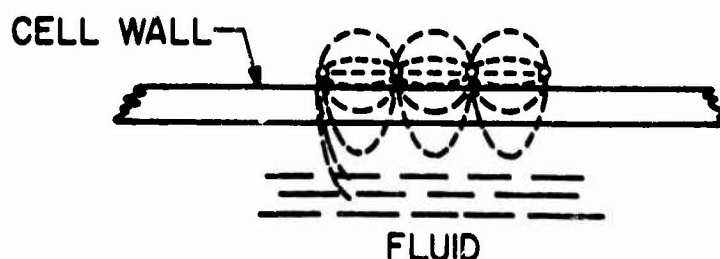
Figure 17. Electric Field Configuration Associated With the Distributed Capacitance

44

The revised symbols become:

$$A = R_o + sL_o + Z_o \tanh(\ell_o s/c) \tag{140}$$

$$B = R_3 + sL_3 + Z_o \tanh(\ell_1 s/c) \tag{141}$$

$$C = R_3 + sL_3 + Z_o \tanh(\ell_2 s/c) \tag{142}$$

$$D = 1/sC_1 \tag{143}$$

$$H = 1/sC_2 \tag{144}$$

The first objective of the solution will be, typically, the formation of a ratio of two polynomials, e. g., I_{RD} may be expressed as

$$I_{RD} = P(s)/Q(s) \tag{145}$$

If one should be so fortunate as to be able to factor $Q(s)$, thus,

$$Q(s) = (s+a_1)(s+a_2) \ldots (s+a_n) \tag{146}$$

then the remainder of the solution becomes simple; one merely performs a partial fraction expansion of the ratio, which leads into an easily performed inverse transformation. Thus, if

$$I_{RD}(s) = K_1/(s+a_1) + K_2/(s+a_2) + \ldots + K_n/(s+a_n) \tag{147}$$

then

$$I_{RD}(t) = K_1 e^{-a_1 t} + K_2 e^{-a_2 t} + \ldots + K_n e^{-a_n t} \tag{148}$$

Obviously, our great difficulty will be with the terms containing the form $\tanh u$. This will not lead to an algebraic expression unless the series expansion of the form is introduced. Then, it may be cut off after sufficient terms and the result treated as a polynomial. That sort of treatment will give reasonable answers if the series has converged sufficiently at the cut-off point. In our case, the convergence has to do with the frequency of concern and with the length of the delay line. For low frequencies and short delay lines, we find early convergence. Roughly, it appears that at least the 7th power must be included if any delay line is as much as one free space wavelength long. At 30 MHz, the wavelength is 5 meters, or above 33 Allison units. Since there is reason to believe that these are near the frequencies of interest, an early cut-off point may be feasible. If a computer can factor the polynomial, the solution will be that much easier. (It should be noted that most of the roots will be complex conjugate pairs).

There are other ways of performing the inverse transformation[21], but these are, for our case, equally as difficult, if not more so. Let us at least attempt the method outlined above; if satisfactory results are not provided, it may at least lead to better methods of solution.

Substitution for the letter symbols should be performed in the current and voltage expressions. The tanh u form may be replaced by sinh u/cosh u. Specifically, let us set

$$Z_o \tanh (\ell_i s/c) = T_i(s) = \frac{M_i(s)}{N_i(s)} \tag{149}$$

where

$$M_i(s) = Z_o \sinh (\ell_i s/c) \tag{150}$$

$$N_i(s) = \cosh (\ell_i s/c) \tag{151}$$

The hyperbolic forms have the series expansions

$$\sinh u = u + u^3/3! + u^5/5! + \ldots \tag{152}$$

$$\cosh u = 1 + u^2/2! + u^4/4! + \ldots \tag{153}$$

These furnish a basis for the formation of the ratio of two polynomials.

Solution 2:

We collect the explicit forms of the letter symbols, substitute the M and N symbols, and begin to attempt the isolation of the polynomial in the denominator.

$$A = (N_o R_o + s N_o L_o + M_o)/N_o \tag{154}$$

$$B = (N_1 R_3 + s N_1 L_3 + M_1)/N_1 \tag{155}$$

$$C = (N_2 R_3 + s N_2 L_3 + M_2)/N_2 \tag{156}$$

$$D = 1/s C_1 \tag{157}$$

$$H = 1/s C_2 \tag{158}$$

$$AB = \left[N_o N_1 R_o R_3 + N_o M_1 R_o + M_o N_1 R_3 + M_o M_1 + s(N_o N_1 R_o L_3 + \right.$$
$$\left. N_o N_1 L_o R_3 + N_o L_o M_1 + M_o N_1 L_3) + s^2 N_o N_1 L_o L_3 \right] / N_o N_1 \qquad (159)$$

$$AC = \left[N_o N_2 R_o R_3 + N_o M_2 R_o + M_o N_2 R_s + M_o M_2 + s(N_o N_2 R_o L_3 + \right.$$
$$\left. N_o N_2 L_o R_3 + N_o L_o M_2 + M_o N_2 L_3) + s^2 N_o N_2 L_o L_3 \right] / N_o N_2 \qquad (160)$$

$$BC = \left[N_1 R_3 N_2 R_3 + M_2 N_1 R_3 + M_1 N_2 R_3 + M_1 M_2 + s(N_1 N_2 R_3 L_3 + \right.$$
$$\left. N_1 N_2 L_3 R_3 + N_1 M_2 L_3 + M_1 N_2 L_3) + s^2 N_1 N_2 L_3 L_3 \right] / N_1 N_2 \qquad (161)$$

$$AH = \left[N_o R_o + M_o + s N_o L_o \right] / s C_2 N_o \qquad (162)$$

$$AD = \left[N_o R_o + M_o + s N_o L_o \right] / s C_1 N_o \qquad (163)$$

$$BH = \left[N_1 RE + M_1 + s N_1 L_3 \right] / s C_2 N_1 \qquad (164)$$

$$CD = \left[N_2 R_3 + M_2 + s N_2 L_3 \right] / s C_1 N_2 \qquad (165)$$

$$DH = 1/s^2 C_1 C_2 \qquad (166)$$

$$C+H = \left[N_2 + s(N_2 R_3 C_2 + C_2 M_2) + s^2 C_2 N_2 L_3 \right] / s C_2 N_2 \qquad (167)$$

$$B+D = \left[N_1 + s(N_1 R_3 C_1 + C_1 M_1) + s^2 C_1 N_1 L_3 \right] / s C_1 N_1 \qquad (168)$$

$$D(C+H) = \left[N_2 + s(N_2 R_3 C_2 + C_2 M_2) + s^2 C_2 N_2 L_3 \right] / s^2 C_1 C_2 N_2 \qquad (169)$$

$$H(B+D) = \left[N_1 + s(N_1 R_3 C_1 + C_1 M_1) + s^2 C_1 N_1 L_3 \right] / s^2 C_1 C_2 N_1 \qquad (170)$$

$$\text{L. C. D., } \Sigma \, AB \dots DH = N_o N_1 N_2 C_1 C_2 s^2 \qquad (171)$$

$$\text{L. C. D., } \quad 1/s \,(C+H) = s^2 C_2 N_2 \qquad (172)$$

$$\text{L. C. D., } \quad 1/s \,(B+D) = s^2 C_1 N_1 \qquad (173)$$

$$\text{L. C. D., } \quad 1/s \, D(C+H) = s^3 C_1 C_2 N_2 \qquad (174)$$

$$\text{L. C. D., } \quad 1/s \, H(B+D) = s^3 C_1 C_2 N_1 \qquad (175)$$

47

Calculate:

$$I_{RD}/V_o, \quad \text{Multiply ADJ } \Sigma \text{ by } 1$$

$$I_{SD}/V_o, \quad \text{Multiply ADJ } \Sigma \text{ by } 1$$

$$V_1/V_o, \quad \text{Multiply ADJ } \Sigma \text{ by } s$$

$$V_2/V_o, \quad \text{Multiply ADJ } \Sigma \text{ by } s$$

$$\text{ADJ } \Sigma = \widehat{AB}(N_2 C_1 C_2 s^2) + \widehat{AC}(N_1 C_1 C_2 s^2) + \widehat{BC}(N_o C_1 C_2 s^2) +$$
$$\widehat{AH}(N_1 N_2 C_1 s) + \widehat{AD}(N_1 N_2 C_2 s) + \widehat{BH}(N_o N_2 C_1 s) +$$
$$\widehat{CD}(N_o N_1 C_2 s) + \widehat{DH}(N_o N_1 N_2) \qquad \frown = \text{numerator} \qquad (176)$$

Useful Relations:

$$\cosh x \cosh y \cosh z = 1/4\Big[\cosh (x+y+z) + \cosh (x+y-z) + \cosh (x-y+z) +$$
$$\cosh (x-y-z)\Big] \qquad (177)$$

$$\sinh a \cosh x \cosh y = 1/4\Big[\sinh (a+x+y) + \sinh (a-x-y) + \sinh (a+x-y) +$$
$$\sinh (a-x+y)\Big] \qquad (178)$$

$$\sinh a \sinh b \cosh x = 1/4\Big[\cosh (a+b+x) + \cosh (a+b-x) + (-1)\cosh (a-b+x) +$$
$$(-1)\cosh (a-b-x)\Big] \qquad (179)$$

$$\widehat{AB}(N_2 C_1 C_2 s^2) = s^2 (N_o N_1 N_2 R_o R_3 C_1 C_2 + N_o M_1 N_2 R_o C_1 C_2 + M_o N_1 N_2 R_3 C_1 C_2 +$$
$$M_o M_1 N_2 C_1 C_2) + s^3 (N_o N_1 N_2 R_o L_3 C_1 C_2 + N_o N_1 N_2 L_o R_3 C_1 C_2 +$$
$$N_o M_2 N_2 L_o C_1 C_2 + M_o N_1 N_2 L_3 C_1 C_2) + s^4 (N_o N_1 N_2 L_o L_3 C_1 C_2) \qquad (180)$$

$$\widehat{AC}(N_1 C_1 C_2 s^2) = s^2 (N_o N_1 N_2 R_o R_3 C_1 C_2 + N_o N_1 M_2 R_o C_1 C_2 + M_o N_1 N_2 R_3 C_1 C_2 +$$
$$M_o N_1 M_2 C_1 C_2) + s^3 (N_o N_1 N_2 R_o L_3 C_1 C_2 + N_o N_1 N_2 L_o R_3 C_1 C_2 +$$
$$N_o N_1 M_2 L_o C_1 C_2 + M_o N_1 N_2 L_3 C_1 C_2) + s^4 (N_o N_1 N_2 L_o L_3 C_1 C_2) \qquad (181)$$

48

$$\widehat{BC}(N_o C_1 C_2 s^2) = s^2(N_o N_1 N_2 R_3^2 C_1 C_2 + N_o N_1 M_2 R_3 C_1 C_2 + N_o M_1 N_2 R_3 C_1 C_2 +$$

$$M_1 M_2 N_o C_1 C_2) + s^3(N_o N_1 N_2 R_3 L_3 C_1 C_2 + N_o N_1 N_2 L_3 R_3 C_1 C_2$$

$$+ N_o N_1 M_2 L_3 C_1 C_2 + N_o M_1 N_2 L_3 C_1 C_2) + s^4(N_o N_1 N_2 L_3^2 C_1 C_2) \quad (182)$$

$$\widehat{AH}(N_1 N_2 C_1 s) = s(N_o N_1 N_2 R_o C_1 + M_o N_1 N_2 C_1) + s^2(N_o N_1 N_2 L_o C_1) \quad (183)$$

$$\widehat{AD}(N_1 N_2 C_2 s) = s(N_o N_1 N_2 R_o C_2 + M_o N_1 N_2 C_2) + s^2(N_o N_1 N_2 L_o C_2) \quad (184)$$

$$\widehat{BH}(N_o N_2 C_1 s) = s(N_o N_1 N_2 R_3 C_1 + M_1 N_o N_2 C_1) + s^2(N_o N_1 N_2 L_3 C_1) \quad (185)$$

$$\widehat{CD}(N_o N_1 C_2 s) = s(N_o N_1 N_2 R_3 C_2 + N_o N_1 M_2 C_2) + s^2(N_o N_1 N_2 L_3 C_2) \quad (186)$$

$$\widehat{DH}(N_o N_1 N_2) = N_o N_1 N_2 \quad (187)$$

$$ADJ\ \Sigma = N_o N_1 N_2 + s\left[N_o N_1 N_2(R_3 C_2 + R_3 C_1 + R_o C_2 + R_o C_1) + M_o N_1 N_2(C_1 + C_2) + \right.$$

$$\left. N_o M_1 N_2 C_1 + N_o N_1 M_2 C_2\right] + s^2\left[N_o N_1 N_2(L_3 C_2 + L_3 C_1 + L_o C_2 + L_o C_1 + \right.$$

$$R_3^2 C_1 C_2 + R_o R_3 C_1 C_2\ (2)) + N_o M_1 N_2(R_3 C_1 C_2 + R_o C_1 C_2) +$$

$$N_o N_1 M_2(R_3 C_1 C_2 + R_o C_1 C_2) + N_o M_1 M_2 C_1 C_2 + M_o N_1 N_2 R_3 C_1 C_2\ (2) +$$

$$\left. M_o M_1 N_2 C_1 C_2 + M_o N_1 M_2 C_1 C_2\right] + s^3\left[N_o N_1 N_2(2R_3 L_3 C_1 C_2 + \right.$$

$$2R_o L_3 C_1 C_2 + 2L_o R_3 C_1 C_2) + M_o N_1 N_2\ 2L_3 C_1 C_2 + N_o M_1 N_2(L_o C_1 C_2 +$$

$$\left. L_3 C_1 C_2) + N_o N_1 M_2(L_o C_1 C_2 + L_3 C_1 C_2)\right] + s^4\left[N_o N_1 N_2(2L_o L_3 C_1 C_2 + \right.$$

$$\left. L_3^2 C_1 C_2)\right] \quad (188)$$

The adjusted summation, ordered in powers of s, represents a polynomial in s which must be factored in order to locate the poles in the s-plane. Once the factoring is completed, the partial fraction expansion can be performed. Actually, the summation is deceptive; it is far from being a simple 4th order polynomial because each of the products, $N_o N_1 N_2$,

$M_o N_1 N_2$, etc., is an infinite series in s. What must be done now is to isolate the coefficients of the powers of s to a "satisfactory" degree. We begin this task by exhibiting the hyperbolic identities for the N, M triples. It is noteworthy that these are functions of sums and differences of the adjustable transmission line lengths.

$$N_o N_1 N_2 = 1/4(\text{Ch}\,\alpha s + \text{Ch}\,\beta s + \text{Ch}\,\gamma s + \text{Ch}\,\delta s) \tag{189}$$

$$M_o N_1 N_2 = Z_o/4(\text{Sh}\,\alpha s + \text{Sh}\,\beta s + \text{Sh}\,\gamma s + \text{Sh}\,\delta s) \tag{190}$$

$$N_o M_1 N_2 = Z_o/4(\text{Sh}\,\alpha s + \text{Sh}\,\beta s - \text{Sh}\,\gamma s - \text{Sh}\,\delta s) \tag{191}$$

$$N_o N_1 M_2 = Z_o/4(\text{Sh}\,\alpha s - \text{Sh}\,\beta s + \text{Sh}\,\gamma s - \text{Sh}\,\delta s) \tag{192}$$

$$N_o M_1 M_2 = Z_o^2/4(\text{Ch}\,\alpha s - \text{Ch}\,\beta s - \smile \quad + \text{Ch}\,\delta s) \tag{193}$$

$$M_o M_1 N_2 = Z_o^2/4(\text{Ch}\,\alpha s + \text{Ch}\,\beta s - \text{Ch}\,\gamma s - \text{Ch}\,\delta s) \tag{194}$$

$$M_o N_1 M_2 = Z_o^2/4(\text{Ch}\,\alpha s - \text{Ch}\,\beta s + \text{Ch}\,\gamma s - \text{Ch}\,\delta s) \tag{195}$$

Where:

$$\text{Sh} = \sinh \tag{196}$$
$$\text{Ch} = \cosh \tag{197}$$
$$\alpha = (\ell_o + \ell_1 + \ell_2)/c \tag{198}$$
$$\beta = (\ell_o + \ell_1 - \ell_2)/c \tag{199}$$
$$\gamma = (\ell_o - \ell_1 + \ell_2)/c \tag{200}$$
$$\delta = (\ell_o - \ell_1 - \ell_2)/c \tag{201}$$

We now find the leading terms in the series expansions of the hyperbolic function triple products.

$$N_o N_1 N_2 = 1 + 1/2(\tau_o^2 + \tau_1^2 + \tau_2^2)s^2 + 1/24(6\tau_o^2\tau_1^2 +$$
$$6\tau_o^2\tau_2^2 + 6\tau_1^2\tau_2^2 + \tau_o^4 + \tau_1^4 + \tau_2^4)s^4 + \ldots \tag{202}$$

$$M_o N_1 N_2 = Z_o\tau_o s + 1/6 Z_o(\tau_o^3 + 3\tau_o\tau_1^2 + 3\tau_o\tau_2^2)s^3 + \ldots \tag{203}$$

$$N_o M_1 N_2 = Z_o\tau_1 s + 1/6 Z_o(\tau_1^3 + 3\tau_1\tau_o^2 + 3\tau_1\tau_2^2)s^3 + \ldots \tag{204}$$

$$N_o N_1 M_2 = Z_o\tau_2 s + 1/6 Z_o(\tau_2^3 + 3\tau_2\tau_o^2 + 3\tau_2\tau_1^2)s^3 + \ldots \tag{205}$$

$$N_o M_1 M_2 = Z_o^2\tau_1\tau_2 s^2 + \ldots \tag{206}$$

$$M_o N_1 M_2 = Z_o{}^2 \tau_o \tau_1 s^2 + \ldots \tag{207}$$

where

$$\tau_o = \ell_o / c \tag{208}$$

$$\tau_1 = \ell_1 / c \tag{209}$$

$$\tau_2 = \ell_2 / c \tag{210}$$

Substitution in the adjusted summation and arrangement by powers of s yields,

$$
\begin{aligned}
\text{ADJ } \Sigma = {} & 1 + s \left[R_3 C_2 + R_3 C_1 + R_o C_2 + R_o C_1 \right] + s^2 \left[1/2(\tau_o{}^2 + \tau_1{}^2 + \tau_2{}^2) + \right. \\
& Z_o \tau_o (C_1 + C_2) + Z_o \tau_1 C_1 + Z_o \tau_2 C_2 + L_3 C_2 + L_3 C_1 + L_o C_2 + L_o C_1 + \\
& \left. R_3^2 C_1 C_2 + 2 R_o R_3 C_1 C_2 \right] + s^3 \left[1/2(\tau_o{}^2 + \tau_1{}^2 + \tau_2{}^2)(R_3 C_2 + R_3 C_1 + \right. \\
& R_o C_2 + R_o C_1) + Z_o \tau_1 (R_3 C_1 C_2 + R_o C_1 C_2) + Z_o \tau_2 (R_3 C_1 C_2 + R_o C_1 C_2) + \\
& \left. Z_o \tau_o 2 R_3 C_1 C_2 + 2 R_3 L_3 C_1 C_2 + 2 R_o L_3 C_1 C_2 + 2 L_o R_3 C_1 C_2 + \right] \\
& s^4 \left[1/24 (6 \tau_o{}^2 \tau_1{}^2 + 6 \tau_o{}^2 \tau_2{}^2 + 6 \tau_1{}^2 \tau_2{}^2 + \tau_o{}^4 + \tau_1{}^4 + \tau_2{}^4 + \right. \\
& 1/6 Z_o (\tau_o{}^3 + 3 \tau_o \tau_1{}^2 + 3 \tau_o \tau_2{}^2)(C_1 + C_2) + 1/6 Z_o (\tau_1{}^3 + 3 \tau_1 \tau_o{}^2 + \\
& 3 \tau_1 \tau_2{}^2) C_1 + 1/6 Z_o (\tau_2{}^3 + 3 \tau_2 \tau_o{}^2 + 3 \tau_2 \tau_1{}^2) C_2 + 1/2 (\tau_o{}^2 + \tau_1{}^2 + \tau_2{}^2) \\
& (L_3 C_2 + L_3 C_1 + L_o C_2 + L_o C_1 + R_3{}^2 C_1 C_2 + 2 R_o R_3 C_1 C_2) + Z_o{}^2 \tau_1 \tau_2 C_1 C_2 + \\
& Z_o{}^2 \tau_o \tau_1 C_1 C_2 + Z_o{}^2 \tau_o \tau_2 C_1 C_2 + Z_o \tau_o 2 L_3 C_1 C_2 + Z_o \tau_1 (L_o C_1 C_2 + \\
& \left. L_3 C_1 C_2) + Z_o \tau_2 (L_o C_1 C_2 + L_3 C_1 C_2) + 2 L_o L_3 C_1 C_2 + L_3{}^2 C_1 C_2 \right] + \\
& \ldots \tag{211}
\end{aligned}
$$

Only the first five terms of the adjusted summation have been computed here. It is not difficult to see that the coefficients of the still higher powers of s will become exceedingly long. It would be inefficient and very expensive in terms of labor and time to work these out without the aid of a computer. Further,

51

the chances for introducing errors increase rapidly if the expansion and rearrangement are carried out by hand.

The reader should note that the lengths of the respective delay lines are now implicit in the time delay factors, τ_o, τ_1, and τ_2. One Allison unit corresponds to a τ of 0.5×10^{-9} second. (Thus, Allison intends that a folded transmission line length l introduces an additional length of $2l$ into the path of the respective "impulse".)

It is interesting (and certainly most gratifying) to observe that the problem reduces exactly to the First High Frequency Approximation, Section I, D, 3, when R_o and R_3 vanish and the delay line lengths (thus, also τ_o, τ_1, and τ_2) are reduced to zero. Even these first few terms will enable us to assess the effect of small resistances and short lengths of delay line, and adjustments of these short lengths, when such are introduced into the pure reactance idealization (Figure 16).

While these first five terms will indicate the trend of the behavior caused by the delay lines and the adjustments of these lines, they are insufficient to predict accurately the effect of long delay lines operated at high frequencies. The infinite series converges too slowly for this latter case and powers as high as 10 or 12 may be needed to study the frequency range of interest. Again, the necessity for a computer solution is obvious.

The next step in the solution of the problem consists of factoring the polynomial formed by cutting off the infinite series in s. Assuming that a computer can factor the polynomial, it is suggested that each polynomial of successive higher power be factored; examination of the factors will enable one to judge when the degree of convergence is adequate.

Let us begin the solution "by hand" by factoring the 4th order polynomial which has been generated thus far. Since it is not convenient to work with the general form, we will substitute typical values for the parameters. One cannot hope to obtain a useful solution from these few terms, but the trends of the main solution may appear.

Typical values for the parameters are as follows:

$$R_o = R_3 = 1 \text{ Ohm} \tag{212}$$

52

$$L_O = L_3 = 2 \times 10^{-6} \text{ Henry} \tag{213}$$

$$C_1 = C_2 = 5 \times 10^{-12} \text{ Farad} \tag{214}$$

$$Z_O = 500 \text{ Ohms} \tag{215}$$

The capacitors C_1 and C_2 are being set equal here for ease of solution. The major area of interest at this moment is the effect of delay line length. Let us substitute the above values to see what form results. The case $C_1 \neq C_2$ may and should be investigated separately.

Substitution yields,

$$
\begin{aligned}
\text{ADJ } \Sigma = 1 &+ s\left[20 \times 10^{-12}\right] + s^2\left[1/2(\tau_O^2 + \tau_1^2 + \tau_2^2) + 25 \times 10^{-10}(2\tau_O + \tau_1 + \tau_2) + \right. \\
&\left. 40 \times 10^{-18}\right] + s^3\left[10^{-11}(\tau_O^2 + \tau_1^2 + \tau_2^2) + 25 \times 10^{-21}(\tau_O + \tau_1 + \tau_2) + \right. \\
&\left. 3 \times 10^{-28}\right] + s^4\left[1/24(6\tau_O^2\tau_1^2 + 6\tau_O^2\tau_2^2 + 6\tau_1^2\tau_2^2 + \tau_O^4 + \tau_1^4 + \tau_2^4) + \right. \\
&25/6 \times 10^{-10}(2\tau_O^3 + \tau_1^3 + \tau_2^3 + 6\tau_O\tau_1^2 + 6\tau_O\tau_2^2 + 3\tau_1\tau_O^2 + 3\tau_1\tau_2^2 + \\
&3\tau_2\tau_O^2 + 3\tau_2\tau_1^2) + 20 \times 10^{-18}(\tau_O^2 + \tau_1^2 + \tau_2^2) + 625 \times 10^{-20}(\tau_1\tau_2 + \\
&\left. \tau_O\tau_1 + \tau_O\tau_2) + 5 \times 10^{-26}(\tau_O + \tau_1 + \tau_2) + 3 \times 10^{-34}\right] + \ldots \tag{216}
\end{aligned}
$$

This simplifies the expression to the point where at least one qualitative observation is possible. The lead wire delay seems to be at least as effective as the reference delay τ_1 and the sample delay τ_2 in determining the roots of the polynomial (and, therefore, the characteristic frequencies of the solution).

The quantitative effects still are far from obvious and a continuing reduction is indicated. A program for this reduction might be as follows:

(1) Establish the polynomial for $\tau_O = \tau_1 = \tau_2 = 0$. In this form it will be, exactly, a closed polynomial because the remainder of the series expansion is non-zero only for non-zero values of τ_O and/or τ_1 and/or τ_2.

(2) Set $\tau_O = 0$ (no delay in the lead wire) and examine the effect of token values of τ_1 and τ_2. A convenient value would be that resulting from $\ell_1 = \ell_2 = 30$ cm. (2 Allison units); thus, $\tau_1 = \tau_2 = 10^{-9}$ sec. The frequency for which 30 cm.

is a quarter-wavelength is 250 Mcps; consequently, the convergence of the series should give reasonable validity to the results for the 50 Mcps vicinity.

(3) Set $\tau_o = 0$, $\tau_1 = 0$, $\tau_2 = 10^{-9}$ sec.

(4) Set $\tau_o = \tau_1 = \tau_2 + 10^{-9}$ sec.

(5) Set $\tau_o = 0$, $\tau_1 = \tau_2 + 2 \times 10^{-9}$ sec.

(6) Set $\tau_o = 0$, $\tau_1 = 0$, $\tau_2 = 2 \times 10^{-9}$ sec.

(7) Set $\tau_o = \tau_1 = \tau_2 = 2 \times 10^{-9}$ sec.

(8) And so on.

The resulting 4th order polynomials will show both the effectiveness of delay line variations and the effect upon the roots. Some extrapolation might be possible without extending the series. Again, the labor involved would seem to warrant the assistance of a computer. Graphical display would be a pole-zero diagram.

Substitution of the various delay line lengths yields the following set of polynomials. The first is closed; the rest are the five leading terms of an infinite series. Note that a change in scale has been employed, viz., $10^{-9} s = m$, in order to avoid the unwieldy exponents. Factorization of these expressions will yield the poles of the current or voltage equations, which, in turn, give the characteristic frequencies of the system. It can be seen even now that these characteristic frequencies change substantially as the delay line lengths are changed.

τ_o τ_1 τ_2
(in units of 10^{-9} sec.)

τ_o	τ_1	τ_2		
0	0	0	$Q(m) = 1 + 0.02m + 40\,m^2 + 0.3\,m^3 + 300\,m^4$	(217)
0	0	1	$Q(m) = 1 + 0.02m + 43\,m^2 + 0.325\,m^3 + 370.46\,m^4 + \ldots$	(218)
0	1	1	$Q(m) = 1 + 0.02m + 46\,m^2 + 0.370\,m^3 + 449.92\,m^4 + \ldots$	(219)
1	1	1	$Q(m) = 1 + 0.02m + 51.5\,m^2 + 0.405\,m^3 + 541.292\,m^4 + \ldots$	(220)
0	0	2	$Q(m) = 1 + 0.02m + 47\,m^2 + 0.390\,m^3 + 484\,m^4 + \ldots$	(221)
0	2	2	$Q(m) = 1 + 0.02m + 54\,m^2 + 0.480\,m^3 + 717.0\,m^4 + \ldots$	(222)
2	2	2	$Q(m) = 1 + 0.02\,m + 66\,m^2 + 0.570\,m^3 + 1022.33\,m^4 + \ldots$	(223)

54

Consequently, in the first moments after the initiation of the impulse, there will be corresponding variations in the rise times of the voltage and current waveforms at the solenoids.

At this point, there no longer is any question about the need for computer assistance, even in the case of numerical solutions for these simple polynomials. We will defer the remainder of the numerical work to Section I, F: let us, however, deal with the first polynomial, $(\tau_0, \tau_1, \tau_2) = (0, 0, 0)$, in an approximate yet rather accurate way so that the reader may gain a feeling for the magnitudes of the numerical values.

It can be seen by inspection that the first power and the cubic terms are small enough in comparison with the rest that they might be neglected in a first attempt to obtain the roots. The approximate polynomial which remains factors into

$$(1 + 10m^2)(1 + 30m^2) \tag{225}$$

whence

$$m = \pm i \, 1/\sqrt{10}, \ \pm i \, 1/\sqrt{30} \tag{226}$$

and thus,

$$s = \pm i \, 10^9/\sqrt{10}, \ \pm i \, 10^9/\sqrt{30} \tag{227}$$

Since $s = \sigma + i\omega$, we see that a pair of characteristic frequencies are predicted:

$$\omega = 10^9/\sqrt{10}, \ 10^9/\sqrt{30} \text{ radians per second} \tag{228}$$

or

$$f = 1/2\pi \, 10^9/\sqrt{10}, \ 1/2\pi \, 10^9/\sqrt{30} \text{ hertz.} \tag{229}$$

These yield

$$f_1 = 50.4 \text{ Megahertz} \tag{230}$$

and

$$f_2 = 29.1 \text{ Megahertz} \tag{231}$$

The current and voltage rise times will be of the order of fractional periods of these frequencies. We must now obtain the remainder of the expressions that are necessary to give a complete solution to the problem. Recall that the problem begins by forming an expression, typically,

$$I_{RD} = P(s)/Q(s) \tag{232}$$

The adjusted summation (ADJ Σ) is the $Q(s)$ expression for currents I_{RD} and I_{SD}. This same adjusted summation, when multiplied by s is the $Q(s)$ expression for the voltages V_1 and V_2. It remains to find the explicit forms of the $P(s)$ expressions for the currents and the voltages. These are readily available from the earlier expressions. Thus,

$$\text{for } I_{RD}, \ P(s) = V_o N_o N_1 C_2 \left[N_2 + s(N_2 R_3 C_2 + C_2 M_2) + s^2 C_2 N_2 L_3 \right] \tag{233}$$

$$\text{for } I_{SD}, \ P(s) = V_o N_o N_2 C_2 \left[N_1 + s(N_1 R_3 C_1 + C_1 M_1) + s^2 C_1 N_1 L_3 \right] \tag{234}$$

$$\text{for } V_1, \ P(s) = V_o N_o N_1 \left[N_2 + s(N_2 R_3 C_2 + C_2 M_2) + s^2 C_2 N_2 L_3 \right] \tag{235}$$

$$\text{for } V_2, \ P(s) = V_o N_o N_2 \left[N_1 + s(N_1 R_3 C_1 + C_1 M_1) + s^2 C_1 N_1 L_3 \right] \tag{236}$$

Finally, we may summarize the complete solutions in $P(s)/Q(s)$ form, giving the normalized forms of the current and voltage expressions.

$$I_{RD}/V_o = N_o N_1 C_1 \left[N_2 + s(N_2 R_3 C_2 + C_2 M_2) + s^2 C_2 N_2 L_3 \right] /ADJ \ \Sigma \tag{237}$$

$$I_{SD}/V_o = N_o N_2 C_2 \left[N_1 + s(N_1 R_3 C_1 + C_1 M_1) + s^2 C_1 N_1 L_3 \right] /ADJ \ \Sigma \tag{238}$$

$$V_1/V_o = N_o N_1 \left[N_2 + s(N_2 R_3 C_2 + C_2 M_2) + s^2 C_2 N_2 L_3 \right] /s \left[ADJ \ \Sigma \right] \tag{239}$$

$$V_2/V_o = N_o N_2 \left[N_1 + s(N_1 R_3 C_1 + C_1 M_1) + s^2 C_1 N_1 L_3 \right] /s \left[ADJ \ \Sigma \right] \tag{240}$$

Let us now review in specific detail the method of solving for, say, $V_1(t)/V_o$. We begin with the $V_1(s)/V_o$ form as given immediately above. That expression can be arranged in the form

$$V_1(s)/V_o = \frac{N_o N_1 N_2 + s(N_o N_1 N_2 R_3 C_2 + N_o N_1 M_2 C_2) + s^2 N_o N_1 N_2 C_2 L_3}{s(1 + a_1 s + a_2 s^2 + \ldots + a_n s^n)} \tag{241}$$

where the infinite series in the denominator has been
cut off after the nth term. Next, one may divide num-
erator and denominator by the coefficient a_n to obtain
the more suitable form

$$V_1(s)/V_o = \frac{1/a_n \left[N_o N_1 N_2 + s(N_o N_1 N_2 R_3 C_2 + N_o N_1 M_2 C_2) + s^2 N_o N_1 N_2 C_2 L_3 \right]}{s(s^n + b_{n-1} s^{n-1} + \ldots + b_o)} \tag{242}$$

where

$$b_{n-1} = a_{n-1}/a_n \tag{243}$$

$$b_o = 1/a_n \tag{244}$$

The denominator is factored, thus

$$V_1(s)/V_o = \frac{1/a_n \left[N_o N_1 N_2 + s(N_o N_1 N_2 R_3 C_2 + N_o N_1 M_2 C_2) + s^2 N_o N_1 N_2 C_2 L_3 \right]}{(s+o)(s+d_1)(s+d_2) \ldots (s+d_n)} \tag{245}$$

Now, one forms

$$V_1(s)/V_o = K_o/s+o + K_1/s+d_1 + K_2/s+d_2 + \ldots K_n/s+d_n \tag{246}$$

where

$$K_o = \left. \frac{1/a_n \left[N_o N_1 N_2 + s(N_o N_1 N_2 R_3 C_2 + N_o N_1 M_2 C_2) + s^2 N_o N_1 N_2 C_2 L_3 \right]}{(s+d_1)(s+d_2) \ldots (s+d_n)} \right|_{s=0} \tag{247}$$

and

$$K_1 = \left. \frac{1/a_n \left[N_o N_1 N_2 + s(N_o N_1 N_2 R_3 C_2 + N_o N_1 M_2 C_2) + s^2 N_o N_1 N_2 C_2 L_3 \right]}{s(s+d_2) \ldots (s+d_n)} \right|_{s=-d_1} \tag{248}$$

$$K_2 = \left. \frac{1/a_n \left[N_o N_1 N_2 + s(N_o N_1 N_2 R_3 C_2 + N_o N_1 M_2 C_2) + s^2 N_o N_1 N_2 C_2 L_3 \right]}{s(s+d_1)(s+d_3) \ldots (s+d_n)} \right|_{s=-d_2} \tag{249}$$

$$\ldots = \rule{8cm}{0.4pt}$$

$$K_n = \frac{1/a_n \left[N_o N_1 N_2 + s(N_o N_1 N_2 R_3 C_2 + N_o N_1 M_2 C_2) + s^2 N_o N_1 N_2 C_2 L_3 \right]}{s(s+d_1)(s+d_2) \ldots (s+d_{n-1})} \Bigg|_{s=-d_n} \tag{250}$$

While it is quite easy, though perhaps laborious to evaluate the K's, the major task is encountered in the factoring of the denominator. Since the coefficient K_o is remarkably easy to evaluate, let us do so to guide the remainder of the work.

For s = 0 (251)

$$N_o(0) = \cosh(0) = 1 \tag{252}$$

$$N_1(0) = \cosh(0) = 1 \tag{253}$$

$$N_2(0) = \cosh(0) = 1 \tag{254}$$

so that

$$K_o = \frac{1/a_n}{d_1 d_2 \ldots d_n} \tag{255}$$

but

$$d_1 d_2 \ldots d_n = 1/a_n \tag{256}$$

whence

$$K_o = 1 \tag{257}$$

To continue the solution of the partial fraction expansion, one makes use of the transform pair

f(t)	F(s)
e^{-dt}	$\dfrac{1}{s+d}$

obtaining therewith the explicit solution

$$V_1(t)/V_o = 1 + K_1 e^{-d_1 t} + K_2 e^{-d_2 t} + \ldots + K_n e^{-d_n t} \tag{258}$$

where we have used the previous evaluation of K_o, and the fact that e^{-0} equals unity.

It is reassuring to see that this expression predicts the correct answer for the circuit of Figure 15 as time t approaches an infinite value. Voltage V_1 does indeed approach the step function value V_o for this limit.

Once the last expression is evaluated numerically, it will be seen that the K's and d's come in complex conjugate

58

pairs. It will be possible to combine these pairs to form sine and/or cosine functions, and this should be done. The real parts of the exponential functions will give exponential damping coefficients to the sinusoidal variations.

It is conjectured that the best approach to a realistic solution is to repeat the solution for ever increasing polynomial orders until the answers begin to show only minor differences from the previous answers; that may be the best assurance of convergence.

6. Concluding Remarks

Circuit Model III is the best representation of the Allison effect equipment for frequencies lying below the (approximately) 50 megahertz limit. Energy considerations lead one to think that the effect can be explained in terms of such frequencies.

The solution of the circuit is given; however, computer assistance will be required if the detailed steps are to yield the numerical results which are necessary for the construction of the desired graphs of the time-varying voltages and currents.

It is recommended that the solutions to the low frequency approximation (Section I, D, 2) and the second high frequency approximation (Section I, D, 5) be carried out in this manner. The exact solution (Section I, D, 4) is so complex, that even a computer solution seems a major undertaking. It is felt that the two approximations can be joined in a logical way to yield a result that is almost as accurate as that which would be given by an exact solution.

E. ADDITIONAL THEORETICAL CONSIDERATIONS

1. Sensitivity of the Allison Effect to Nuclear Type Properties

One is forced by the experimental evidence documented in the literature to include some property or properties of the nucleus in the final explanation of the Allison effect. The specific experimental evidence is contained in the work done by various investigators on isotopes [11, 12, 13, 14, 15, 16, 22, 23, 24].

The properties of the nucleus which might have some direct effect in the Allison experiment are the mass, the magnetic moment, and the electric quadrupole moment. Each of these properties produces a bulk effect in the materials containing the nuclei, and this bulk effect enters into the circuit

properties. Microwave gyrators, Faraday rotators, isolators, and circulators are concrete examples of the practical application of the magnetic moment of the electron. The magnetic moment of the nucleus could cause similar effects in principle, although the radio frequencies would be considerably lower due to the larger mass of the nucleus. All the magneto-optic effects and the electro-optic effects are associated with transitions between energy levels of atoms and molecules. Since these energy levels are affected by interactions with the magnetic moment, the electric quadrupole moment, and with combined effects of these moments, and, since, for a given element, these moments vary with the isotopes, one may expect differences in the magneto-optic and the electro-optic behavior of materials composed of various isotopes. All the known effects should be given some attention in the light of the small variations caused by the nuclear properties.

The magnetic moment and the electric quadrupole moment of the nucleus would relate to the electric circuit used in the Allison experiments through their effect on the bulk susceptibility of the liquid media used in the cells. They do affect the bulk susceptibility or susceptibilities which, in turn, determine the permeability and permittivity. These latter are responsible for the inductive and capacitive. properties of the circuit elements involved.

The major reason why these nuclear properties evoke interest is that they introduce exceedingly sharp resonances in certain electrical circuits. Nuclear magnetic resonance (NMR) experiments and electric quadrupole resonance experiments are familiar because of their widespread use in chemical analysis and physical research. If the reader is unfamiliar with the technique and theory, he may find it interesting to read a review such as is given by Andrew[25].

If these nuclear properties were active in the Allison effect, they would provide a basis for the reported identification of isotopes. As was mentioned earlier in this paragraph, the nucleus must somehow be involved. Unfortunately, the case for NMR and quadrupole effects is extremely weak, to the point, in fact, where they may be discarded from our considerations, if we are to accept the experimental evidence of the observers (referenced in this paragraph) who attributed certain minima in the Allison effect experiments to the presence of isotopes.

The specific reason for discarding the possibility that NMR (or quadrupole) effects are active in the Allison experiments is that the nucleus does not possess any observable magnetic moment or electric quadrupole moment if it contains both an even number of protons and an even number of neutrons. In the Allison effect experiments, different minima positions are reported for isotopes of a given element where these isotopes do not possess a magnetic moment (nuclear) or a nuclear electric quadrupole moment. Specifically, to document this statement, one might consider the work of Bishop, Lawrenz, and

Dollins on lead isotopes[13]. Lead, atomic number 82, has an even number of protons, viz., 82. The above investigators report different minima positions for isotopes of mass number 202, 204, 206, 208, 210, 212, 214, and 216; all of these have an even number of neutrons as well as an even number of protons and would not possess net nuclear moments.

The same case may be made for radium, uranium, and other elements. The conclusion to be drawn here is that the isotope discrimination in the Allison effect most likely is due to mass.

2. Concentration Sensitivity of the Allison Effect

The extreme sensitivity claimed for the Allison effect is one characteristic which often is viewed with disbelief. It should be made a matter of record in this report that there are numerous other areas of experimental science where a small concentration of active centers causes an unusually large bulk effect; there is ample precedence for the detection of weak concentrations by relatively simple apparatus.

One such area is that of semiconductor materials. It is well known that the smallest trace of an impurity will cause a drastic change in the bulk conductivity of an intrinsic semiconductor. The presence of $1:10^{10}$ of a donor or acceptor impurity is detectable easily. A knowledge of the ultimate sensitivity is limited experimentally by the inability of technology to produce a completely "pure" specimen of the intrinsic material.

In electron spin resonance work, where the presence of active centers is detected by a radio frequency circuit, one can, for example, detect the generation of broken bonds caused by light irradiation of a material to a sensitivity of $1:10^{11}$. In fact, this type of apparatus will detect the presence of burning tobacco somewhere in the same room by means of the free radicals produced in the charring process.

Earlier investigators attributed the Allison effect to a time delay in the Faraday magneto-optic effect. Currently, however, there is cause for reconsideration of this early opinion. If, nevertheless, it develops that the Faraday effect does enter in some subtle way, it certainly can be demonstrated by means of a theoretical model that a small concentration of active centers can produce a significant Faraday rotation. The classical theory of the Faraday magneto-optic effect relates this bulk effect to the density of active centers by the following expression:

$$\theta = -\left[N q^3 B_o \, \ell/2 \, (K+1)^2 \, m^2 \, C \, \varepsilon_o \right] \left[1/(\omega_o - \omega) \right]^2 \qquad (259)$$

(the angular rotation in radians)

where:

    N = density of the charges, molecules per cubic meter

    q = charge of an electron

    B_o = magnetic flux density in webers per square meter

    ℓ = length of path in meters

    K = ratio, ω_o/ω

    m = mass of an electron

    C = velocity of light in meters per second

    ϵ_o = permittivity of free space in Farads per meter

    ω_o = resonant angular frequency associated with the active center

    ω = angular frequency of the illuminating light

Large angles of rotation are predicted (and found in experimental work) for light frequencies, ω, which are in the close vicinity of some natural resonance associated with the active centers. This latter resonance is characterized by an absorption line centered at frequency ω_o. The greatest effect is obtained, of course, when the illuminating spectral line is very narrow and the absorption line also is very narrow; the difference $(\omega_o - \omega)$ can be very small under those circumstances.

3. Resolution of Minima

a. Importance of the Light Frequency Used in the Experiment

The possibility of using a more stable light source for the Allison effect experiment, for example, high intensity Mercury vapor or Xenon lamps, has been considered. It is completely and inescapably logical that a minimum would be smeared over an increment of trolley displacement, depending on the breadth of the spectral line illuminating the sample. A very narrow spectral line, such as is available from a continuous wave laser emission, would be the best possible source for the light. The basis for this assertion is Allison's work[3] concerning the effect of wave length on the position of the minimum for a particular substance. In the paper referred to, Allison shows that the position of the minimum, in the case of Xylene (C_8H_{10}), for example, shifts 100 centimeters when the light frequency is changed by approximately 1400Å.

The significance of this is that a spectral source only 14Å wide would smear the minimum over a 1 centimeter range of trolley adjustment; it is doubtful that good results could be obtained under these circumstances. Now, a high pressure mercury arc or Xenon arc has a very broad spectrum, considerably broader than 14Å, so that such sources could not be used directly.

It might be possible to utilize one of the modern interference filters, but even here a 5Å transmission band is quite an achievement and obtainable only at a great loss in intensity. Compare this to the typical line width of 0.02Å to 0.1Å for spectral lines normally used in the Allison effect experiments.

One answer to the problem is the laser, which has a line width that is orders of magnitude below that of the spectral line now in use. Incomparable resolution would be obtained; it is possible, even, that an enhancement of the minimum would result from the elimination of the dispersion that now is present. The extraordinarily high intensity of the laser beam is a well known fact; a further advantage is the possibility of modulating the laser beam with a sub-carrier frequency. This would permit the use of phase detection which, in turn, would improve the sensitivity of the detector by orders of magnitude beyond that of the d.c. method now in use.

b. Significance of Phase Displacement vs. Resolution

It has often been observed in the literature, sometimes implicitly[26], that the approximately 3 mm resolution of a minimum in the Allison effect experiment requires a rise time of the order of 10^{-11} second. One interpretation of this figure is that frequency components of the order of 10 gigahertz should be present in the impulse that travels along a conductor. This observation is based upon the natural law

$$\Delta\omega\Delta t = 1 \tag{260}$$

There is another way of looking upon this experiment, one which would predict much lower frequency components. The apparatus is to be thought of as a phase comparator; that is, we seek to discriminate between the phases of the two signals incident upon the two solenoids, the relative adjustment of the two phase angles being affected by a shift in trolley position. In this case, the applicable formula

$$\theta = \beta l \tag{261}$$

which gives phase angle θ in terms of the transmission line phase shift constant β and the displacement along the transmission line l, allows us to relate an incremental phase difference to an incremental relative displacement. Thus,

$$\Delta\theta = \beta\Delta l \tag{262}$$

The phase constant of the transmission line is

$$\beta = \frac{\omega}{C} = \frac{2\pi f}{C} \tag{263}$$

63

Accordingly, we may write

$$f = \frac{C \Delta \theta_{/}}{2\pi \Delta \ell} \qquad (264)$$

Now, the $\Delta \ell$ is of the order of 1 cm; if we could arrive at a number for $\Delta \theta$, we could calculate the frequency that would give us this degree of resolution. After some thought, it appears that the signal to noise ratio (S/N) of a phase detector is the determining factor. Conventional phase detectors are able to resolve 1 milliradian without difficulty. If we use this number, we find that a frequency of about 5 megahertz is sufficient to permit minima resolution of 1 cm. A resolution of 3 mm would require a corresponding frequency of 15 megahertz. Now the Allison effect apparatus might be thought of as a phase detector; the problem is that of ariving at a realistic value for the S/N ratio, for this will give us the minimum $\Delta \theta$. Until we know more about the applicable phenomenon, we cannot tell which part of the impulse is signal and which part is noise. If the basic frequency of the exponentially damped oscillation were indeed the signal, then a 1 milliradian phase resolution might be realistic. On the other hand, if some minor component in the frequency spectrum of the burst were responsible for the effect, then the noise would be considerable. At any rate, with this point of view, it would be possible to justify a displacement resolution for relatively low radio frequency values of relatively long rise times.

4. Light Modulation Effects

Every facet of the Allison effect experiment should be explored in our search for a possible explanation. Accordingly, it should be pointed out that the Allison effect apparatus is, intentionally or unintentionally, a light modulator. Carbon bisulfide, for example, is an excellent medium for this purpose; it possesses both strong electro-optic and magneto-optic properties, and indeed has been used in successful light modulators driven by radio frequencies of all values including microwave frequencies[27]. Thus, both the Kerr effect and the Faraday effect are possible mechanisms here. In considering these effects, the investigator is cautioned not to idealize the symmetry of the interaction cells; small components of the main fields could be capable of producing an observable effect. This is true especially for the Kerr effect. The crossed polarizers (also other orientations) and the interaction cells are elements of light modulators. In the case of the Allison experiment, there are two modulators in cascade. It is quite possible that light beats could take place that were visible to the human eye. The eye can discriminate against a very poor S/N ratio and can pick out a minor detail against a background that totally would confuse an electronic detector. It is interesting to note that the cascaded modulators would respond to a phase difference produced by a displacement of modulator cells as well as a phase difference produced by a trolley displacement. In considering the possibility of modulation, it should not be forgotten that light modulation can be produced by absorption modulation as well as electro-optic or magneto-optic modulation.

64

5. B and E as a Function of Time

The explicit solutions for $\underline{B}$ and $\underline{E}$ have not been developed; however, the solutions are given implicitly by the solenoid current expressions of Circuit Model II.

First

One forms the expression for the magnetic vector potential $\underline{A}$ by substituting the solenoid current expression in the formula

$$\underline{A} = (\mu/4\pi)\oint Id\underline{l}/r \tag{265}$$

where μ is the permeability of the medium in the cell and r is the radial distance from the current element $Id\underline{l}$ on the solenoid to the point in the cell at which the vector $\underline{A}$ is being evaluated. The line integral will be over the length of the solenoid; the external leads make only a negligible contribution.

Second

Having $\underline{A}$, one can immediately find the $\underline{B}$ vector from the well-known relation

$$\underline{B} = \nabla \times \underline{A} \tag{266}$$

Third

Having $\underline{B}$, one can find the $\underline{E}$ vector from Maxwell's equation

$$\nabla \times (\underline{B}/\mu) = \frac{\partial}{\partial t} \varepsilon \underline{E} \tag{267}$$

The vector solutions of the wave shapes of the transient solution will contain the magnitude and the direction of the specific field intensity. The helical geometry of the solenoid is taken into account by the line integral of the $\underline{A}$ vector expression. The proximity effect of the two solenoids is taken into account in an indirect way because the mutual inductance of the arrangement plays a part in the determination of the solenoid current expressions for Circuit Model III. (It should be noted that this field interaction is important only for the low frequency components where the mutual inductance is effective.)

The question arises: Should the retarded potential $\underline{A}$ be used, i. e. , should we consider the fields in the solenoids to be radiation fields? The present judgement is that this is not necessary because the dimensions of the solenoid are small compared to the wavelength of the highest frequency for which the current expressions are valid. Naturally, this opinion must remain open to revision in case it turns out that frequencies much over 100 Mcps are involved, or that unusually high dielectric constants are active. Perhaps we should worry about this a little because the dielectric constant of pure water is 81; hence, our cell is effectively a quarter wavelength long at about 75 Mcps. If it does become necessary to employ the retarded potential, the same $\underline{A}$ expression is

used, merely employing (t-r/c) in place of t in the current expressions (t is time and c is the speed of light in the medium -- or actually the speed of the electro-magnetic wave at the frequency involved). In this case, the permittivity of the liquid enters in two ways. Needless to say, the complexity of the solution increases greatly if the retarded potential must be used.

The reader is referred to the spiraling displacement current concept presented in Section I, C, 4. When the A vector is calculated for this current, it will be necessary to transform the line integral to a surface integral because the displacement current must be treated as a surface current.

In a recent NASA publication, Sass and Stoll[28] have used the current sheet concept to calculate the magnetic fields in a finite helical solenoid via the Biot-Savart law (which is closely related to the defined magnetic vector potential). This work appears to be directly applicable to our problem. One is cautioned to associate their helical angle α with the displacement current sheet direction, not the direction of the physical wire turns.

It would be of limited value to run an expensive computer program on the geometry of an arbitrary apparatus. It would be more reasonable to use the theoretical guidelines developed thus far to construct an effective apparatus, and then to insert the numerical values for the parameters of that equipment.

6. Effect of Humidity on Circuit Parameters

Insofar as the circuit analysis is concerned, one can do little more at the moment than relate the humidity to increasing corona losses. This is valid because the corona losses are clearly visible in the equipment and it is well known that they are a function of the humidity. Such losses would be reflected in the circuit analysis as an increase in the effective circuit resistances shown in the various equivalent circuit models. They would cause more rapid damping (increasing resistance), which would result in a spread of the band width of the power spectra around the characteristic frequencies. The trolley lines would become lossy transmission lines; in general, the high frequency energy would be reduced.

Optically, it may be that the water molecules in the atmosphere absorb light frequencies that are needed to produce effects in the water cell. While this is merely conjecture, it is still a strong suspicion that must be checked out by continuing research into the Allison effect.

F. COMPUTER SOLUTION OF SECOND HIGH FREQUENCY APPROXIMATION OF CIRCUIT MODEL III

1. Introduction

The objective of the computer solution of the second high frequency approximation was to find and evaluate expressions for the reference coil current and voltage (I_1, V_1 respectively) and the sample coil current and voltage (I_2, V_2 respectively) for varying values of line delay factors (τ_o, τ_1, τ_2) for the lengths of lead line (l_o), reference line (l_1), and sample line (l_2) respectively. This program has been carried out only for the voltages under consideration; additional work is necessary to extend the program for the current parameters. The derivation of the equations used in these calculations was carried out in paragraph D, 5, Solution 2, of this section.

The Laplace transforms of these quantities, denoted by the additional subscript D, can be expressed in the form

$$V_{1D}(s) = V_o \cdot P(s)/Q(s) \qquad (268)$$

To find $V_1(t)$, $V_{1D}(s)$ must first be expanded into partial fractions. If

$$Q(s) = \prod_{i=1}^{n} (s + a_i) \qquad (269)$$

then

$$V_{1D}(s)/V_o = \prod_{i=1}^{n} \frac{K_i}{(s + a_i)} \qquad (270)$$

where

$$K_i = \frac{P(-a_i)}{\prod_{\substack{j=1 \\ j \neq i}}^{n} (-a_i + a_j)} \qquad (271)$$

To continue, one uses the transform pair

$$F(s) \longrightarrow f(t) \qquad (272)$$

$$\frac{1}{s+a} \longrightarrow e^{-at} \qquad (273)$$

Hence,

$$V_1(t)/V_o = \sum_{i=1}^{n} K_i e^{-a_i t} \qquad (274)$$

which gives $V_1(t)$ explicitly in terms of t.

67

Figure 18 is a graphic presentation of the steps in the computer solution for the voltages and currents.

Schmidt's solution[2] involves the term $\prod\limits_{i=0}^{2} Z_o \tanh(\tau_i s)$.

Since the inverse Laplace transform of this expression is unknown, it is necessary to set

$$Z_o \tanh(\tau_i s) = \frac{M_i(s)}{N_i(s)} \tag{275}$$

$$M_i(s) = Z_o \sinh(\tau_i s) \tag{276}$$

$$N_i(s) = \cosh(\tau_i s) \tag{277}$$

Each of the M's and N's is expressible as an infinite series in s, and, by cutting off these series at a given point, each of the quantities $Z_o \tanh(\tau_i s)$ is approximated by the ratio of two polynomials. Then, the product of the three hyperbolic tangents is approximated by the ratio of the product of the three numerator polynomials and the product of the three denominator polynomials. This ratio, substituted into expression (269), results in the aforementioned fraction $P(s)/Q(s)$.
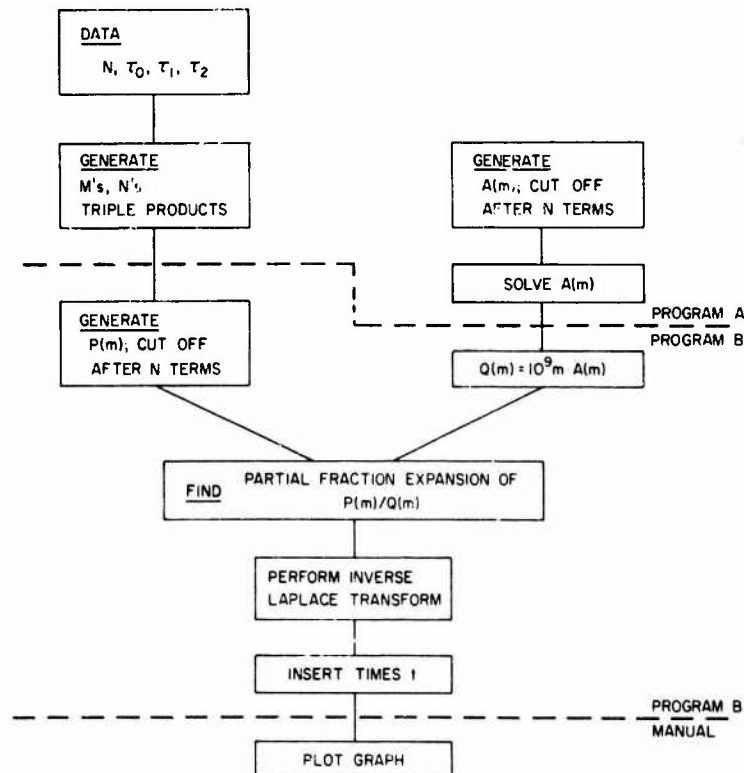
Figure 18. Flow Diagram for Computer Solutions

2. Program A

This program (see Appendix I, A) has as its object the calculation of the polynomical A(m) related to Q(s) by

$$Q(s) = s \cdot A(10^{-9} s) = s \cdot A(m) \tag{278}$$

$$Q(m) = 10^9 \, m \cdot A(m) \tag{279}$$

where
$$m = 10^{-9} s \tag{280}$$

The quantities read in (as DATA) are N, T_o, T_1, and T_2. The integer N is the number of terms after which A(m) is to be cut off, and

$$T_1 = \tau_i \tag{281}$$

Also read in (as DATAFACT) are the values 1/n! for n=o to n=19. These data are stored in the first twenty cells of the vector F. The M_i and N_i series are then computed and stored in

$$M_j (I) = T_j(I-1) \cdot \frac{1}{(I-1)!} \cdot Z_o \tag{282}$$

$$N_j (I) = T_j (I-1) \cdot \frac{1}{(I-1)!} , \quad j = 1, 2, 3 \tag{283}$$

If any of the T_i's is zero, the corresponding M_i and N_i are directly set to 0 and 1, respectively, in order to save computer time.

Each of the M_i and N_i is cut off after N terms, and the various triple products of the M's and N's are calculated and also cut off after N terms. Each of the N terms is an exact term of the infinite series.

The calculation of the triple products is extremely important, since it is here that the restriction $N \leq 7$ is placed upon the number of terms N to which A(m) can be calculated with this program. The Burroughs 220 computer, on which this program was run, can handle quantities of magnitudes from 10^{-51} to 10^{48}. Calculation of a number of magnitude greater than 10^{50} will result in the error message ARITHMETIC OVERFLOW. Any quantity smaller in magnitude than 10^{-51} is set identically equal to zero. The polynomial A(m) has coefficients of reasonable size, but the corresponding polynomial in s, which must be found first, does not. This latter polynomial, the ADJSIGMA (refer to paragraph D, 5, Solution 2 of this section), is stored by the computer in a vector with each term multiplied by 10^{45}, a step necessary to prevent some of the coefficients from being set identically equal to zero because of their small magnitude. The cause of this complication is that the Nth term of ADJSIGMA (s) is of approximate magnitude $(10^{-9})^{N-1}$. This fact was the reason that the

69

substitution of m for 10^{-9} s was originally made in equation (224). Division by $(N-1)!$ reduces the magnitude of the Nth term somewhat further.

It has been estimated in Section I, D, 5 that sufficient convergence and accuracy will not be achieved without twelve or fourteen terms, or possibly more; whether this will be sufficient can be determined only by comparing the final results (the currents and voltages) for various values of N.

Since all terms of ADJSIGMA (s) are less than or equal to 1, it might be thought that the program as it stands could be used to generate ADJSIGMA to ten terms. Unfortunately, this is not the case. The actual limiting factor lies in the calculation of the triple products of M's and N's. For a triple product to be exact to N terms, each of the factor polynomials must also be exact to N terms. This is the reason why each of the M and N polynomials is multiplied by 10^{15} rather than the triple products being multiplied by 10^{45} in their calculation. If the latter were done, the three factor polynomials would be exact only to six terms, all thereafter being zero; hence, the product would be exact to only six terms. The first term in each factor polynomial being 1, the coefficient of a given term in each factor polynomial enters into the coefficient of the term of the same order in the product polynomial. In the equations, if

$$A = 1 + \sum_i^\infty a_i \cdot s^i \tag{284}$$

$$B = 1 + \sum_i^\infty b_i \cdot s^i \tag{285}$$

$$C = 1 + \sum_i^\infty c_i \cdot s^i \tag{286}$$

it follows that

$$(ABC)_i = (a_i + b_i + c_i + \text{other terms}), \quad i \geq 2 \tag{287}$$

where $(ABC)_i$ denotes the ith term of the product series.

Therefore, multiplying each of the factor polynomials by 10^{15} will result in the greatest number of exact terms. Any larger factor will cause the early coefficients of the product to exceed 10^{50}. Now

$$-50 - 15 = -65 \tag{288}$$

If eight terms are to be computed, it must hold that

$$-9(8-1) - \log_{10}\left[(8-1)!\right] > -65 \tag{289}$$

or

$$-63 - 3.7 \qquad\qquad > -65 \tag{290}$$

70

which barely fails to hold. Hence, the largest N, i.e., the greatest number of exact terms able to be generated by the program as it stands, is 7.

As was noted previously, however, it will probably be necessary to go out to twelve, fourteen, or more terms. To do this, a new program is being planned which would create two separate cells for each quantity, instead of just one. In one of the two (cell A) would be stored the (integral) exponent of the quantity when written in scientific notation, or at least the greatest part of it. In the other (cell B) would be stored the first eight significant digits of the quantity, with its sign and an exponent (to base 10) of much smaller magnitude than the integer stored in cell A. In equation form, if a is the integer in cell A and b the number in cell B,

$$b = b_1 \cdot 10^{b_2}, \tag{291}$$

where

$$.1 < b_1 < 1, \text{ and } b_2 \text{ integral,}$$

the actual quantity being represented will be

$$q = b \cdot 10^a = (b_1 \cdot 10^{b_2}) \cdot 10^a = b_1 \cdot 10^{a+b_2} \tag{292}$$

By keeping all quantities in this form, two quantities can be added by setting the integer in the A cell of the first quantity equal to that of the second quantity, adjusting the b_2 of the first quantity accordingly, and then adding the B cells together. In symbols, if

$$p = (b_{1_p} \cdot 10^{b_{1} p}) \cdot 10^{a_p} \tag{293}$$

$$q = (b_{1_q} \cdot 10^{b_2 q}) \cdot 10^{a_q} \tag{294}$$

then

$$p + q = (b_{1_p} \cdot 10^{b_2 p + a_p - a_q} + b_{1_q} \cdot 10^{b_2 q}) \cdot 10^{a_q} \tag{295}$$

Multiplication is less complicated:

$$pq = (b_{1_p} \cdot b_{1_q} \cdot 10^{b_2 p + b_2 q}) \cdot 10^{a_p + a_q} \tag{296}$$

From the size of the program, it is evident that such a necessary procedure will be time consuming in terms of both writing and computer time.

After A(m) has been computed, it is printed out on a line in increasing term order. The original data are also printed out. Thereafter, the coefficients of A(m) are reversed in their array, with the coefficient of the Nth term taken

71

out of the array and called AO. This change was made to fit the second part of the program. Then (and here some confusion may result) the denotation of N is changed. Henceforth, N denotes the <u>degree</u> of A(m), not the number of terms. The degree is one less than the number of terms, because the first term (1) has degree 0.

The rest of Program A solves for the roots of A(m). This part of the program, as noted in the COMMENT declaration, is a polynomial solver[29], modified for this program with regard to output-format and exists from the procedure. Precisely how the procedure works is unknown, but it appears to be a version of either the Bairstow or the Bernoulli iteration method. It was tested and found to work relatively consistently. If the iterations do not converge, PROCEDURE FAILS is printed. Another unplanned failure occurs occasionally when the procedure finds only one pair of complex roots and declares that the rest of the roots are identical. That is, multiple roots are reported to occur when, in reality, they do not. These deficiencies will be eliminated in the future by using a standard polynomial solver, probably employing the "down-hill" method.

It was noticed from the results from Program A that the real components of complex roots of A(m) are very small, less that 10^{-3}. Hence, to save time and effort, they are neglected in the further calculations given in Program B. From the complex values, the frequencies are computed. The characteristic frequency ω is simply the imaginary part of the root of Q(s), or 10^9 times the imaginary part of P(s). Figures 19 to 21 show the characteristic frequencies for several variations of the τ's; each pair of complex, conjugate roots generates one frequency, as demonstrated in Equations (225) to (231).

3. <u>Program B</u>

The object of Program B (see Appendix I, B) is to generate the P(m) polynomial of the P(m)/Q(m) ratio, which is terminated after N terms, and then to find the partial fraction expansion of the ratio P(m)/Q(m). It then performs the inverse Laplace transform, substitutes various times T, and prints out the voltage at these times.

For convenience, only odd N are used where N again denotes the number of <u>terms</u>. (This change in N again was made so as to be able to use some data cards made out beforehand using the old meaning of N.) This means that only the imaginary parts of complex roots are used in the calculations. Read in (as DATAFACT) are the same inverted factorials as in Program A. Also read in (as AR) were N, T_o, T_1, T_2, the polynomial A(m), and the complex parts of its roots (stored in the array V).

The M's and N's are again generated, along with some necessary triple products. Once more, the meaning of N is changed to denote the <u>degree</u> of A(m).

72
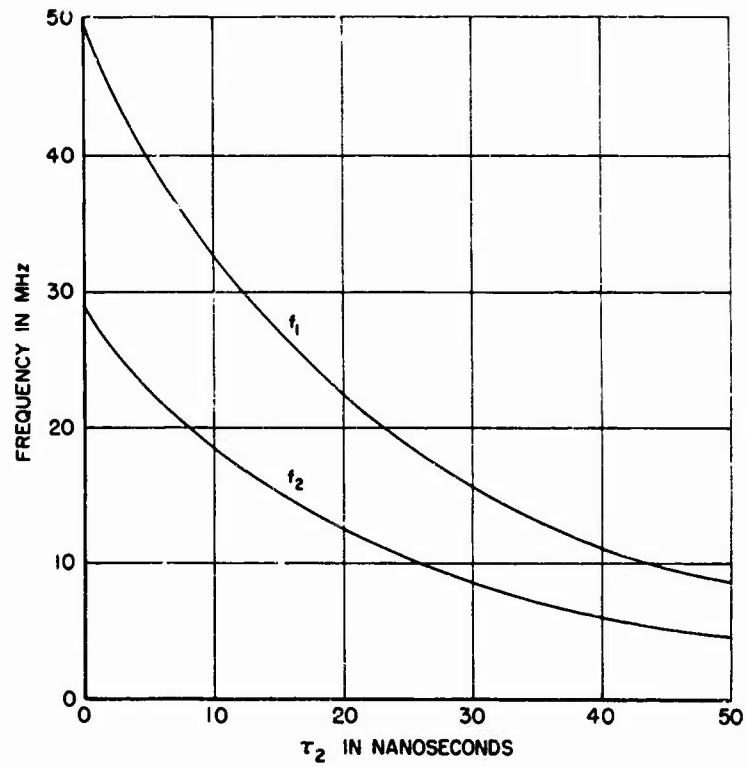
Figure 19. Characteristic Frequencies of an Unbalanced Circuit, $\tau_O = \tau_1 = 0$, τ_2 Variable, N = 4
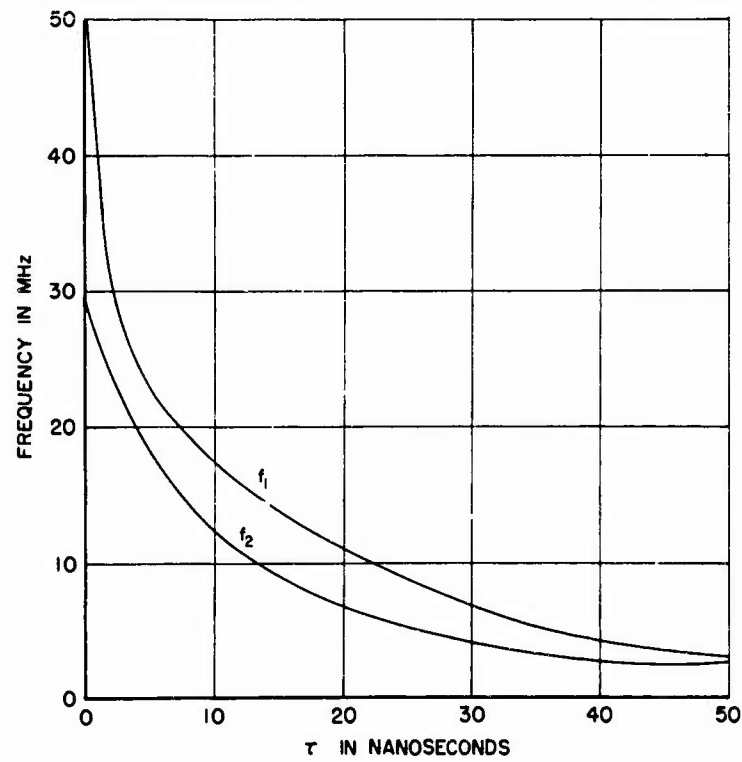
Figure 20. Characteristic Frequencies of a Balanced Circuit, $\tau = \tau_O = \tau_1 = \tau_2$, N = 4

73
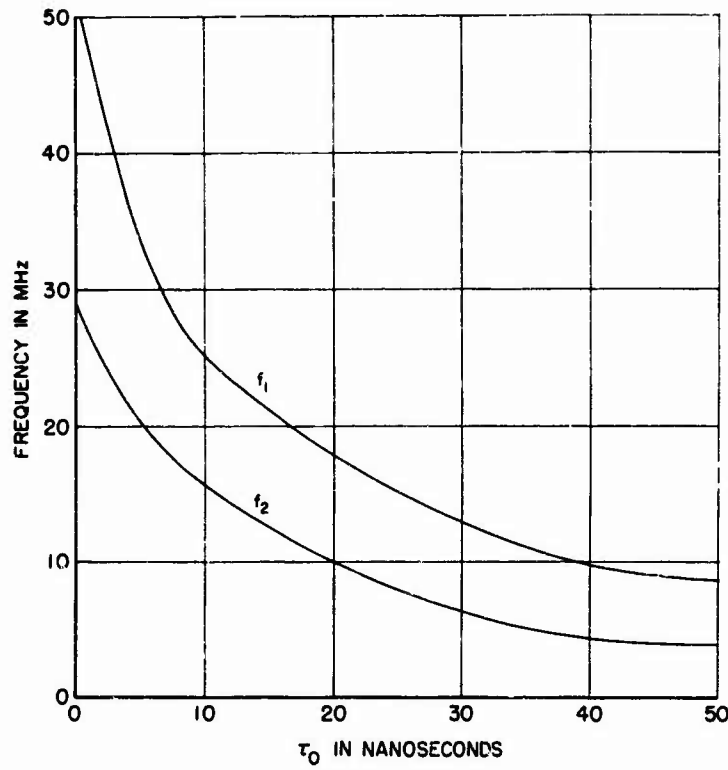
Figure 21. Characteristic Frequencies of an Unbalanced
Circuit, $\tau_1 = \tau_2 = 0$, τ_0 Variable, $N = 4$

The polynomial $P(m)$ is calculated by rearranging equation (233):

$$P(s)/V_o = C_1 N_o N_1 N_2 + s(C_1 C_2 R_3 N_o N_1 N_2 + C_1 C_2 N_o N_1 M_2)$$

$$+ s^2 (C_1 C_2 L_3 N_o N_1 N_2) \tag{297}$$

where

$$s = 10^9 m \tag{298}$$

remembering that the triple products are infinite series. The calculation of $P(m)$ involves the same limitation noted above in connection with $A(m)$. It was decided to calculate $P(m)$ to as many terms as $A(m)$. Thus, it has one less term than

$$Q(m) = 10^9 m \cdot A(m) \tag{279}$$

Then

$$V_1 D / V_o = \frac{P(s)}{Q(s)} = \frac{P(s)}{s \cdot A(s)} \tag{299}$$

To perform the inverse Laplace transformation and find V_1 / V_o, it is necessary to find the partial fraction expansion of $P(s)/Q(s)$:

74

$$\frac{P(s)}{Q(s)} = \sum_{i=1}^{m} \frac{K_i}{(s + a_i)} \tag{300}$$

where the a's are the roots of Q.

The problem is to find the K's. There are two theoretical considerations of great importance to be noted:

(1) The coefficients of the partial fractions for $P(s)/Q(s)$ are the same as for $P(m)/Q(m)$.

(2) For a pair of complex conjugate roots of Q, the coefficients of the corresponding partial fractions are complex conjugates.

Proof of (1):

$$m = 10^{-9}s \quad \text{again,} \tag{280}$$

consider

$$\frac{P(x)}{Q(x)} = \frac{C(x-x_A)(x-x_B) \cdots (x-x_z)}{(x-x_1)(x-x_2) \cdots (x-x_n)} \tag{301}$$

$$\frac{P(x)}{Q(x)} = \sum_{i=1}^{n} \frac{K_{i,x}}{x-x_i} \tag{302}$$

and

$$\frac{P(kx)}{Q(kx)} = \frac{C(kx-x_A)(kx-x_B) \cdots (kx-x_z)}{(kx-x_1)(kx-x_2) \cdots (kx-x_n)} \tag{303}$$

let

$$w = kx \tag{304}$$

$$\frac{P(kx)}{Q(kx)} = \frac{C(w-x_A)(w-x_B) \cdots (w-x_z)}{(w-x_1)(w-x_2) \cdots (w-x_n)} \tag{305}$$

$$\frac{P(kx)}{Q(kx)} = C \sum_{i=1}^{n} \frac{K_{i,w}}{kx-x_i} \tag{306}$$

by equation (303) on the preceding page, with the same K's as before, except that their previous dimension was $1/w$, whereas it now is $1/x$.

In the application to the present case,

$$x \equiv m \tag{307}$$

$$k \equiv 10^{-9} \tag{308}$$

$$w = kx \equiv s \tag{309}$$

$$x_i = a_i \tag{310}$$

Hence,

$$\frac{P(m)}{Q(m)} = \sum_{i=1}^{n} \frac{K_{i,m}}{m - a_i} \tag{311}$$

$$\frac{P(s)}{Q(s)} = \sum_{i=1}^{n} \frac{K_{i,s}}{s - a_i} \tag{312}$$

$$= \sum_{i=1}^{n} \frac{K_{i,s}}{10^{-9} \cdot m - a_i} \tag{313}$$

$$= \sum_{i=1}^{n} \frac{10^{9} \cdot K_{i,s}}{m - 10^{9} \cdot a_i} \tag{314}$$

The right-hand side has the dimension $1/s$ built into the constant $K_{i,s}$, whereas the right hand side of equation (311) has the dimension $1/m$ built into the constant $K_{i,m}$; the underlying reason for this being that Q is of one degree greater than P. The equation of conversion for the constants is

$$K_{i,s} = K_{i,m} \cdot 10^{-9} \tag{315}$$

Consequently,

$$V_{1D}/V_o = \frac{P(s)}{Q(s)} = \sum_{i=1}^{n} \frac{K_{i,m}}{m - 10^{9} \cdot a_i} \tag{316}$$

End of Proof.

76

The procedure of the program is to calculate the $K_{i,m}$'s from equation (311) using the relationship

$$K_{i,m} = \frac{P(-a_i)}{\prod_{\substack{j=1 \\ j \neq i}}^{n}(-a_i + a_j)} \tag{271}$$

Actually, the denominator polynomial $Q(m)/m^2 + a_1^2$ is generated by synthetic division and both it and $P(m)$ were evaluated by transforming to polar coordinates and using the convenience of DeMoivre's Formula. (Most of the program was written for more general cases than the special case considered here, which involves (1) no real roots, meaning the entire BEGIN --- END segment after IF U(I) EQL O was never executed; and (2) neglecting the real facts of the complex roots, meaning DeMoivre's formula is overcomplicated for the present situation. The programming was done as generally as possible, for the future.) The vectors $V_1, \ldots, V_6$ are needed for this complex arithmetic which is, in general, straightforward. The matrix KK, a 2-column array, is introduced to hold the real and imaginary part of the partial fraction coefficients.

Proof of (2):

Let the pair of roots be $x_1 = a+bi$, $x_2 = a-bi$.

Then

$$K_{x_1} = \frac{P(a+bi)}{B(a+bi) \cdot 2bi} \tag{317}$$

$$K_{x_2} = \frac{P(a-bi)}{B(a-bi) \cdot (-2bi)} \tag{318}$$

where

$$B(x) = \frac{Q(x)}{x^2 - 2ax + b^2} \tag{319}$$

B(a+bi) can be expressed

$$B(a+bi) = C + Di + Ei^2 + Fi^3 \tag{320}$$

$$= C + Di - E - Fi = (C-E) + i(D-F) \tag{321}$$

Then

$$B(a+bi) = C - Di - E + Fi = (C-E) - i(D-F) \tag{322}$$

77

More simply,

$$B(a+bi) = G + Hi \qquad (323)$$

$$B(a-bi) = G - Hi \qquad (324)$$

Similarly,

$$P(a+bi) = R + Si \qquad (325)$$

$$P(a-bi) = R - Si \qquad (326)$$

Then,

$$K_{x_1} = \frac{R+Si}{(G+Hi) \cdot 2bi} \qquad (327)$$

$$K_{x_2} = \frac{R-Si}{(G-Hi) \cdot (-2bi)} \qquad (328)$$

Realizing the denominators,

$$K_{x_1} = \frac{(R+Si)\ (G-H)(-i)}{(-2b)\ (G^2+H^2)} = \frac{(HR-GS) + i\ (RG+HS)}{(-2b)\ (G^2+H^2)} \qquad (329)$$

$$K_{x_2} = \frac{(R-Si)\ (G+Hi)(-i)}{(-2b)\ (G^2+H^2)} = \frac{(HR-GS) - i(RG+HS)}{(-2b)\ (G^2+H^2)} \qquad (330)$$

It is evident now that the two coefficients are complex conjugates.

<u>End of Proof.</u>

Call the two coefficients $A+Bi$, $A-Bi$ (not to be confused with the polynomials of the same name). Then

$$V_{1D}/V_o = \dots + \frac{A+Bi}{s-(a+bi)} + \frac{A-Bi}{s-(a-bi)} + \dots \qquad (331)$$

The inverse Laplace transform of this is

$$V_1/V_o = \dots + (A+Bi)\ e^{(a+bi)t} + (A-Bi)\ e^{(a-bi)t} + \dots \qquad (332)$$

<u>t expressed in nanoseconds</u>
The reason for this lies in equation (316).

$$V_1 / V_o = \ldots + e^{at} \Big[A \cos bt + i A \sin bt + Bi \cos bt$$

$$+ A \cos bt - i A \sin bt - Bi \cos bt + Bi^2 \sin bt \Big] + \ldots \quad (333)$$

$$= \ldots + 2e^{at} \Big[A \cos bt - B \sin bt \Big] + \ldots \quad (334)$$

If there is a real root c, with corresponding partial fraction coefficient C, then its inverse Laplace transform is Ce^{ct}.

The quantity TOTAL is the evaluation of V_1 / V_o at a particular time t; the number 1 added on to TOTAL is the contribution due to the root $s = 0$ of $Q(s)$. That this contribution is 1 was shown in equation (256). The whole process is then reiterated for V_2, starting with a different $P(m)$ polynomial.

The output shows V_1 / V_o for various values of T (in nanoseconds): T=1, 2, ... 20, 30, 40, 50, 100, and the same for V_2 / V_o. At T=0, both voltages should be zero; derivations for this are probably due to the neglect of the real parts of the roots of $Q(m)$.

Figures 22 to 27 show how the two voltages vary with variation of the τ's.

The case $\tau_o = \tau_1 = \tau_2 = 0$ has been completely calculated by hand and found to agree with the computer's solution. It might be noted that, for this case, the second high frequency approximation is identical to the first.

In this instance,

$$V_1 / V_o = V_2 / V_o = 1 - \cos \left(\sqrt{10} \cdot 10^8 t \right) \quad (335)$$

<u>t in nanoseconds</u>

Similar explicit equations can be written for other combinations of the τ's.
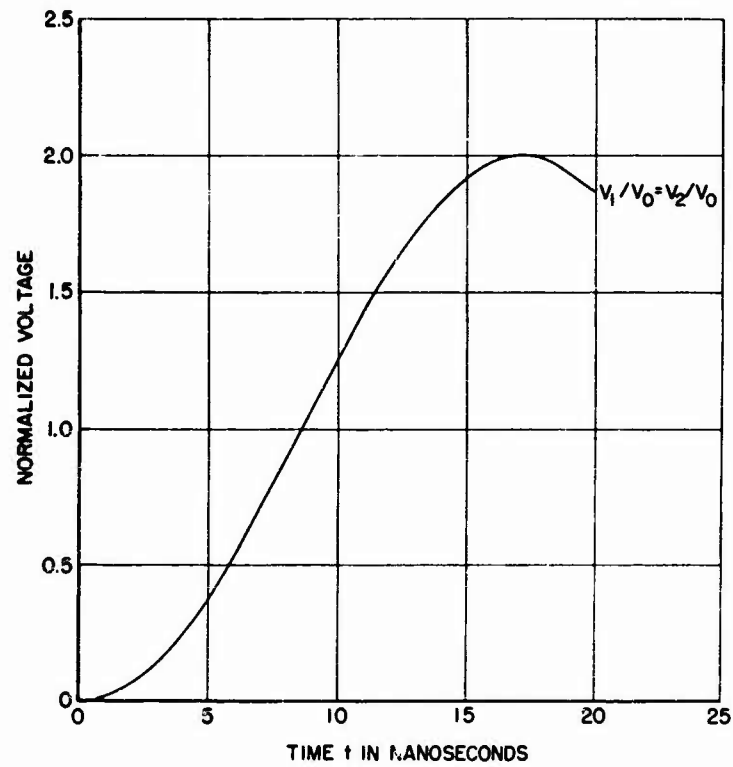
Figure 22. Balanced Circuit, V_1/V_o, V_2/V_o Coincide,
$\tau_o = \tau_1 = \tau_2 = 0$, $N = 4$

Figure 23. Unbalanced Circuit, $\tau_o = \tau_1 = 0$,
$\tau_2 = 2$ nanoseconds, $N = 4$

80

Figure 24.   Unbalanced Circuit, $\tau_0 = \tau_1 = 0$,
$\tau_2 = 2$ nanoseconds, $N = 6$
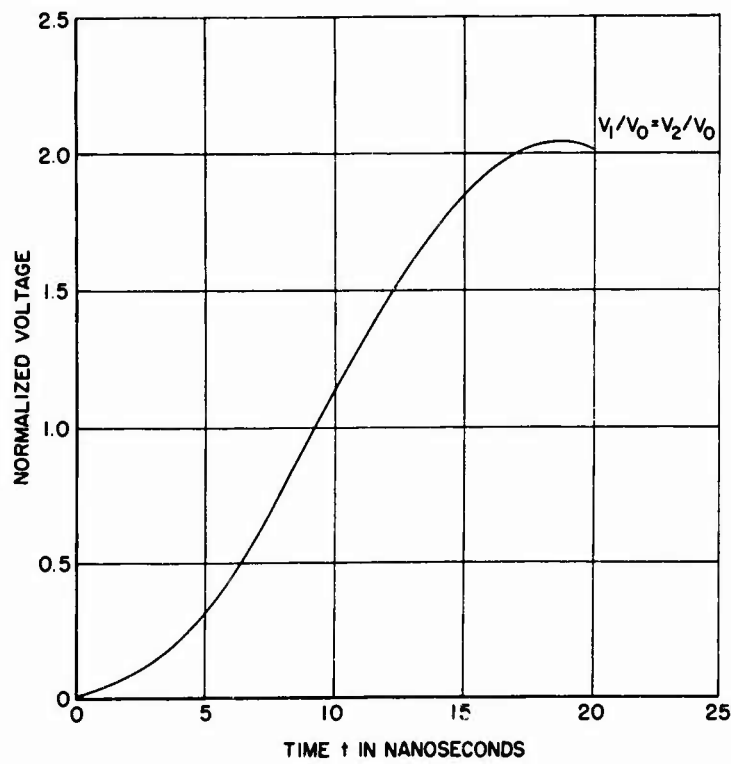
Figure 25.   Balanced Circuit, V_1/V_0, V_2/V_0 Coincide,
$\tau_1 = \tau_2 = 0$, $\tau_0 = 1$ nanosecond, $N = 4$

81
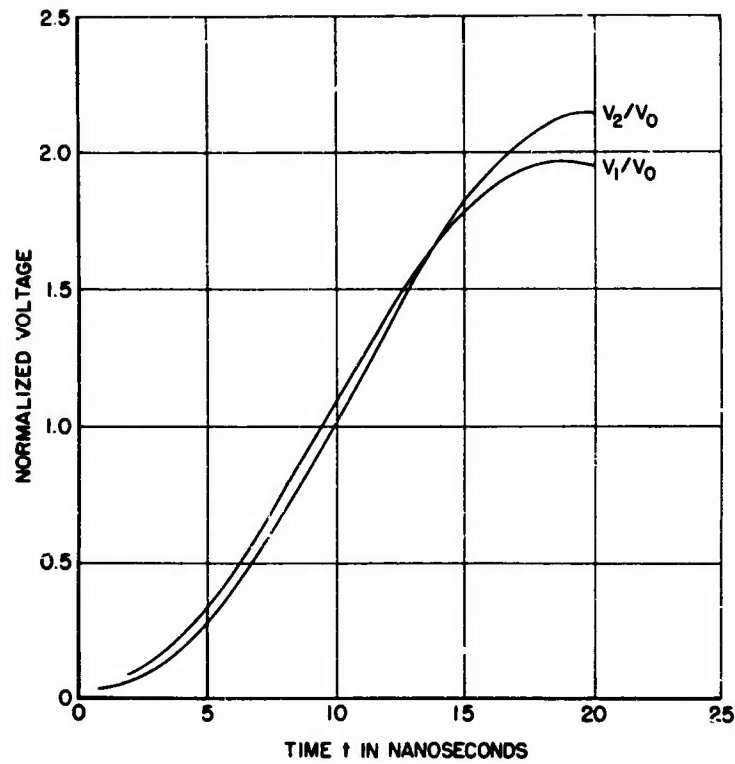
Figure 26. Unbalanced Circuit, $\tau_0 = \tau_2 = 1$ nanosecond, $\tau_1 = 0$, $N = 4$
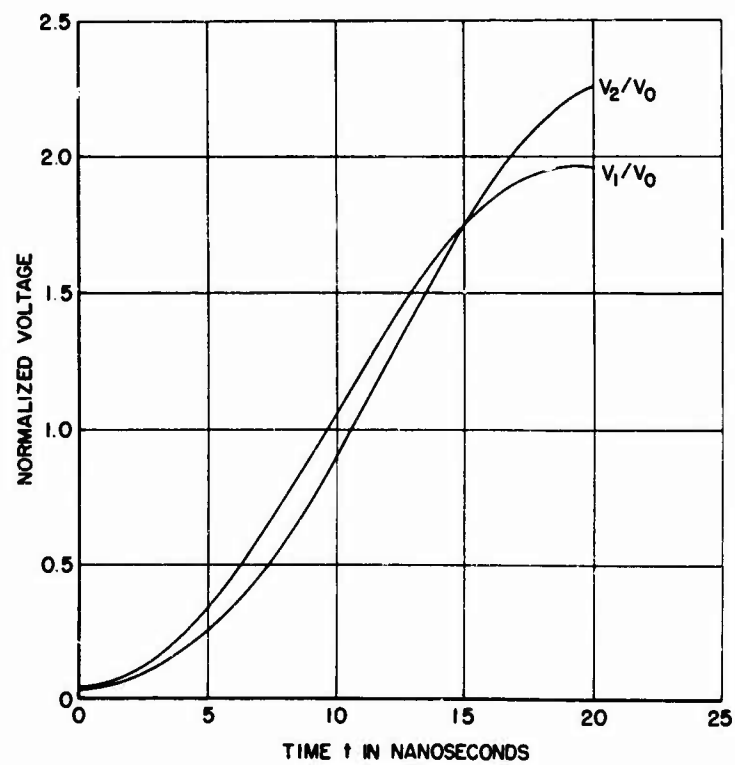
Figure 27. Unbalanced Circuit, $\tau_0 = 1$ nanosecond, $\tau_1 = 0$, $\tau_2 = 2$ nanoseconds, $N = 4$

82

SECTION II

EXPERIMENTAL INVESTIGATIONS

The experimental phase of this program was concerned primarily with the gathering of clear, objective evidence coordinated to assist in the theoretical circuit analysis developed by Schmidt[2]. In particular, those experimental techniques and observations which would substantiate the theoretical assumptions and conclusions were given the utmost consideration.

A. ALLISON EFFECT APPARATUS

1. Introduction to Circuits and Apparatus

As the program developed, extensive measurements and observations were performed on three separate apparatuses constructed to demonstrate the Allison effect: a) the original apparatus, which will be referred to as APL-1 (Aero Propulsion Laboratory, Allison Effect Apparatus Model 1); b) an apparatus currently in use by Allison; c) the subsequent modification of APL-1 to APL-2 (Aero Propulsion Laboratory, Allison Effect Apparatus Model 2). For future reference and apparatus design considerations, these apparatuses will be discussed in detail, particularly with relation to the latest configuration employed by Allison.

2. Circuit Description and Construction of APL-1

Initial investigations conducted in the program were performed with the electrical apparatus illustrated in Figure 28, which was furnished by the Aero Propulsion Laboratory. The design and construction of this system was based upon the theoretical considerations given to the physical construction of earlier apparatuses as described by Allison and more clearly defined by Cooper[17]. However, certain liberties were taken with the physical layout of the trolley lines to facilitate the use of the apparatus in the confines of a normal laboratory area.

Trolley line construction consisted of two sets of parallel-spaced (10.26 centimeters) lines approximately ten and a half Allison units long (one Allison unit being equal to a 15 centimeter scale length). It was the intention that equivalent additional lengths of the line could be introduced by switching in successive two-meter lengths in the sample trolley lines as required.

The reference and sample coil construction consisted of 60 turns of number 18 enameled solid copper wire wound on a 1.5 inch diameter polystyrene core form 5 inches long, which in turn was supported by a phenolic holder.

83

Electrically, the capacitor charging circuit utilized a half-wave high-vacuum rectifier tube V (type 8020), a 5 volt center tapped transformer T_1 (Thordarson - 27F125), and a 0-25 kilovolt high voltage transformer T_2 (Thordarson - 24P79) for stepping up the powerstat controlled (T_5 - Superior Q117U) primary voltage to the desired level for stable spark breakdown. The charging capacitor itself consisted of a series-parallel combination of 0.05 microfarad, 3000 volt-rated capacitors to yield an equivalent 0.02 microfarad (0.0183 actual) capacitor with a high maximum voltage rating. Transformers T_3 and T_4 were used as line isolation transformers.
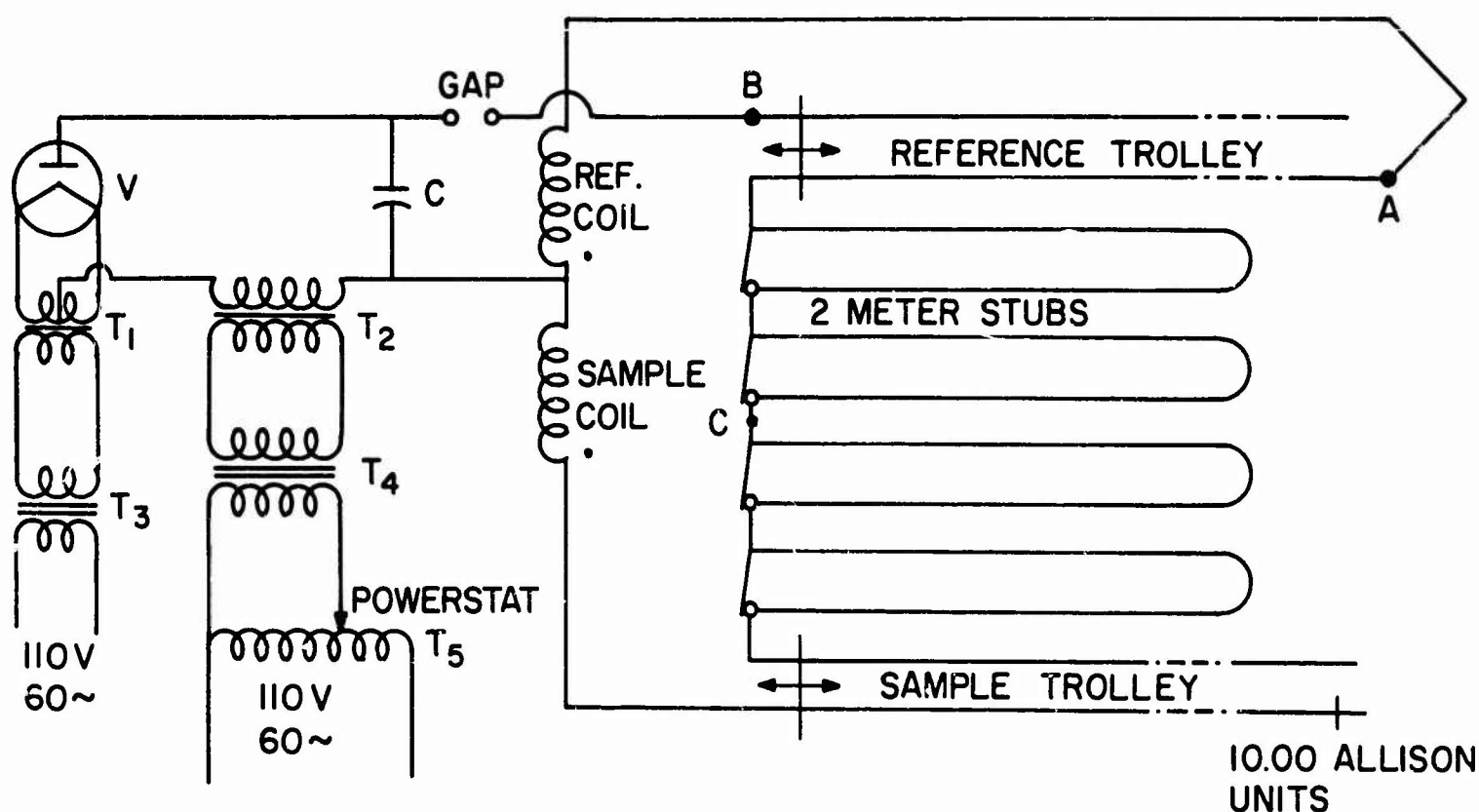
Figure 28. Electrical Circuit Layout APL-1

The optical components employed in the apparatus consisted of: a) double convex lens (focal length 15 centimeters); b) filter (Kodak Wratten Gelatin numbers 35 and 47B); c) Glan Thompson polarizing prism; d) Nicol polarizing prism mounted in a divided analyzing circle equipped with vernier scale graduated in tenths of a degree; e) glass cells and spacers (see Figure 29).

Each component was supported as illustrated in Figure 30 and could readily be adjusted in any of three axes by screw adjustments on the optical bench carriers. All critical wire leads and terminations were supported from the apparatus surface with polystyrene spacers.
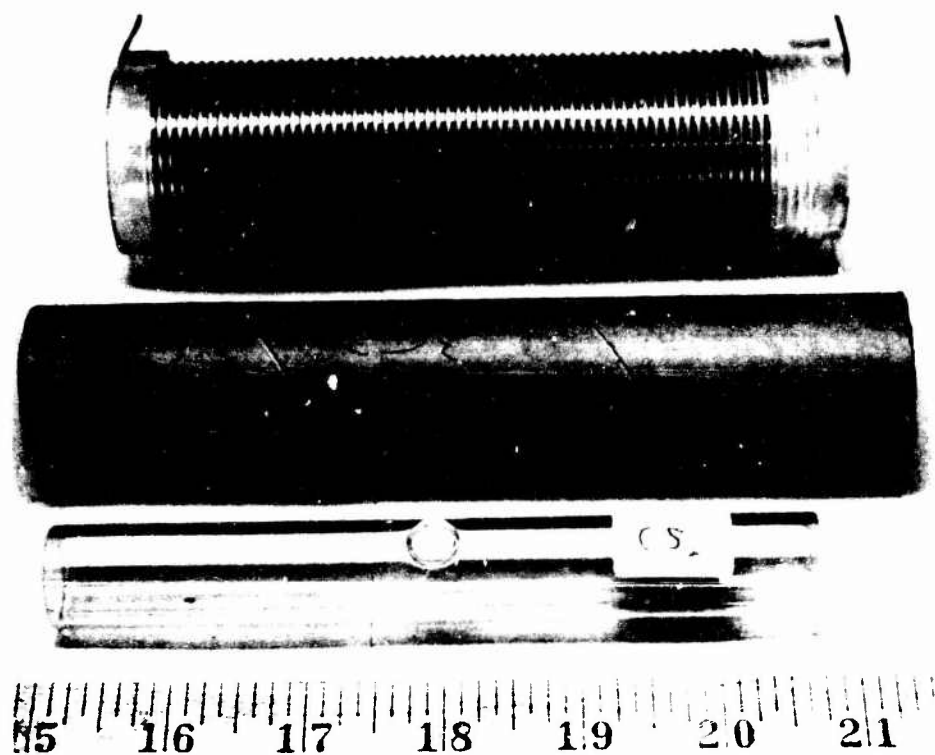
Figure 29. Coil Assembly, Paper Spacer, Glass Cell
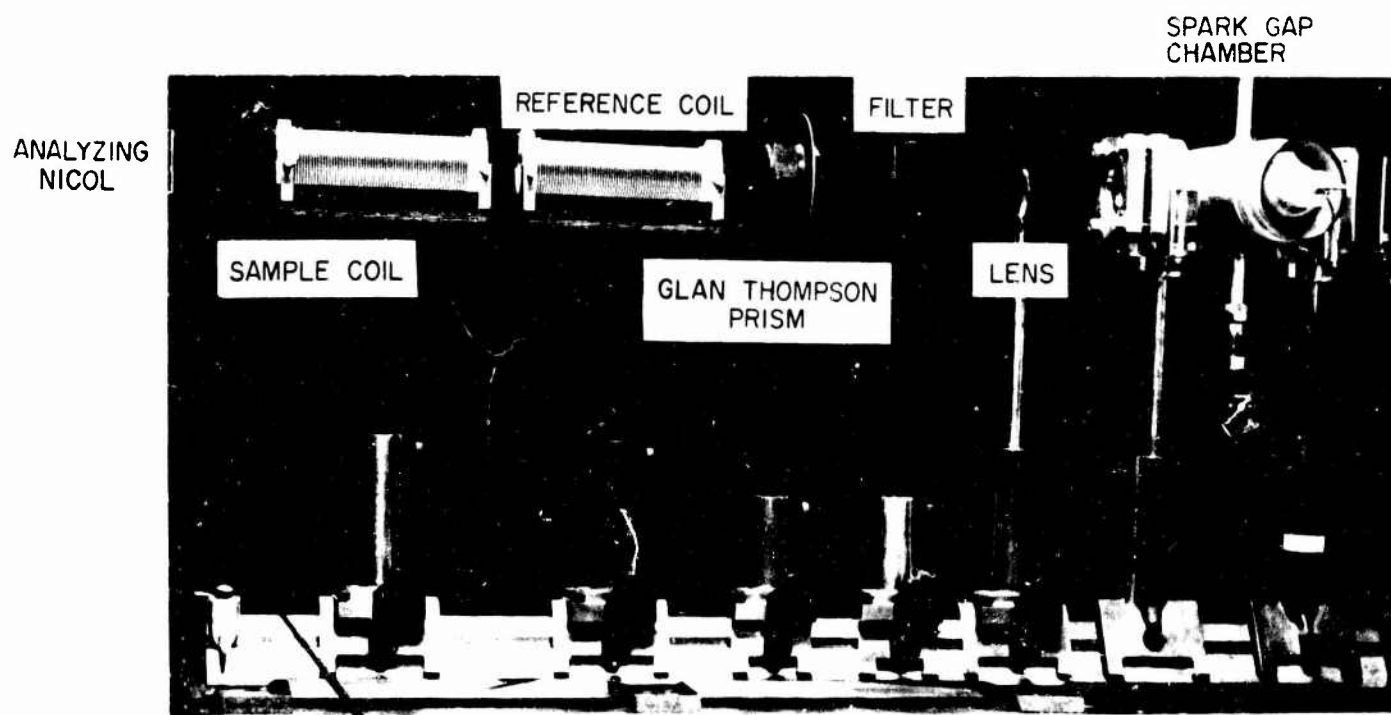
Figure 30. APL-1 Component Placement

85

3. Circuit Description and Construction of Allison's System

To bring the available sources of information up to date, a visual inspection of this system was performed, and subsequent discussions indicated the latest revisions that Allison performed on his original apparatus. This latest configuration is presented in schematic form in Figure 31.
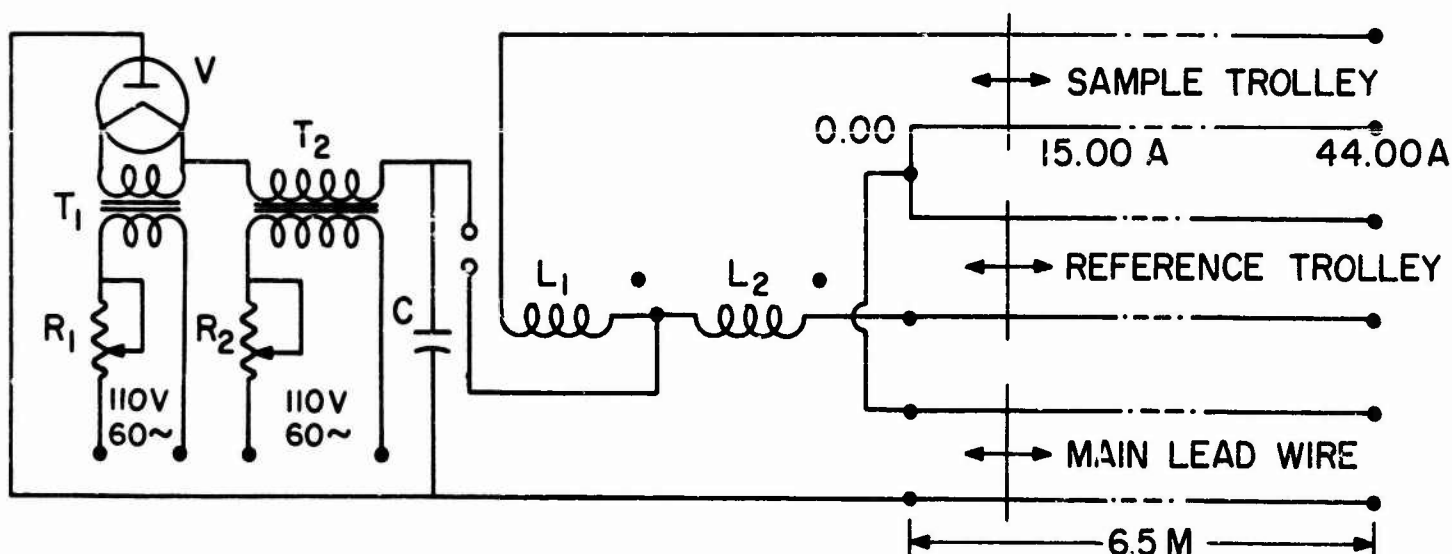
Figure 31. Electrical System of Allison's Apparatus

The installation of the trolley lines for this particular apparatus is usually restricted only by the confines of the maximum dimensions of the particular laboratory room available (in this case, 6.5 meters). That is to say, for convenience, the trolley lines are attached by polystyrene insulators to panels secured to opposite walls of the room. The spacing of the number 18 gauge solid copper wire lines is approximately 20 centimeters apart. Additional parallel trolley lines are available but are not in use at the present time. The main variation in the treatment of the trolley lines from earlier papers is that Allison no longer uses trolley lines symmetrical about each coil as originally shown in discussions of his work. In addition, he has now incorporated a main slidewire immediately preceding the distribution to the sample and reference trolley lines.

Electrically, the charging circuit has remained the same, a vacuum rectifier tube V (Kenotron KP2), the high voltage transformer T_2 (Thordarson type R, 110-24kv), two filament transformers in series T_1 (G. E. type Y2052), an adjustable 45 ohm power resistor R_1 in the primary of the filament transformer, and an adjustable 95 ohm power resistor R_2 in the primary of the high voltage transformer.

86

The construction of the coils (L_1 and L_2) consisted of 73 turns of number 18 gauge solid copper enameled wire wound on a bakelite core form six inches long. The inductance of the coils was checked and found to be 51 microhenries. A capacitor (C) was constructed of parallel sheets (6 inches x 18 inches) of copper stock with a 4.2 millimeter glass separator. Eight sections similarly constructed were connected in parallel for an equivalent capacitance measured to be 0.0152 microfarads.

Optically, the system has two Nicol polarizing prisms, one placed between the lens and reference coil, and the other located in the analyzing circle. The lens is a camera quality lens with a focal length of approximately 22 centimeters. Of significant importance is the fact that the lens is no longer placed at the focal point with respect to the spark gap, but slightly beyond. Although the image is not as sharp, this makes it possible to obtain a larger spot diameter which is controlled by light stops at the lens and the first Nicol prism.

With regard to the spark gap, additional comments are necessary to the satisfactory operation of the spark for the generation of the light source and electrical pulses. To reduce the effective electrode wear, the use of one magnesium and one tungsten electrode is incorporated into the spark gap assembly. Electrode diameters are approximately forty to sixty thousandths of an inch in diameter, with flattened ends to restrict the region over which the spark discharges can arc across. Electrode spacing is usually on the order of one-eighth of an inch. Equally as important with regard to electrode wear is the placement of the tungsten electrode in the line connected to the secondary of the high voltage transformer. Interchanging of electrodes results in much faster electrode ablation, with the consequence that the light level fluctuates and is rapidly attenuated due to the deposit of magnesium oxide powder over the aperture windows of the assembly. There is usually some small trace of oxygen present in the argon gas due to the nature of the process used to prepare the gas.

4. Circuit Description and Construction of APL-2

This particular apparatus evolved from the previous model, additional knowledge gathered from experience with Allison's apparatus, and other modifications used to improve the functional operation of the apparatus.

Four major changes were made. The existing trolley lines were replaced with lines similar to those on Allison's apparatus but limited in length to approximately 5 meters due to the size of the room. The double convex lens was replaced by a Wollensak 162 millimeter enlarging Raptar lens with a built-in adjustable stop. An additional light stop was placed between the Glan Thompson polarizing prism and the reference coil (see Figure 32), and a
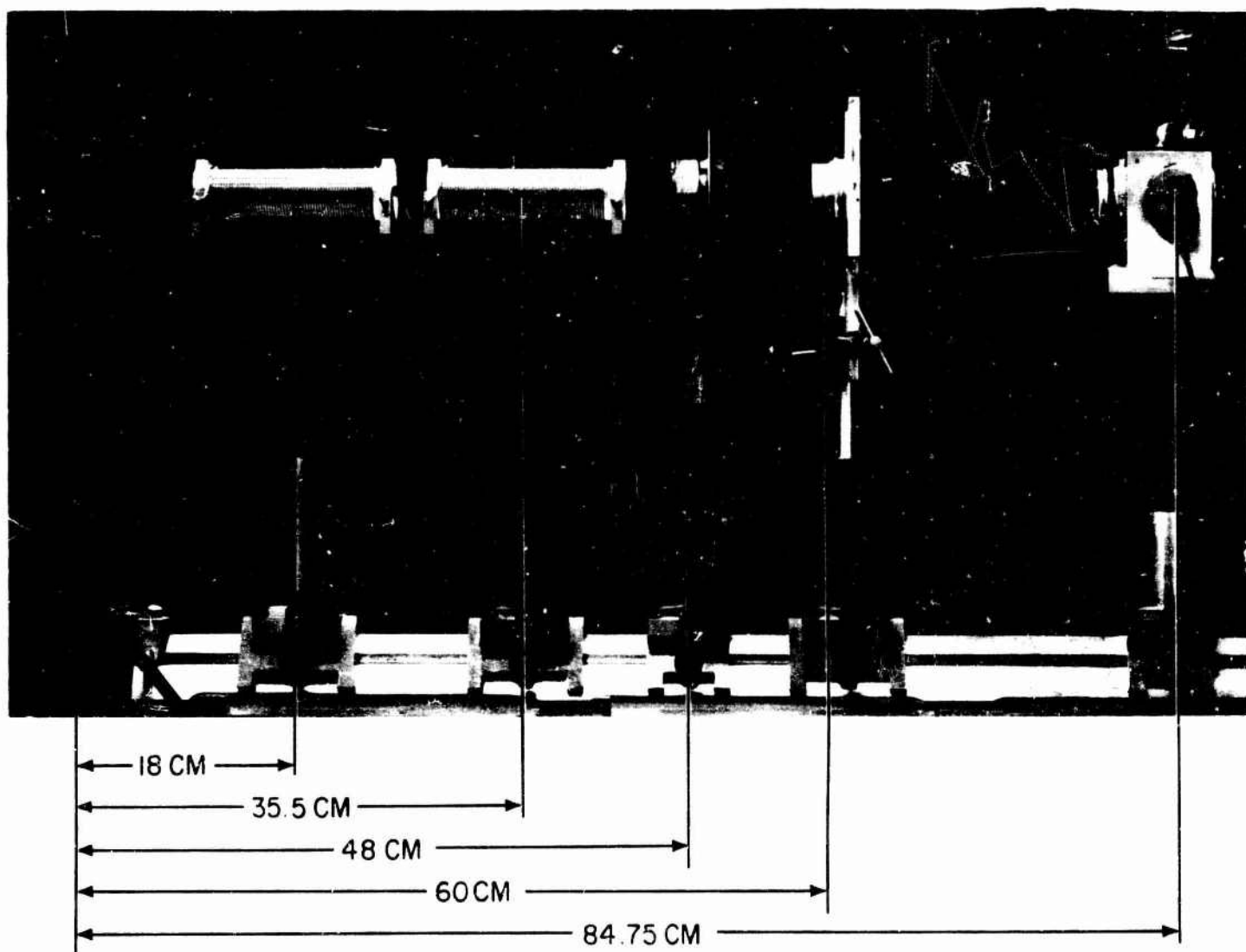
Figure 32. APL-2 Component Placement
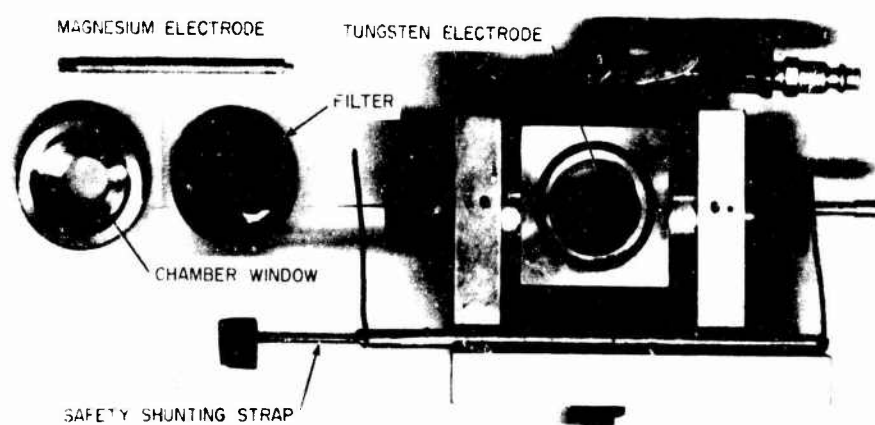
Figure 33. Spark Gap Assembly

redesigned spark gap assembly was adapted to the rapid dissassembly of the electrodes and aperture windows for ease of adjustment and maintenance (see Figure 33).

The electrical configuration of the trolley lines and capacitor charging supply is shown in Figure 34, which includes a close approximation of the layout of the lines.
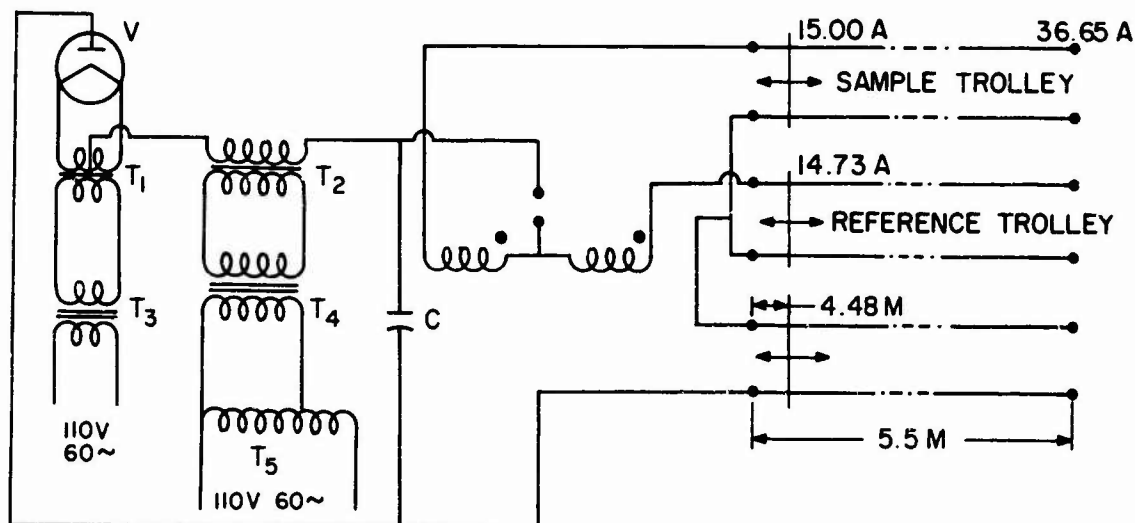
Figure 34. Electrical Circuit APL-2

B. MEASUREMENT OF SAMPLE AND REFERENCE COIL PARAMETERS

1. Introduction to Coil Measurements

During the course of the initial investigations conducted with the APL-1 apparatus, the coils used in the system were extensively measured and compared with regard to their characteristic parameters over a frequency range of 150 kilohertz to 4 megahertz. During the development of the earlier theoretical models of the apparatus, this frequency range was considered to be the area of primary interest for these particular measurements. In addition, the range was restricted by the limitations of the test equipment available, although subsequent modifications were performed tc extend the range within a certain degree of accuracy. The curves presented in the following paragraphs were plotted from calculations performed with the data recorded from a Boonton Q-Meter, Model 160 A.

2. Inductance vs. Frequency

The procedure used in testing the coils was as follows: the inductance of each coil was measured over the frequency range of 200 kilohertz to 4 megahertz under six separate conditions, the coil alone, the coil and a paper spacer tube

within the coil, the coil with the glass cell, the coil with the paper spacer tube and glass cell, the coil with triple distilled water in the cell, and the coil with carbon disulfide in the cell.

Using the equation to calculate the effective inductance,

$$L_s = \frac{1}{(2\pi)^2 \, f_r^2 \, C_1} \tag{336}$$

where f_r is the resonant frequency selected on the Q-Meter, and C_1 is the value of the tuning capacitance required to peak the tuning of the coil at resonance. The distributed capacitance of the coils can also be determined simply by placing the coil across the input terminals, dialing a particular value of tuning capacitance C_1, resonating the Q circuit by adjusting the oscillator frequency, regulating the frequency to $f_r/2$, and retuning the Q circuit by adjusting the tuning capacitance C_2. Then the distributed capacitance can be determined from the equation

$$C_d = \frac{C_2 - 4C_1}{3} \tag{337}$$

This procedure was repeated several times over different frequency ranges and an average value determined.

In Figure 35, a presentation of data and calculations for each coil is plotted in comparison with the worst case, that is, with the coil and triple distilled water in the cell. In general, even when compared to the worst case, the curves are the same until the frequency is raised above 2 megahertz. At this point, the curve for the coil with the cell and triple distilled water increases at a faster rate for an increase in frequency. Over this frequency range, the average inductances for the sample coil and reference coil are 38.5 micro-henries and 38.8 microhenries respectively. The distributed capacitances of each coil are 7.85 picofarads and 7.8 picofarads respectively.

3. Series Resistance vs. Frequency

The series resistance for each coil under the same conditions (as in Section II. B. 1) was also measured and calculated from the equation

$$R_s = \frac{1}{2\pi f_r Q_r C_1} \tag{338}$$

where f_r is again the resonant frequency, C_1 is the tuning capacitance for resonance, and Q_r is the peak meter reading at the resonant point. The graphs
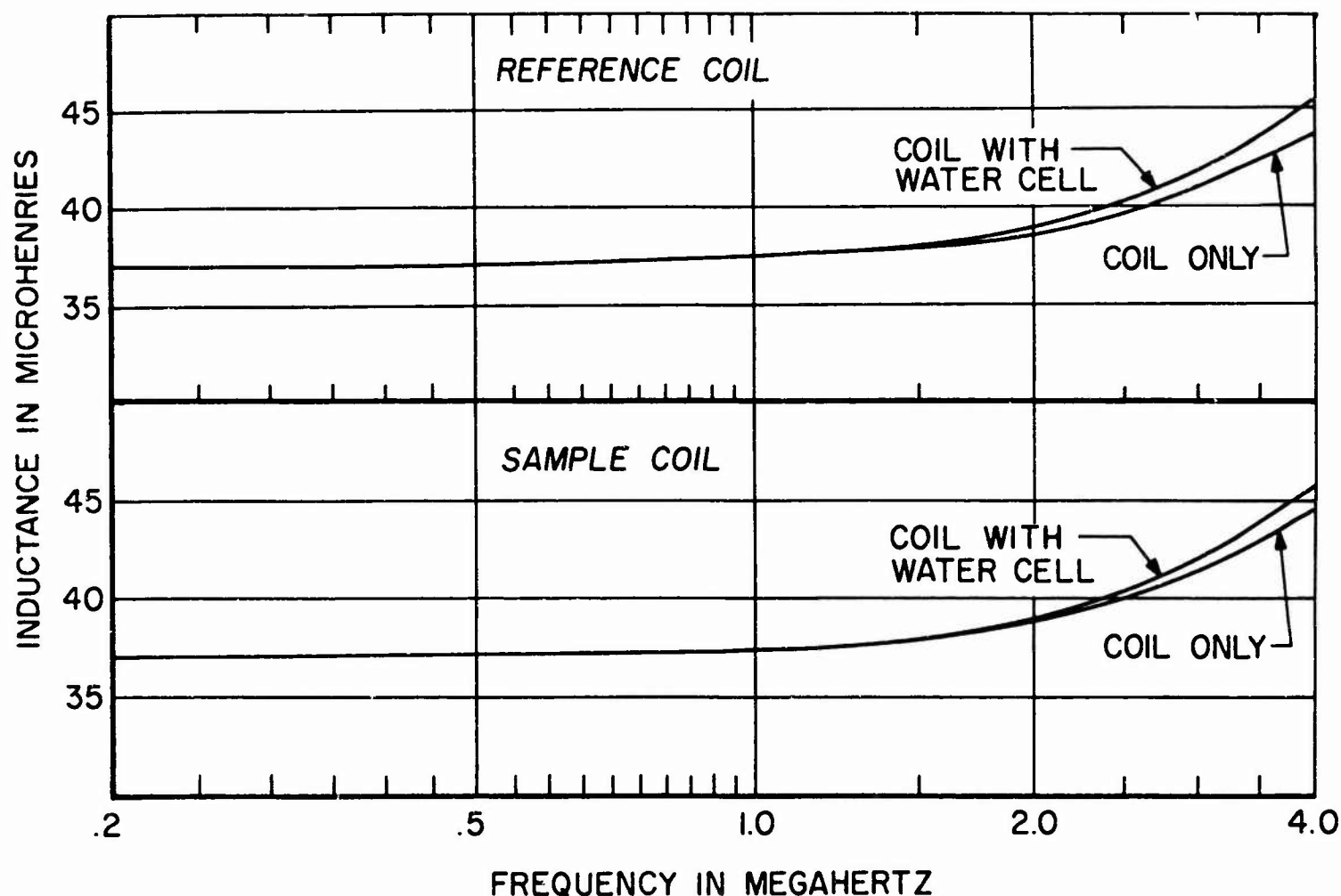
Figure 35.   Inductance vs. Frequency - Sample and Reference Coil

presented in Figure 36 are a comparison of the individual coils only; there is very little difference in the change in resistance under the other conditions examined.

The dc resistance of the sample coil was measured on a Queen Kelvin Bridge and found to be 0.204 ohms; the reference coil measured 0.200 ohms.

4.   Q vs. Frequency

The Q values recorded during the particular parameter measurement were plotted in Figures 37 and 38 for each of the coils, along with the plot of the worst case condition which again occurred with the glass cell containing triple distilled water.   Below 1.0 megahertz, the Q of the coils compared to the Q under the respective conditions is the same.   Above this frequency, the curves rapidly diverge, the curve for the coil with the sample of water falling off much more quickly.   The peak Q of the coils occurs at 3.0 megahertz, while with the sample of water in the cells the peak Q value occurs at 2.5 megahertz.
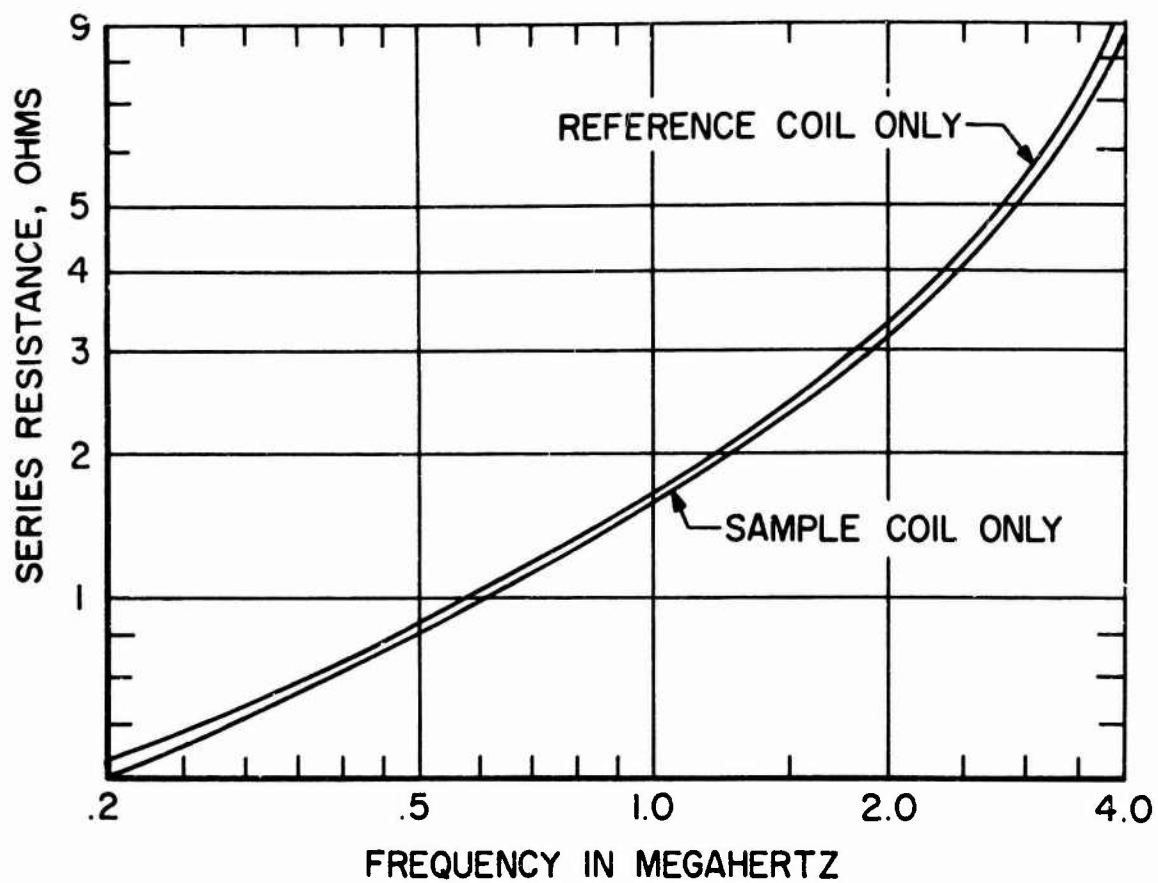
Figure 36. Series Resistance vs. Frequency
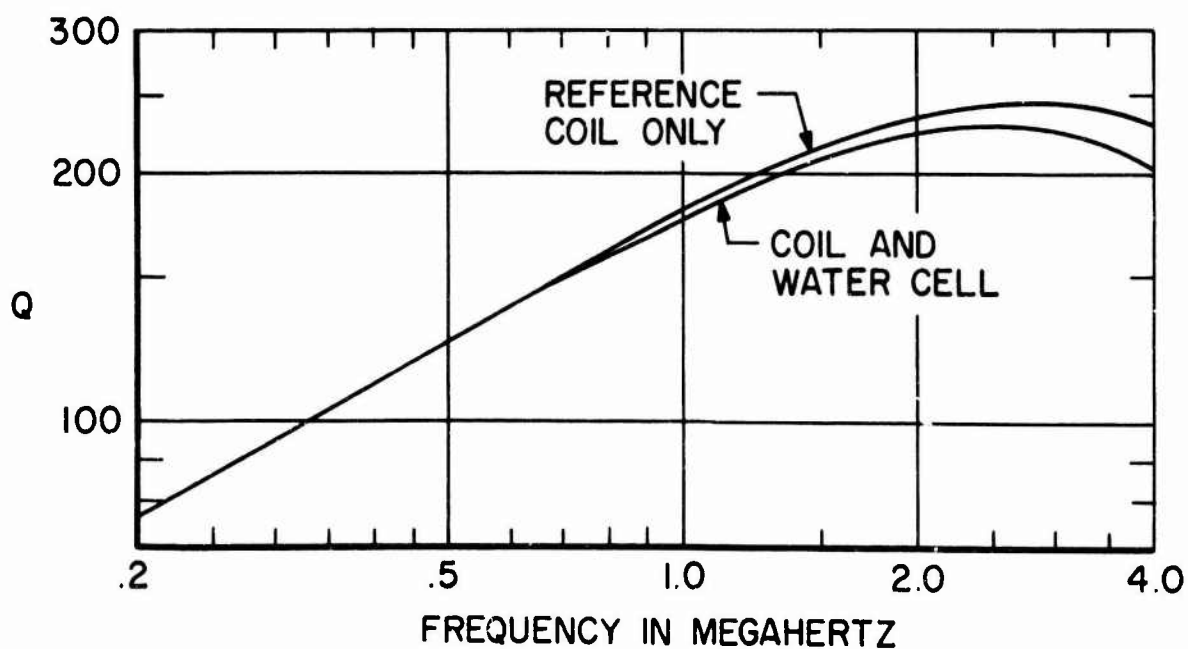
Figure 37. Q vs. Frequency - Reference Coil

92
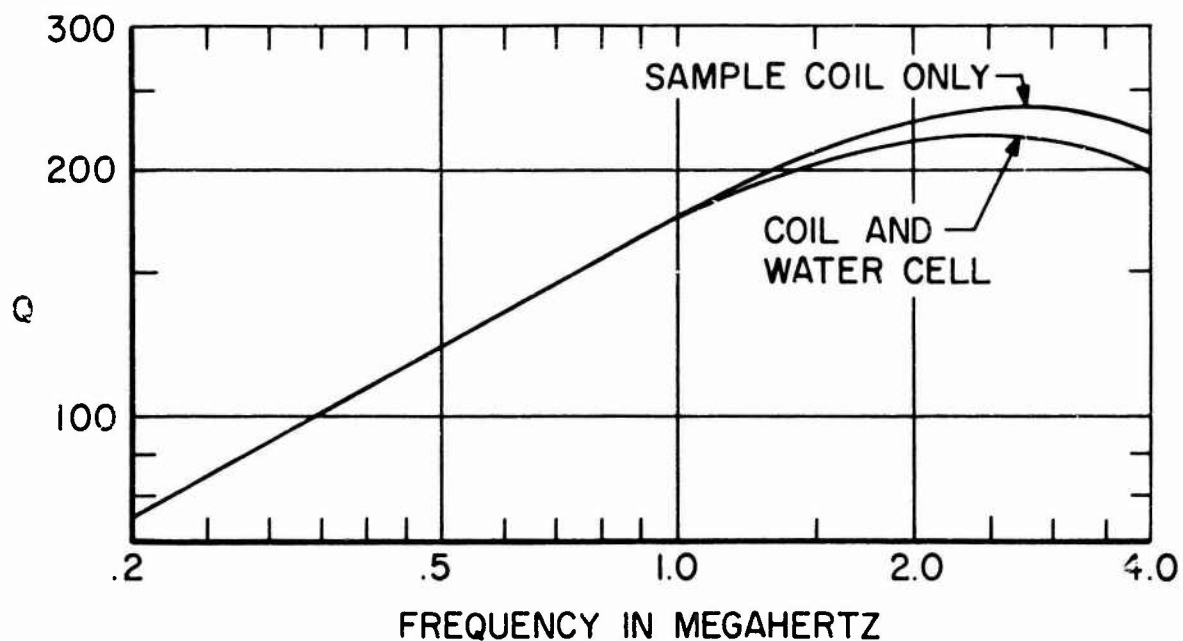
Figure 38. Q vs. Frequency - Sample Coil

5. Mutual Inductance Between Sample and Reference Coils

The mutual inductance of the coils with the normal liquids in the cells and without any material in the coils was determined from the equation

$$M = \frac{L_a - L_o}{4} \quad (339)$$

where L_a is the inductance measured with the coils connected in series aiding configuration, and L_o is the inductance measured with the coils connected in series opposition. These measurements were carried out over the limits of the tuning capacitance range for the resonant frequencies, for gap spacing between coils of 1/2 inch, 1 inch, and 2 inches. In Figure 39, a plot of this data reveals that the mutual inductance falls off rapidly as the gap distance increases, and it is severely affected as the frequency increases, particularly for the larger gap spacing.

The coefficient of coupling between the two coils can readily be determined as follows:

$$K = \frac{M}{\sqrt{L_1 L_2}} \quad (340)$$

Assuming $L_1 = L_2 = 37.8$ microhenries, and $M = 0.23$ microhenries from Figure 39, the coefficient of coupling will be 0.6 percent.

93
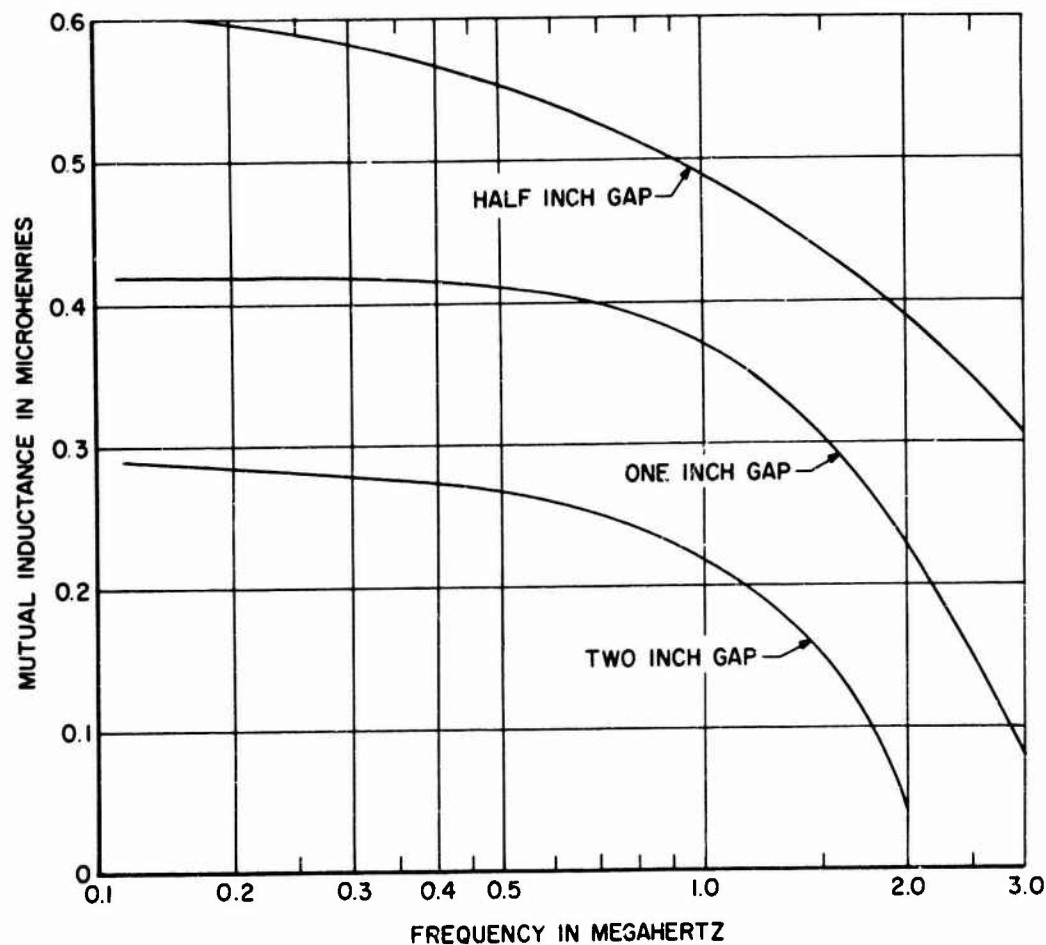
Figure 39. Mutual Inductance vs. Frequency for Different Coil Spacing

6. Self-Resonant Frequency

With the aid of a Measurements Corporation Grid Dip Oscillator and an oscilloscope, a search for the self-resonant point or points was conducted with each coil over a frequency range of 2 to 400 megahertz. Particular consideration was given both to the possible effects of various media within the core of the coil on this parameter and to the effect of coupling produced by the close proximity of the coils in the apparatus. From the observations performed, it appeared that there were no evident effects produced by these changes on the self-resonant frequency data measured with each individual coil. The sharpest grid dip indication of self-resonance occurred at 38.5 and 39 megahertz for the respective coils. The next sharpest indication occurred at 56 megahertz for both coils, although a broad dip was also observed between 9 - 11 megahertz. Due to the construction of the coils, a broad span for the self-resonant frequency could be expected. The higher frequencies indicated can be attributed to the coils acting as an open wire transmission line and the values expressing the frequencies of reflections on the line.

94

C. THE FREQUENCY SPECTRUM OF THE TRANSIENT PULSE

1. A Basis for the Measurement of the Frequency Spectrum

With the development of the theory for Circuit Model II presented in Section I, C, we can see that enough detail is available to resolve the transient risetime to approximately 10 or 15 nanoseconds. In order to investigate a higher resolution, we must bring in certain third order details which would greatly magnify the circuit analysis problem. Relevant experimental evidence is the most satisfactory means for arriving at a properly based decision as to whether it is realistic to go into the theoretical detail further. The experimental evidence we seek is the actual risetime of the voltage and current transient in the apparatus. If the risetime is faster than 10 or 15 nanoseconds, then we have not gone far enough in detailing the circuit model; if the risetime is indeed 10 or 15 nanoseconds or longer, then we have included the significant parameters and are justified in completing the theoretical circuit analysis on that basis.

2. Spectrum Analysis Technique

The technique consists of obtaining the frequency spectrum of the transient, since the risetime is implicitly contained in the spectrum and can readily be determined by applying the Fourier transform theory, which relates the time domain representation of a transient to the frequency representation. Equivalent representations for the transient with which we are dealing are shown in Figure 40.
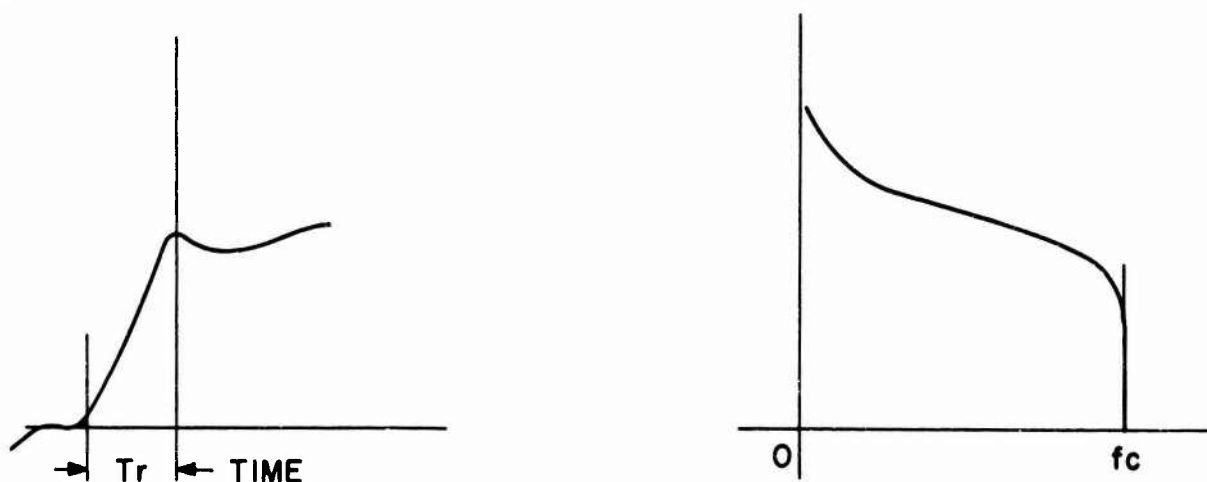
Figure 40. Equivalent Representations

The important feature of the equivalent representation is that the rise-time of the time domain representation is theoretically related to the cutoff frequency in the frequency domain representation. The expression which relates these two parameters is

$$f_c = 1/2T_r \qquad (341)$$

95

The derivation and treatment of this expression may be found in any standard text [30, 31].

To apply this theory, one couples a receiver to the system and measures the frequencies that are present, searching especially for the point in the frequency spectrum where the output falls to a negligible value. This will indicate an excellent approximation for the cutoff frequency f_c. The risetime T_r can then be computed from expression (341).

Only the leading edge of the transient corresponds to the transient of Figure 40. However, this is the part of the waveform which gives rise to the high frequencies shown in the frequency representation. The low frequency oscillatory behavior contributes only to the low frequency portion of the representation and has no bearing on the cutoff frequency. Such variations will affect the envelope of the frequency representation, but the cutoff frequency is a clearly defined quantitative point at the most rapid time-varying part of the waveform. Thus, 1 nanosecond risetime corresponds to a 500 megahertz cutoff frequency. While the sketch in Figure 40 idealizes the situation insofar as the immediate problem is concerned, the frequency domain plot can be associated with the ringing of the RLC circuit of Circuit Model II. This will introduce a large peak around the resonant frequency position. In addition, there is a (sin X/X) multiplying factor associated with the exponentially damped rf burst. This will prevent an abrupt cutoff at frequency f_c. Instead, there will be an extended curve of gradually diminishing high frequency components far out into the ultra high, and possibly the microwave, frequencies. The amplitudes of these components can be predicted: what we must look for is a frequency region where a very rapid attenuation in amplitude can be observed over and above the attenuation predicted for the exponentially damped rf burst. In this manner, the cutoff frequency can be identified.

3. Experimental RF Spectrum Measurements

The experimental spectrum analysis was exploratory in nature, and the noise and field intensity receivers employed (Empire Devices Model NF 105 and Polarad FIM-B) were the best equipment available at that time for the type of impulse being studied. The procedure followed was to place the proper antenna in the desired orientation with relation to the spark gap of the APL-1 apparatus, and then to scan through the particular frequency band of the tuning plug-in unit, successively observing and recording alternate maxima and minima signal amplitudes at the frequency indicated. A frequency range of 14 kilohertz to 7.74 gigahertz was covered in this manner. Both vertical and horizontal antenna polarizations were studied with the antenna placed one meter from the spark gap. The results of these observations are plotted in Figure 41. Examination of the curves reveals that the spectrum is exceedingly complex, containing many maxima and minima points. The reader is cautioned not to underestimate the magnitude of the fluctuations between maxima and minima

96
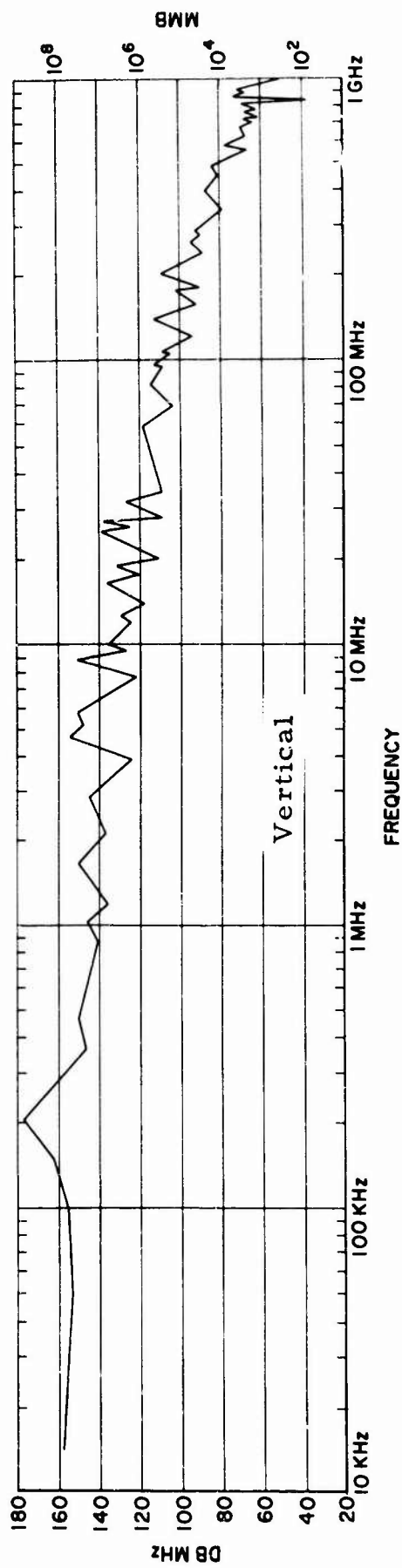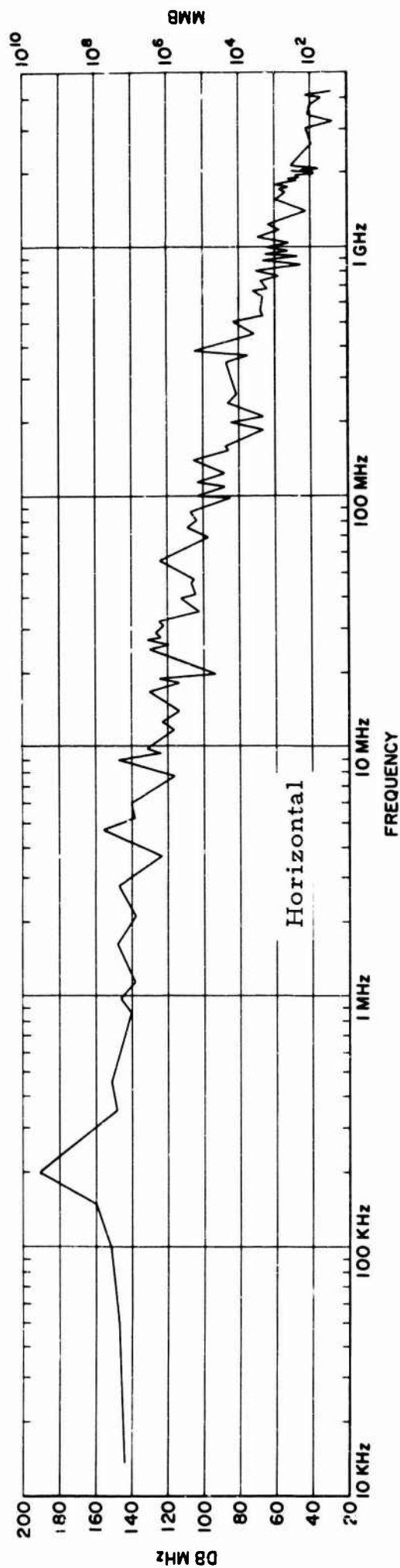
Figure 41. Radiated Noise Spectrum from Spark Gap Discharge, Antenna Oriented in Horizontal and Vertical Position, one Meter from Gap, Pulse Repetition Frequency of 60 prf

97

because the logarithmic scale in microvolts per megahertz bandwidth is deceptive in this respect, since it tends to compress the range.

A study of Figure 41 reveals a characteristic that is shown in Figure 42. In this illustration, the low frequency and high frequency asymptotes of the field intensity peaks are drawn. We can ignore a small percentage of the unusually large peaks in making this construction, on the basis that some of these are due to resonances or a fortuitous constructive interference from the various radiating elements of the apparatus. The break point of the
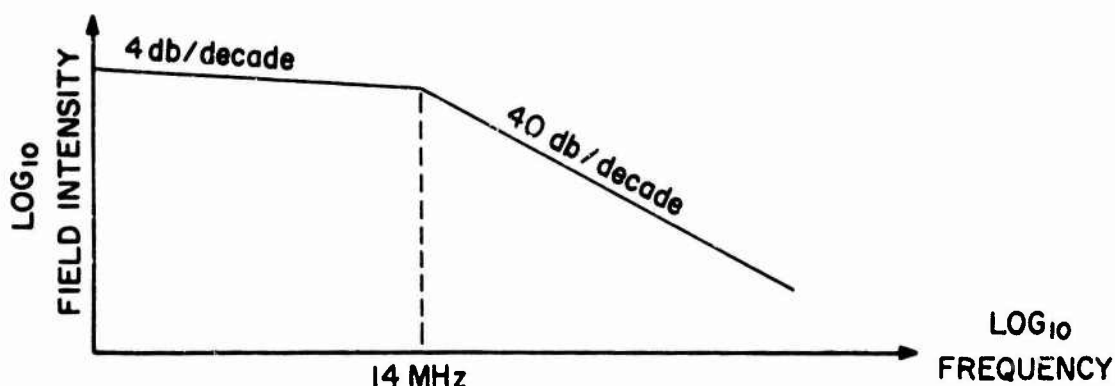
Figure 42. Asymptotic Behavior of Peak Field Intensity Spectrum

asymptotic construction occurs at 14 megahertz. Above this value, there is a 40 db per decade negative slope which extends to approximately 4.2 gigahertz, the frequency where the signal merges into the receiver noise level. The low frequency asymptote is characterized by a 4 db per decade negative slope. At the break point, the open circuit voltage at the receiver terminals is of the order of 10 volts per megahertz bandwidth.

This number must be interpreted extremely carefully. It is incorrect, for example, to conclude that as a consequence there are 10 microvolts per hertz bandwidth. The proper interpretation is that there is a power density of (10^2) / R_T watts per megahertz, where R_T is the sum of the antenna radiation resistance and the input resistance of the receiver. The power density may be divided by 10^6 to convert the previous number to watts per hertz bandwidth. Thus, on the hertz bandwidth basis, the open circuit voltage at the receiver terminals is 10 millivolts per hertz bandwidth at the 14 megahertz break point.

4. Evidence for a Cutoff Frequency

To consider the implication of the break point, another plot of the asymptotic data is shown in Figure 43. This illustration uses linear scales for field intensity and frequency. The 14 megahertz break point is the basis for a normalized amplitude scale.
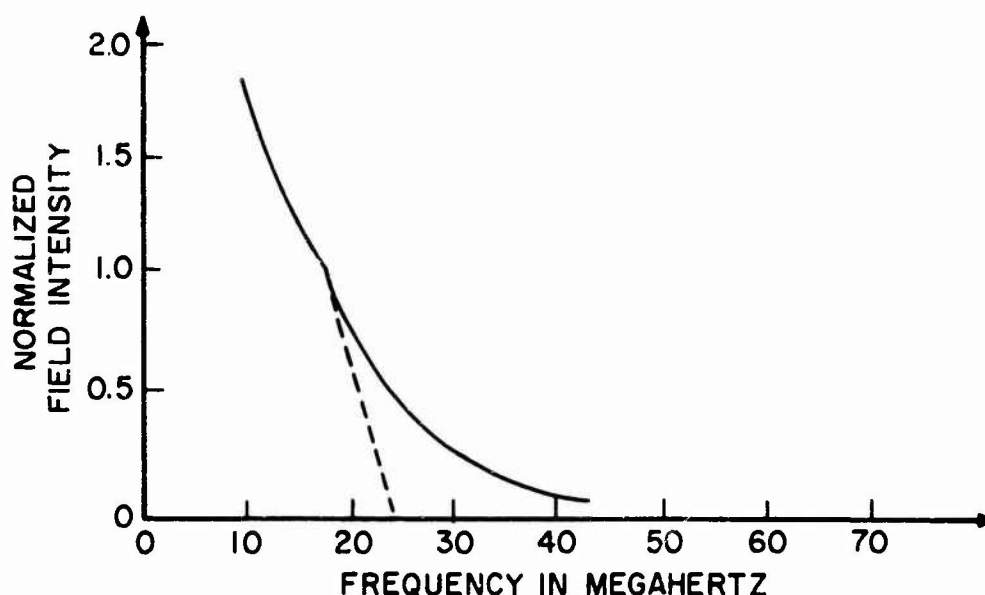
Figure 43. Asymptotic Behavior of Peak Field Intensity
Spectrum Transformed to Linear Scales

The interesting feature, however, is the rapidly decaying signal. The field intensity falls off with a $1/f^2$ characteristic (where f is the frequency) instead of the $1/f$ characteristic that would be expected for the sidelobes of a pulse spectrum or the spectrum of a damped oscillatory train of waves.

Based on the prediction in paragraph C of this section, there is good justification for assigning this rapid drop-off of the cutoff region in the spectrum of the step function with a leading edge having a definite risetime. To obtain a number for the cutoff frequency, we can arbitrarily project the slope of the upper part of the drop-off curve until it intersects the frequency axis, as illustrated in Figure 43. The cutoff frequency indicated by this method is approximately 23 megahertz. However, we could use any other reasonable criterion. The (1/10) power point (relative to the power at the break point), for example, would occur at the 0.316 normalized field intensity value. This method defines a cutoff frequency of 35 megahertz.

The precise value is not really critical; it is of more importance that the region of the cutoff frequency seems to be localized in the vicinity of 30 megahertz. Applying equation (341), a risetime for the impulse of approximately 17 nanoseconds is predicted. This experimental result is in good agreement with the theoretically predicted risetime of 15 nanoseconds (see Section I, C. 4). Another conclusion which follows from the experimental results is that the breakdown time of the spark gap is less than approximately 15 nanoseconds.

5. Magnitude of UHF and Microwave Power

Although microwave radiation was not unexpected, it is interesting to find such high frequencies in the spectrum (Figure 41). Their presence

99

presents two questions: (1) by what mechanism do the microwave frequencies originate?, and (2) is there sufficient microwave energy to cause a possible optical effect?

It is conjectured that very little of the microwave energy is traceable to the plasma in the spark gap. In other words, the spark performs the function of a switch rather than that of a generator. This conjecture is based upon the shape of the high frequency end of the frequency spectrum, which is more consistent with that of an impulse spectrum. If plasma generated oscillations were present, one would expect to find a strong peak in the microwave region considerably more prominent than any of the maxima appearing in the observed structure of that region. An estimate of the microwave signal strength yields magnitudes of 10^{-12} watts per hertz bandwidth in the vicinity of 1.0 gigahertz, which represents the total available power per hertz bandwidth at the sample or reference coil.

Additional receiver measurements enable us to determine, with reasonable assurance, the magnitude of the maximum microwave or UHF signal available at the sample or reference coil, in order to assess the possible importance of these frequencies in connection with the Allison effect. Figures 44 and 45 show the results of receiver measurements taken with the dipole antenna placed in a horizontal and vertical orientation 3 inches away from the coils. In either case, the open circuit receiver voltage is of the order of 10^4 microvolts per megahertz bandwidth.
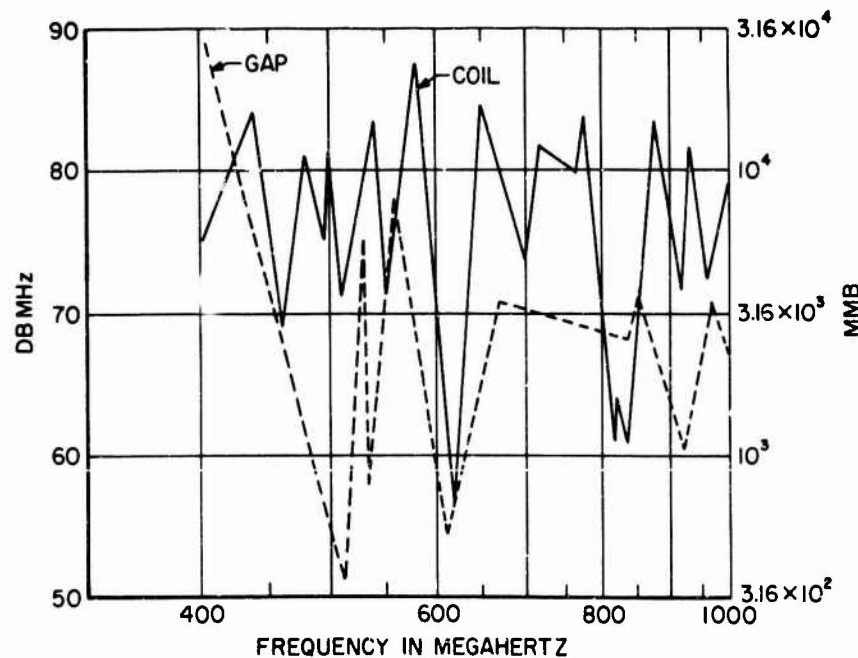
Figure 44. Radiated Noise Spectrum from Spark Gap Discharge,
Antenna Oriented in Horizontal Position, Three Inches
from Gap and Three Inches from Coils (PRF = 60 pps)
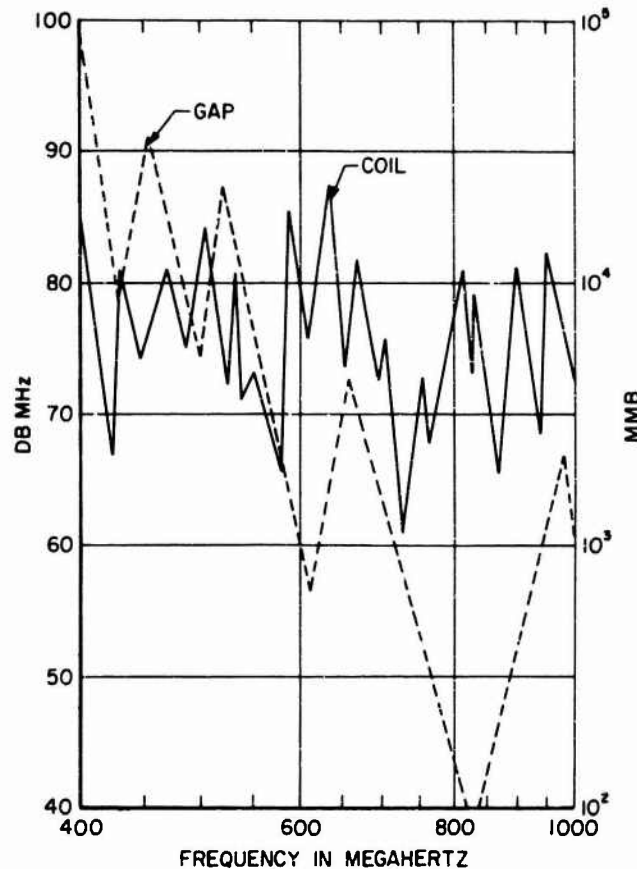
Figure 45. Radiated Noise Spectrum from Spark Gap Discharge,
Antenna Oriented in Vertical Position, Three Inches
from Gap and Three Inches from Coils (PRF = 60 pps)

The measuring circuit, consisting of the coil and the antenna, is very
complex. However, the approximate equivalent circuit of Figure 46 renders
an order of magnitude value for the coil voltage. Using the 1.0 gigahertz
dipole antenna, a conservative value of 1 picofarad coupling capacitance
between the antenna and coil can be assumed. For the larger lower frequency
antennas, the capacitance will increase. At 1.0 gigahertz, the reactance of
this coupling element is about 160 ohms; the receiver has a 50 ohm input
impedance. Accordingly, the voltage across the coil can be computed by
means of the potential divider formula. In this case, the coil voltage is less
than 10^5 microvolts per megahertz bandwidth. We must also assume an
effective bandwidth from which the sample in the coil absorbs or utilizes RF
energy. A Q of 1000 for the resonance associated with the Allison phenomenon
would be conservative considering the various physical resonances which could
be involved in producing the effect. The relation between the Q and bandwidth is

$$Q = \frac{fr}{BW} \tag{342}$$

At 1.0 gigahertz, a Q of 1000 indicates a bandwidth of 1 megahertz. Thus,
the effective coil voltage is 10^5 microvolts.
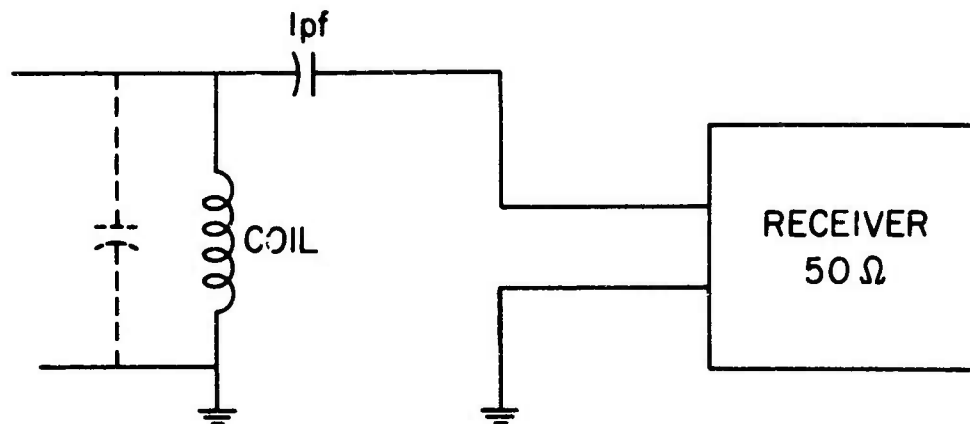
Figure 46. Representation of Measuring Circuit

6. Maxima and Minima Observations

The origin of the abundance of maxima and minima observed during the spectrum analysis is attributable to three causes: interference, presence of high Q circuits, and the shape of the impulse. Interference enters into the picture above 50 megahertz . At this point, the apparatus becomes an efficient radiator, or antenna, because its size is an appreciable fraction of a wave-length. Wires, coils, and other metal objects are distributed throughout the apparatus. In addition, there are metallic objects located near the apparatus. A receiving antenna placed in the vicinity receives electromagnetic signal components having different amplitudes and phases from all the active elements and from the passive reflectors. As the frequency to which the receiver is tuned varies, the amplitudes and phases vary. The received signal amplitude depends upon the type of interference. The destructive interference results in a minimum, the constructive interference in a maximum. The frequencies corresponding to the maxima and minima caused by interference effects do not follow a set pattern, because the various radiating and reflecting elements do not form a simple configuration.

The various high Q resonant circuits in the equipment are the second cause of maxima and minima. These circuits ring when they are excited by the discharging capacitor. Some are lumped parameter circuits and others are formed from elements having distributed parameters. The most prominent of the peaks is that due to the fundamental 200 kilohertz resonant circuit. A shorted section of parallel wire transmission line displays numerous resonances; the fundamental value is that frequency for which the length of line is a quarter wavelength long. Other frequencies correspond to wavelengths for which the line length represents odd and even multiples of a quarter wavelength. The peaks in the experimental data which correspond to such resonances are difficult to identify by inspection; however, their positions can be calculated by a numerical solution of the equivalent circuit.

A third set of maxima and minima arise from the shape of the impulse. Fourier analysis of an impulse often contains a (sin X/X) multiplying factor. When we deal with a periodically repeated impulse, there is always a basic discrete spectrum that gives rise to peaks.

Two of the characteristic features of this impulse which have come to light thus far are: (1) an exponentially damped oscillatory transient (with a modified structure of the first or so cycle), and (2) a relatively fast rise at the beginning of the transient, that is, a physical approximation of a step function. Neither of these features possess a (sin X/X) term in their frequency spectrum; they both have a smooth continuous spectrum. However, it is quite likely that there are impulse variations in the waveform which will generate such a term. The observed leading edge is quite complex. Certainly, there is a discrete structure corresponding to the 60 pps repetition frequency of the impulse; however, the elements of this discrete spectrum are so close together (about 17 elements per kilohertz or 17,000 per megahertz) that it is impossible for a conventional receiver to resolve them, since many elements are contained in the overall bandwidth of such a receiver. Furthermore, the jitter due to the uncertainty in gap breakdown would tend to smear out these elements, even though a very narrow bandwidth or phase detection were used.

The frequency spectrum has been examined carefully for evidence of regularly spaced minima, but nothing really conclusive has been found. The region below 50 megahertz would be the most likely range for these minima. Above that value, the minima caused by interference effects would tend to mask this effect. It is very possible that the deep minima located around 3.9 megahertz and 7.8 megahertz are minima of the third type; if so, this would indicate the presence of some sort of pulse structure at the very beginning of the impulse, the pulse being approximately 250 nanoseconds wide. Again, the finite bandwidth of the receiver prevents accurate location of the minima; if it were necessary to resolve these locations more accurately, a receiver with a very narrow IF bandwidth would be required. A suitable spectrum analyzer would, of course, be the ideal instrument for this task, providing the tendency of the pulse repetition rate of the spark gap to shift could be eliminated.

Finally, some of the amplitude fluctuations are due to the variations in response of the antenna and the receiver. Offhand, the fluctuations within plus or minus 5 db of the average amplitude may be suspected as being of this nature.

7. <u>Summary of Experimental RF Spectrum Analysis</u>

There are two major experimental results:

(1) The RF spectrum analysis predicts the existence of an approximately 15 nanosecond risetime at the beginning of the

oscillatory transient. The intensities of the frequency components begin to reduce sharply in the corresponding frequency region. This is in agreement with previous theoretical predictions.

(2) There is a long curve of decreasing amplitude in the experimental RF spectrum. Measureable frequency components which are part of the extreme spectrum of the damped oscillatory transient exist out to approximately 4 gigahertz. The intensities fall off more rapidly than is predicted by theory, but the UHF and microwave components are weak and would not be detectable without the aid of a fairly sensitive UHF or microwave receiver.

In addition, there are a number of minor experimental results:

(3) The predicted fundamental resonance of the charging capacitor and the inductance of the line and coil system have been confirmed at 200 kilohertz for our apparatus.

(4) There are numerous maxima and minima in the RF spectrum which would be much more pronounced if a receiving instrument with a higher resolution were available.

(5) The UHF and microwave energy generated in the system reaches the sample and reference coils without suffering great attenuation. (It was observed, see Figures 44 and 45, that the field intensity measured near a coil was greater than that measured near the spark gap. This can be explained by the fact that the coil is a much more effective radiator of the high frequency electromagnetic energy than the enclosed spark gap and the distributed parameters extending from it.)

The experimental results serve to narrow the search to two independent areas:

(1) If the classical type of magneto-optic or electro-optic effect is active, then the important frequency range seems to lie below approximately 30 megahertz, because only at these frequencies is the field intensity high enough to produce observable optical effects, even for resonances. In this area, Circuit Model II (with the elaboration required by the two parallel paths and the mutual inductance) contains all the necessary parameters to permit a theoretical study.

(2) The region above approximately 30 megahertz would be important only if an amplifying type of quantum phenomenon were active in producing the Allison effect. Even here, Circuit Model II

would be useful, since the UHF and microwave components seem to form the "tail" of the RF spectrum of a wave shape generated by the basic circuit. Since the experimental evidence portrays the spark gap mainly as a passive switch and not as an active source, the only additional theoretical work on the circuit might be a study of a coil as a slow wave structure, and this would not be necessary unless it is decided to research the possibility of the above mentioned quantum effect.

Such frequencies (either 1 or 2 above) had not been considered by previous investigators except, perhaps, by Snoddy [19], although his work was not of a quantitative nature.

D. OBSERVATIONS WITH PULSE GENERATOR INPUT AND NORMAL OPERATION

1. Basis for Experimental Application of Pulse Generator

The erratic behavior of the usual spark gap as employed in this apparatus defeats any attempt at precision analysis, even with the most modern oscillographic equipment. However, if the spark gap is simulated by use of a pulse generator with its perfectly reproducible pulses occurring at exactly defined intervals, then full advantage can be taken of the capabilities of cathode ray oscilloscope equipment. Although the main objective of the pulse generator technique was to analyze, check, and trouble-shoot the experimental electrical circuit, there is now clear evidence to indicate that it may have disclosed phenomena which can be correlated with the Allison effect.

2. Spark Gap Simulation - APL-1 Apparatus

To simulate the electrical pulse generated by the spark gap breakdown, the electrical circuit of APL-1 was adapted as shown in Figure 47. The 5 ohm component of the voltage divider network was used to approximately simulate the spark gap resistance. The matching network itself was dictated by the specifications of the pulse generator (Hewlett-Packard Model 214A) for developing the maximum output, that is, 50 volts across a 50 ohm load.

It can be noted in comparing Figures 47 and 28 that the spark gap simulating resistance has been placed in the opposite line returning to the charging capacitor and high voltage transformer secondary. The purpose of this circuit manipulation was to furnish a common ground point on the same level for the pulse generator and the single-ended oscilloscope inputs. Introducing the pulses in the former configuration would yield unsatisfactory results due to probe grounding problems.

The pulse generator output at the 5 ohm resistor was adjusted to develop approximately 4-to 5-volt pulses 80 microseconds in duration, at a pulse repetition frequency of 100. The risetime of the pulses generated was determined to be approximately 10 nanoseconds.

In these measurements, consideration was given to the resistive, capacitive, and risetime characteristics of the passive oscilloscope probes, which is necessary to obtain realistic results. After preliminary checks with available equipment, the measuring components for the low voltage inputs comprised a Tektronix 585A oscilloscope with type 82 dual-trace plug-in unit and type P6008 passive probes. This combination results in an optimum measurement system with a 4. 5 nanosecond risetime, 10 megohm input resistance, and 7 picofarad input capacitance, which is ideal for our immediate application.
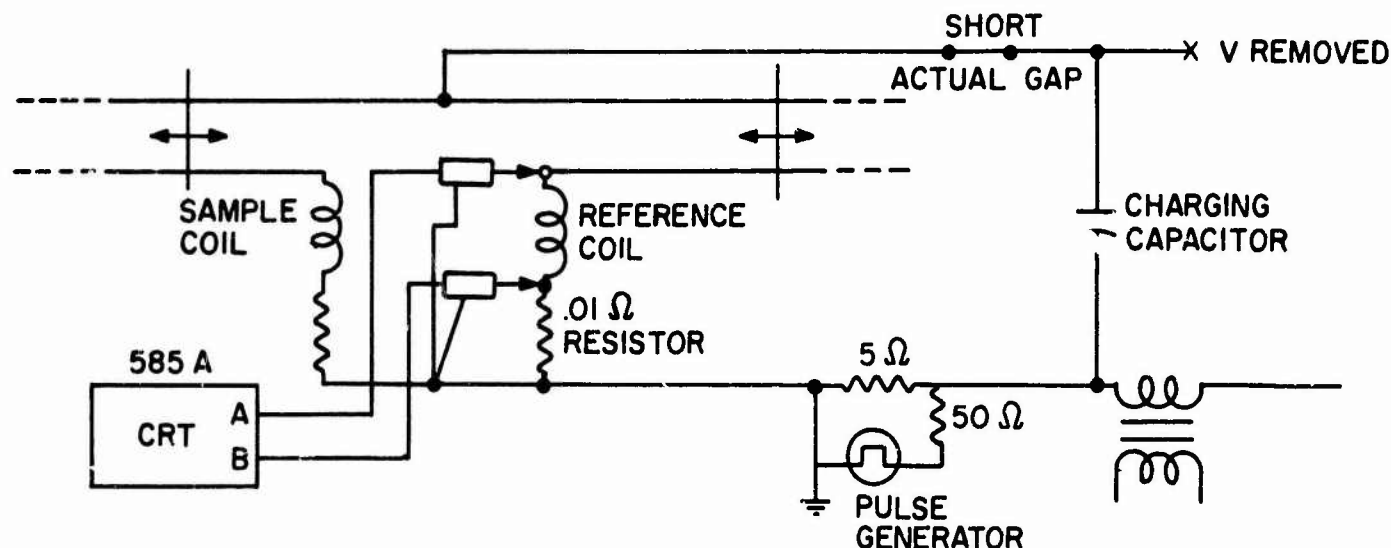
Figure 47. Pulse Simulation and Measurement Circuit

Prior to actual measurements, extreme care must be exercised in matching the initial slope and amplitude of the probes at the fastest sweep speed. Following this procedure, the probes are placed as shown in Figure 47 for a particular measurement where the voltage across a coil and the current through the coil (voltage drop across a 0. 01 ohm resistor) is of interest.

A series of sweep speed exposures from 0. 05 to 5 microseconds per centimeter is shown in Figure 48 a) through e) of the voltage waveforms across the reference coil and 0. 01 ohm resistor as described above. In these exposures, it is evident that the current waveform (lower trace) leads the voltage waveform (which has a risetime of 10 nanoseconds) and has an initial frequency of about 30 megahertz for the first cycle. The characteristic waveform observed at this stage can best be described as an initial section combining a high-frequency nonsymmetrical damped oscillation which evolves into a second section with a smooth exponentially damped 200 kilohertz oscillation lasting 50 microseconds. The total period occurs in approximately 60 microseconds.

106

Voltage

Current

a)   0.05 μsec/cm

Voltage

Current

b)   0.1 μsec/cm

Voltage

Current

c)   0.2 μsec/cm

Voltage

Current

d)   1.0 μsec/cm

Voltage

Current
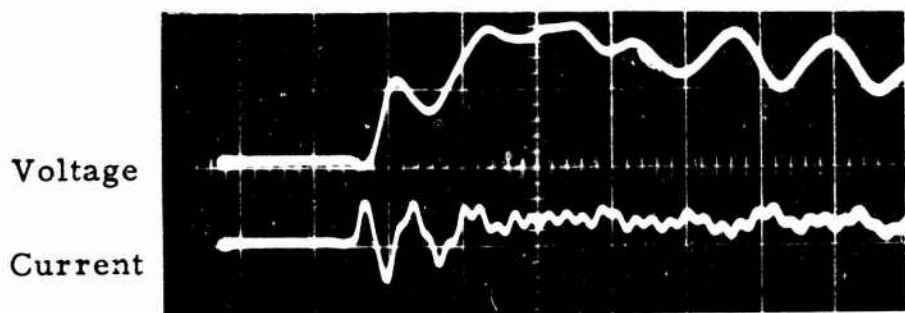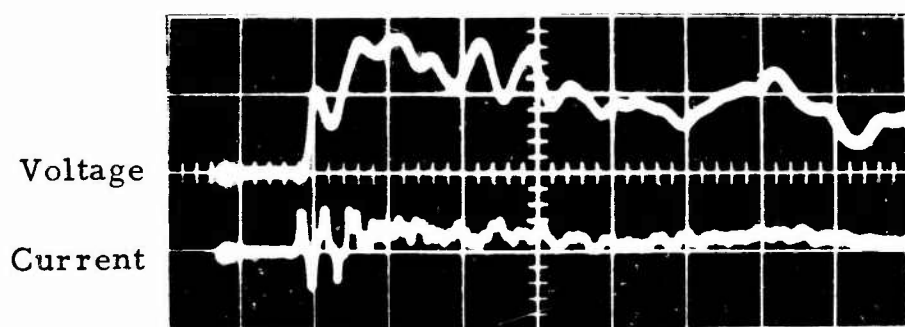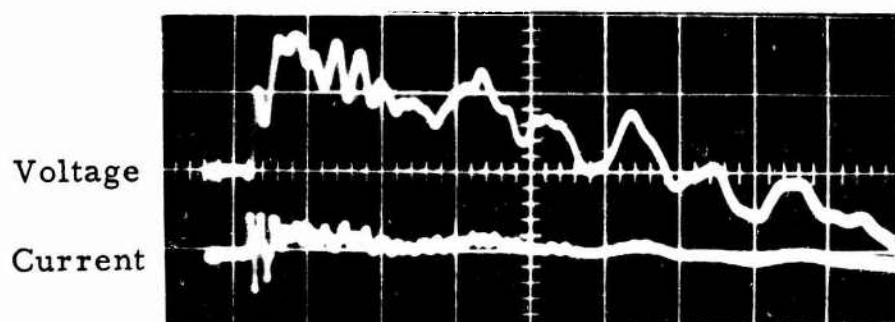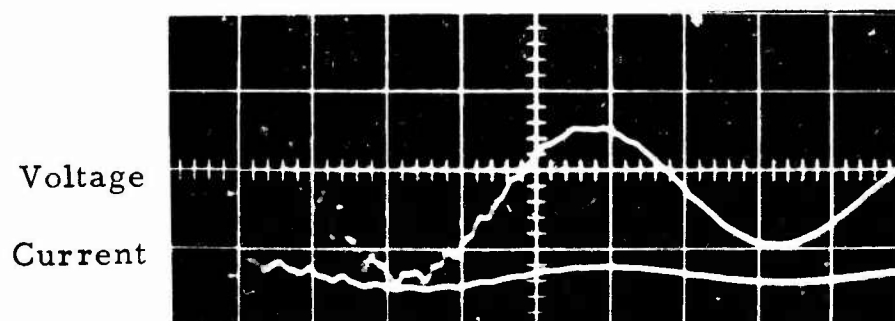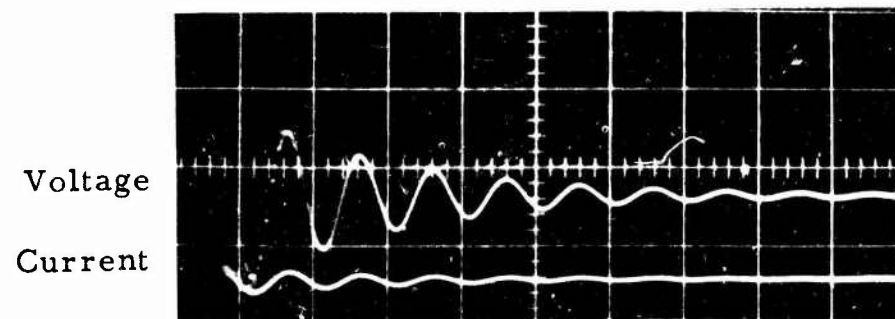
e)   5.0 μsec/cm

Similar exposures were taken of measurements in the sample coil circuit which were comparable except for minor waveform dissimilarities at the high-frequency end as shown in Figure 49, where a composite exposure illustrates the waveforms across both the sample and reference coil superimposed and individually. The obvious dissimilarities between the waveforms can be attributed to construction irregularities in the lines which result in electrical coupling between the trolley as shown in Figure 28. These dissimilarities will be evident during the first microsecond of the waveform; below this point, the resolution between the two oscilloscope traces will not permit further discrimination.

Observations conducted to determine the effect of moving the sample trolley on the waveform resulted in the initial conclusion that the only evident effect was a reduction in sample signal amplitude (regardless of whether a sample was in the coils or not) due to the

Figure 48. Voltage and Current Signals Present in Reference Coil, APL-1 Apparatus, Pulse Generator Input, Vertical Sensitivities - Upper Trace 2 v/cm, Lower Trace 0.1 v/cm

107

circuit parameters as the length of the trolley line was increased from 0 to 10 Allison units.

A closer examination of the superimposed waveforms during the first 0.1 microsecond reveals a significant change in amplitude, phase, and waveform characteristic for five positions of sample trolley with respect to the reference trolley position. Figure 50 illustrates a composite photograph of the five trolley positions with both traces superimposed. Considering
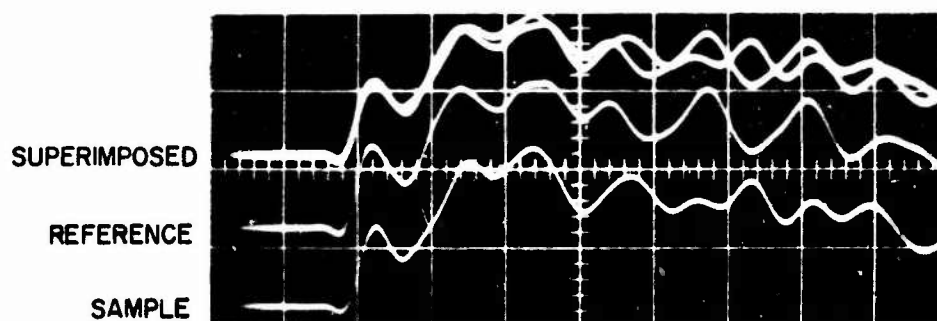
Figure 49. Comparison of Reference and Sample Coil Voltage Waveforms, APL-1 Apparatus, Horizontal Sweep Speed - .05 μsec/cm, Vertical Sensitivity - 2 v/cm

the amplitude change first, the amplitude decreases as the length of the sample trolley is increased, whereas the reference signal amplitude remains the same. The change in waveform characteristic is due to constructive or destructive reinforcement of the waveform as reflections on the line increase with a corresponding increase in line length. Finally, a significant observation which was not given a great deal of consideration at the time was the phase change between the two signals at the initial risetime slope from position 0.00 to 2.5 Allison units. The significance of this observation with relation to apparatus constructions and calibration will be brought out in paragraph E. 1) of this section.

Further observations were conducted to experimentally detect and compare the waveform effect of displacing the reference coil with respect to the sample coil along the optical bench[1]. As observed in Figure 50, a similar shift in phase between the waveforms occurs, and is illustrated in Figures 51 and 52, even though there are physical limitations to the extent to which a practical displacement of the coils on the bench can be made.

3. Normal Operation Observations - APL-1 Apparatus

With the APL-1 system connected for normal operation (as in Figure 28), the initial waveform of the voltage across the reference and

sample coils and the current through the coils (voltage drop across 0.01 ohm) were recorded as shown in Figures 53 and 54.

O Progressive Waveform Changes
△ Amplitude Changes
◊ Phase Shift

0.00   2.5   5.0   7.5   10.0   Units

Figure 50. Reference and Sample Signal Changes as a Function of Sample Trolley Position, APL-1 Apparatus, Horizontal Sweep Speed .05 μsec/cm, Vertical Sensitivity 1 v/cm

1.35"
2.75"
5.50"
16.00"
19.00"
48.00"
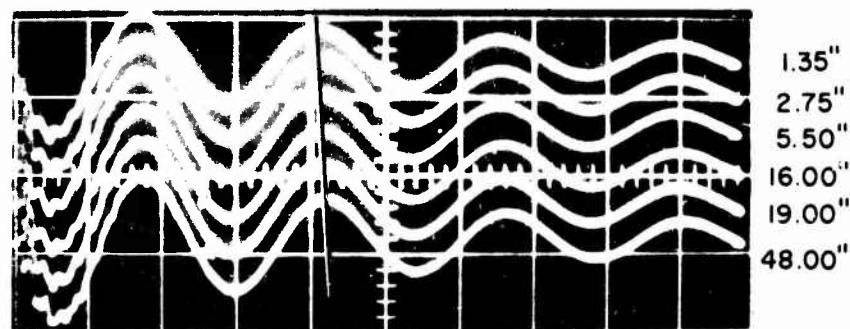
Figure 51. Sample Signal Phase Shift Induced by Coil Separation - Low-frequency End, APL-1 Apparatus, Horizontal Sweep Speed - 2 μsec/cm, Vertical Sensitivity - 2 v/cm

COIL SEPARATION

1.35"
2.75"
5.50"
19.0"
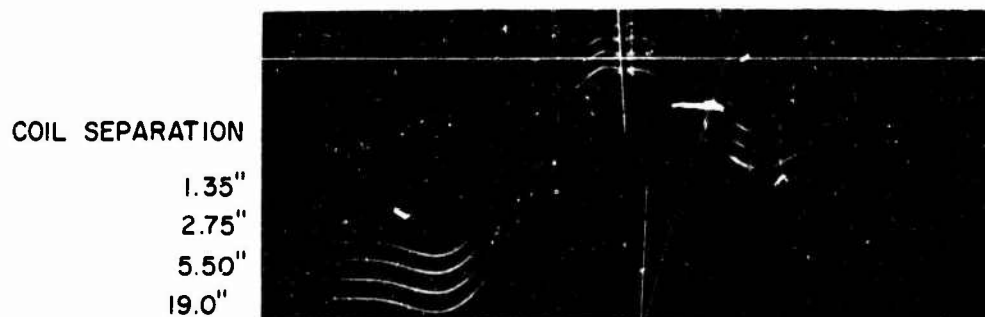
Figure 52. Sample Signal Phase Shift Induced by Coil Separation - High-frequency End, APL-1 Apparatus, Horizontal Sweep Speed - 10 nsec/cm, Vertical Sensitivity - 0.5 v/cm
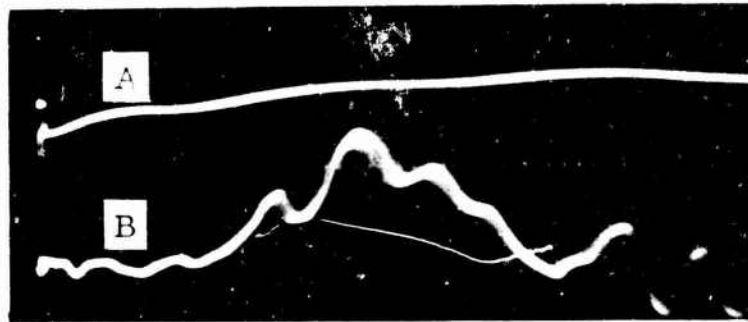
Figure 53.   Initial Voltage and Current Waveforms at Reference
Coil, APL-1 Apparatus, A - Voltage, B - Current,
Horizontal Sweep Speed - 10 nsec/cm, Vertical
Sensitivity - A - 5 kv/cm and B - 50 v/cm
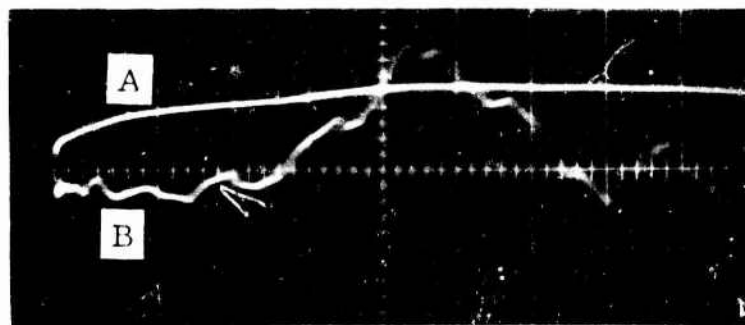
Figure 54.   Initial Voltage and Current Waveforms at Sample Coil,
APL-1 Apparatus, A - Voltage, B - Current, Hori-
zontal Sweep Speed - 10 nsec/cm, Vertical Sensitivity -
A - 5 kv/cm and B - 50 v/cm

An examination of these waveforms indicates a peak voltage pulse of
approximately 5 kilovolts (negative) when the spark gap breaks down. The
peak current pulse occurs at about 50 nanoseconds after the spark gap
breaks down and has a maximum amplitude of 10,000 amperes. However,
one must be cautioned in seriously considering this magnitude as indicative
of the actual current present in the coil. There are indications that a
significant portion of this amplitude is due to rf fields inducing a voltage
drop across the purely resistive element (.01 ohm) and the resistive
component of the high input impedance probe. Attempts at eliminating this
pickup have thus far been unsuccessful. One evident difficulty is that from
a rf measurement standpoint the system construction, while unavoidable,
is undesirable. The physical lengths of line and leads involved are a serious
drawback when rf radiation is present. For example, the ground side in the
system is several feet long, offering an ideal antenna element for picking up rf.
However, the current waveform contour can be considered as representative
of the actual current in the coils. In comparing the current waveforms for
each coil, it is quite evident that the signals differ considerably due to a
nonsymmetrical trolley line construction.

In an attempt to check the effect (pulse generator input) of the line symmetry on the waveforms, the circuit shown in Figure 28 was changed by moving the lead from point A to point B, and the lead from the gap to point C, keeping these leads and trolley lengths approximately equal wherever possible. The recorded results shown in Figure 55, when compared to Figure 49, show considerable improvement in waveform similarity. The lower pair of superimposed figures shows the effect of moving the lead to point C (see Figure 28), seven inches closer to the sample trolley.
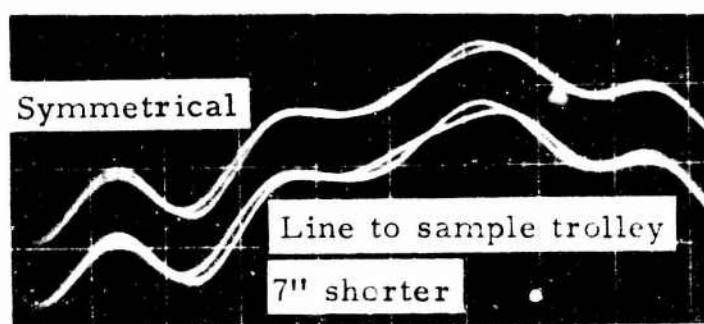
Figure 55. Coil Waveforms with Symmetrical Lines, APL-1,
Pulse Generator Input, Horizontal Sensitivity -
20 nsec/cm, Vertical Sensitivity - 2 v/cm

4. Spark Gap Simulation - Allison's Apparatus

Extensive observations and measurements were conducted using Allison's apparatus[18] (see Figure 31) . The same series of observations shown in Figure 48 was repeated with this system and appears in Figure 56. As before, the current waveform leads the voltage waveform, but now the first peak and successive peaks are not as high or as smooth as observed with the APL-1 apparatus. An examination and comparison of the voltage waveforms of the two apparatuses reveals a considerable difference in the first three microseconds. The initial cycle is much lower in amplitude but of approximately the same risetime and duration. With regard to successive cycles (a comparison should also be made with Figure 8 and the accompaning theoretical prediction), the effect of reflections cancelling or reinforcing the exponentially damped waveform is obvious in this symmetrical system. After the first 3 microseconds, the voltage waveforms can be considered identically the same, and resolves into an exponentially damped oscillation (10 cycles) lasting about 50 microseconds.

Similar exposures were taken of measurements in the sample coil circuit which were more comparable with this apparatus as shown in Figure 57, where a composite exposure illustrates the waveforms across both the sample and reference coils superimposed and individually.

a) 0.05 μsec/cm

Voltage

Current

b) 0.1 μsec/cm

Voltage

Current

c) 0.2 μsec/cm

Voltage

Current

d) 1.0 μsec/cm

Voltage

Current

e) 5.0 μsec/cm

Current
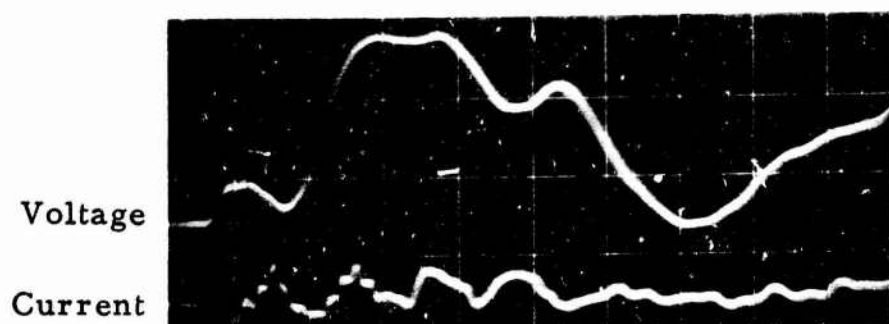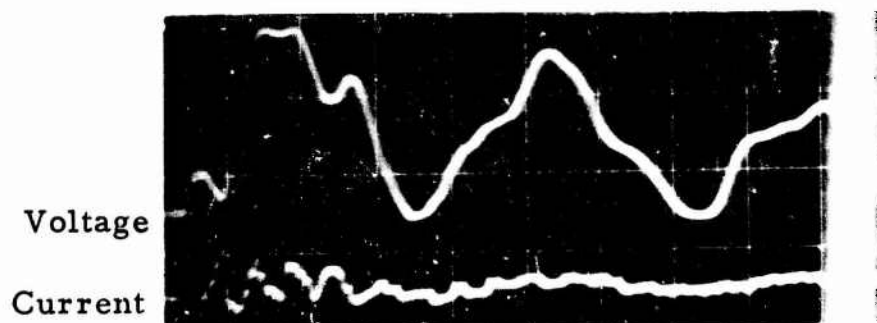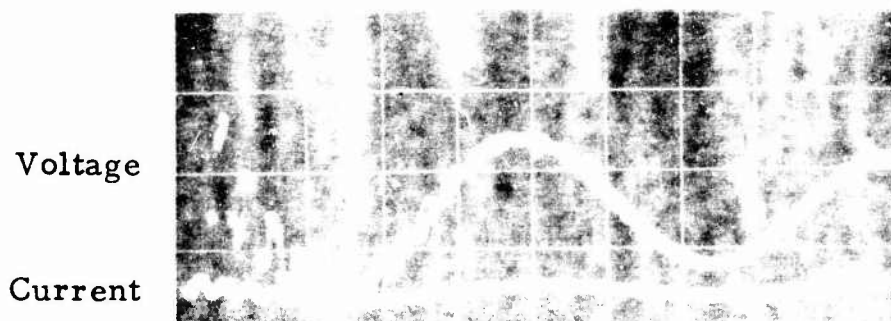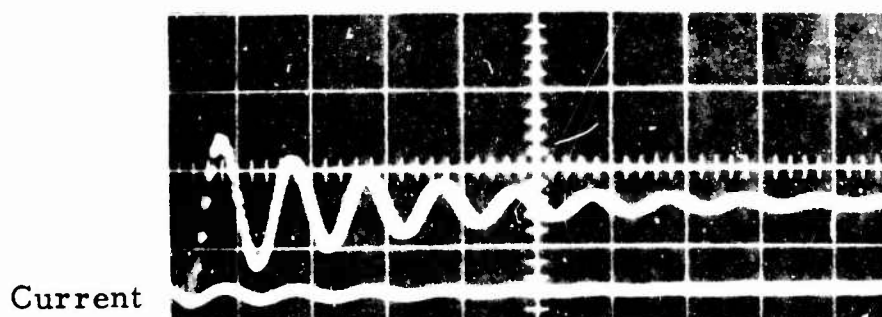
The minor dissimilarities which still exist between the waveforms can best be attributed to minor characteristic electrical differences between the two trolley lines which affect the high frequency components of the signals.

A closer examination of the superimposed waveforms during the first 0.1 microsecond again reveals a significant change in amplitude, phase, and waveform characteristic for six positions of sample trolley with respect to the calibrated reference trolley position. Figure 58 illustrates a composite photograph of the six trolley positions with both traces superimposed. In this photograph, a change in amplitude between the two waveforms the initial riset ⌐ not apparent. The most apparent effect of moving the sample trolley over 18 Allison units from the calibrated position (15.00) is the shift in phase between the two signals and the effect on the reference waveform. At the calibrated position, the leading edge of the two signals coincide perfectly (within the resolution of the

Figure 56. Voltage and Current Signals Present in Reference Coil, APL-1 Apparatus, Pulse Generator Input, Vertical Sensitivities - Upper Trace 2 v/cm, Lower Trace 0.1 v/cm

112

Superimposed
Reference
Sample
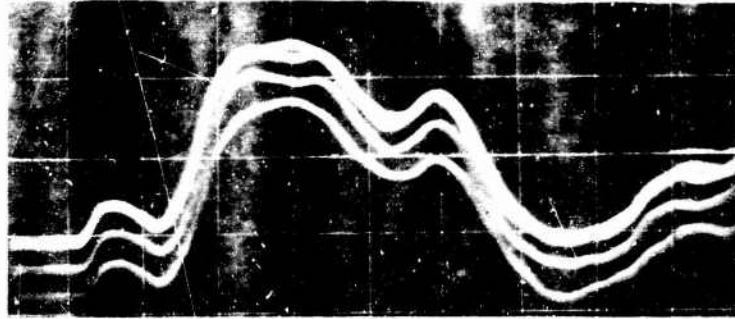
Figure 57.   Comparison of Reference and Sample Coil
Voltage Waveforms, Allison's Apparatus,
Horizontal Sweep Speed - 0.05 μsec/cm,
Vertical Sensitivity - 2 v/cm
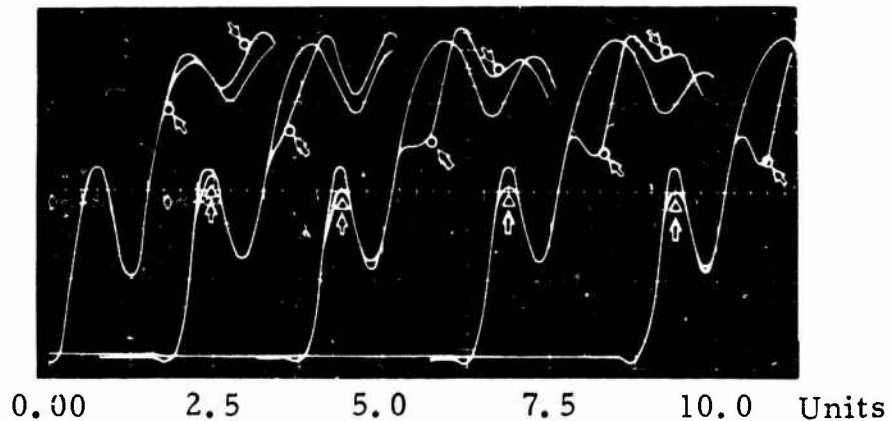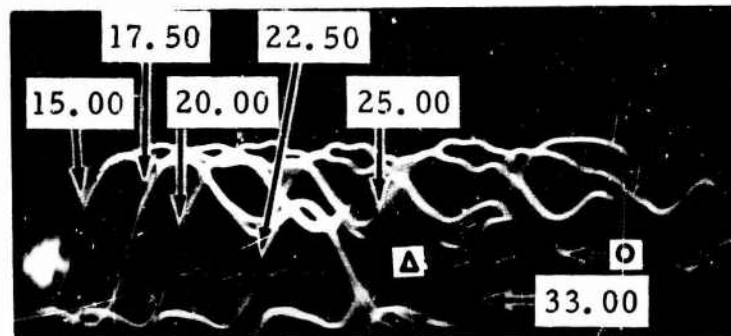

Figure 58.   Reference and Sample Signal Changes as a
Function of Sample Trolley Position,
Allison's Apparatus, Horizontal Sweep
Speed - 0.05 μsec/cm, Vertical Sensi-
tivity - 2 v/cm

trace widths at this sweep speed), and, as the sample trolley is moved
up-scale, the phase of the sample signal lags the reference signal.

Further observations of the waveforms were recorded in Figure 59
with the sample trolley at 3.00, 15.00, and 27.00 Allison units. With a
sweep speed of 10 nanoseconds per centimeter, the phase shift of the
sample signal from a leading position to in-phase and then to a lagging
position is obvious. In other words, we can match the initial leading
edges of the voltage waveform signals relatively well, simply by matching
the oscilloscope presentation as the sample trolley is moved through the
calibrated position. The accuracy would depend on the sweep speed and
resolution to which an operator could detect a difference between the two
traces. The only difficulty in matching the two waveforms would be due
to the presence of an excessive dissimilarity in the waveforms caused by
different characteristic impedance between the two trolley lines.

113

Allison Units

3.00
15.00
27.00
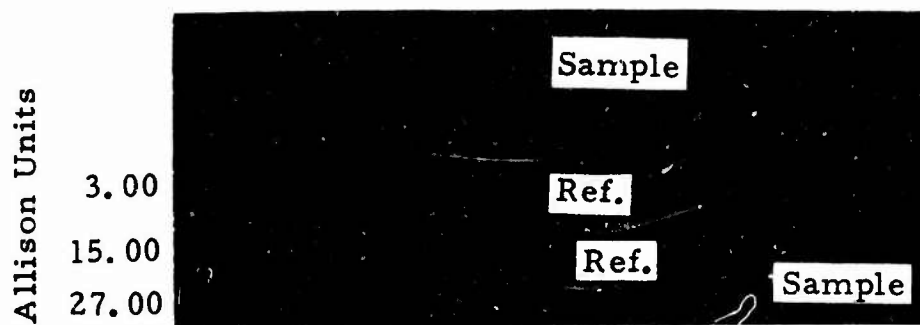
Figure 59. Reference and Sample Signal Changes as a
Function of Sample Trolley Position, Allison's
Apparatus, Horizontal Sweep Speed-10 nsec/cm,
Vertical Sensitivity - 2 v/cm

As with the APL-1 system, further observations on Allison's system
were conducted to experimentally detect and compare the waveform effect of
displacing the reference coil with respect to the sample coil along the
optical bench. As observed in Figure 52, a similar shift in phase occurs
and is shown in Figure 60; although the effect is not as obvious, a slight
change could be observed at the high frequency end of the voltage waveform.

0.8"
4.0"
8.0"
14.5"

Figure 60. Sample Signal Phase Shift Induced by Coil Separation,
High-frequency End, Allison's Apparatus, Horizontal
Sweep Speed - 10 nsec/cm, Vertical Sensitivity - 2 v/cm

A further experiment conducted with Allison's apparatus consisted of
changing the position of the main slidewire termination from 0 to 36 meters
total length (0 - 18 meters parallel transmission line), with the reference
and sample trolleys at the calibrated position. The effect of these changes
is shown in Figure 61. As might be expected, the risetime of the waveforms
increased as the main slidewire length is increased. The optimum phase
match between the two waveforms occurs when the total length of line is
9 meters long. At this point, we can also observe that the initial risetime
of the waveforms could also be considered optimum in comparison to the
other curves.

114
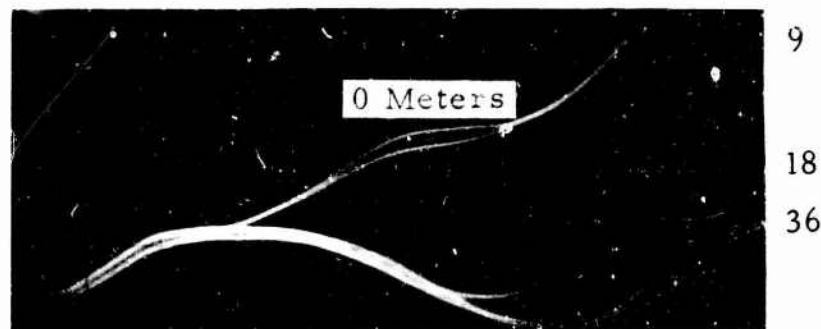
Figure 61.   Comparison of Reference and Sample Coil Voltage
Waveforms as a Function of Main Slidewire,
Horizontal Sweep Speed - 10 nsec/cm, Vertical
Sensitivity - 1.0 v/cm

5.   Normal Operation Observations - Allison's Apparatus

With Allison's system connected for normal operation (as in Figure
31), the initial waveform of the voltage across the reference and sample coils
and the current through the coils were recorded as shown in Figures 62 and 63.
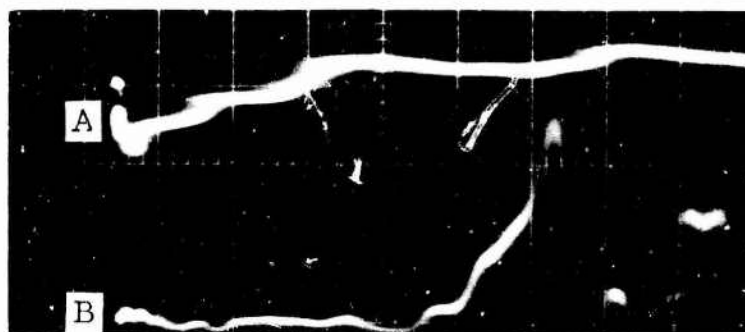
Figure 62.   Initial Voltage and Current Waveforms at Reference
Coil, Allison's Apparatus, A - Voltage, B - Current,
Horizontal Sweep Speed - 10 nsec/cm, Vertical
Sensitivity - A - 5 kv/cm and B - 50 v/cm
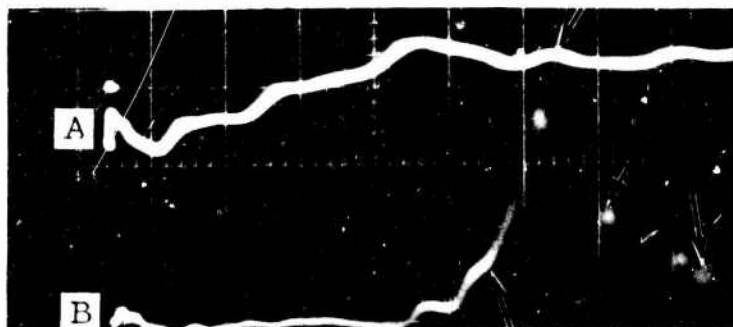
Figure 63.   Initial Voltage and Current Waveforms of Sample
Coil, Allison's Apparatus, A - Voltage, B - Current,
Horizontal Sweep Speed - 10 nsec/cm, Vertical
Sensitivity - A - 5 kv/cm and B - 50 v/cm

115

In comparison to the waveforms in Figures 54 and 55, the voltage wave-forms observed on Allison's system have a longer duration to the initial peak. In addition, the peak current pulse occurs approximately 50 nanoseconds after the voltage pulse (10 nanoseconds later than on the APL-1 apparatus). The similarity between the current pulses for the first cycle is apparent; succeeding cycles, however, are different in contour and amplitude. At the same time, additional observations were recorded to show the effect on the sample voltage and current waveforms for increased sample trolley lengths as shown in Figure 64 a) and b).
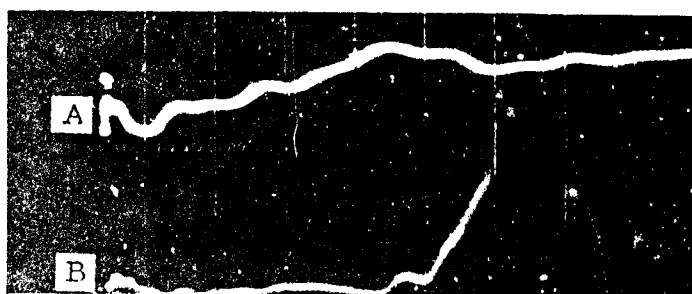
a)   Sample Trolley at 25 Allison Units

b)   Sample Trolley at 33 Allison Units

Figure 64.   Initial Voltage and Current Waveforms of Sample Coil as a Function of Sample Trolley Position, Allison's Apparatus, A - Voltage, B - Current, Horizontal Sweep Speed - 10 nsec/cm, Vertical Sensitivity - A-5 kv/cm and B - 50 v/cm

At the indicated points, a significant change in the waveform has been observed which can be attributed to constructive or destructive reinforcements of the signal set up on the trolley lines for a given length of line. Extreme care must be exercised in these measurements, particularly with regard to observing time lapse, electrode spacing and wear, and gas pressure. A minor change in any one of these variables has been observed to affect the risetime and amplitude considerably. An example of the effect of electrode

116

spacing change is shown in Figure 65, where the resulting waveform amplitude and contour effects are apparent when compared to Figure 62 for the same observation.

Figure 65. Electrode Spacing Change Effect on Reference
Voltage and Current Waveforms, Allison's Apparatus,
A - Voltage, B - Current, Horizontal Sweep Speed -
10 nsec/cm, Vertical Sensitivity - A - 5 kv/cm and
B - 50 v/cm

Further waveform observations were conducted with the parallel plate capacitor mount indicated in Section I A b). This mount, which included its own sample coil and form for holding the capacitor plates, was substituted for the normal coil thus far used. The coil inductance was measured and found to be 30 microhenries, and the capacitor size was calculated at 7 picofarads for the particular plate spacing chosen for the observations. When using this coil and capacitor mount configuration, it was observed that the amplitude of the current waveforms appears to be higher in magnitude (see Figure 66 a). In addition, the second pulse current cycle is almost of the same magnitude as the initial peak. With the capacitor plates placed in the mount, the only observable difference in the waveforms occurs during the initial few cycles of the signals as shown in Figure 66 b). The first and second peak of the current waveform appear to have been modified by a destructive component of frequency, while the first valley appears to be constructively reinforced.

In Figure 66 c), the effect of a polystyrene dielectric material (1/4 x 2 x 8-1/2 inches) placed between the capacitor plates can also be observed. The placing of this material between the plates slightly decreases the interference effect of the frequency component previously observed.

In Figure 67 a) through c), the effect on the current waveform of a "water cell" capacitor[5] was observed and recorded for comparison with Figure 66 (for improving clarity of minima under humid weather conditions). The term "water cell" refers to a capacitor plate system composed of two curved foil plates secured, diametrically opposing, against the inside diameter walls of the core form of the sample cell coil and connected to the coil terminals.

117
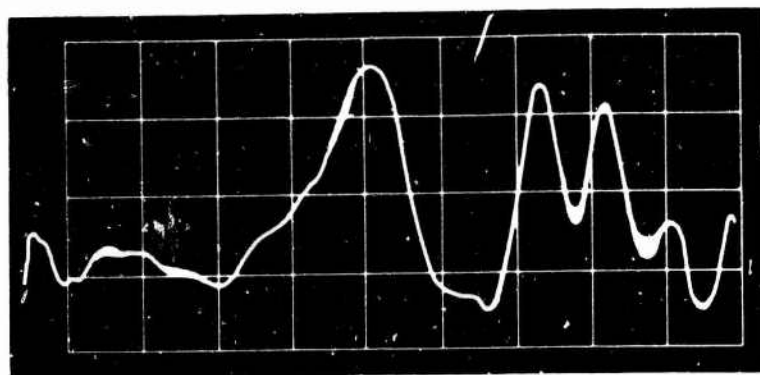
a) Coil and Mount Only
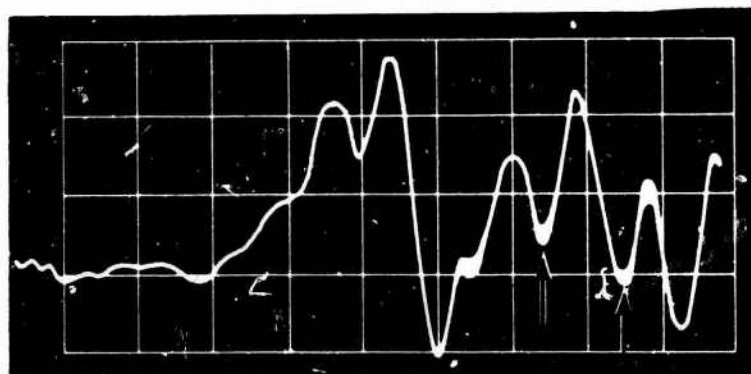
b) Capacitor Plates Inserted and Connected
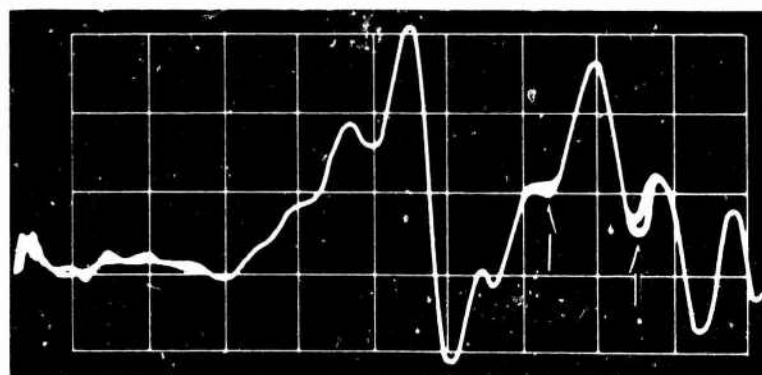
c) Polystyrene Dielectric Plate Added

Figure 66. Parallel Plate Capacitor Effects on Current
Waveform, Horizontal Sweep Speed - 10 nsec/cm,
Sensitivity - 50 v/cm
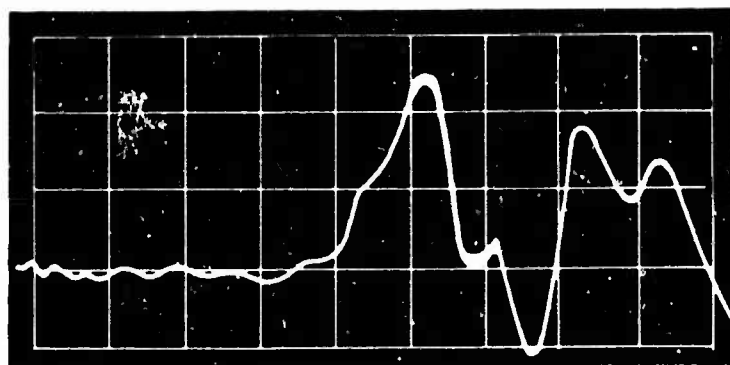
a) Water Cell Capacitor Out, Water Filled Cell in Position
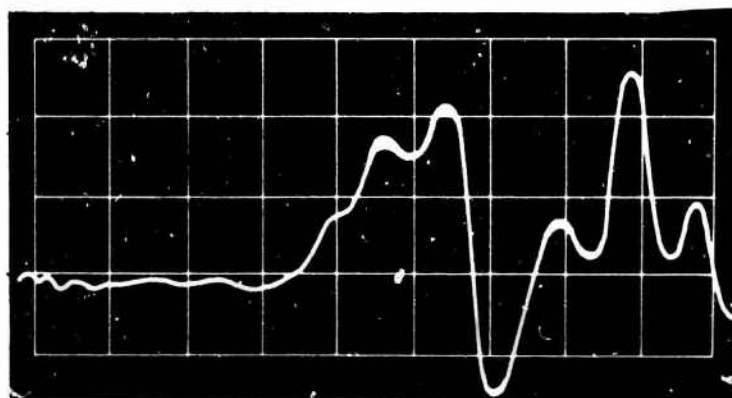
b) Water Cell Capacitor in Place and Connected, Water Filled Cell Out
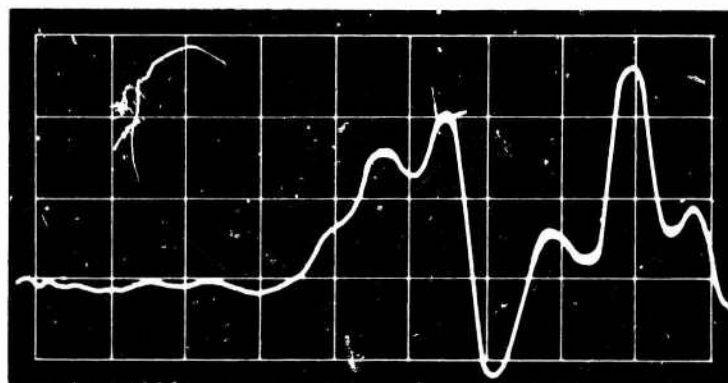
c) Water Cell Capacitor in Place and Water Filled Cell in Position

Figure 67. Water Cell Capacitor Effects on Current Waveform, Horizontal Sweep Speed - 10 nsec/cm, Vertical Sensitivity - 50 v/cm

119

A similarity between these photographs and those presented in Figure 66 for the parallel plate capacitor is apparent to the observer. With the capcitor out of the circuit, but the plates physically in position, the waveforms in Figures 66 a) and 67 a) are similar except for the large negative swing of each cycle. Connecting the capacitors electrically in the circuit also has similar effects on the current waveforms as shown in Figures 66 b) and 67 b). The waveform has been modified similarly as described before by a component of frequency. The effective waveform change introduced by placing a dielectric, in this case the water-filled cell between the capacitor plates, is also similar in Figures 66 c) and 67 c). The preshoot and undershoot for that portion of the waveforms, which contains the second highest pulse, can be observed to decrease in magnitude with the addition of dielectric material. Two additional assumptions which may be drawn from these figures are that, in general, the current waveforms with the water cell capacitor in the circuit are more clearly defined than with the parallel plate capacitor method, and the time of the initial peak current occurs 10 nanoseconds later with the water cell capacitor in place.

The series of observations on Allison's apparatus was concluded with an examination of the charging voltage build-up across the capacitor prior to the spark gap breakdown and the damped oscillation following the breakdown. Figure 68 a) represents the initial charging curve of the capacitor. A peak to
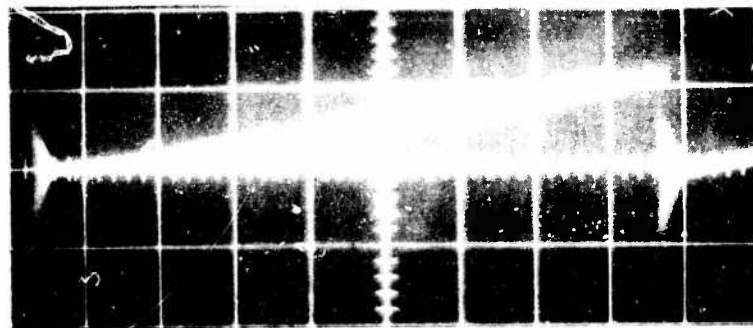
a) Charging Curve Across Capacitor, Horizontal
Sweep Speed - 0.2 ms/cm, Vertical Sensitivity -
2 kv/cm
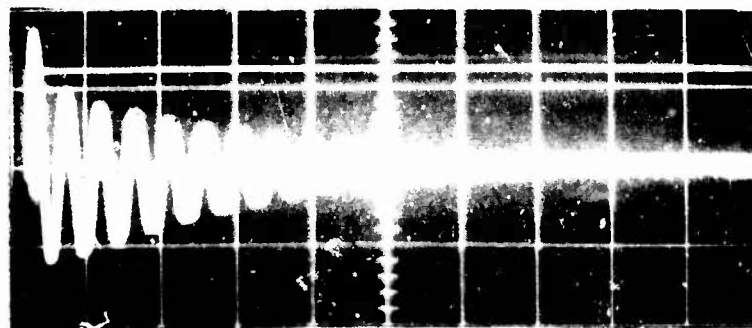
b) Discharge Waveform after Spark Gap Break-
down, Horizontal Sweep Speed - 10 μsec/cm,
Vertical Sensitivity - 2 kv/cm

Figure 68. Voltage Waveforms Across Charging Capacitor

120

peak voltage pulse of approximately 4 kilovolts with random 2 kilovolt spurious discharges riding on the same charging curve with a charging cycle period of 60 hertz is normally observed during operation. Figure 68 b) illustrates the duration of the capacitor discharge, which is approximately 65 microseconds from the time the spark gap breaks down. The exponentially damped discharge oscillation has a frequency of 200 kilohertz and damps out in some 14 cycles in this 65 microsecond period.

6. Spark Gap Simulation - APL-2 Apparatus

After the modification of the APL-1 apparatus to the APL-2 configuration (Section II, A. 4), the same observations and techniques used to detect circuit change effects were repeated. Using the pulse generator input to the system, a series of photographs was recorded as shown in Figure 69. With the reference and sample coil voltage waveforms superimposed as before (and the trolleys at their calibrated position), a comparison on an extended sequence of time base exposures was recorded to present two complete pictures of the electrical system response with pulse input. Those segments of the waveform where the two signals diverge due to the characteristics of the trolley lines is evident at the faster sweep speeds. As the sweep speed is decreased, further discrepancies are no longer discernible due to the corresponding loss in CRT resolution between the two signals. The waveforms observed have an initial 4. 0 megahertz damped oscillation which decays into the 200 kilohertz resonant frequency of the electrical system. There is also some indication of a high frequency small amplitude component superimposed on the first few cycles of the response waveforms.

As was observed previously with Allison's apparatus, moving the sample trolley through six positions effectively shifts the leading edge of the sample voltage waveform from an in-phase position (with the main slide-wire on 8. 96 meters total length, reference trolley on 14. 73, and the sample trolley on 15. 10 Allison units) to a lagging position with respect to the reference waveform. Results of these observations, which are shown in Figure 70 a), indicate an approximate shift of 5 nanoseconds for a trolley change of 15 Allison units. Further observations, as shown in Figure 70 b), were made in which the sample trolley was placed at 12. 00, 15. 00, and 18. 00 Allison units. A phase shift of the initial leading edge of the sample signal from a leading position to in-phase and then to a lagging position is quite apparent.

These same observations were recorded and are shown in Figure 70 a) and b) for the first half-cycle in order to demonstrate the general waveform change and phase shift of the signals as the relative position of the sample trolley was changed with respect to the calibrated reference trolley position.

121
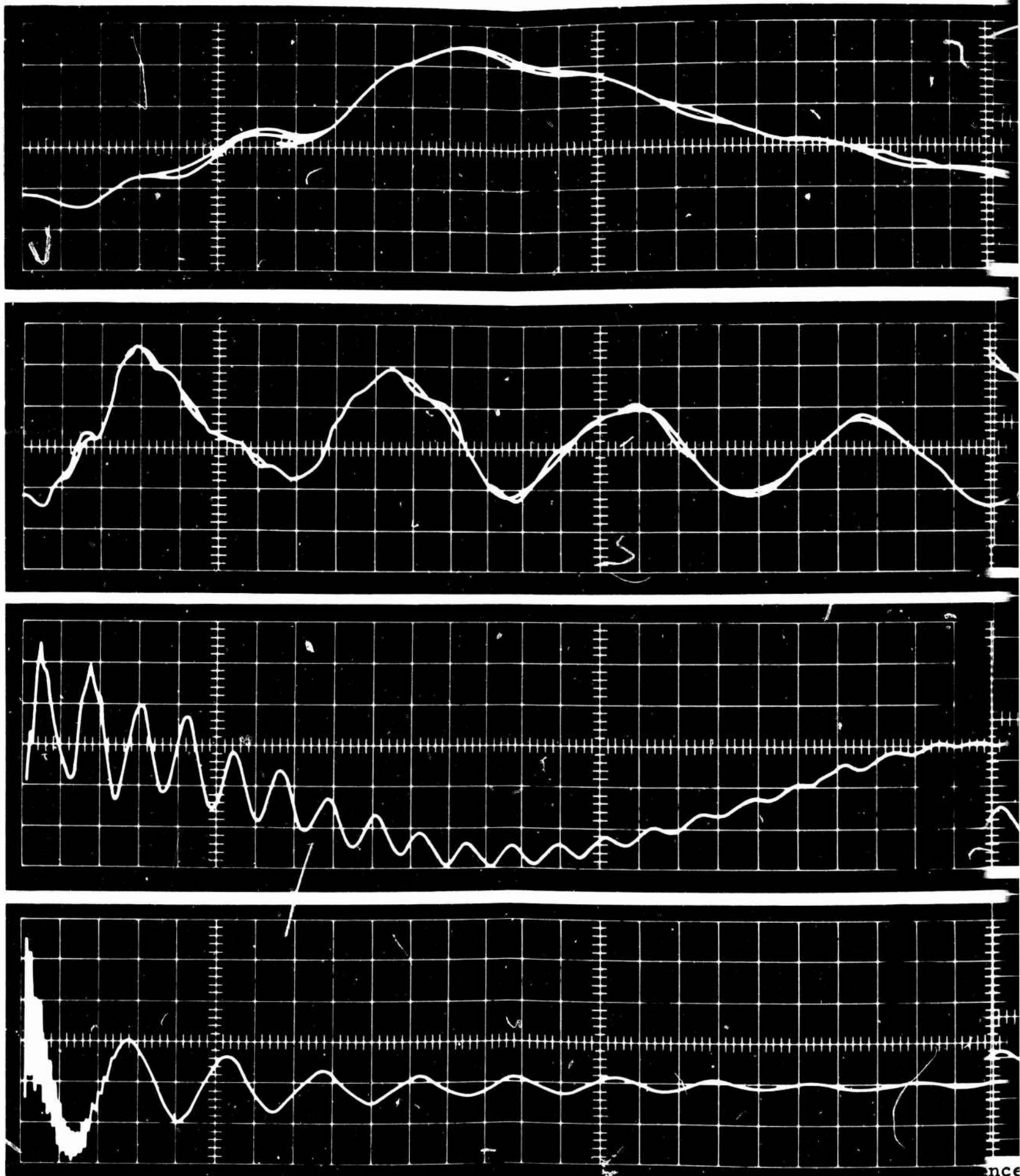
Figure 69. Reference and Sample Coil Voltage Waveforms, APL-2 Appar.
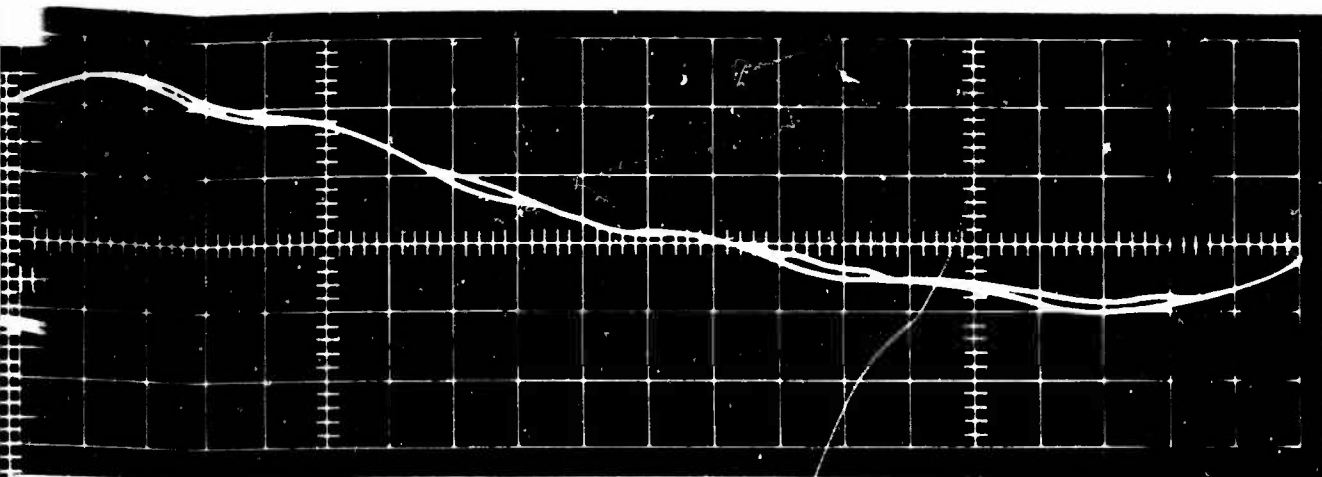
A) First 0.3 μsec., Horizontal Sweep Speed 10 nsec/cm, Vertical Sensitivity 1 v/cm
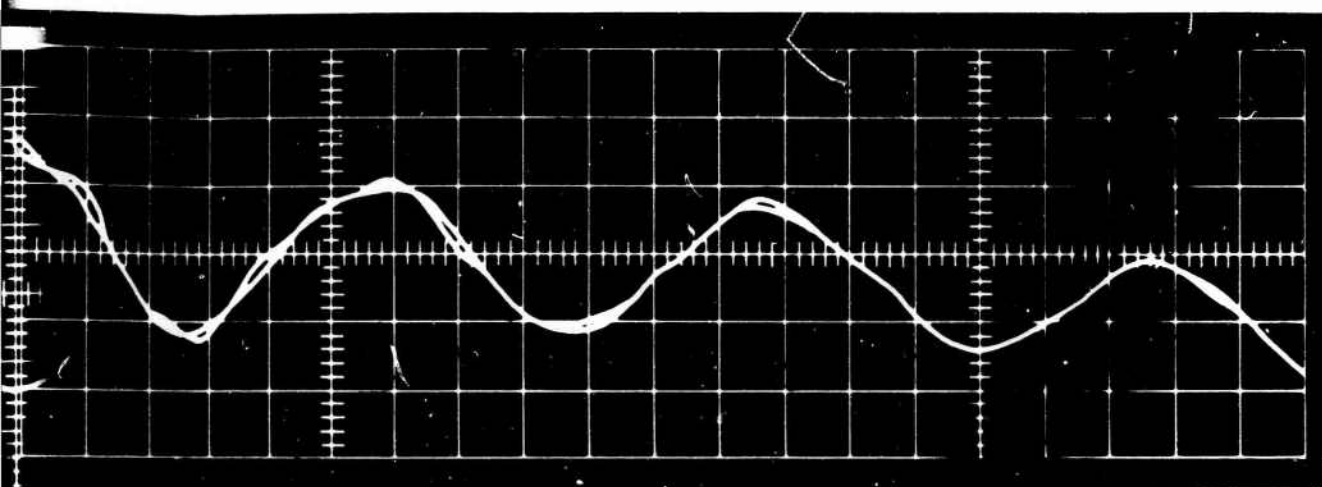
B) First 1.2 μsec., Horizontal Sweep Speed 40 nsec/cm, Vertical Sensitivity 1 v/cm

C) First 6 μsec., Horizontal Sweep Speed 0.2 sec/cm, Vertical Sensitivity 1 v/cm

D) First 60 μsec., Horizontal Sweep Speed 2 sec/cm, Vertical Sensitivity, 1 v/cm

nce and Sample Coil Voltage Waveforms, APL-2 Apparatus, Pulse Generator Input

122

B

a) Sample Trolley at 15.00, 18.00, 21.00,
    24.00, 27.00, and 30.00 Allison Units

12.00   15.00 18.00

b) Sample Trolley at 12.00, 15.00, and
    18.00 Allison Units
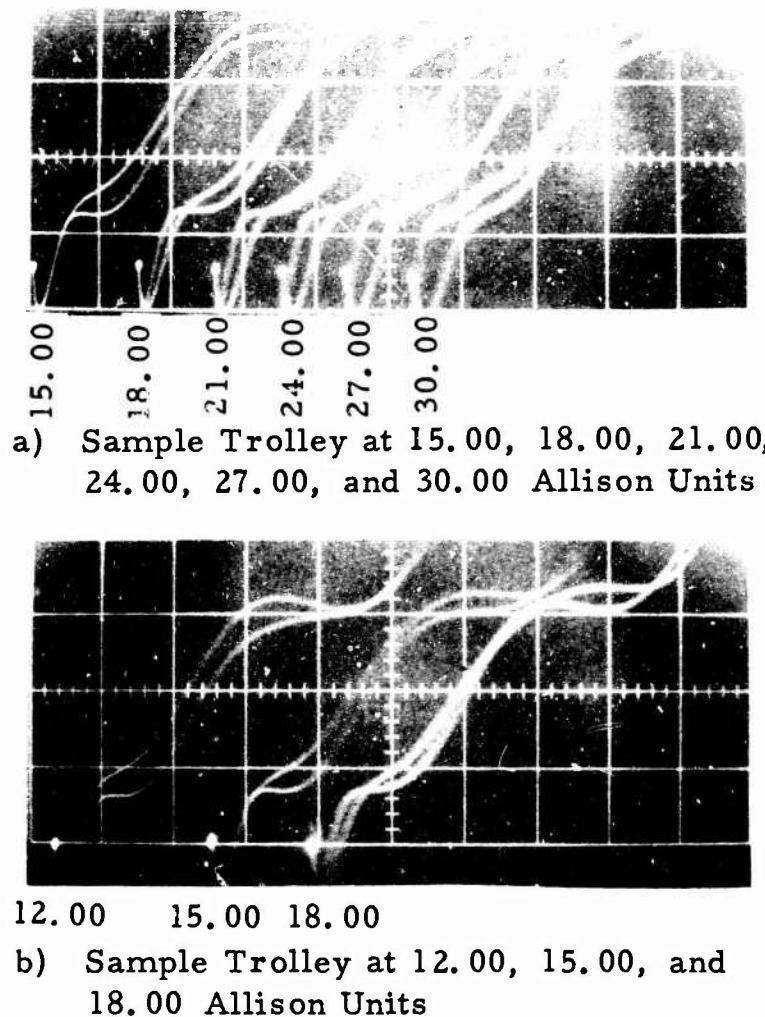
Figure 70. Effect of Sample Trolley Position on Phase Relation
            Between Reference and Sample Coil Voltage Wave-
            form, Pulse Generator Input, APL-2 Apparatus,
            Horizontal Sweep Speed - 10 nsec/cm, Vertical
            Sensitivity - 0.5 v/cm

In both photographs of Figure 71, the extreme sample trolley position
compared to the calibration position (15.00 Allison units) clearly exhibits a
severe waveform mismatch. The phase shift, as indicated by the relative
position of the leading edges of the two waveforms, still can be detected for
large changes in sample trolley position, even at this sweep speed.

A further observation was conducted with this apparatus in which the
position of the main slidewire termination from 0 to 11 meters total length
(0 - 5.5 meters parallel transmission line) was moved with the reference and
sample trolleys at the calibrated position. The effect of these changes, shown
in Figure 72, can be compared with the observations with Allison's apparatus
shown in Figure 61. The optimum phase match (for a laboratory relative
humidity level of 57 percent at the time these exposures were recorded) between
the two waveforms occurs when the total length of line is about 11 meters long,
although in actual operation the 8.96 meter length (45 percent relative humidity)
with the optimum risetime is used.

123

6. 00   12. 00   15. 00

a) Sample Trolley at 6.00, 12.00 and 15.00
    Allison Units

15. 00   18. 00   21. 00

b) Sample Trolley at 15.00, 18.00 a:d 21.00
    Allison Units

Figure 71. Effect of Sample Trolley Position on Phase and Wave-
            form Relation Between Reference and Sample Voltage
            Waveforms, Pulse Generator Input, APL-2 Apparatus,
            Horizontal Sweep Speed - .05 μsec/cm, Vertical Sensi-
            tivity - 1 v/cm

0 Meters
6. 96
8. 96
11. 0C

Figure 72. Comparison of Reference and Sample Coil Voltage
            Waveforms as a Function of Main Slidewire Length,
            APL-2 Apparatus, Horizontal Sweep Speed - 10 nsec/cm,
            Vertical Sensitivity - 1 v/cm

124

7. Normal Operation Observations - APL-2 Apparatus

With the APL-2 apparatus connected for normal operation, as in Figure 34, the initial waveform of the voltage across the sample coil and the current through the coil were recorded as shown in Figure 73. This photograph was recorded using a Fairchild 766H oscilloscope with a 6 x 10 cm screen for the purpose of presenting the waveforms on a larger scale. The one apparent drawback with this oscilloscope was the inability to trigger the sweep on the initial voltage pulse. Approximately 40 nanoseconds delay is observed before the trigger level is sufficient to start the sweep. However, the total current waveform is presented in its entirety.
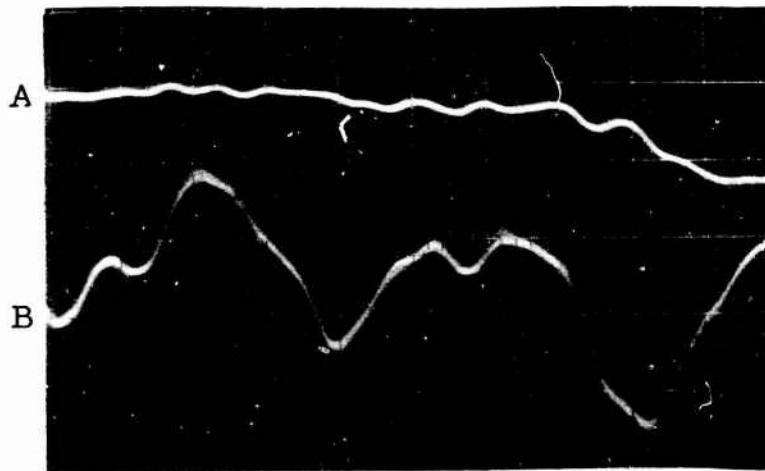
Figure 73. Initial Voltage and Current Waveform of Sample Coil, Normal Operation, APL-2 Apparatus, A - Voltage, B - Current, Horizontal Sweep Speed - 10 nsec/cm, Vertical Sensitivity - A - 2 kv/cm and B - 200 v/cm

In this figure, the major difference when compared to Figure 63 is the longer initial period for the first cycle, approximately 15 nanoseconds. The risetime and falltime of the current pulse on Allison's apparatus are much faster, and the peak amplitude of the current pulse is much higher than on the APL-2 apparatus. It must be remembered that this signal is not an exact indication of current magnitude due to the significant rf pickup encountered in this measurement.

Figure 74 displays several interesting features which furnish experimental clues to the electrical behavior of the system. Consider the behavior of the waveform in the 60 to 70 nanosecond range. As the length of the sample delay line is increased, the prominence in that time interval shifts to the left. The same behavior is observed in the case of the second major prominence in the 0 to 10 nanosecond interval. The direction of shift is contrary to what

might be expected from a theoretical analysis based on variations in time delay, since, on that basis, the voltage waveform observed at the sample coil should shift to the right as the length of the delay line in the sample circuit is increased.
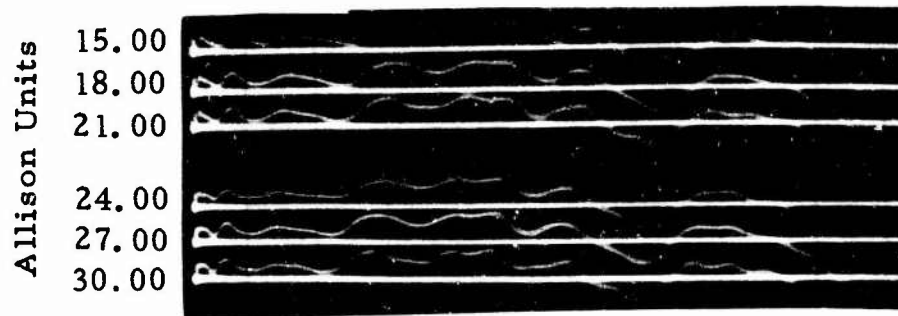
Figure 74. Sample Coil Voltage Waveform Effect as Sample Trolley Position Increases, Horizontal Sweep Speed - 10 nsec/cm, Vertical Sensitivity - 2 kv/cm

The experimental results become even more interesting when they are compared to those obtained with the pulse generator substituted for the spark gap. Figure 70 a) clearly exhibits a progressive delay (or shift to the right) in the sample waveform when the length of the delay line in the sample circuit is increased.

Some of the shift to the left in Figure 74 could be attributed to a progressive delay in CRO triggering due to a progressive decrease in slope of the leading edge. However, this would seem to be an insignificant amount. Furthermore, it would not explain why there is a marked decrease in the relative spacing between the prominence in the 0 to 10 nanosecond range and that in the 60 to 70 nanosecond range.

All these experimental data may be reconciled if one interprets the behavior in terms of phase shifts and amplitude changes in the Fourier components of the waveforms. In this light, the short-circuited parallel wire transmission line takes on the appearance of a circuit element. If, to a certain frequency, it is shorter than a quarter wavelength, then it appears as an inductive element. If it is longer than a quarter wavelength (but less than a half wavelength), it appears to be a capacitive element. For a given initial line length, a phase retardation (shift to right) could be expected for low frequency Fourier components as the sample line length is increased. A phase advance (shift to left) could be expected for those higher frequencies where the sample line length makes a transition to second quarter of the wavelength. (The inductive behavior repeats for odd quarter wavelength multiples and the capcitive behavior repeats for even quarter wavelength multiples.)

The initial 15 Allison unit length of the sample line is a quarter wavelength shorted section for 33 megahertz and a three-quarter wavelength shorted

section for 100 megahertz. A study of the traces in the 60 to 70 nanosecond range indicates that frequency components just above the 33 megahertz value are responsible for the fluctuations observed, and a study of the waveform in the 0 to 10 nanosecond range reveals the probable presence of frequencies at or above 100 megahertz. Accordingly, a shift to the left would be predicted in both these instances as the length of the shorted section is increased.

If we return now to Figure 70 a), it is easy to see that the slowly increasing part of the sample waveform must be associated with frequency components well below the 33 megahertz value. In this case, an increase in sample line length should increase the phase retardation, and such behavior is evident in the figure.

Similar observations of the voltage waveform across the reference coil as a function of sample line length, shown in Figure 75, display only an amplitude change in the waveform in the 60 to 70 nanosecond range. A comparable
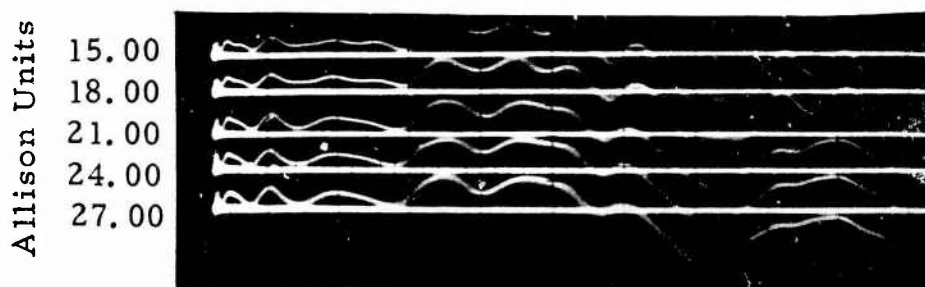
Figure 75. Reference Coil Voltage Waveform Effect as Sample Trolley Position Increases, Horizontal Sweep Speed - 10 nsec/cm, Vertical Sensitivity - 2 kv/cm

shift in the waveform for increased sample line length is absent, but the loss of one of the Fourier components of the waveform can be observed as a gradua peaking of the waveform for an increased sample line length.

It may be concluded, then, that the experimental evidence seems to indicate that sample trolley adjustment produces relative phase shifts between identical Fourier components in the two channels of the apparatus; naturally, amplitude changes will be produced also.

In Figure 76, a series of current and voltage waveforms for the sample cell coil (which is also representative of the waveforms on the reference coil) is illustrated for discrete intervals of time. The purpose of this exhibit is to present to the reader a more fully developed picture of the complex waveforms present in this particular system. Figure 76 a) represents the waveforms observed during the first 0.3 microsecond after each spark discharge. The rf

Figure 76. Voltage and Current Waveforms, APL-2 Apparatus,

128
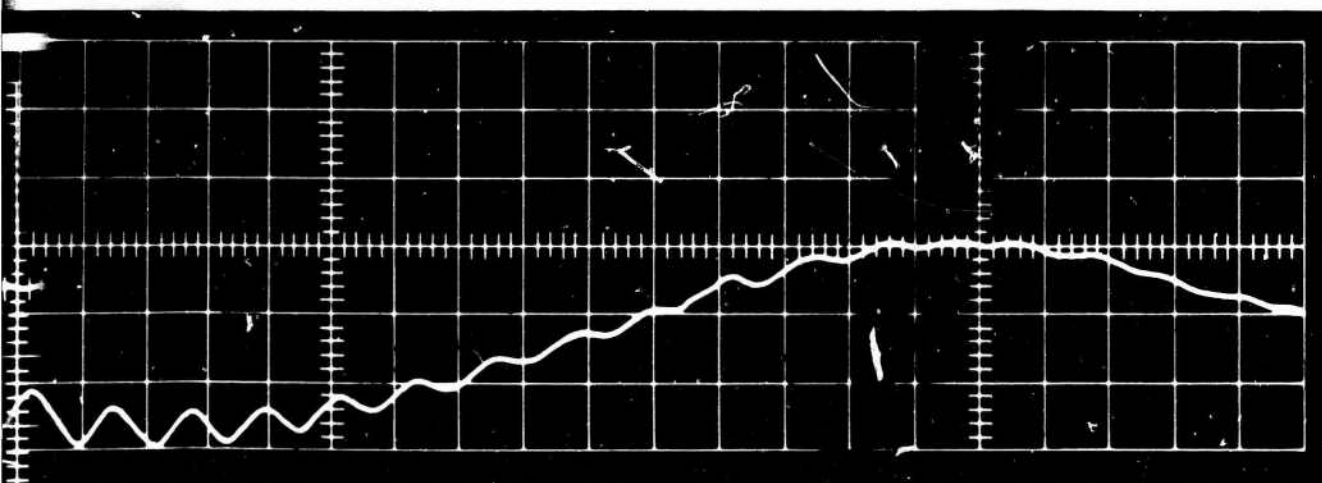
A
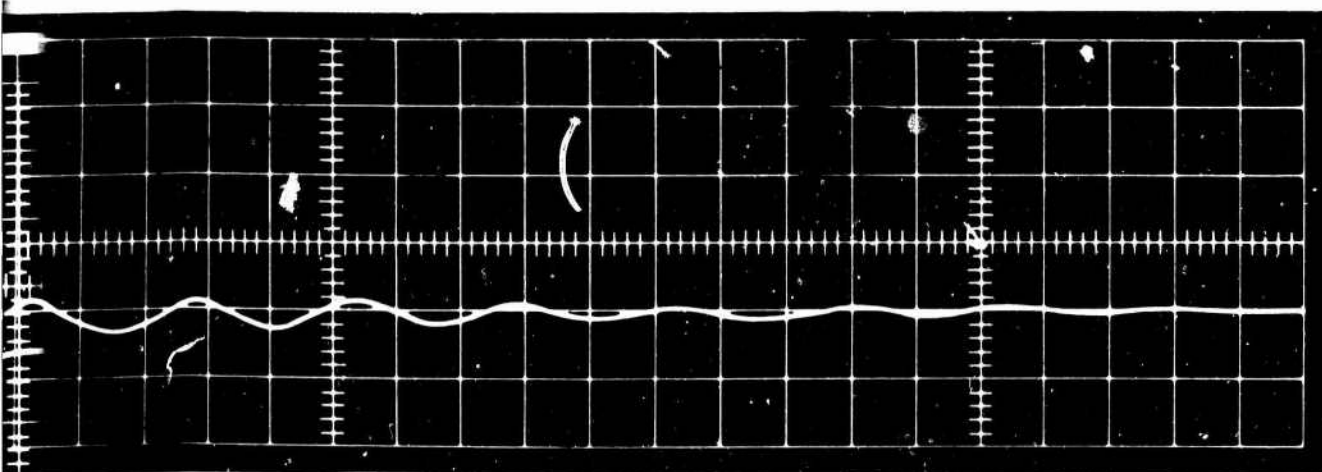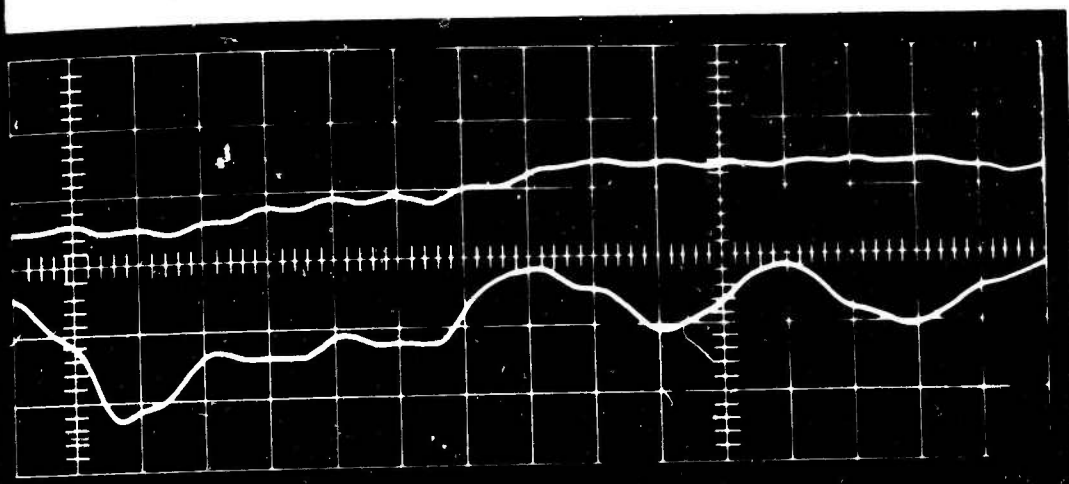
A) First 0.3 μsec,
Horizontol Sweep
Speed 10 nsec/cm,
Vertical Sensitivity
2 kv/cm
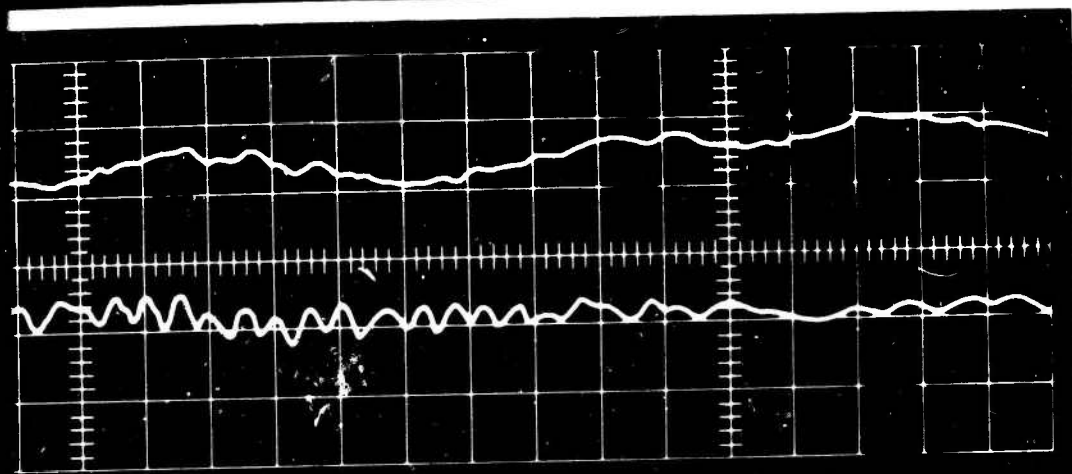
B) First 1.2 μsec,
Horizontal Sweep
Speed 40 nsec/cm,
Vertical Sensitivity
2 kv/cm
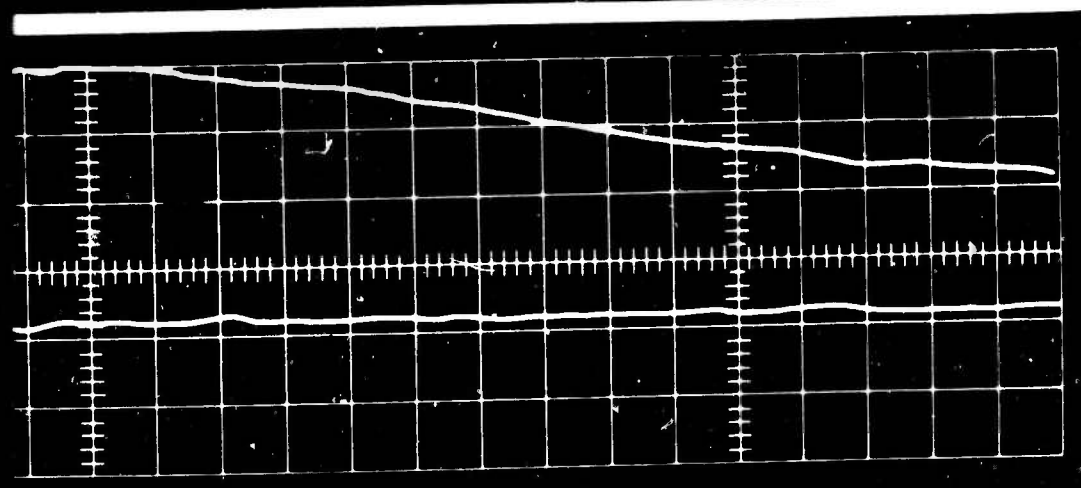
C) First 6 μsec,
Horizontal Sweep
Speed 0.2 nsec/cm,
Vertical Sensitivity
2 kv/cm
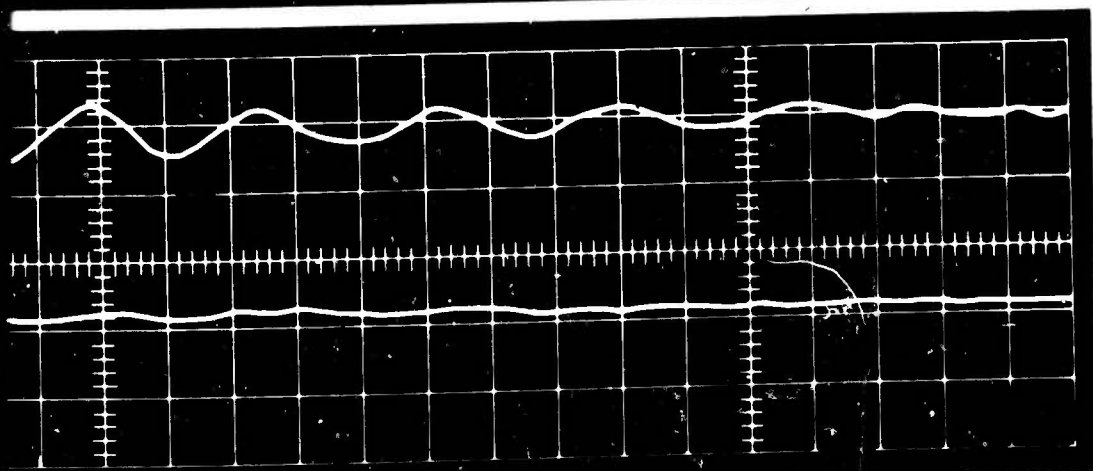
D) First 60 μsec,
Horizontal Sweep
Speed 2 sec/cm,
Vertical Sensitivity
2 kv/cm

rrent Waveforms, APL-2 Apparatus, Normal Operation

B

current waveform reaches a peak value in about 20 nanoseconds and develops into an initial frequency component of 25 - 28 megahertz waveform, with a damped higher frequency (approximately 50 megahertz) component of lower amplitude superimposed upon it. The 25 megahertz component of the current waveform rapidly decays in about 1 microsecond (Figure 76 b) into the natural frequency component, which is barely discernible on this scale. The voltage waveform reaches a maximum value (negative) in approximately 150 nanoseconds. This does not include the initial breakdown voltage pulse which is not presented in these photographs taken with the Fairchild 766H oscilloscope. As mentioned previously, the first 40 nanoseconds of the signal are lost due to triggering delays in the oscilloscope. A small amplitude high frequency component also can be observed superimposed on the voltage waveform. Indications are that this component may have a frequency component of approximately 100 megahertz. As shown in Figure 76 c) and d), this waveform evolves into the natural frequency response of the electrical system in approximately 1.5 microseconds, which then dampens out in 65 microseconds with some 13 cycles of oscillation.

Loading effects of the probe (approximately 4 pf capacitive) on the current waveform, shown in Figure 73, are clearly evident when examining Figure 77, in which we have removed the high voltage probe from across the coil while still measuring the current through the coil (voltage drop across 0.01 ohm resistor). A decrease in risetime with a substantial increase in amplitude for the first few cycles is apparent. The component of frequency contained in the initial few cycles would be more clearly defined than before, and exhibits a frequency of 23.8 megahertz during the initial portion of the waveform. At this point, the possibility of the initial waveform appearing as a perfectly damped 20 - 25 megahertz sinusoid without any distortion might be considered, if the waveform could be observed without any probe loading.

Figure 77. Current Waveform Change Due to Removing One Probe from Measuring Circuit, Horizontal Sweep Speed - 10 nsec/cm, Vertical Sensitivity - 200 v/cm

The series of initial observations on the APL-2 apparatus was concluded with an examination of the charging voltage build-up across the capacitor prior to the spark gap breakdown and the damped oscillation following the breakdown.

129

Figure 78 a) represents the initial charging curve of the capacitor in the APL-2 apparatus. A peak to peak voltage pulse of approximately 5 kilovolts with a charging cycle of 60 hertz is normally observed during operation. In comparing this waveform to Figure 68 a), we can observe that an opposite polarity exists between the two waveforms of the charging pulses. This can readily be explained
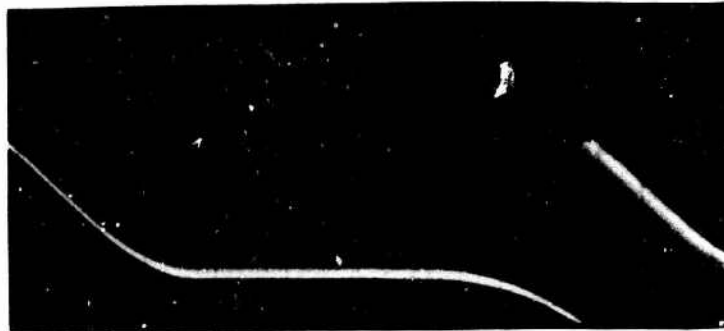
a) Charging Curve Across Capacitor, Horizontal
   Sweep Speed - 2 ms/cm, Vertical Sensitivity -
   2 kv/cm
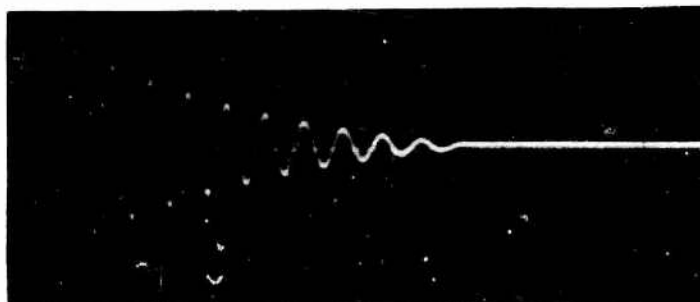
b) Discharge Waveform After Spark Gap Break-
   down, Horizontal Sweep Speed - 10 μs/cm,
   Vertical Sensitivity - 2 kv/cm

Figure 78. Voltage Waveforms Across Charging Capacitor
          APL-2 Apparatus

by the fact that, during the course of measurements on Allison's apparatus, the high voltage probe ground had to be placed at the junction point of the capacitor, high voltage transformer secondary, and gap in order to observe the charging waveform. Placing the probe with its ground on the rectifier anode side of the charging capacitor would result in a loading effect on the charging circuit and subsequent erratic operation. With the APL-2 apparatus, however, this probe connection was possible because of the isolation from ground, as shown in Figure 34; it was used for these measurements, due to the location of the leads and capacitor for convenience.

The discrepancies which are apparent when examining the slope of the charging waveform can best be explained in this manner. The waveform shown

in Figure 78 a) would be the normal curve expected from a half-wave rectifier signal charging a capacitor with very little inductive and resistive loading. The linear charging waveform in Figure 68 a), however, can be attributed only to the resistive effect of the rheostat control used in Allison's system being reflected in the secondary of the high voltage transformer and thereby appreciably contributing to the resistance of the secondary charging circuit. This would have the effect of smoothing out the charging curve. In the APL-2 apparatus, the control element is a powerstat which could enhance only any inductive effect appearing in the secondary of the transformer.

Figure 78 b) illustrates the duration of the capacitor discharge, which is approximately 64 microseconds from the time the spark gap breaks down. The exponentially damped discharge oscillation has a frequency of 200 kilohertz and dampens out in about 11 cycles in this 64 microsecond period.

E. CALIBRATION AND OBSERVATION OF MINIMA WITH ALLISON EFFECT APPARATUS

1. Calibration - APL-1 Apparatus

In paragraph D, 2 and 3 of this section, we had indicated that liberties taken in the construction of this particular apparatus created inherent difficulties when attempts were made to match the waveforms across the coils. The importance of electrical symmetry of the trolley lines used in the system became apparent when the apparatus was to be calibrated prior to observing minima. Using the standard procedure outlined in several papers in the past[1, 3, 7, 17, 26], we experienced negative results in observing even the broad Faraday minima for carbon disulfide samples. In light of the experience gained with oscilloscope observations on Allison's apparatus, it was surmised first that the trolley lines must be symmetrical for optimum matching of the waveforms. In addition, the trolley lines must be of sufficient length to permit the shorting link of the sample trolley to move completely through the zero phase matching point of the two waveforms. As shown in Figure 31, the actual zero calibration point of the sample trolley is 15.00 Allison units from the end of the parallel wire transmission line. Subsequently, in order to continue the investigations, this system was modified to conform more rigidly to the original design of an Allison effect apparatus.

2. Calibration - APL-2 Apparatus

With this system, initial efforts at calibration were encouraging; we could now observe the broad Faraday minima extending ±5.00 units about the 15.00 scale reading. The difficulty encountered at this point was in detecting the minimum light level over this extreme range, due to the small relative change in dimming of light compared to the existing light level, which is on the order of ten percent of the light emitted by the spark breakdown after filtering (4481 Å). To compensate for this low level of light when calibrating the system

with identical samples of carbon disulfide, an additional step was incorporated into the procedure which appears to overcome the difficulty. Immediately after first observing the broad minima and adjusting the sample trolley position to the point where a change in level or dimming cannot be detected by eye, the operator then uncrosses the analyzing Nicol by 1/4 degree to let more light through. With this additional light level, he can then narrow the spread of the minima even further. By repeating this procedure once again, the calibration position was successfully determined to within ± 0.01 units, with an error of one hundredth of a unit between three different operators. As a check, the minima points for hydrochloric acid are observed and correlated with data reported by Allison and others. For this apparatus, the correlation between the data was very satisfactory; the final calibrated position for the reference trolley was determined to be 14.73 units.

In addition to the modified standard method of calibrating an Allison effect apparatus, it has also been determined that the pulse generator and fast rise-time oscilloscope can be used to great advantage. With identical samples of carbon disulfide in the cells as usual, an operator monitoring the superimposed voltage waveforms across the sample and reference coils can effectively set the sample trolley on its calibrated position with relative ease. Using a high vertical sensitivity (on the order of 0.2 volts per centimeter), fast sweep speed (10 nanoseconds per centimeter), and a properly adjusted (focus, astigmatism, and intensity) trace, the calibration point can be determined within ± 0.1 Allison units on the first pass through the 15.00 scale reading. With stable triggering and careful observation of the leading edge of the waveforms, an observer can maneuver the sample trolley position (adjusted by an assistant) to within ± 0.02 units of the exact calibrated position.

3. Observation for Minima - Allison's Apparatus

During the course of the experimental observations conducted with Allison's apparatus, several attempts were made to observe the minima of a prepared sample. At the time these observations were conducted, the relative humidity conditions experienced in the laboratory area were almost always in excess of sixty percent. At first, the detection of the proper minima point was extremely difficult due to unfamiliarity with differentiating between a light change and the light dimming due to the spark. Once an operator overcomes this difficulty and can distinguish between a clearly defined minima for a known sample and a spark fluctuation, then it becomes relatively easy to pick out a minima if it exists in the sample under examination. Nevertheless, the process is very fatiguing, requiring, of necessity, many short periods (less than a minute) of observation for an operator to determine the validity of an observation.

The observations for minima conducted with Allison's apparatus under the humid conditions were greatly improved through the use of the water cell capacitor configuration discussed in paragraph D.5 of this section.

4. Observations for Minima - APL-2 Apparatus

In addition to the calibration observations previously discussed, we have repeatedly observed minima for three different compounds. These are separate samples of hydrochloric acid, lithium fluoride, and calcium phosphate diluted in solutions of one part per million in tripled distilled water.

Repeated observations by trained observers have indicated that the system as presently constructed is in working order, and that the observed minima are in excellent agreement both in number and position with reported data for the samples investigated.

F. QUALITATIVE AND QUANTITATIVE OBSERVATIONS

The experimental investigations were concluded with an initial study of oscilloscope observations of the qualitative and quantitative effects of samples on the coil waveforms during normal operation.

By recording multiple exposure photographs of the reference and sample coil waveforms as shown in Figure 79, the waveforms can be compared at the zero scale position (15.00), and then at the particular sample point. In the first instance, a sample of calcium phosphate (diluted 1 part per million) was compared in the upper pair of traces at 15.00 units and then at 23.20 units (one of the three minima points for this compound) of the scale. Although the two high voltage probes used have slightly different risetimes (4 and 7 nanoseconds), a definite shift to an in-phase comparison of the two waveforms as the sample trolley approaches the correct scale reading can be observed.

15.00 units

23.20 units

Figure 79. Sample Trolley Position Effects on Voltage Waveforms Calcium Phosphate (1 ppm) in Sample Cell, Carbon Disulfide in Reference Cell, Horizontal Sweep Speed - 10 ns/cm, Vertical Sensitivity - 2 kv/cm

The general shape of these waveforms should also be compared with those of Figure 80, in which carbon disulfide was placed in a sample cell and compared at 15.00 units with total main leadwire lengths of 6.96, 8.96, and 10.96 meters

133

total length. On this particular day, the waveforms matched best with a total length of approximately 11 meters. The presence of carbon disulfide in both cells appears to smooth out the contour of the waveform to some degree.

Figure 80. Main Leadwire Effect on Voltage Waveforms, Carbon Disulfide in Both Reference and Sample Cells, Horizontal Sweep Speed - 10 nsec/cm, Vertical Sensitivity - 2 kv/cm

In Figure 81, we have recorded successive exposures of the two waveforms with calcium phosphate in the sample cell. Each of the three minima points for this compound were observed along with a point midway between. Only by careful examination of an enlargement of the photograph could a shift in position or phase of the waveforms be observed. This shift for the extreme positions is much less than 0.1 nanosecond and beyond the resolution of oscilloscope.

Figure 81. Waveform Comparison for Three Minima Positions of Calcium Phosphate (1 ppm), Horizontal Sweep Speed - 10 nsec/cm, Vertical Sensitivity - 2 kv/cm

To compare the effect of sample concentration on the waveform, a series of exposures was recorded as shown in Figure 82 a) to d). In these photographs, we initially observed the waveforms with just triple distilled water in the sample coil, first at 15.00 units and then at 23.20 units, the lower minima point of the compound. The results shown in Figure 82 a) are lacking in the high frequency component that is evident in Figure 79 for the calcium phosphate sample. The

134
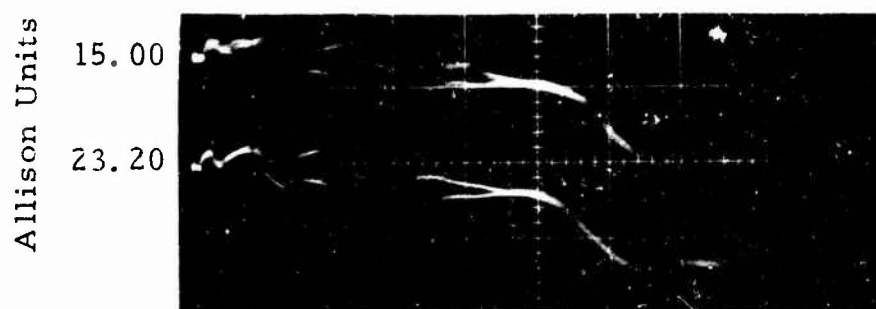
a) Reference Cell - Carbon Disulfide, Sample Cell - Triple Distilled Water

b) Reference Cell - Carbon Disulfide, Sample Cell - Calcium Phosphate 1 part per 10 million

c) Reference Cell - Carbon Disulfide, Sample Cell - Calcium Phosphate 1 part per 2 million

d) Reference Cell - Carbon Disulfide, Sample Cell - Calcium Phosphate 1 part per million

Figure 82. Concentration Effects on Waveform, Horizontal Sweep Speed - 10 nsec/cm, Vertical Sensitivity - 2 kv/cm

135

sample signal approaches the phase of the reference signal, but a good wave-form match cannot be accomplished after repeatedly passing through the 23.20 scale reading. When a 10 percent solution of one part per million calcium phosphate is added thereby resulting in an approximate solution of one part in ten million, it was extremely difficult to observe any change in the waveform as shown in Figure 82 b). The effect of increasing the concentration to one part in two million, however, can be distinguished from the previous obser-vations. A distinct high frequency component has appeared on the waveforms. Further increases in the concentration to one part per million show little change between Figure 82 c) and d).

Visual observations of oscilloscope waveforms indicate that, for the concentrated samples, we can easily detect an area of broad matching (±1.0 unit) about the proper minima points for the compounds used in these experi-ments. These results are very encouraging considering the difficulties encountered in triggering and observing the waveforms produced by the spark gap discharges. With the development of a more repetitive spark discharge system, further quantitative and qualitative investigations along this line are judged necessary.

SUMMARY

The efforts documented in this report represent a new and different approach to the study of the Allison effect and the Allison effect apparatus. A final objective of the continuing program is to make the effect useful and convenient for chemical analysis of known fluids containing trace impurities. Accordingly, it is necessary to discover which parameters of the optical and electrical systems are active, what can be done to enhance the presently marginal responses, and what latitude is available in simplifying, modernizing, and miniaturizing the components of these systems.

In a joint experimental and theoretical effort, a replica apparatus of a standard Allison type was analyzed in its every detail by modern electronic test equipment in order to provide accurate information about the voltages and currents that are present in the apparatus while the effect is being produced. A concurrent theoretical analysis attempted to predict these same electrical values. A circuit model was generated to represent the physical circuit and its excitation. The solutions of the circuit model were to be compared with the experimental counterparts. In addition, the optical characteristics of the equipment were studied both from the experimental and theoretical points of view.

There was a coordinated effort and a mutually cooperative spirit throughout the current work. The theoretical phase suggested promising directions of activity for the experimental group and there was experimental feedback to guide the theoretical study.

The experimental phase of this program has produced significant data on the systems which previously had not been reported. These data include evidence that:

     1. The light emitted by the spark is intensity modulated by the time varying current.

     2. The spark gap has the characteristics of a passive switch with a low value, linear resistance.

     3. A continuous frequency spectrum containing various resonant peaks and extending up to 4000 megahertz is generated by the electrical transient. However, the amplitudes of the signal components fall off sharply above approximately 30 megahertz.

     4. Successful operation of the apparatus seems to depend upon simultaneous optical and electrical balance between the two solenoid circuits.

137

5. Relative phase shifts occur between high frequency signal components in the two branches of the circuit when trolley adjustments are made. These signal frequencies appear to be in the 30 to 100 megahertz range.

6. Trace impurities of the order of parts per million produce observable disturbances in the electrical signals.

There are a number of areas of agreement between the theoretical analysis and the experimental results, even when a highly idealized electric circuit model is employed. The circuit model finally chosen to represent the physical circuit is a compromise between an oversimplified model and one which would lead to intractable mathematical expressions. The solutions become more difficult because the apparatus contains series combinations of lumped and distributed parameters. At present, only the Laplace transforms of the current and voltage solutions are available, and it is clearly evident that an extensive computer program will be required to reduce these expressions to the final useful form. Significantly, it was possible to obtain initial computer solutions valid for selected operational modes of the equipment, and the results are very encouraging. They indicate risetimes and waveform behavior consistent with the experimentally observed traces.

The theoretical study has suggested a basis for the trolley displacement resolution of the minima; phase comparison of frequencies in the 30 megahertz range will permit such high resolution as has been observed. This possibility had not been considered in previous discussions of the Allison effect because earlier investigators were unaware of the range of frequencies present in the apparatus. If this suggestion leads to a confirmation of the fact, it will further lead directly to an enhancement of the Allison effect and the long awaited objective experimental evidence. The obvious step is to eliminate those frequencies which do not contribute to the effect, thus improving the signal to noise ratio of the system.

The theoretical investigation also suggests that the optical section of the apparatus plays the part of the detector in the electrical phase comparison of the solenoid signals. The process suggested is one of light modulation by means of an electro-optical interaction in the fluids in the cells. The Cotton-Mouton magneto-optic effect seems a logical possibility in view of the high electrical frequencies present which give rise primarily to axially directed displacement currents in the solenoid distributed capacitances.

There is as yet no theoretical explanation for the extreme sensitivity of the Allison effect. Based upon the suggested frequency effect, a conjecture would tend to attribute the phenomenon to the presence of some common factor in the reference and sample cells. One possibility that may be significant is the presence of water as a trace contaminant in all fluids unless extreme

138

measures are taken to eliminate it. Trace contaminants in the sample cell
may form complex structures with water molecules, resulting in a small con-
centration of active centers which would still be relatively effective because
of resonance. The trace water in the reference cell may, in the presence of
the host fluid, form similar complex structures. The type of impurity in the
sample cell may cause slight variations in the resonance which then lead to
variations in the trolley settings. Another factor which lends some plausibility
to this conjecture is the adverse effect of humidity on the observation of minima.
Due to the nature of the apparatus construction, humidity adds water molecules
to the light path of the system.

CONCLUSIONS AND RECOMMENDATIONS

The two-pronged experimental-theoretical investigation of the Allison effect has produced once more the same subjective evidence observed by previous experimenters. In addition, it has yielded a body of experimental data on the electrical operation of the apparatus such as had not been obtainable previously because of technological limitations in instrumentation. A theoretical analysis of the electric circuit has been performed; however, the solutions are available presently only in the form of Laplace transforms. An initial computer solution has been performed which shows promise, but it is valid only for the first tens of nanoseconds and only for very small lengths of the delay lines, a maximum of one or two Allison units in each of the three lines. It is estimated that this trial computer solution represents no more than one percent of the effort required for a complete solution of the expressions. After the complete solution is performed, an even greater effort will be required to substitute the results into expressions leading to the electric and magnetic fields in the solenoids. Even now it is possible to see that important amplitudes at frequencies in the tens of megahertz will be predicted and there is a growing conviction that the Allison effect will be traceable to definite frequency components in the transient.

It is therefore recommended that:

1. The complete computer solution be delayed until the experimental work on bandwidth limitation has produced either positive or negative results. If a positive result is obtained, then the solution will simplify to that of the steady state problem, a much easier problem requiring only a nominal effort.

2. A further analysis be conducted on the recorded waveforms to discover the frequency content of the transient. There are techniques whereby the waveforms of Figures 74 and 75 (Section II) could be transferred to magnetic tape. A closed loop of tape could be passed repeatedly through a pickup and the output applied to an audio frequency spectrum analyzer. The frequencies of the resolved Fourier components could be multiplied by the appropriate scale factor to give the frequencies actually present in the transient. By analyzing the successive recordings, it would be possible to determine the effect of adjusting the trolley position.

3. There is sufficient evidence to warrant tests where the signals applied to the solenoid circuits are limited to frequency bands that are fixed by appropriate band pass filters. If the Allison effect persists when this is done, it will be conclusive that relative phase shifts are instrumental in the production of the effect. In the limit, the effect could be produced without benefit of the spark gap. A coherent radio frequency signal generator could excite the electrical circuit and the optical elements could be illuminated by a continuous emission, a continuous magnesium arc for example. The trolley adjustment would produce

the phasing necessary for the production of a minimum. A relatively low power signal generator would be effective; remember that the present transient contains considerable electrical power, but it is distributed over a continuous radio frequency spectrum and only a small amount of power is present at a given frequency. There is a suspicion that the modulation of the light source is important. Such modulation could be produced easily by means of an electro-optic cell. Finally, a photodetector could be operated efficiently by tuning its output to the radio frequency value. The only difficulty would be that of determining which radio frequency value is active in the Allison effect; the recommended experiments employing band pass filters would help in locating these.

4. A triggered spark gap be used so that a more accurate spectrum analysis of the impulse will be possible. The standard Allison effect apparatus has several characteristics which make it particularly difficult to apply modern measurement techniques. One is the randomness in the initiation of the spark. Spark gap triggering will have little effect upon the electrical or optical nature of the spark. Triggering can be accomplished by means of a third electrode to which a triggering impulse is applied at a predetermined time; or, the usual two electrode gap can be triggered by means of a sharp voltage spike applied in series with the charging capacitor.

5. The light source be stabilized by an optical arrangement. An undesirable characteristic is the tendency of the spark to wander about in the region of the electrodes. This has been a common complaint in the literature and it is surprising that nothing has been done to improve the situation. The optical background noise detracts the eye from its observation of minima and, undoubtedly, is one of the factors that makes electronic detection of light minima virtually impossible. It has been suggested that a converging "light pipe" arrangement be used. A tapered cone will gather the light from the spark; total internal reflection will converge the light into a small well-localized spot.

6. The use of a laser as a light source for the Allison effect apparatus be investigated. The undesirable intensity fluctuations in the spark (from impulse to impulse) would be eliminated if a steady c. w. gas laser plus a controlled electro-optic shutter were substituted for the present arrangement. Since this is a radical change, it should be considered only as a sequential improvement to follow a successful implementation of the measures recommended for improving the present spark gap source. It will be important to consult authoritative sources for information regarding safety precautions. Direct visual observation of a laser beam is to be prohibited.

7. The Cotton-Mouton magneto-optic effect be considered as a possible means for optical interactions. Since the high frequency currents flow in the axial direction and over the skin of the solenoids, they produce magnetic fields which are mainly perpendicular to the axial direction. This magneto-optic effect is produced by a magnetic field perpendicular to the light direction. Also, it is an effect produced in liquid media.

APPENDIX I

A. COMPUTER PROGRAM A

B. COMPUTER PROGRAM B

Program A

```
-BALGL      CAMPBELL  /COMBINEGENSOLV 9323760  PROD      04/07/66.15.38

0200                   BAC-220 SPECIAL VERSION  2/22/64

0200      INTEGER N,I,J,T$

0200      ARRAY M0(50),M1(50),M2(50),N0(50),N1(50),N2(50),N0N1N2(50),

0200             M0N1N2(50),N0M1N2(50),N0N1M2(50),N0M1M2(50),M0M1N2(50),

0200             M0N1M2(50),F(50),ADJSIGMA(50),A(50),HH(50)$

0200      R0=R3=1$ L0=L3=2**-6$ C1=C2=5**-12$ Z=500$

0211      INPUT DATAFACT (FOR I=(1,1,20)$F(I))$

0232      READ ($$DATAFACT)$

0236      INPUT DATA (N,T0,T1,T2)$

0252      START..

0252      WRITE($$EJECT)$

0256      READ ($$DATA)$

0260      IF T0 NEQ 0$ BEGIN FOR I=(2,2,N+1)$

0276             M0(I) = 10.0*15.T0*(I-1).F(I).Z$            END$

0294      IF T1 NEQ 0$ BEGIN FOR I=(2,2,N+1)$

0310             M1(I) = 10.0*15.T1*(I-1).F(I).Z$            END$

0328      IF T2 NEQ 0$ BEGIN FOR I=(2,2,N+1)$

0344             M2(I) = 10.0*15.T2*(I-1).F(I).Z$            END$

0362      IF T0 NEQ 0$ BEGIN FOR I=(1,2,N)$

0375             N0(I) = 10.0*15.T0*(I-1).F(I)$             END$

0392      IF T1 NEQ 0$ BEGIN FOR I=(1,2,N)$

0405             N1(I) = 10.0*15.T1*(I-1).F(I)$             END$

0422      IF T2 NEQ 0$ BEGIN FOR I=(1,2,N)$

0435             N2(I) = 10.0*15.T2*(I-1).F(I)$             END$

0452      FOR  I=(N+2,1,50)$ BEGIN M0(I)=M1(I)=M2(I)=N0(I)=N1(I)=N2(I)=0$ END$

0473      IF T0 EQL 0$ BEGIN FOR I=(1,1,N+1)$BEGIN M0(I)=N0(I)=0$ END END$

0495      IF T1 EQL 0$ BEGIN FOR I=(1,1,N+1)$BEGIN M1(I)=N1(I)=0$ END END$

0517      IF T2 EQL 0$ BEGIN FOR I=(1,1,N+1$BEGIN M2(I)=N2(I)=0$ END END$
```

144

```
0539      IF TO EQL 0$ NO(1)=1.0**15$ IF T1 EQL 0$ N1(1)=1.0**15$ IF T2 EQL 0$
0539                      N2(1)=10.0*15$
0557      FOR I=(1,1,50)$ BEGIN NON1N2(I)=NOM1N2(I)=NOM1M2(I)=MON1N2(I)=
0557          MOM1N2(I)=NON1M2(I)=MON1M2(I)=ADJSIGMA(I)=A(I)=HH(I)=0$
0580      END$
0581      FOR T=(1,1,N)$ FOR I=(1,1,T)$ FOR J=(1,1,T+1-I)$ BEGIN
0623          IF (I+J) LEQ (T+1)$ BEGIN
0623          NON1N2(T)=NON1N2(T)+NO(I).N1(J).N2(T+2-I-J)$
0644          NOM1N2(T)=NOM1N2(T)+NO(I).M1(J).N2(T+2-I-J)$
0658          NOM1M2(T)=NOM1M2(T)+NO(I).M1(J).M2(T+2-I-J)$
0672          MON1N2(T)=MON1N2(T)+MO(I).N1(J).N2(T+2-I-J)$
0686          MOM1N2(T)=MOM1N2(T)+MO(I).M1(J).N2(T+2-I-J)$
0700          NON1M2(T)=NON1M2(T)+NO(I).N1(J).M2(T+2-I-J)$
0714          MON1M2(T)=MON1M2(T)+MO(I).N1(J).M2(T+2-I-J)$
0728                                          END    END$
0731      RC = R3.C2 + R3.C1 + RO.C2 + RO.C1$ CC= C1 + C2$
0749      LRC = L3.C2 + L3.C1 + LO.C2 + LO.C1 + R3.R3.C1.C2 +2RO.R3.C1.C2$
0777      RC2 = R3.C1.C2 + RO.C1.C2$ LC2 = LO.C1.C2 + L3.C1.C2$
0795      RLC2 = 2R3.L3.C1.C2 + 2LO.R3.C1.C2 + 2RO.L3.C1.C2$
0815      L2C2 = 2LO.L3.C1.C2 + L3.L3.C1.C2$
0827          ADJSIGMA(1) = NON1N2(1)$
0829          ADJSIGMA(2) = NON1N2(2) +
0829              RC.NON1N2(1   ) +CC.MON1N2(1   ) + C1.NOM1N2(1   )+
0829              C2.NON1M2(1   ) $
0845          ADJSIGMA(3) = NON1N2(3) +
0845              RC.NON1N2(2   ) +CC.MON1N2(2   ) + C1.NOM1N2(2   )+
0845              C2.NON1M2(2   ) +
0845              LRC.NON1N2(1   ) + RC2.NOM1N2(1   ) + RC2.NON1M2(1   ) +
```

```
0845          C1.C2.NOM1M2(1   ) + 2R3.C1.C2.MON1N2(1   )        +

0845          C1.C2.MOM1N2(1) + C1.C2.MON1M2(1) $

0895       ADJSIGMA(4) = NON1N2(4) +

0895          RC.NON1N2(3   ) +CC.MON1N2(3   ) + C1.NOM1N2(3   )+

0895          C2.NON1M2(3   ) +

0895          LRC.NON1N2(2   ) + RC2.NOM1N2(2   ) + RC2.NON1M2(2   ) +

0895          C1.C2.NOM1M2(2   ) + 2R3.C1.C2.MON1N2(2   )        +

0895          C1.C2.MOM1N2(2) + C1.C2.MON1M2(2) +

0895          RLC2.NON1N2(1   ) + 2L3.C1.C2.MON1N2(1   ) +

0895          LC2.NOM1N2(1   ) + LC2.NON1M2(1   ) $

0964    FOR T=(5,1,N   )$ BEGIN

0964          ADJSIGMA(T) = NON1N2(T) +

0964          RC.NON1N2(T-1) +CC.MON1N2(T-1) + C1.NOM1N2(T-1) +

0964          C2.NON1M2(T-1) +

0964          LRC.NON1N2(T-2) + RC2.NOM1N2(T-2) + RC2.NON1M2(T-2) +

0964          C1.C2.NOM1M2(T-2) + 2R3.C1.C2.MON1N2(T-2)        +

0964          C1.C2.MOM1N2(T-2) + C1.C2.MON1M2(T-2) +

0964          RLC2.NON1N2(T-3) + 2L3.C1.C2.MON1N2(T-3) +

0964          LC2.NOM1N2(T-3) + LC2.NON1M2(T-3) +

1050          L2C2.NON1N2(T-4)$               END$

1051    FOR T=(1,1,N)$ A(T) = ADJSIGMA(T).(10.0*(-45+(T-1)9))$

1076    A(1) = 1$

1078    OUTPUT MINOR (N,FIX   ((10*9)T0),FIX   ((10*9)T1),FIX   ((10*9)T2))$

1118    FORMAT MINORF (*N=*,I2,B5,*T0=*,I2,B5,*T1=*,I2,B5,*T2=*,I2,B5,

1118          *TAUS IN NANOSECONDS*,W6)$

1137    WRITE ($$MINOR,MINORF)$

1145    A0=A(N)$ FOR I=(1,1,N-1)$ HH(I)=A(N-I)$ FOR I=(1,1,N-1)$ A(I)=HH(I)$

1190    N=N   -1 $
```

146

```
1190

1193      COMMENT.   THIS PROGRAM FINDS THE ROOTS OF AN NTH DEGREE POLYNOMIAL.    SOLVER**

1193                 PROGRAM BY HERB DERSHEM, MODIFIED BY PAUL J. CAMPBELL$

1193      INTEGER NN,M,R,QQ$

1193      INTEGER G$

1193      BOOLEAN          RL$

1193      ARRAY            LMDA(50),B(50),C(50)$

1193      ARRAY S(20), U(20)$

1193      OUTPUT           ROUT(XST), DATAOUT (A0,FOR I=(1,1,N!$A(I)),

1224                       COUT(XST,YST,XST,YST,FREQ)$

1243      FORMAT           EJECT(W4,W4)$

1247      FORMAT           RFORM(*X = *,X10.4,W4),

1247                       CFORM(*X = *,X10.4,B2,*+*,X10.4,B2,*I*,W4,

1247                           *X = *,X10.4,B2,*-*,X10.4,B2,*I*,B5,

1247                           *FREQUENCY IN MC = *,X7.2,W4)$

1275      FORMAT           DATAOUTPUT (*COEFFICIENTS*,(F15.6),W4

1275                       *SOLUTIONS*,W4)$

1285      PROCEDURE        SYNDV(N,K$B(),C())$

1285      COMMENT     THIS PROCEDURE WILL DIVIDE SYNTHETICALLY AN NTH DEGREE

1285                  POLYNOMIAL.  A0.XN+A1.X(N-1)+...+AN BY A KTH DEGREE

1285                  POLYNOMIAL, XK+B1X(K-1)+...+BN.  THE ARRAY

1285                  B()=(A0,A1,...AN) AND C()=(-B1,-B2,....-BK).  THE QUOTIEN

1285                  POLYNOMIAL WILL BE FOUND IN THE FIRST N-R+1 CELLS OF THE B

1285                  ARRAY WITH THE REMAINING R CELLS CONTAINING THE

1285                  COEFFICIENTS OF THE REMAINDER POLYNOMIAL$

1285                  BEGIN

1285                       INTEGER N,K,I,J$

1289                       FOR I = (2,1,N)$

1300                       FOR J = (0,1,K-1)$
```

```
1315                        B(I+J) = B(I+J)+C(J+1).B(I-1)$

1342                        RETURN END SYNDV()$

1351        1..

1351                        WRITE(SSEJECT)$ WRITE (SSDATAOUT,DATAOUTPUT)$

1363        G = 0$

1364                        FOR I=(1,1,N)$

1375        BEGIN

1375                A(I) = A(I)/A0$

1381                B(I+1) = A(I)$

1384        END$

1385                        B(1)=1$

1387                        NN=N$ IF N LEQ 2$

1387                        GO TO 4$

1395        STARTT..        PX=PRSQ=PRCOSTH=PLMDA=PPLMDA=0.0$ QQ=0$

1401                        EITHER IF B(2) EQL 0$ LMDA(2)=0$ OTHERWISE$

1412                        LMDA(2) = B(2)/(2B(3)-B(2)*2)$

1417                        M = 2$

1419        2..            M = M + 1$

1422                        PXI = B(M)-M.B(M+1)/B(2)$

1431                        FOR R=(2,1,M-1)$

1445                    BEGIN

1445                        XI = PXI.LMDA(R)+B(M-R+1)$

1457                        PXI = XI$

1459                    END$

1460                        LMDA(M) = -1.0/XI$

1465                        X = 1.0/LMDA(M)$

1470                        PX= 1.0/LMDA(M-1)$

1475                        PRSQ = RSQ$
```

148

```
1477                    IF M LEQ N $   GO TO 2$

1483                    IF M GEQ 50$ GO SCRATCH$

1489                    IF M GEQ 3$

1489          BEGIN

1497                    RSQ = (LMDA(M)-LMDA(M-1))/((LMDA(M-1).LMDA(M)).

1503                    (LMDA(M-1)-LMDA(M-2)))$

1509                    PRCOSTH = RCOSTH$

1511                    RCOSTH = (LMDA(M)-LMDA(M-2))/(LMDA(M)(LMDA(M-1) -

1517                    LMDA(M-2)))$

1523          END$

1523                    EITHER IF (ABS(X-PX) LEQ ABS(X(1**-3)))$

1523          GO TO REEL$

1539                    OR     IF (ABS(RSQ-PRSQ) LEQ ABS(RSQ(1**-3))) AND

1557                    (ABS(RCOSTH-PRCOSTH) LEQ ABS(RCOSTH(1**-3)))$

1557                    GO TO CMPLX$

1572                    OR IF RSQ GTR 0$

1572                    GO CMPLX$

1577                    OTHERWISE$

1577                    GO TO 2$

1579    REEL..          RL = 1$

1581                    YST = 0.0$

1582                    XST = X$

1584                    GO TO 3$

1585    CMPLX..         RL = 0$

1586                    XST = RCOSTH/2.0$

1590                    ZETA = RSQ - XST.XST$ ZETAP = ABS(ZETA)$

1596                    YST = SQRT(ZETAP)$

1600                    IF YST LSS 1**-4$

1600                    GO TO REEL$
```

```
1606        3..                 ALFA = GMA = 1.0$

1609                            BETA = DLTA = 0.0$   QQ=QQ+1$

1614                            FOR R = (1,1,N)$

1625                      BEGIN PALFA = ALFA$   PBETA = BETA$

1630                            PGMA = GMA$ PDLTA = DLTA$

1634                            ALFA = A(R) + XST.PALFA - YST.PBETA$

1643                            BETA = XST.PBETA + YST.PALFA$

1650                            GMA = ALFA + XST.PGMA - YST.PDLTA$

1658                            DLTA = BETA + XST.PDLTA + YST.PGMA$

1666                      END$

1667                            X=XST$ Y=YST$

1671                            XST = X - (ALFA.PGMA+BETA.PDLTA)/(PGMA*2+PDLTA*2)$

1690                            IF QQ GEQ 50$ GO SCRATCH$

1696                            YST = Y - (BETA.PGMA-ALFA.PDLTA)/(PGMA*2+PDLTA*2)$

1715                            IF (ABS(X-XST) GTR ABS(XST).(1**-7))

1728                            OR (ABS(Y-YST) GTR ABS(YST).(1**-7))$

1728                            GO TO 3$

1746                            IF  RL$

1746                      BEGIN

1746                            C(1) = XST$

1750                            SYNDV(NN,1$B(),C())$

1766                            B(NN+1) = 0.0$

1768                            NN = NN - 1$

1771                            G = G + 1$

1774                            S(G) = XST$

1777                            WRITE($$ROUT.RFORM)$

1785                            GO TO 4$

1786                      END$

1786                            C(1) = 2XST$
```

150

```
1789                          C(2) =-XST*2 - YST*2$

1798                          SYNDV(NN,2$B( ),C( ))$

1814                          B(NN+1) = B(NN) = 0.0$

1817                          NN=NN-2$

1820                          G = G + 1$

1823                          S(G) = XST$   U(G) = YST$

1829                          FREQ = (YST/6.2831853).(1.0**3)$

1834                          WRITE ($$COUT,CFORM)$

1842        4..              IF NN GTR 2$

1842                          GO TO STARTT$

1848                          SWITCH NN,(SW1,SW2)$

1852                          GO TO START$

1853        SW1..            XST =-B(2)$

1855                          YST = 0.0$

1856                          RL = 1$   GO TO 3$

1859        SW2..            DISC = B(2)*2 - 4B(3)$

1866                          IF DISC LSS 0$

1866                    BEGIN

1866                          XST = -B(2)/2.0$

1873                          YST = SQRT(-DISC)/2.0$

1879                          RL = 0$    GO TO 3$

1881                    END$

1881                          XST = (-B(2)+SQRT(DISC))/2.0$

1888                          RL = 1$    YST = 0.0$  GO TO 3$

1892        SCRATCH..  FORMAT ZOT (*PROCEDURE FAILS*,W4)$

1899                          WRITE ($$ZOT)$  GO START$

1904        FINISH$
COMPILED PROGRAM ENDS AT 1904
PROGRAM VARIABLES BEGIN AT 3246
```

N= 5   T0= 0   T1= 0   T2= 0   TAUS IN NANOSECONDS

COEFFICIENTS   .300000, 03   .300000, 00   .400000, 02   .200000,-01   .100000, 01SOLUTIONS

X =   -.0002 + .3162 I
X =   -.0002 - .3162 I   FREQUENCY IN MC =   50.37
X =   -.0002 + .1825 I
X =   -.0002 - .1825 I   FREQUENCY IN MC =   29.05

N= 6   T0= 0   T1= 0   T2= 0   TAUS IN NANOSECONDS

COEFFICIENTS   .000000, 00   .300000, 00   .300000, 00   .400000, 02   .200000,-01   .100000, 01SOLUTIONS

X = -299.9994

PROCEDURE FAILS

N= 7   T0= 0   T1= 0   T2= 0   TAUS IN NANOSECONDS

COEFFICIENTS   .000000, 00   .000000, 00   .300000, 03   .300000, 00   .400000, 02   .200000,-01   .100000, 01SOL

X =   .0005 + 17.3166 I
X =   .0005 - 17.3166 I   FREQUENCY IN MC =   2756.03

152

X =   -.0002 + .3163 I

X =   -.0002 - .3163 I   FREQUENCY IN MC = 50.34

X =   -.0002 + .1825 I

X =   -.0002 - .1825 I   FREQUENCY IN MC = 29.05

N= 5   TO= 0   T1= 0   T2= 1   TAUS IN NANOSECONDS

COEFFICIENTS .370458, 03   .335000, 00   .430000, 02   .200000,-01   .100000, 01SOLUTIONS

X =   -.0002 + .2896 I

X =   -.0002 - .2896 I   FREQUENCY IN MC = 46.09

X =   -.0002 + .1793 I

X =   -.0002 - .1793 I   FREQUENCY IN MC = 28.54

Program B

```
-BALGL    CAMPBELL    /PARTIALFRACT   93374-60 PROD      05/06/66-11.41
0200                      BAC-220 SPECIAL VERSION  2/22/64
0200      COMMENT ONLY ODD N ARE BEING USED, AND ALL ROOTS ARE COMPLEX$
0200      COMMENT REAL COMPONENTS OF ROOTS, WHICH ARE LESS THAN 10*-3, HAVE BEEN
0200             NEGLECTED$
0200      INTEGER I,J,K,N,G,W,M,AI$
0200      INTEGER T$
0200      INTEGER G$
0200      BOOLEAN AS$
0200      ARRAY A(20),B(20),P(20),S(20),U(20),KK(20,2), L(20),C(20),V(6)$
0200      ARRAY NON1N2(20),NON1M2(20),NON2M1(20),M1(20),M2(20),N0(20),N1(20),
0200             N2(20),HH(20)$
0200      ARRAY F(20)$
0200      R0=R3=1$ L0=L3=2**-6$ C1=C2=5**-12$ Z=500$
0211      RC = R3.C2 + R3.C1 + R0.C2 + R0.F1$ FF= F1 + F2$
0229      LRC = L3.C2 + L3.C1 + L0.C2 + 00.F1 + R6.R3.C1.C2 +2R0.R3.C1.C2$
0257      RC2 = R3.C1.C2 + R0.C1.C2$ LC2 = L0.C1.C2 + L3.C1.C2$
0275      RLC2 = 2R3.L3.C1.C2 + 2L0.R3.C1.C2 + 2R0.L3.C1.C2$
0295      L2C2 = 2L0.L3.C1.C2 + L3.L3.C1.C2$
0307      PROCEDURE SYNDV(N,K$B(),C())$
0307      BEGIN
0307             INTEGER I,J,K,N$
0311      FOR I = (2,1,N)$
0322           FOR J = (0,1,K-1)$
0337               B(I+J) = B(I+J) + C(J+1).B(I-1)$
0364           RETURN                        END SYNDV()$
0373      INPUT DATAFACT (FOR I=(1,1,20)$F(I))$
0394      READ ($$DATAFACT)$
0398      INPUT AR (N,T0,T1,T2,FOR I=(N-1,-1,1)$A(I),A0,FOR I = (1,1,(N-1)/2)$
```

```
0449                         U(I))$

0457        BB..

0457        READ ($$AR)$

0461        IF T1 NEQ 0$ BEGIN FOR I=(2,2,N+1)$

0477            M1(I) = 10.0*15.T1*(I-1).F(I).Z$          END$

0495        IF T2 NEQ 0$ BEGIN FOR I=(2,2,N+1)$

0511            M2(I) = 10.0*15.T2*(I-1).F(I).Z$          END$

0529        IF T0 NEQ 0$ BEGIN FOR I=(1,2,N)$

0542            N0(I) = 10.0*15.T0*(I-1).F(I)$            END$

0559        IF T1 NEQ 0$ BEGIN FOR I=(1,2,N)$

0572            N1(I) = 10.0*15.T1*(I-1).F(I)$            END$

0589        IF T2 NEQ 0$ BEGIN FOR I=(1,2,N)$

0602            N2(I) = 10.0*15.T2*(I-1).F(I)$            END$

0619        FOR  I=(N+2,1,20)$ BEGIN        M1(I)=M2(I)=N0(I)=N1(I)=N2(I)=0$ END$

0639        IF T0 EQL 0$ BEGIN FOR I=(1,1,N+1)$BEGIN        N0(I)=0$ END END$

0660        IF T1 EQL 0$ BEGIN FOR I=(1,1,N+1)$BEGIN M1(I)=N1(I)=0$ END END$

0682        IF T2 EQL 0$ BEGIN FOR I=(1,1,N+1)$BEGIN M2(I)=N2(I)=0$ END END$

0704        IF T0 EQL 0$ N0(1)=1.0**15$ IF T1 EGL 0$ N1(1)=1.0**15$ IF T2 EQL 0$

0704                    N2(1)=10.0*15$

0722        FOR I = (1,1,20)$ BEGIN N0N1N2(I)=N0N2M1(I)=N0N1M2(I)=HH(I)=0$

0739        END$

0740        FOR T=(1,1,N)$ FOR I=(1,1,T)$ FOR J=(1,1,T+1-I)$ BEGIN

0782            IF (I+J) LEQ (T+1)$ BEGIN

0782            N0N1N2(T)=N0N1N2(T)+N0(I).N1(J).N2(T+2-I-J)$

0803            N0N2M1(T)=N0M1N2(T)+N0(I).M1(J).N2(T+2-I-J)$

0822            N0N1M2(T)=N0N1M2(T)+N0(I).N1(J).M2(T+2-I-J)$

0836                                                    END    END$

0839        N = N-1$

0842        G=N/2$
```

```
0846        P(1) = NON1N2(1).(10.0*-45)$

0853        P(2) = (NON1N2(2) + R3.C2.NON1N2(1) + C2.NON1M2(1)).(10.0*-36)$

0869        FOR I = (3,1,N+1)$

0883             P(I) = (NON1N2(I) + R3.C2.NON1N2(I-1) + C1.NON1M2(I-1)

0898                  + C2.L3.NON1N2(I-2)).(10.0*(-45+9(I-1)))$

0912        OUTPUT MINOR (N,FIX   ((10*9)T0),FIX   ((10*9)T1),FIX   ((10*9)T2))$

0952        OUTPUT O2 (FOR W=(N,-1,1)$A(W),A0)$

0976        OUTPUT O3 (FOR W=(1,1,G)$U(W))$

0997        OUTPUT O4 (FOR W=(1,1,N+1)$P(W))$

1021        OUTPUT O5 (AS+1)$

1029        OUTPUT O6 (KK(G+1,1))$

1040        OUTPUT O7 (KK(I,1),(-1)*(J -1)KK(I,2))$

1070        OUTPUT O8 (T,TOTAL)$

1080        FORMAT MAJORF ((F10.4,B5),W)$

1086        FORMAT F2 (*A(M) POLY*,B5,(F10.4,B5),W)$

1095        FORMAT F3 (*U(M) ROOTS (ALL IMAGINARY)*,B5,(F10.4,B5),W)$

1108        FORMAT F4 (*P(M) POLY*,B5,(F10.4,B5),W)$

1117        FORMAT MINORF (*N=*,I2,B5,*T0=*,I2,B5,*T1=*,I2,B5,*T2=*,I2,B5,

1117             *TAUS IN NANOSECONDS*,W6)$

1136        FORMAT F8 (I3,B5,F15.6,W)$

1142        FORMAT F9 (*  T*,B12,*V*,I1,*/V0*,W)$

1150        WRITE ($$MINOR,MINORF)$

1158        WRITE ($$O2,F2)$

1166        WRITE ($$O3,F3)$

1174        A(N+2) = 0$

1179        FOR I = (1,1,N)$ B(I+1) = A(I)$

1195        B(1) = A0$

1197        U(G+1)=0$

1199        COMMENT IT HAS BEEN ASSUMED THAT THERE ARE NO MULTIPLE ROOTS. IF THERE ARE,
```

```
1199              THE MESSAGE *FRACTIONS FAIL* WILL BE PRINTED.$

1199       PARTIALFRACTIONS..

1199       BC..

1203       WRITE ($$04,F4)$

1207       FORMAT F5 (*THE PARTIAL FRACTION EXPANSION OF V*,I1,*/VO = P(M)/(A(M).

1207       M) HAS, CORRESPONDING TO THE ROOTS ABOVE, THESE COEFFICIENTS--*,W4,

1207       *REAL PART*,B6,*IMAGINARY*,W)$

1241       WRITE ($$05,F5)$

1249       FOR I = (1,1,G)$

1260       BEGIN

1260              IF U(I) EQL 0$

1260              BEGIN

1260       AI = 1$

1267                  R = C(1) = S(I)$

1271       FOR K = (1,1,N+1)$ A(K) = B(K)$

1290              SYNDV(N+1,1$A(),C())$

1307              QS = 0$ PS = 0$

1309              FOR J = (1,1,N+1)$

1323              BEGIN

1327                  QS = QS + A(J).R*(N-J+1)$

1335                  PS = PS + P(J).R*(J-1)$

1345                                          END$

1346              IF QS EQL 0$ GO TO FRACTFAIL$

1350              KK(I,1) = PS/QS$

1358                  FOR J = (1,1,AI)$

1369                                  WRITE ($$07,MAJORF)$

1379                                      END$

1379          IF U(I) NEQ 0$

1379          BEGIN
```

157

```
1379      AI = 2$

1384              C(1) = 2S(I)$

1388              C(2) = -S(I).S(I) - U(I).U(I)$

1396      FOR K = (1,1,N+1)$ A(K) = B(K)$

1415              SYNDV(N+1,2$A(),C())$

1432              V(1) = SQRT (-C(2))$

1436              EITHER IF S(I) EQL 0$ V(2) = 1.5707963SIGN(U(I))$

1448              OTHERWISE$ /(2) = ARCTAN (U(I)/S(I))$

1456      V(3) = V(4) = V(5) = V(6) = 0$

1460              FOR J = (1,1,N)$

1471              BEGIN

1474                  AD = V(1)*(N-J).A(J)$   AE = (N  -J)V(2)$

1487                  V(3) = V(3) + AD.COS(AE)$

1493                  V(4) = V(4) + AD.SIN(AE)$

1499                  AF = V(1)*(J-1).P(J)$   AG =(J-1).V(2)$

1514                  V(5) = V(5) + AF.COS(AG)$

1520                  V(6) = V(6) + AF.SIN(AG)$

1526                                          END$

1527      V(5) = V(5) + V(1)*N.P(N+1).COS(N(V(2)))$

1543      V(6) = V(6) + V(1)*N.P(N+1).SIN(N(V(2)))$

1559                  VV = V(3).V(3) + V(4).V(4)$

1566              IF VV EQL 0$ GO FRACTFAIL$

1570              KK(I,2) = -(V(5).V(3) + V(4).V(6))/(VV.2U(I))$

1592              KK(I,1) =  (V(6).V(3) - V(4).V(5))/(VV.2U(I))$

1612                  FOR J = (1,1,AI)$

1623                              WRITE ($$07,MAJORF)$

1633                                      END$

1633                                          END$

1634      WRITE ($$05,F9)$
```

```
1642       FOR T=(0,1,20),(30,10,50),100$

1666                                              BEGIN

1666       TOTAL = 0$

1670       FOR I=(1,1,G)$

1681                                              BEGIN

1682       IF KK(I,2) EQL 0$

1696       TOTAL = TOTAL +  EXP(S(I).T).KK(I,1) $

1707             TOTAL = TOTAL + 2EXP(S(I).T).(KK(I,1)COS(U(I).T)

1724                   -KK(I,2)SIN(U(I).T))$

1749                                              END$

1750       TOTAL = TOTAL + 1$

1753       COMMENT THE ADDITION OF 1 TAKES INTO CONSIDERATION THE TERM 1/M OF THE

1753             CONTINUED FRACTION EXPANSION OF V/V0 = P(M)/A(M), SINCE A(M) =

1753             M.Q(M).$

1757       WRITE ($$C8,F8)$

1761                                              END$

1762       P(2) = (NON1N2(2) + R3.C1.NON1N2(1) + C1.NON2M1(1)).(10.0*-36)$

1778       FOR I = (3,1,N+1)$

1792             P(I) = (NON1N2(I) + R3.C2.NON1N2(I-1) + C2.NON2M1(I-1)

1807                   + C1.L3.NON1N2(I-2)).(10.0*(-45+9(I-1))))$

1821       IF AS EQL 1$ BEGIN AS=0$ GO BB$ END$

1828       AS = 1$

1830       GO BC$

1831       GO TO FINIS$

1832       FRACTFAIL..FORMAT AC (*FRACTIONS FAIL*,W2)$ WRITE ($$AC)$

1842       GO TO BB$

1843       FINIS..

1843       FINISH$
```

159

N= 4   TO= 0   TI= 0   T2= 0   TAUS IN NANOSECONDS

A(M) POLY .1000, 01   .2000,-01   .4000, 02   .3000, 00   .3000, 03
Q(M) ROOTS (ALL IMAGINARY)   .3162, 00   .1825, 00
P(M) POLY .1000, 01   .5000,-02   .1000, 02   .0000, 00   .0000, 00

THE PARTIAL FRACTION EXPANSION OF V1/V0 = P(M)/(A(M),M) HAS, CORRESPONDING TO THE ROOTS ABOVE, THESE COEFFICIENTS--
REAL PART   IMAGINARY
.4142,-04   .3958,-03
.4142,-04   -.3958,-03
-.5002, 00   -.6867,-03
-.5002, 00   .6867,-03

T	V1/V0
0	-.324100,-03
1	.162887,-01
2	.655852,-01
3	.145943, 00
4	.254708, 00
5	.388774, 00
6	.542211, 00
7	.711404, 00
8	.890727, 00
9	.107273, 01
10	.125783, 01
11	.142455, 01
12	.158715, 01
13	.172039, 01
14	.183466, 01
15	.192116, 01
16	.197702, 01
17	.200027, 01
18	.199045, 01
19	.194760, 01
20	.187325, 01
30	.307880, 00
40	.474894, 00
50	.195619, 01
100	.173223, 00

P(M) POLY .1000, 01   .5000,-02   .1000, 02   .0000, 00   .0000, 00

THE PARTIAL FRACTION EXPANSION OF V2/V0 = P(M)/(A(M),M) HAS, CORRESPONDING TO THE ROOTS ABOVE, THESE COEFFICIENTS--
REAL PART   IMAGINARY
.4142,-04   .3958,-03
.4142,-04   -.3958,-03
-.5002, 00   -.6867,-03
-.5002, 00   .6867,-03

T	V2/V0
0	-.324100,-03
1	.162887,-01
2	.655852,-01
3	.145943, 00
4	.254708, 00
5	.388774, 00
6	.542211, 00

160

7	.711404, 00
8	.890227, 00
9	.107773, 01
10	.125283, 01
11	.142455, 01
12	.158215, 01
13	.172039, 01
14	.183466, 01
15	.192116, 01
16	.197702, 01
17	.200037, 01
18	.199045, 01
19	.194760, 01
20	.187325, 01
30	.307880, 00
40	.474894, 00
50	.195619, 01
100	.173223, 00

N= 4   TO= 0   T1= 0   T2= 2   TAUS IN NANOSECONDS

A(M) POLY	.1000, 01	.2000,-01	.4700, 02	.3900, 00	.4840, 03
Q(M) ROOTS (ALL IMAGINARY)		.2561, 00	.1774, 00	.1000,-01	
P(M) POLY	.1000, 01	.5000,-02	.1700, 02	.2400, 02	

THE PARTIAL FRACTION EXPANSION OF V1/VO = P(M)/(A(M).M) HAS, CORRESPONDING TO THE ROOTS ABOVE, THESE COEFFICIENTS--

REAL PART	IMAGINARY
-.5432,-02	.4743,-03
-.5432,-02	-.4743,-03
-.4695, 00	.7081,-04
-.4695, 00	-.7081,-04

T	V1/VO
0	.499394,-01
1	.648183,-01
2	.109414, 00
3	.182301, 00
4	.281141, 00
5	.402762, 00
6	.543266, 00
7	.698151, 00
8	.862461, 00
9	.103094, 01
10	.119877, 01
11	.135902, 01
12	.150819, 01
13	.164104, 01
14	.175341, 01
15	.184179, 01
16	.190344, 01
17	.193649, 01
18	.193999, 01
19	.191391, 01
20	.185918, 01
30	.459365, 00
40	.362557, 00
50	.178762, 01

100
P(M) POLY   .571789, 00
             .1000, 01   .5000,-02   .1200, 02   .1000,-01   .2066, 02

THE PARTIAL FRACTION EXPANSION OF V2/V0 = P(M)/(A(M),M) HAS, CORRESPONDING TO THE ROOTS ABOVE, THESE COEFFICIENTS--

REAL PART	IMAGINARY
.1395, 00	.1544,-02
.1395, 00	-.1544,-02
-.6176, 00	.1586,-03
-.6176, 00	-.1586,-03

T	V2/V0
0	.438868,-01
1	.533313,-01
2	.833795,-01
3	.134016, 00
4	.705116, 00
5	.296348, 00
6	.407062, 00
7	.536169, 00
8	.682016, 00
9	.842282, 00
10	.101390, 01
11	.119304, 01
12	.137510, 01
13	.155483, 01
14	.172639, 01
15	.188364, 01
16	.202032, 01
17	.213033, 01
18	.220807, 01
19	.224876, 01
20	.224871, 01
30	.277484, 00
40	-.377011,-01
50	.232025, 01
100	.697036, 00

APPENDIX II

LIST OF EQUIPMENT USED IN PROGRAM

EQUIPMENT USED IN PROGRAM:

	INSTRUMENT	MANUFACTURER	TYPE	S/N
1.	Oscilloscope	Tektronix	585A	000658
2.	Plug In Unit	Tektronix	P80	000870
			L	013965
			K	015088
			53/54C	16451
3.	Plug In Unit	Tektronix	82	4363
4.	Square Wave Generator	Tektronix	105	006552
			107	00248
5.	High Voltage Probe	Tektronix	P6013	
			P6015	
6.	Q Meter	Boonton Radio Corp.	160A	4862
			160A	2439
7.	V.O. M.	Triplet	630A	95072
8.	AC-DC VTVM	Kalpa Scientific		No S/N
9.	Electronic Frequency Converter		AN-APR4Y	1459
	Tuning Unit		40-1000MHz	1544
			975-2200MHz	1456
10.	Megacycle Meter (GDO)	Measurements Corp.	159	6100
			159	6178
11.	Noise and Field Intensity Meter	Empire Devices	NF105	2367
			NF105	2579
12.	Noise and Field Intensity Meter	Empire Devices	NF105	149
13.	Noise and Field Intensity Meter	Stoddard	NM20B	No S/N
14.	Microwave Receiver	Polarad	Model R	153
15.	Noise and Field Intensity Meter	Polarad	FIM-B	Not Avail.
16.	Unit Pulser	General Radio	1217B	No S/N
17.	Pulse Generator	Dumont	404	835

	INSTRUMENT	MANUFACTURER	TYPE	S/N
18.	Pulse Generator	Hewlett-Packard	214A	433-01430
19.	Scope Camera	Beattie Coleman	12445	1538
20.	Queen Kelvin Bridge	Queen	E-3273	8936
21.	Resistor 0.01 ohm	Weston	0042211	No S/N

REFERENCES

1. Beams, J.W., and Allison, Fred, "The Difference in the Time Lags of the Faraday Effect Behind the Magnetic Field in Various Liquids", Phys. Rev., 29, (1927), 161.

2. Schmidt, B.M., "A Theoretical Analysis of the Electric Circuit Used in the Allison Effect Experiments" Research Institute, University of Dayton, Dayton, Ohio, Chronological Log, Unpublished Paper, April - November 1965.

3. Allison, Fred, "The Effect of Wave-Length on the Difference in the Lags of the Faraday Effect Behind the Magnetic Field for Various Liquids", Phys. Rev., 30, (1927), 66.

4. Allison, Fred, and Murphy, E.J., "A Magneto-Optic Method of Chemical Analysis", Jour. Am. Chem. Soc., 52, (1930), 3796.

5. Roquemore, M., Private Communication, May 19, 1965.

6. Allison, Fred, "Magneto-Optic Method of Analysis as a New Research Tool", Ind. and Chem. Eng., (Anal. Ed.), 4, (1932), 9.

7. Allison, Fred, "The Magneto-Optic Method of Analysis", Jour. Chem. Ed., 10, (1933), 70.

8. Cooper, Stancil S., "The Magneto-Optic Method of Chemical Analysis, I", Jour. Chem. Ed., 13, (1936), 210.

9. Cooper, Stancil S., "The Magneto-Optic Method of Chemical Analysis, III", Jour. Chem. Ed., 13, (1936), 326.

10. Allison, Fred, and Murphy, E.J., "The Probable Number of Isotopes of Eight Metals as Determined by a New Method" (letter), Phys. Rev., 36, (1930), 1097.

11. Bishop, Edna R., "Copper Isotopes", Phys. Rev., 40, (1932), 16.

12. Bishop, Edna R., Lawrenz, Margret, and Dollins, C.B., "Lead Isotopes", Phys. Rev., 43, (1933), 43.

13. Bishop, Edna R., and Dollins, C.B., "Radium Isotopes", Phys. Rev., 43, (1933), 48.

14. Goslin, Roy and Allison, Fred, "The Isotopes of Uranium, Thorium and Thallium", Phys. Rev., 43, (1933), 49.

REFERENCES CONT.

15. Piggot, Charles S., "Isotopes of Uranium, Thorium and Lead, and Their Geophysical Significance", Phys. Rev., 43, (1933), 51.

16. Westman, H. P., (Ed.), Reference Data for Radio Engineers, 4th Edition, International Telephone and Telegraph Corp., New York, (1962).

17. Cooper, Stancil S., "The Magneto-Optic Method of Chemical Analysis, II", Jour. Chem. Ed., 13, (1936), 276.

18. Mildrum, H. F., "Summary of Experimental Efforts Conducted at Auburn University on Dr. Allison's Magneto-Optic System" Research Institute University of Dayton, Dayton, Ohio, Unpublished Notes, August 9-13, 1965.

19. Snoddy, L. B., "Allison's Magneto-Optic Effect" (letter), Phys. Rev., 44, (1933), 691.

20. Cobine, J. D., Gaseous Conductors, McGraw-Hill Co., New York, (1941).

21. Thomson, W. T., Laplace Transformation, 2nd Ed., Prentice-Hall, Inc., Englewood Cliffs, New Jersey, (1960).

22. Allison, Fred, and Bishop, Edna R., "Bismuth Isotopes", Phys. Rev., 43, (1933), 47.

23. Latimer, W. H., and Young, H. A., "The Isotopes of Calcium by Magneto-Optic Method" (letter), Phys. Rev., 44, (1933), 61.

24. Ball, T. R., and Cooper, S. S., "A Study of the Isotopes of Cobalt by the Magneto-Optic Method", J. A. C. S., 55, (1933), 3207.

25. Andrew, E. R., Nuclear Magnetic Resonance, Cambridge University Press, New York, (1956).

26. Webb, J. S., and Morey, D. R., "On the Existence of Time Lags in the Faraday Effect", Phys. Rev., 44, (1933), 589.

27. Gaddy, O. L., Holshouser, D. F., and Stanfield, R. E. "Microwave and Electro-Optical Properties of Carbon Disulfide", Quantum Electronics, Proceedings of the Third International Congress, 2, Columbia University Press, New York, (1965), 1679.

28. Sass, A. R., and Stoll, J. C., "Magnetic Field of a Finite Helical Solenoid", NASA Technical Note, NASA TN D-1993, (1963).

REFERENCES CONT.

29. Dershem, H., University of Dayton Computation Laboratory, October, 1965.

30. Guillemin, et al., The Mathematics of Circuit Analysis, John Wiley and
    Sons, Inc., New York, (1949).

31. Glasford, G. M., Linear Analysis of Electronic Circuits, Addison-Wesley,
    Reading, Mass., (1965).

BIBLIOGRAPHY

Allison, Fred, "The Effect of Wave-Length on the Difference in the Lags of the Faraday Effect Behind the Magnetic Field for Various Liquids" (abstract), Phys. Rev. 29, (1927), 370.

Allison, Fred, "The Magneto-Optic Method of Analysis and Some Recent Applications", Science, 77, (1933), 494.

Allison, Fred, "Influence of X-rays upon the Time Lags of the Faraday Effect and upon Optical Rotation in Several Liquids" (letter), Nature, 120, (1927), 729.

Allison, Fred, "The Effect of X-rays upon the Faraday Time Lags, the Faraday Effect, and the Optical Rotation in Several Liquids" (abstract), Phys. Rev., 31, (1928), 158.

Allison, Fred, "Further Studies in the Effect of X-rays upon Certain Optical Properties of Liquids and Glass" (abstract), Phys. Rev., 31, (1928), 306.

Allison, Fred, "Time Lag Differences of the Faraday Effect in Several Mixtures and Chemical Compounds" (abstract), Phys. Rev. 31, (1928), 313.

Allison Fred, Bishop, Edna R., Sommer, Anna L., and Christensen, J.H., "Further Research on Element 87", Jour. Am Chem. Soc., 54, (1932), 613.

Allison, Fred, Bishop, Edna R., and Sommer, Anna L., "Concentration, Acids, and Lithium Salts of Element 85", Jour. Am. Chem. Soc., 54, (1932), 616.

Allison, Fred, and Condon, John L., "An Experiment in Support of the Hypothesis of a Time Lag in the Faraday Effect" (letter), Phys. Rev., 40, (1932), 1021.

Allison, Fred, Christensen, J.H., and Waldo, Geo. V., "A Preliminary Report of the Application of the Photo-Electric Cell to the Reading of Minima in a Magneto-Optic Method of Analysis" (letter), Phys. Rev., 37, (1931), 1003.

Allison, Fred, Christensen, J.H., and Waldo, Geo. V., "The Nature of the Phenomenon Underlying the Magneto-Optic Method of Analysis" (abstract), Phys. Rev., 40, (1932), 1052.

Allison, Fred, and Goslin, Roy, "The Transformation Product of Potassium" (letter), Phys. Rev., 40, (1932), 1015.

BIBLIOGRAPHY CONT.

Allison, Fred, and Murphy, E. J., "A Magneto-Optic Method of Chemical Analysis" (abstract), Phys. Rev., 35, (1930), 124.

Allison, Fred, and Murphy, E. J., "Evidence of the Presence of Element 87 in a Sample of Pollucite and Lepidolite Ores" (letter), Phys. Rev., 35, (1930), 285.

Allison, Fred; Murphy, E. J.; Bishop, Edna R.; and Sommer, Anna L., "Evidence of the Detection of Element 85 in Certain Substances", (letter) Phys. Rev., 37, (1931), 1178.

Ball, T. R., and Crane, Keith D., "Intermediate States of Reduction of Chromic Acid", J. A. C. S., 55, (1933), 4860.

Beams, J. W., and Allison, Fred, "The Difference in the Time Lags in the Disappearance of the Electric Double Refraction Behind that of the Electric Field for Several Liquids", Phil. Mag., 3, (1927), 1199.

Beams, J. W., and Lawrence, E. O., "On Relaxation of Electric Fields in Kerr Cells and Apparent Lags of the Kerr Effect", Jour. Frank. Inst., 206, (1928), 169.

Bishop, Edna R., "Radioactive Families", Phys. Rev., 43, (1933), 38.

Bishop, Edna R., and Allison, Fred, "Isotopes of Chlorine" (letter), Phys. Rev., 44 (1933), 419.

Bishop, Edna R., and Dollins, C. B., "Quantitative Determination of Calcium by the Magneto-Optic Method", J. A. C. S., 54, (1932), 4585.

Bishop, Edna R.; Dollins, C. B.; and Otto, Irene G., "Magneto-Optic Nicol Rotation Method for Quantitative Analysis of Calcium", J. A. C. S., 55, (1933), 4365.

Bishop, Edna R.; Otto, Irene G.; and Baisden, Louis, "The Magneto-Optic Nicol Rotation Method for the Quantitative Analysis of Copper" (note), J. A. C. S., 56, (1934), 408.

Bitter, F., "Magnetic Resonance in Radiating or Absorbing Atom", Applied Optics, 1, (1962), 1.

Document, "Meeting Between B. Schmidt, M. Roquemore, and H. Mildrum", unpublished, April 8, 1965.

Dollins, C. B., and Bishop, Edna R., "Isotopes of Sodium and Cesium ", J. A. C. S., 55, (1933), 4372.

BIBLIOGRAPHY CONT.

Gaviola, E., "On Time Lags in Fluorescence and the Kerr and Faraday Effects", Phys. Rev., 33, (1929), 1023.

Hughes, Gordon, and Hopkins, B.S., "Observations of the Rare Earths. XXXIIIa. The Basicity of Illinium and Yttrium", J.A.C.S., 55, (1933), 3121.

Jones, Herman D., and Goslin, Roy, "Some Further Remarks on the Use of the Magneto-Optic Method" (letter), J.A.C.S., 55, (1933), 3500.

Langford-Smith, F., Radiotron Designer's Handbook, 4th Ed., Wireless Press, Sydney, Australia.

Latimer, Wendell M., and Young, Herbert A., "Isotopes of Hydrogen by the Magneto-Optic Method. The Existence of H^3" (letter), Phys. Rev., 44, (1933), 690.

Lawrence, E.O., and Beams, J.W., "On the Time Required for the Photo-Electric Ejection of an Electron by Visible Light" (abstract), Phys. Rev., 31, (1928), 709.

Loeb, L.B., "Ionizing Waves of Potential Gradient", Science, 148, (1965), 1417.

Lorentz, H.A., The Theory of Electrons, (B.G. Teubner, Leipzig, 1916).

McGhee, J.L., and Lawrenz, Margret, "Tests for Element 87 by the Use of Allison's Magneto-Optic Apparatus" (letter), Jour. Am. Chem. Soc., 54, (1932), 405.

McGhee, J.L., and Lawrenz, Margret, "Magneto-Optic Minima of Organic Compounds" (letter), J.A.C.S., 55, (1933), 2614.

McGhee, J.L., and Lawrenz, Margret, "Scale Readings of Isometric Esters on the Magneto-Optic Apparatus" (letter), J.A.C.S., 55, (1933), 4333.

Otto, Irene G., and Bishop, Edna R., "Manganese Isotopes", J.A.C.S., 55, (1933), 4371.

Papish, J., and Shuman, A.C., "A Critical Study of the Magneto-Optic Method of Analysis" (abstract), Science, 74, (1931), 636.

Papish, Jacob, and Wainer, Eugene, "Element 87" (Preliminary Paper), Jour. Am. Chem. Soc., 53, (1931), 3818.

Schawlow, A.L., "Lasers", Science, 149, (1965), 13.

BIBLIOGRAPHY CONT.

Schmidt, B., Williams, J., and Williams, D., "Magneto-Optic Modulation of a Light Beam in Sodium Vapor", J.O.S.A., 54, (1964), 454.

Shurcliff, W. A., Polarized Light, (Harvard University Press, Cambridge, Mass., 1962).

Slack, Francis G., "The Magneto-Optic Method of Chemical Analysis", Journal of the Franklin Institute, 218, (1934), 445.

Slack, F. G., and Breazeale, W. M., "The Magneto-Optic Rotation by Condenser Discharge" (abstract), Phys. Rev., 40, (1932), 1052.

Slack, F. G., and Breazeale, W. M., "Magneto-Optic Rotation by Condenser Discharge", Phys. Rev., 42, (1932), 305.

Slack, Francis G., and Peoples, James A., Jr., "The Magneto-Optic Method of Chemical Analysis" (abstract), Phys. Rev., 45, (1934), 126.

Wissink, G. M., "A Magneto-Optic Method of Determining the Vitamin Content of Various Substances", Physics, 5, (1934), 31.

Wissink, G. M. and Woodrow, Jay W., "The Detection of Vitamin A by Means of the Magneto-Optic Apparatus" (abstract), Phys.Rev., 45, (1934), 126.

Yoe, John H., "Lead Isotopes by the Magneto-Optic Method" (letter), Phys. Rev., 44, (1933), 420.

Yoe, John H., and Wingard, R. E., "The Formation of Formaldehyde by the Action of Ultraviolet Light on Carbon Dioxide and Water: An Application of the Allison Magneto-Optic Apparatus" (letter), Jour. Chem. Phys., 1, (1933), 886.

DOCUMENT CONTROL DATA - R&D			
(Security classification of title, body of abstract and indexing annotation must be entered when the overall report is classified)			
1 ORIGINATING ACTIVITY *(Corporate author)* University of Dayton Research Institute Dayton, Ohio 45409		2a REPORT SECURITY CLASSIFICATION Unclassified	
		2b GROUP	

3 REPORT TITLE

"Allison Method of Chemical Analysis"

4 DESCRIPTIVE NOTES *(Type of report and inclusive dates)*
Final Report (April 1965-December 1966)

5 AUTHOR(S) *(Last name, first name, initial)*

Mildrum, Herbert F.
Schmidt, Bernhard M.

6. REPORT DATE April 1966	7a. TOTAL NO. OF PAGES 187	7b. NO. OF REFS 31
8a. CONTRACT OR GRANT NO. AF 33(657)-9175 b. PROJECT NO. 8119 c. d.	9a. ORIGINATOR'S REPORT NUMBER(S) UDRI TR-106 9b. OTHER REPORT NO(S) *(Any other numbers that may be assigned this report)* AFAPL-TR-66-52	

10. AVAILABILITY/LIMITATION NOTICES

Distribution of this report is unlimited.

11. SUPPLEMENTARY NOTES	12. SPONSORING MILITARY ACTIVITY Air Force Aero Propulsion Laboratory Wright-Patterson Air Force Base, Ohio

13. ABSTRACT

This report describes the theoretical study and experimental circuit investigations conducted on the Allison effect apparatus used for chemical analysis.

The inherent electrical behavior of an Allison effect apparatus has been well defined by using modern high speed oscillographic techniques and frequency selective equipment. A continuous radio frequency spectrum characterized by numerous resonances rapidly diminishes into the noise level at 4000 megahertz. A theoretical analysis of the apparatus has generated a valid equivalent circuit model. A review of the extensive data indicates that the Allison effect apparatus functions primarily as a phase comparator for radio frequencies in the 30 to 100 megahertz range. An rf-optical interaction in the cells, possibly by means of the Cotton-Mouton effect, is thought to produce a characteristic light modulation effect when phase matching occurs.

DD FORM **1473**

14. KEY WORDS	LINK A		LINK B		LINK C	
	ROLE	WT	ROLE	WT	ROLE	WT
Allison Effect Observation of Allison Effect Minima Allison - Magneto-Optic Apparatus						

INSTRUCTIONS

I. ORIGINATING ACTIVITY: Enter the name and address of the contractor, subcontractor, grantee, Department of Defense activity or other organization (corporate author) issuing the report.

2a. REPORT SECURITY CLASSIFICATION: Enter the overall security classification of the report. Indicate whether "Restricted Data" is included. Marking is to be in accordance with appropriate security regulations.

2b. GROUP: Automatic downgrading is specified in DoD Directive 5200.10 and Armed Forces Industrial Manual. Enter the group number. Also, when applicable, show that optional markings have been used for Group 3 and Group 4 as authorized.

3. REPORT TITLE: Enter the complete report title in all capital letters. Titles in all cases should be unclassified. If a meaningful title cannot be selected without classification, show title classification in all capitals in parenthesis immediately following the title.

4. DESCRIPTIVE NOTES: If appropriate, enter the type of report, e.g., interim, progress, summary, annual, or final. Give the inclusive dates when a specific reporting period is covered.

5. AUTHOR(S): Enter the name(s) of author(s) as shown on or in the report. Enter last name, first name, middle initial. If military, show rank and branch of service. The name of the principal author is an absolute minimum requirement.

6. REPORT DATE: Enter the date of the report as day, month, year; or month, year. If more than one date appears on the report, use date of publication.

7a. TOTAL NUMBER OF PAGES: The total page count should follow normal pagination procedures, i.e., enter the number of pages containing information.

7b. NUMBER OF REFERENCES: Enter the total number of references cited in the report.

8a. CONTRACT OR GRANT NUMBER: If appropriate, enter the applicable number of the contract or grant under which the report was written.

8b, 8c, & 8d. PROJECT NUMBER: Enter the appropriate military department identification, such as project number, subproject number, system numbers, task number, etc.

9a. ORIGINATOR'S REPORT NUMBER(S): Enter the official report number by which the document will be identified and controlled by the originating activity. This number must be unique to this report.

9b. OTHER REPORT NUMBER(S): If the report has been assigned any other report numbers (either by the originator or by the sponsor), also enter this number(s).

10. AVAILABILITY/LIMITATION NOTICES: Enter any limitations on further dissemination of the report, other than those imposed by security classification, using standard statements such as:

(1) "Qualified requesters may obtain copies of this report from DDC."

(2) "Foreign announcement and dissemination of this report by DDC is not authorized."

(3) "U. S. Government agencies may obtain copies of this report directly from DDC. Other qualified DDC users shall request through

_____ ."

(4) "U. S. military agencies may obtain copies of this report directly from DDC. Other qualified users shall request through

_____ ."

(5) "All distribution of this report is controlled. Qualified DDC users shall request through

_____ ."

If the report has been furnished to the Office of Technical Services, Department of Commerce, for sale to the public, indicate this fact and enter the price, if known.

11. SUPPLEMENTARY NOTES: Use for additional explanatory notes.

12. SPONSORING MILITARY ACTIVITY: Enter the name of the departmental project office or laboratory sponsoring (paying for) the research and development. Include address.

13. ABSTRACT: Enter an abstract giving a brief and factual summary of the document indicative of the report, even though it may also appear elsewhere in the body of the technical report. If additional space is required, a continuation sheet shall be attached.

It is highly desirable that the abstract of classified reports be unclassified. Each paragraph of the abstract shall end with an indication of the military security classification of the information in the paragraph, represented as (TS), (S), (C), or (U).

There is no limitation on the length of the abstract. However, the suggested length is from 150 to 225 words.

14. KEY WORDS: Key words are technically meaningful terms or short phrases that characterize a report and may be used as index entries for cataloging the report. Key words must be selected so that no security classification is required. Identifiers, such as equipment model designation, trade name, military project code name, geographic location, may be used as key words but will be followed by an indication of technical context. The assignment of links, rules, and weights is optional.